



City Research Online

City, University of London Institutional Repository

Citation: Abu Shousha, R. I. (1991). Hot ductility of steels. (Unpublished Doctoral thesis, City, University of London)

This is the accepted version of the paper.

This version of the publication may differ from the final published version.

Permanent repository link: <https://openaccess.city.ac.uk/id/eprint/28474/>

Link to published version:

Copyright: City Research Online aims to make research outputs of City, University of London available to a wider audience. Copyright and Moral Rights remain with the author(s) and/or copyright holders. URLs from City Research Online may be freely distributed and linked to.

Reuse: Copies of full items can be used for personal research or study, educational, or not-for-profit purposes without prior permission or charge. Provided that the authors, title and full bibliographic details are credited, a hyperlink and/or URL is given for the original metadata page and the content is not changed in any way.

HOT DUCTILITY OF STEELS

by

020173836

R. I. ABU SHOUSA

A dissertation submitted to
The CITY UNIVERSITY
in fulfilment of the requirement
for the degree of
Doctor of Philosophy

October 1991

THE CITY UNIVERSITY

DEPARTMENT OF MECHANICAL ENGINEERING & AERONAUTICS

CONTENTS

	PAGE
LIST OF TABLES	1
LIST OF FIGURES	2
ACKNOWLEDGEMENTS	20
DECLARATION	21
ABSTRACT	22
LIST OF SYMBOLS	23
CHAPTER 1 INTRODUCTION	24
CHAPTER 2 LITERATURE SURVEY	28
2.1 The continuous casting process	29
2.2 Mechanics of the slab straightening process	31
2.3 Methods for reducing transverse cracking	33
2.4 High temperature strength and structure	36
2.4.1 Dynamic recovery	38
2.4.2 Dynamic recrystallization	42
2.4.3 Influence of structure on dynamic recrystallization	45
2.5 FRACTURE MODES RELATED TO THE DUCTILITY TROUGH	48
2.5.1 The right- hand side of the trough (H.D.H.T)	48
2.5.2 Region of embrittlement (inter granular fracture)	50
2.5.3.Mechanism's of crack formation for steels which have been solution treated	54
2.5.4 High carbon steel and C-Mn-Al steels which high Al and N levels.	56

2.5.5 Steels in which micro alloying precipitation occurs at the γ boundaries and precipitation free zones (PFZ) are present.	56
2-5-6 The left hand side high ductility low temperature region (H.D.L)	58
2.6 FACTORS INFLUENCING HOT DUCTILITY	59
2.6.1 Effect of strain rate	60
2.6.2 Influence of grain size on hot ductility.	62
2.6.3 Influence of composition on hot ductility	66
2.6.4 Precipitation in steels	67
2.6.5 The effect of precipitation on the hot ductility	68
2.6.6 Effect of Nb	71
2.6.7 Influence of Ti on hot ductility	74
2.6.8 Effect of Al	76
2.6.9 Effect of vanadium	79
2.6.10 Influence of S on hot ductility	80
2.6.11 Influence of carbon	83
2.6.12 Other elements	85
CHAPTER 3 EXPERIMENTAL TECHNIQUES	87
3.1 Introduction	88
3.2 Methods for studying hot ductility	88
3.3 Hot tensile tests	91
3.3.1 Induction heating tests	91
3.3.2 Instron tests	92
3.3.3 Measurement of Reduction in Area	94
3.4 Carbon extraction replica preparation	95

CHAPTER 4 EFFECT OF CALCIUM ON THE HOT DUCTILITY OF STEEL	96
4.1 Introduction	97
4.1.1 Ductility at room temperature	97
4.1.2 Ductility at high temperature	98
4.2 Experimental	100
4.2.1 As cast steels	100
4.2.2 Melted and reheated steels	101
4.3 RESULTS	102
4.3.1 Hot ductility of C-Mn-Al steels in the as cast state, steels directly cast and cooled down to the test temperature	102
4.3.2 Hot ductility of C-Mn-Nb-Al steels. Steels directly cast.	103
4.3.3 Melted and reheated C-Mn-Al Steels. Samples heated up to 1330°C after melting and cooling to the test temperature.	103
4.3.4 Dynamic recrystallization	104
4.4 FRACTOGRAPHY	105
4.4.1 SEM examination	105
4.4.2 Metallography	107
4.4.3 TEM examination	107
4.5 DISCUSSION	109
4.5.1 As cast condition	109
4.5.2 As cast and reheated condition	112
4.5.3 Hot-rolled and solution treated steels, cooled directly to test temperature.	114
4.6. CONCLUSIONS	115

CHAPTER 5 THE INFLUENCE OF S AND Nb ON THE HOT DUCTILITY	116
5.1 Introduction	117
5.2 Experimental	120
5.3 Results	121
5.3.1 Hot ductility curves	121
5.3.2 Stress/Elongation curves	121
5.3.3 Metallography	122
5.3.4 Replica examination	123
5.4 Discussion	124
5.4.1 Hot ductility behaviour of C-Mn-Al steels	124
5.4.2 Influence of Nb on hot ductility	128
5.5 Conclusions	131
CHAPTER 6 EFFECT OF TITANIUM ON THE HOT DUCTILITY	132
6.1. Introduction	133
6.2 Experimental	136
6.3 Results	138
6.3.1 Hot ductility curves	138
6.3.2 Stress/Elongation curves	138
6.3.3 Metallography	140
6.3.4 Fracture appearance for Nb/Ti and Nb steels	140
6.3.5 Replica examination	141
6.4 Discussion	143
6.4.1 As-cast	143
6.4.2 As-cast reheated	145
6.5 Conclusions	146

CHAPTER 7 EFFECT OF TI AND C ON THE HOT DUCTILITY OF C-Mn-AI STEEL	148
7.1. Introduction	149
7.2 Experimental	151
7.3 Results	153
7.3.1 Hot ductility curves	153
7.3.2 Stress/Elongation curves	153
7.3.3 Metallography	155
7.3.4 Replica examination	156
7.4 Discussion	157
7.4.1 Influence of Ti on hot ductility	157
7.4.2 Influence of C on the hot ductility	159
7.5 Conclusions	163
CHAPTER 8 EFFECT OF AI AND N ON HOT DUCTILITY	164
8.1. Introduction	165
8.2 Experimental	167
8.3 Results	170
8.3.1 Hot ductility curves	170
8.3.2 Stress/Elongation curves	172
8.3.3 Metallography	173
8.3.4 Transmission electron microscope results	174
8.4 Discussion	176
8.5 Conclusions	180
CHAPTER 9 EFFECT OF 'RESIDUALS ELEMENTS' ON HOT DUCTILITY	182

9.1. Introduction	183
9.2 Experimental	186
9.3 Results	188
9.3.1 Hot ductility curves	188
9.3.2 Fracture examination	190
9.3.3 Metallography	190
9.4 Discussion	191
9.5 Conclusions	193
CHAPTER 10 EFFECT OF C ON HOT DUCTILITY	194
10.1. Introduction	195
10.2 Experimental	197
10.3 Results	199
10.3.1 Hot ductility curves	199
10.3.2 Stress/Elongation curves	200
10.3.3 Metallography	200
10.4 Discussion	202
10.5 Conclusions	206
CHAPTER 11 SUMMARY AND RECOMMENDATIONS	207
11.1. Introduction	208
11.2 Summary	209
11.3 Future work and recommendations	213
11.4 Industrial recommendations	217
APPENDIX	218
Publications	219

LIST OF TABLES

- 4.1 Composition of the steels examined.
- 4.2 Grain size μm of steels examined.
- 5.1 Composition of the steels examined.
- 6.1 Composition of the steels examined.
- 6.2 Austenite grain size for the steels examined at the two cooling rates in (micron).
- 6.3 Precipitation observed in the grain boundaries and in the matrix for the steels examined.
- 7.1 Composition of the steels examined.
- 8.1 Composition of the steels examined.
- 9.1 Composition of the steels examined.
- 10.1 Composition of the steels examined.

LIST OF FIGURES

- 2.1 Profile of Gray slab caster (After Lankford, 1972).
- 2.2 Schematic representation of friction force and tensile force on the skin surface. (After Lankford, 1972).
- 2.3 Ductility trough controlled by phase transformation in coarse grained steels (grain size 200 μm). (After Mintz et al 1991).
- 2.4 Hot ductility for Al and Nb containing steels. (After Mintz and Arrowsmith, 1979).
- 2.5 Surface strain and strain rate resulting from bending (After Lankford, 1972).
- 2.6 Comparison of temperature distribution between mist cooling and spray cooling. (After Kawasaki et al, 1987).
- 2.7 Stress strain curves for a plain carbon and a 2.91% silicon steels tested at 1000°C (After Sakai and Ohashi., 1981).
- 2.8 Schematic Models showing the formation of wedgecracks due to grain boundary sliding The arrows indicate a sliding boundary and the sense of translation. (After Chang and Grant, 1956).
- 2.9 Mechanism for void formation at grain boundary ledge (After Gifkin, 1959).
- 2.10 Schematic diagram showing the mechanisms for transformation induced intergranular failure. (After Mintz et al 1991).

- 2.11 Flow stress at strains of 0.001 and 0.100 for 0.005% C steel, illustrating difference in strength, temperature dependence, and work hardening rate for α and γ phases (After Wray 1981).
- 2.12 Schematic illustrations showing intergranular microvoid coalescence of niobium-bearing steels by deformation (After Maehara and Ohmori 1984).
- 2.13 Influence of strain rate on the hot ductility of C-Mn-Al-Nb steel. (After Mintz and Arrowsmith, 1979).
- 2.14 The effect of strain rate on hot ductility and grain boundary sliding in a C-Mn-Nb-Al steel. (After Ouchi and Matsumoto, 1982).
- 2.15 Effect of grain size on the hot ductility of plain C-Mn steels (After Crowther and Mintz 1986).
- 2.16 The influence of D_0 (the initial grain size) on the minimum R. of A. value. (After Mintz et al 1991).
- 2.17 Solubilities of carbides and nitrides in austenite. (After Narita 1975).
- 2.18 **Hot brittlement** due to AlN precipitation (After **Funnell** and Davies 1978).
- 2.19 Influence of soluble Aluminium on the hot ductility of C-Mn-Nb-Al steels (After Mintz and Arrowsmith 1979).
- 2.20 Hot ductility curves for different micro-alloy steels, showing the effect of V (After Mintz and Arrowsmith, 1980).

- 2.21 Hot ductility curves for Al containing steels examined with different carbon levels (After Z.Mohamed, 1988).
- 2.22 Hot ductility curves for Nb containing steels with different carbon contents (After Z.Mohamed, 1988).
- 3.1 Schematic illustration of induction heating equipment for high temperature tensile testing.
- 3.2 Induction test specimen.
- 3.3 Schematic illustration of Instron high temperature testing equipment.
- 3.4 Instron test piece.
- 4.1 Experimental arrangement for measuring hot ductility in the as-cast condition.
- 4.2 Hot ductility curves for C-Mn-Al steels with and without calcium. Steels directly cast and cooled to test temperature.
- 4.3 Hot ductility curves for C-Mn-Nb-Al steels with and without calcium. Steels directly cast and cooled to test temperature.
- 4.4 Hot ductility curves for C-Mn-Al and C-Mn-Nb-Al steels at two S levels.
- 4.5 Hot ductility curves for the calcium treated C-Mn-Al steel, steel (A) after casting and casting followed by reheating.
- 4.6 Hot ductility curves for as-cast and as-cast reheated C-Mn-Al steel. Steel (C).

- 4.7 Hot ductility curves for as-cast and as-cast reheated C-Mn-Al steel. Steel (B).
- 4.8 Stress/Elongation curves for Ca containing C-Mn-Al steel (A).
- 4.9 Stress/Elongation curves for Ca free C-Mn-Al steel (C).
- 4.10 Stress/Elongation curves for Ca free high S, C-Mn-Al steel (B).
- 4.11 Stress/Elongation curves for as-cast C-Mn-Nb-Al steels.
- 4.12 Fracture surface of as-cast C-Mn-Al-steel tested at 900°C showing intergranular micro-void coalescence and intergranular decohesion, (steel C).
- 4.13 Typical dendritic region found on fracture surface of as-cast C-Mn-Al steel, steel (C), tested at 750°C.
- 4.14 Dendritic failure in C-Mn-Al steel as-cast and reheated, and tested at 800°C, (steel C).
- 4.15 Fracture surface of as-cast C-Mn-Al steel showing grain boundary sliding. Steel (B), tested at 900°C.
- 4.16 Mixture of interdendritic and ductile voiding fracture observed in C-Mn-Al-Ca steel (A), tested at 850°C.
- 4.17 Interdendritic fracture in as-cast calcium containing steel, steel (A) tested at 850°C.

- 4.18 Fracture surface of as-cast reheated C-Mn-Al-Ca, steel (A) showing high temperature ductile rupture fracture, steel tested at 850°C.
- 4.19 Fracture surface of as-cast C-Mn-Nb-Al steel showing a mixture of intergranular micro-void coalescence and intergranular decohesion, (steel D), tested at 800 °C.
- 4.20 Fracture surface of the Ca containing as-cast C-Mn-Nb-Al, steel (D) tested at 800°C, Showing intergranular fracture due to grain boundary sliding.
- 4.21 Sulphide inclusions found in C-Mn-Al steel. The steel was as-cast and reheated, and tested at 900°C. (steel B).
- 4.22 Isolated inclusions in Ca containing steel, in the as cast reheated condition, steel (A) tested at 900°C.
- 4.23 Example of NbCN precipitation observed in the as-cast C-Mn-Nb-Al steel, (D) tested at 900°C.
- 4.24 NbCN observed at sub-boundaries for Ca treated steel, steel (D) tested at 900°C.
- 4.25 NbCN eutectic observed in the Ca free steel. Steel (G) tested at 800°C.
- 4.26 CaS inclusions observed in the as cast steel (A), tested at 900°C.
- 4.27 MnFeS inclusions found in as-cast steel (B), tested at 900°C.

- 4.28 Fine sulphide inclusions found in the as-cast and reheated steel, steel (B) tested at 900°C.
- 4.29 Hot ductility curves for C-Mn-Al steels with and without calcium. Steels solution treated and cooled to test temperature (After Mintz et al, 1989).
- 4.30 Hot ductility curves for C-Mn-Nb-Al steels with and without calcium. Steels solution treated and cooled to test temperature (After Mintz et al 1989).
- 5.1 Hot ductility curves for all the steels examined.
- 5.2 Stress/Elongation curves for all the steels examined.
- 5.3 Evidence of deformation induced ferrite in low Nb/high S Steel (D), tested at 850°C.
- 5.4 Evidence of deformation induced ferrite in high Nb/high S Steel C, tested at 850°C.
- 5.5 Evidence of dynamic recrystallization found in steel (D), tested at 900°C.
- 5.6 Fracture surface of low S/high Nb steel (B) showing intergranular micro-void coalescence and intergranular decohesion.
- 5.7 Fracture surface of high S/high Nb, steel (C) Showing intergranular micro-voids.
- 5.8 Fracture surface of low S/high Nb, steel (B) Showing grain boundary sliding plus ductile voiding, steel tested at 800°C.
- 5.9 Micro-void coalescence around sulphide inclusions observed in high S/Nb steel (C) tested at 800°C.

- 5.10 Spherical sulphides found on dendrite nodules in High S/Nb steel (C), tested at 850°C.
- 5.11 Sulphide inclusions found in high S/Nb steel (C). Steel tested at 850°C.
- 5.12 Typical interdendritic fracture observed in Low Nb high S, steel (D) tested at 850°C.
- 5.13 (Mn,Fe)S inclusions present at interdendritic boundaries found in steel (D).
- 5.14 Very coarse (Mn,Fe)S inclusions found in steel (D), tested at 900°C.
- 5.15 Very fine Fe-oxysulphides found in high S steel, steel (D) tested at 900°C.
- 5.16 Very fine Fe-oxysulphides found in high S steel, steel (D) tested at 900°C.
- 5.17 Very fine Nb(CN) matrix precipitation found in low S high Nb, steel (B), tested at 900°C.
- 5.18 Nb(CN) precipitation in the grain sub-boundary found in high S high Nb, steel (C), tested at 900°C.
- 5.19 Nb(CN) precipitation in the sub-boundary found in high S high Nb, steel (C), tested at 900°C.
- 5.20 Mixture of Nb(CN) with (Mn,Fe)S found in high S/Nb steel (C), tested at 900°C.
- 5.21 Nb(CN) eutectic found in high S/Nb steel (C), tested at 900°C.

- 5.22 (Mn.Fe)S eutectic found in high S/Nb steel C, tested at 900°C.
- 6.1 Hot ductility curves for Nb/Ti steel.
- 6.2 Hot ductility curves for Nb containing steel.
- 6.3 Stress/Elongation curves for Nb/Ti containing steel.
- 6.4 Stress/Elongation curves for Nb/Ti free steel.
- 6.5 Fine grain structure in as-cast reheated Ti containing steel, tested at 800°C. Cooling rate 100°C/min.
- 6.6 Typical wedge type crack found in Ti containing steel tested at 850°C, cooling rate 100°C/min.
- 6.7 Typical wedge type crack found in Ti as-cast steel tested at 850°C, cooling rate 25°C/min.
- 6.8 Evidence of deformation induced ferrite in the as-cast Ti free steel tested at 850°C. Cooling rate 100°C/min.
- 6.9 Fracture surface of as-cast Ti steel, tested at 850°C, showing a mixture of inter granular microvoid coalescence and intergranular decohesion (R of A 47%).
- 6.10 Fracture surface of as-cast Ti containing steel tested at 850°C, showing evidence of grain boundary boundary sliding. (R of A 38%) cooling rate 25°/min.

- 6.11 Interdendritic failure observed in Ti free steel tested at 900°C. (R of A 63%). Cooling rate 25°C/min.
- 6.12 Fracture surface of as-cast Ti containing steel tested at 850°C, showing isolated dendritic region with spherical MnS inclusions on the nodule surface. Cooling rate 100°C/min.
- 6.13 Dendritic regions found in the as-cast reheated Ti containing steel tested at 850°C. Cooling rate 100°C/min.
- 6.14 Typical high temperature rupture fracture in Ti containing steel, tested at 950°C, (R of A 74%). Cooling rate 100°C/min.
- 6.15 Fracture surface of as-cast reheated Ti containing steel tested at 900°C showing a mixture of intergranular micro-void coalescent, inter-granular decohesion failure and interdendritic failure. (R of A 40%). Cooling rate 100°C/min.
- 6.16 Fracture surface of as-cast reheated Ti containing steel, tested at 900°C showing a mixture of intergranular micro-void coalescence and interdendritic failure (RofA 40%). Cooling rate 100°C/min.
- 6.17 Fracture surface of as-cast reheated Ti containing steel, tested at 900°C showing a mixture of intergranular micro-void coalescence and intergranular decohesion. (RofA 40%). Cooling rate 100°C/min.
- 6.18 Ti eutectic found in the Ti containing steel tested at 1000°C, cooling rate 100°C/min.

- 6.19 Nb rich eutectic observed in Ti containing steel tested at 1000°C, cooling rate 100°C/min.
- 6.20 Coarse Nb rich precipitation found in the Ti containing steel, tested at 1000°C. cooling rate 100°C/min.
- 6.21 Fine Nb(CN) precipitation found in the Ti containing steel, tested at 850°C, cooling rate 100°C/min.
- 6.22 Fine Nb(CN) precipitation found in Ti containing steel tested at 850°C, cooling rate 100°C/min.
- 6.23 Fine Nb(CN) precipitation found in Ti containing steel, tested at 850°C, cooling rate 100°C/min.
- 6.24 Fine Nb(CN) precipitation found in the Ti containing steel, tested at 850°C. Cooling rate 100°C/min.
- 6.25 Fine Nb(CN) precipitation found in Ti free steel, tested at 850°C, cooling rate 100°C/min.
- 6.26 Fine Nb(CN) precipitation found in Ti free steel, tested at 850°C cooling rate 100°C/min.
- 6.27 Fine Nb(CN) precipitation found in Ti free steel, tested at 850°C, cooling rate 100°C/min.
- 6.28 Nb and Ti precipitation found in Ti containing steel tested at 850°C cooling rate 25°C/min.
- 6.29 NbC precipitation found in Ti containing steel, tested at 850°C, cooling rate 25°C/min.

- 6.30 Nb and Ti precipitation found in the Ti containing steel, tested at 850°C, cooling rate 25°C/min.
- 6.31 Nb precipitation found in Ti free steel, tested at 850°C, cooling rate 25°C/min.
- 6.32 Nb and Ti precipitation found in as-cast reheated Ti containing steel, tested at 850°C. Cooling rate 100°C/min,
- 6.33 Nb and Ti precipitation found in as-cast reheated Ti containing steel, tested at 850°C. Cooling rate 100°C/min,
- 6.34 Nb and Ti precipitation found in as-cast reheated Ti containing steel, tested at 900°C. Cooling rate 100°C/min.
- 6.35 Nb and Ti precipitation in as-cast reheated Ti containing steel, tested at 900°C. Cooling rate 100°C/min.
- 7.1 Hot ductility curves for 0.05% C.
- 7.2 Hot ductility curves for 0.15% C.
- 7.3 Influence of C on hot ductility for Ti free steels.
- 7.4 Influence of C on hot ductility for Ti containing steels.
- 7.5 Influence of carbon content on the difference in temperature between A_{e3} temperature and the A_{r3} temperature.
- 7.6 Stress/Elongation curves for the 0.05% C steels.
- 7.7 Stress/Elongation curves for the 0.15% C steels.

- 7.8 Evidence of deformation induced ferrite in Ti free, 0.15% C steel, tested at 800°C.
- 7.9 Typical wedge crack found in Ti free, 0.15% C, tested at 900°C.
- 7.10 Fracture surface of Ti containing, 0.15% C steel, Showing intergranular microvoid coalescence, tested at 800°C. R of A 23%.
- 7.11 Fracture surface of Ti containing, 0.15% C steel, Showing intergranular microvoid coalescence, tested at 800°C. R of A 23%.
- 7.12 Fracture surface of Ti containing, 0.15% C steel, Showing grain boundary sliding, steel tested at 900°C, R of A 83%.
- 7.13 Fracture surface of Ti free, 0.05% C steel showing ductile voiding, steel tested at 900°C. R of A 83%.
- 7.14 Fracture surface of Ti free 0.15% C steel showing isolated dendritic region, tested at 900°C. (R of A 57%).
- 7.15 TiN precipitation found in 0.15% C steel tested at 850°C.
- 7.16 TiN precipitation found in 0.15% C steel tested at 850°C.
- 7.17 TiN precipitation found in 0.05% C steel tested at 850°C.
- 7.18 TiN and Al rich particles found in 0.15% C steel tested at 850°C.

- 7.19 Al rich particle found in 0.15% C Ti free steel tested at 850°C.
- 8.1 Hot ductility curves for C-Mn-Al steels and C-Mn steel. Steels were given short holding times. Dashed curve is for C-Mn steel heat-treated to give a coarse grain size.
- 8.2 Hot ductility curves for C-Mn-Al steels and C-Mn steel given long holding times. Dashed curves are for short holding time heat-treatments for the C-Mn-Al steels.
- 8.3 Stress/Elongation curves for the steels examined, after the short holding times.
- 8.4 Stress/Elongation curves for the steels examined, after being given long holding times.
- 8.5 Example of intergranular micro-void coalescence fracture observed in the 0.023% Al steel tested at 800°C and given the short holding time treatment.
- 8.6 Example of deformation induced ferrite observed in the 0.058% Al steel tested at 850°C and fast cooled after fracture. Calculated Ae_3 temperature was ~850°C. Steel given short holding times.
- 8.7 **Example** of ductile rupture observed in an 0.058% Al steel tested at 850°C and given the short holding times.
- 8.8 Example of ductile voiding observed in an C-Mn steel tested at 800°C, the steel was given short heat-treatment and had a fine grain size.

- 8.9 Austenite grain size for C-Mn-Al and C-Mn steels, after solution treatment to 1330°C. for 5 mins, and quenching in water.
- 8.10 Example of intergranular fracture due to grain boundary sliding and micro-void coalescence observed in the 0.058% Al steel tested at 900°C. The steel was given the long heat-treatment.
- 8.11 Example of intergranular fracture due to grain boundary sliding and micro-void coalescence observed in the 0.058% Al steel tested at 850°C. The steel was given the long heat-treatment.
- 8.12 Wedge cracks observed in the 0.058% Al steel tested at 850°C. Steel had been given the long heat-treatment prior to testing.
- 8.13 Very coarse AlSiO_2 particles found in 0.023% Al steel tested at 850°C. Steel was given short holding times.
- 8.14 A very coarse Al_2O_3 precipitation found in 0.058% Al steel tested at 850°C. Steel was given short holding times.
- 8.15 Alumina silicate particles found in 0.023% Al steel tested at 850°C. Steel was given short holding times.
- 9.1 Hot ductility curves for 0.5% Cu steel in the solution treated condition with and without argon, and after casting and testing in an argon atmosphere.

- 9.2 Hot ductility curves for 0.5%Ni steel in the solution treated condition with and without argon, and after casting and testing in an argon atmosphere.
- 9.3 Hot ductility curves for CuNi steel in the solution treated condition with and without argon, and after casting and testing in an argon atmosphere.
- 9.4 Hot ductility curves for all the steels examined after solution treating, using an argon atmosphere through-out the tests.
- 9.5 Hot ductility curves for all the steels examined after solution treating in air.
- 9.6 Hot ductility curves for all the steels examined in the as-cast condition, using an argon atmosphere for protection.
- 9.7 Hot ductility curves for all the steels examined in the as-cast condition argon was switched off at 1500°C.
- 9.8 Hot ductility curves for all the steels examined in the as-cast condition using an argon atmosphere for protection. The dashed lines are for the steels ~~when~~ argon was switched off after melting.
- 9.9 Stress/Elongation curves for the reheated solution treated steels tested in an argon atmosphere.
- 9.10 stress/Elongation curves for the reheated steels solution treated and tested in air.
- 9.11 Stress/Elongation curves for the as-cast steels protected with an argon atomsphere.

- 9.12 Stress/Elongation curves for all the steels examined in the as-cast condition with the argon flow discontinued at a temperature of 1500°C.
- 9.13 Ductile rupture fracture found in 0.5% Ni containing steel reheated to 1300°C, and protected with argon. Sample tested at 1000°C
- 9.14 Grain boundary sliding found in the CuNi steel in the as-cast condition. Steel tested at 900°C
(a) argon flow stopped at 1500°C
(b) argon flow on all the time.
- 9.15 Grain boundary sliding found in 0.5% containing Ni steel. Steel was solution treated, tested at 900°C. Sample was protected by argon.
- 9.16 As-cast 0.5% Cu steel, tested at 800°C, showing a mixture of grain boundary sliding and micro-void coalescence.
- 9.17 Intergranular fracture due to micro-void coalescence, found in the CuNi steel tested at 800°C. Sample was protected by argon.
- 9.18 Ductile voiding found in 0.5% Ni steel, tested in air at 850°C.
- 9.19 Wedge cracks found in 0.5% Cu steel.
- 9.20 Decarburization and internal oxidation found in 0.5% Cu containing steel solution treated and tested in air at 900°C (R.of.A is 35 %).

- 9.21 Decarburization and internal oxidation found in as-cast CuNi steel tested at 900°C. Argon was turned off at 1500°C.
- 9.22 Virtual absence of decarburization and internal oxidation found in the as-cast 0.5% Cu steel protected throughout the test by argon. Steel was tested at 900°C.
- 10.1 Schematic diagram of the quenching unit.
- 10.2 Hot ductility curves for low and high carbon steels.
- 10.3 Stress/Elongation curves for high and low carbon steels.
- 10.4 Evidence of dynamic recrystallization for high carbon steel, tested at 750°C.
- 10.5 Evidence of dynamic recrystallization for high carbon steel, tested at 780°C.
- 10.6 Example of intergranular micro-void coalescence fracture observed in low carbon steel, tested at 850°C.
- 10.7 ~~Example~~ of high temperature ductile rupture fracture found in high carbon steel tested at 750°C.
- 10.8 Example of intergranular micro-void coalescence fracture observed in high carbon steel, tested at 700°C.
- 10.9 Evidence of deformation induced ferrite in high carbon steel tested at 700°C.

- 10.10 Grain boundary sliding found in high carbon steel, tested at 670°C.
- 10.11 Typical pearlitic fracture found in high carbon steel tested at 620°C.
- 10.12 First evidence of pearlitic structure formation in high carbon steel. Steel heated to 1330°C, held for 5 min, cooled at 25°C/min to 650°C, held 5 min, and then quenched in water.
- 10.13 High carbon steel tested at 670°C showing austenite grains with ferrite films surrounding the grains.
- 10.14 Hot ductility curves for a series of plain C-Mn steels with different carbon levels. (After Crowther and Mintz, 1986).

ACKNOWLEDGEMENTS

I would like to express my thanks to Dr. B. Mintz for his invaluable supervision, encouragement and the knowledge he has imparted on the subject.

Thanks are due to Professor G. Done for the provision of laboratory facilities and to the staff of the Mechanical Engineering Department for their help, particularly Mr. R. Vipond and Dr J. Walker and Mr T. Rose.

Gratitude is also expressed to Mr. G.D. McPhail of the Physics Department for his help in the use of the electron microscope

Thanks are also due to British Steel, in particular to Dr. D.N. Crowther for supplying the steel

Finally I would like to thank my husband for his encouragement, and my son Mohamed for helping me with the preparation and typing of this thesis.

DECLARATION

I grant powers of discretion to the University Librarian to allow this thesis to be copied in whole or in part without further reference to me. This permission covers only single copies made for study purposes, subject to normal conditions of acknowledgement.

ABSTRACT

The hot tensile test has been used for to examine the influence of such factors as precipitation, composition, inclusions, phase transformation and grain size on hot ductility. Tests were performed mainly in the as-cast condition but also after solution treatment (1330°C) so as to obtain a coarse grain size similar to that found in the continuously cast slab process. Test temperatures in range of 750-1000°C and strain rates between 10^{-3}s^{-1} - $3 \times 10^{-3}\text{s}^{-1}$ inclusive were examined, these being the temperature range and strain rate in which the straghtening operation is performed. The ductility trough arises as a result of stress and strain concentrations at the austenite boundaries caused by the presence of thin films of the softer deformation induced ferrite enveloping the austenite grains, or by grain boundary sliding in the austenite. Both failure mechanisms are encouraged by the presence of grain boundary precipitation and inclusions. The depth and width of the trough is dependent on the size and volume fraction of these precipitates. Dynamic recrystallizaion is also found to be a very important factor controlling the ductility trough at the high temperature end of the trough. Precipitation and inclusions can retard the dynamic recrystallization so extending the trough to higher temperatures. Reheating the C-Mn-Al low S level steels after casting can be beneficial to the hot ductility as a result of refining the grain size. For C-Mn-Nb-Al and C-Mn-Al high S level steels reheating causes the precipitation of NbCN and FeMnS in the latter, which are finer and have a closer inter-particle spacing than in the as-cast state. These particles precipitate on the austenite grain boundaries and within the matrix during the tests leading to a delaying of the onset of dynamic recrystallization. Grain boundary sliding and cavitation are enhanced leading to poor ductility. Improved hot ductility has been achieved by adding Ca to steels which reduces the amount of sulphides inclusions precipitated on cooling from the as-cast condition to the test temperature. Ti additions give rise to only a slight improvement in hot ductility in the as-cast condition when the cooling rate to the test temperature is 100°C/min but is very beneficial when the cooling rate after casting is reduced to 25°C/min.

This probably arises because coarse Ti rich particles allow the Nb to precipitate out at high temperature leaving less available to precipitate out in a detrimental form at lower temperature. Raising the C level was found to move the ductility troughs to lower temperatures as a result of lowering the transformation temperature. These troughs are controlled by the presence of deformation induced ferrite which forms in the temperature range between the A_{r3} and A_{e3} .

It is found that removal of deformation induced ferrite leads to dynamic recrystallization. Ductility is found to deteriorate when Al is added to steels, and the AlN solubility product is high, 2 to 3×10^{-4} . Increasing the solution treatment time probably allows the AlN to precipitate out in a finer form giving inferior ductility. Addition of Cu to the C-Mn-Nb-Al steels can be detrimental to the hot ductility especially when the as-cast steels were tested in air. The segregation of Cu to the boundaries and the oxidation of Fe at the surfaces leads to Cu enrichment and hot shortness.

LIST OF SYMBOLS

a	numerical constant
A	numerical constant
b	numerical constant
dg	grain diameter
do	initial grain size
ds	diameter of subgrains
L	gauge length during continuously cast slab straightening
M	grain boundary mobility
n	stress exponent
p	driving force for grain boundary migration
Q	activation energy for deformation
R	universal gas constant
R	bending radius for straightening of continuously cast slab
t	slab thickness
T	absolute temperature
v	grain boundary migration velocity
V	continuous casting speed
Z	Zener-Hollomon parameter
α	numerical constant
α	ferrite
γ	austenite
δ	solidified skin thickness in continuously cast slab
Δ	tangent point to first bending roll
$\dot{\epsilon}$	strain rate
ϵ_c	critical strain for the nucleation of dynamic recrystallisation
ϵ_{gb}	grain boundary strain
ϵ_p	strain at peak stress
ϵ_s	surface strain at continuously cast slab
ϵ_t	total strain
σ	stress
σ_f	flow stress
σ_p	peak stress
τ_c	critical shear stress for wedge crack nucleation
ν_r	inclusion relative plasticity

CHAPTER 1

INTRODUCTION

INTRODUCTION

The essential properties required in material used for oil platform and pipe line applications are high fracture toughness and strength. Before around 1950 the maximum strength for structural steel was 300 Mpa. In 1960 additions of micro-alloying elements such as Al, Nb, V and Ti, in small amounts led to improvement in grain refinement, giving improved strength and impact behaviour. This was achieved by the formation of a fine precipitation of aluminium nitride (AlN), niobium carbide (NbCN), vanadium carbide, and titanium nitride or titanium carbide at the austenite grain boundaries which prevented the boundaries from moving by a pinning action. Strengths of 490 Mpa were now possible in normalised steels and 550 Mpa in controlled rolled steels. However, this ability of micro-alloying additions to refine grain size by pinning boundaries although giving excellent toughness and strength in the finished product, produces problems on continuous casting and can give rise to a wide variety of defects in the solidified slab during continuous casting, (Lankford, 1972; Brimacombe and Sorimachi, 1977). One such defect is known as transverse cracking described in chapter [2]. These cracks are particularly deleterious since they form on the slab surface and hence cannot weld up during subsequent rolling and sometimes the whole slab must be scrapped, (Crowther, 1988). Considerable understanding has been made of the problem in the last 20 years using a simple

laboratory hot tensile test and most steel companies have to a large extent solved the problem to their own satisfaction. It is therefore perhaps surprising that so much research effort is still being carried out in this area both at steel research laboratories and universities. This arises through the following reasons:-

- 1- Transverse cracking can often arise when new continuous casters are introduced into production.
- 2- Information is required for new steels programmed through the continuous casting route.
- 3- Scarfing is needed at times for the most difficult grades of steel. Cracks are also formed at the edges of the strand and it is not uncommon to roll wide and trim off the edges, adding considerably to scrap losses.
- 4- With the advent of direct rolling it is essential to obtain a defect clean surface for the economic production of steel (Mintz et al, 1991).

Thus there is a strong incentive to gain an understanding into the formation of these defects in order to prevent their occurrence. To achieve this aim, hot tensile tests have been performed.

In most of the previous work the tests were performed

after solution treating, or heating the sample from room temperature to the test temperature. Such tests although giving useful information, are often inadequate in simulating the commercial processing route, in which the as-cast structure may dominate ductility. Only a few investigations have been carried out on steel cast in situ followed by direct cooling to the test temperature, (Lankford, 1972; Harding et al, 1977; Suzuki et al, 1982; Rogberg, 1983; Mintz and Mohamed, 1988).

The present work has therefore concentrated on obtaining hot ductility curves for as-cast steel. The influence of Calcium, Niobium, Sulphur, Titanium, Carbon, and residual elements on the hot ductility of directly cast steels have been examined. In addition the influence of Aluminium and Nitrogen additions on hot ductility after solution treatment has been examined in more detail.

CHAPTER 2

LITERATURE SURVEY

2 LITERATURE SURVEY

2.1 The continuous casting process

The continuous casting operation is shown schematically in Fig. 2.1. The molten steel is poured from a ladle via a tundish into an oscillating water cooled copper mould and is generally cast in a curve, the strand requiring straightening or unbending at a certain point. The mould oscillates to prevent sticking, and this oscillation introduces transverse ripples onto the surface and these may act as stress concentrators and under certain conditions cracks may form along the oscillation marks on the top surface and edges of the strand. These cracks are often difficult to see on the original slab and scarfing is necessary to reveal them. Normally the crack depth varies from 1-15 mm and the width is approximately 0.2 mm, (Brimacombe and Sorimachi, 1977), although at the corners the crack depth may be as much as 50 mm, (Farkas et al, 1971; Hater et al, 1973). It is believed that the cracks form in the mould and propagate during the straightening process, (Schmidt and Josefsson, 1974; Mercer and Mcpherson, 1980). In addition Schmidt and Josefsson, (1974) have shown that the cracks propagate along the austenite boundaries, and that coarse grained regions are particularly prone to cracking. A variety of particles have^{been} identified on the crack surface including AlN (Mori, 1974; Cochrane, 1982), and MnS, NbCN and various oxides (Cochrane, 1982), and

these are believed to encourage intergranular failure. The straightening operation which unbends the strand and puts the top surface and edges into tension is carried out in the temperature range 700-1000°C which is just the temperature range in which ductility is poor in a hot tensile test, Fig 2.2. The failure mechanism in the trough is intergranular and believed to be the same as that which produce transverse cracks. Essential two mechanisms have been proposed to account for intergranular failure

1- Transformation induced as in Fig. 2.3.

2- Failure by grain boundary sliding (gbs) which is aggravated by precipitation at boundaries e.g. AlN or NbC precipitation, Fig. 2.4 and these will pin boundaries allowing cracks formed by gbs to join up.

2.2 Mechanics of the slab straightening process

Transverse cracks propagate during the slab straightening process, and several estimates have been made to determine the surface strain and strain rate experienced by the slab during the straightening process. Fig. 2.5 illustrates the surface strain and strain rate developed. These strains may be the greatest to which the slab is subjected during the continuous casting operation.

The surface strain ϵ_s due to the bending is given approximately by the following equation:

$$\epsilon_s = t / 2R \dots\dots\dots 2.1$$

Where t is the slab thickness and R is the bending radius. For typical R values of 10 m and slab thickness of 0.23 m, a surface strain of 1.15% is expected. The strain rate, $\dot{\epsilon}$, is given by

$$\dot{\epsilon} = \epsilon_s V/L \dots\dots\dots 2.2$$

Where V is the casting speed and L is the gauge length. The uncertainty in the value of the gauge length over which the full bending strain is developed could lead to over or underestimating of the actual strain rate (Lankford, 1972). He has given 3 values for this gauge length L , Fig. 2.5, the distance from tangent point to the first bending rolls (Δ), a distance equal to the skin thickness (δ) or a distance equal to the slab thickness (t).

For a typical casting speed of 0.9 m/min and a suitable

value for L (6-10 m) the surface strain is in the range of 1.7×10^{-3} to $2.9 \times 10^{-3} \text{ s}^{-1}$

Similar results for surface strain and strain rate have been calculated by Bernard et al, (1978).

It should be noted that these calculations are approximate, and deal with the deformation of the slab as a whole. Locally, at the bottom of the oscillation marks for example values ϵ_s and $\dot{\epsilon}$ may be higher.

2.3 Methods for reducing transverse cracking

The temperature range in which a loss of ductility occurs for micro-alloying steels is reported to be between 600-1000°C when using a strain rate in the range $10^{-4} - 10^{-3} \text{ s}^{-1}$. This temperature range is just the range in which the straightening operation is performed and where the transverse cracks are believed to propagate. In order therefore to produce crack free slabs, it is necessary to select either a soft cooling pattern to give a slab surface temperature in excess of this temperature range as shown in Fig. 2.6, or hard cooling patterns to give slab surface temperatures below the low ductility region. Offerman et al, (1981); Mercer and Macpherson, (1979) have reported a reduction in the incidence of transverse cracking using a soft cooling pattern. However this method presents problems as the extent of the trough is dependent on composition. Straightening temperatures therefore, have either to be adjusted for a particular composition or kept at a temperature high enough to avoid the ductility trough. Also casting speed must be adjusted carefully if a soft pattern is used, as rapid casting can result in incomplete solidification at the straightener, while a casting speed which is too low can produce a straightening temperature close to the ductility trough. Birat et al, (1981) have used a hard cooling pattern which reduces the surface temperature at the straightener to 700°C and this produced a decrease in the frequency of

transverse cracking. Nozaki et al, (1978); Schmidt and Josefsson, (1974) have also used a hard cooling pattern and found reduced transverse cracking. The latter authors attributed the reduction in cracking to the elimination of the coarse austenite grains which they had previously related to the transverse cracking. The disadvantages of a hard cooling pattern are reported by Offerman et al, (1981). Reducing the slab surface temperature below 700°C will at some point below the slab surface cause the temperature to be high enough to place it in the low ductility region, leading to the formation of sub-surface transverse cracks. Also uniform cooling over the slab surface using the hard cooling pattern is very difficult to achieve (Offerman et al, 1981). For example clogged spray nozzles can produce localized bands at the surface which are at elevated temperature, and the cracking can then occur along the bands. The impingement of cooling sprays can lead to oscillations in the slab temperature near the slab surface. This rapid cooling leads to thermal stresses and these may be enough to form a crack (Tomono, 1977). In addition, thermal cycling below the A_{r3} temperature can increase the rate of AlN precipitation at the austenite boundaries (Suzuki et al, 1982), and hence reduce hot ductility. Uniform cooling patterns which reduce these temperature oscillations have been found to reduce transverse cracking (Suzuki et al, 1984; Coleman and Wilcox, 1985; Mintz et al, 1987). The latter workers have also found that small cyclic oscillations in temperature reduce the amount of NbCN

precipitation and improve ductility.

Mould oscillation frequency can also effect transverse cracking by reducing the depth of the oscillation marking and the BS Ravenscraig plant has shown that an increase in mould oscillation frequency can lead to a significant reduction in plate rejection levels, presumably by reducing the stress concentration effect of the oscillation marks (Mercer and Mcpherson, 1979).

2.4 High temperature strength and structure

In hot working, extremely large strains are applied to materials at high rates of strain at temperatures above about 0.7 T_m where T_m is the melting point in degrees Kelvin. Strength and ductility under these conditions are markedly dependent on both temperature and rate of straining (Tegart, 1968). The strength and also the ductility of a metal is governed by the balance between work hardening and dynamic softening processes. If the work hardening predominates, strength is high but ductility is low. If softening predominates strength is low but ductility is high. Various attempts have been made to formulate a relation between strength (σ), temperature T and strain rate $\dot{\epsilon}$. The most successful attempt appears to be that of Sellers and Tegart (1966) who proposed that:-

$$\dot{\epsilon} = A (\sinh \alpha \sigma)^n \exp (-Q/RT) \dots \dots \dots 2.3$$

Where A , α , n are temperature independent constants and Q is the activation energy.

Equation 2.3 can also be expressed in terms of Z , the Zener-Hollomon parameter where

$$Z = \dot{\epsilon} \exp (Q/RT) \dots \dots \dots 2.4$$

So that 2.3 can be written as

$$Z = (A \sinh \alpha \sigma)^n \dots \dots \dots 2.5$$

This relationship has been successfully applied for a number of alloys including plain carbon steels (Tegart 1968; Crowther and Mintz, 1986) and to micro alloyed steels (Sankar et al, 1979) in the austenitic state. The

value for Q may remain unchanged over a wide range of strain rates, but in some cases different values are obtained for creep and hot working conditions (Jonas, et al, 1968). In the former cases, the constant value of the activation energy, close to that for self diffusion of Fe indicates that the recovery is operative over the whole range, and in the latter cases, the values suggest that the softening process is recovery under creep conditions but may be by dynamic recrystallization during hot working (Tegart, 1968). For steels hot worked in the austenitic state at intermediate strain rates, dynamic recrystallization is the operative softening process, (Jonas et al, 1968; Mintz and Crowther, 1987).

It is generally found that materials which have a high stacking fault energy favour recovery as thermally activated cross slip is easy, whereas materials which have low stacking fault energy encourage build up of dislocations in the matrix favouring dynamic recrystallization. The ferrite phase therefore favours recovery while the austenite phase favours dynamic recrystallization.

2.4.1 Dynamic recovery

This softening process occurs at all strains for ferrite but generally only at small strains for austenite. The micro-structural evidence for dynamic recovery has been reviewed by Jonas et al (1968). This review indicates that the grains of the original micro-structure elongate in the direction of hot working and appear fibrous. This distortion of grain boundaries is accompanied by sub-grain formation until the final structure is reached with narrow and well defined sub-grains. Sub-grain size and mis-orientation, and dislocation density between the sub-boundaries remain constant. A situation is reached in which dislocation generation and annihilation rates are equal, and the strain hardening rate is then reduced to zero, leading to the establishment of a steady flow as shown in Fig. 2.7. For iron, it has been shown that the sub-grains assume their final size at strains of 0.2-0.3 for strain rates of 0.05 to 1.5 s⁻¹, Glover and Sellars (1973). The mean sub-grain size is increased by decreasing strain rate and temperature, and is related to the Zener-Hollomon parameter Z by

$$d_s^{-1} = a + b \log Z \dots \dots \dots 2.6$$

where d_s is the mean sub-grain diameter, a and b are constants and $Z = \dot{\epsilon} \exp(Q/RT)$, (McQueen et al, 1967). A correlation has also been observed by many workers between flow stress and sub grain size. The most general relationship being of the form:-

$$\sigma_f = \sigma_0 + Kd_s^{-m} \dots \dots \dots 2.7$$

Where σ_f is the flow stress and σ_0 , K and m are constants. In general, solid solution alloying additions reduce stacking fault energy and hence make dynamic recovery more difficult, and as a consequence the flow stress is increased. Metals containing stable second phase particles develop substructure more rapidly than an equivalent particle free alloy, and these particles finally stabilize the sub structure. Subgrain diameter can be reduced to the order of the interparticle spacing. If the second phase particle is less stable, particle coarsening and coalescence can occur. This process is greatly accelerated by hot deformation as sub-boundaries act as paths for diffusion at higher rates than the lattice. This process can lead to a decrease in the flow stress during hot deformation. Generally ductility is very good when a high percentage of ferrite is present in the micro structure at the low temperature side of the trough in the region of 700°C, (Ouchi and Matsumoto, 1982; Crowther and Mintz, 1986; Maki et al 1985). At this temperature, recovery in the ferrite will be complete, sub-grain size will be large and the flow stress will be low.

In the trough, failure is intergranular and cracks are often nucleated by grain boundary sliding. In creep tests, it has been observed that with increasing stress, crack nucleation sites change from grain boundary edges and particles to triple points. Materials in which dynamic recovery occurs readily, like ferrite, have low

flow stresses and flow readily at triple points to relieve stress concentrations and thus diminish the initiation of "w" type cracks. In addition these materials may form "scalloped" grain boundaries, which diminishes grain boundary sliding and hence reduces intergranular crack nucleation (McQueen et al, 1975). For metals which are susceptible to dynamic recovery ductility increases with increasing temperature because the stress relieving processes are more sensitive to temperature than those promoting crack nucleation (Gittins, 1977). However, this is not the case for lower stacking fault materials like austenite, and this is always the main phase present in the trough. Strains in the trough can also be insufficient to allow dynamic recrystallization and the only recovery mechanism available is then dynamic recovery. For low stacking fault energy materials like austenite, dynamic recovery is low and ductility may decrease with increasing temperature in the lower part of the high temperature range, because of ^{an} increase in the amount of grain boundary sliding (White and Rossard, 1968).

In general, solid solution alloying and precipitation tend to reduce ductility. This is partly because the smaller subgrains often formed in these materials are not as effective in producing scalloped grain boundaries, so that grain boundary sliding is not impeded to the same extent. The scalloping is also reduced by the retarding effect solute and precipitation

exert on grain boundary migration. In addition the decreased ease of dynamic recovery associated with alloying and precipitation raises the flow stress considerably, which is instrumental in nucleating and opening up cracks.

Increasing the strain rate by increasing the dislocation density and hence flow stress might be expected to reduce the hot ductility of ferrite (White and Rossard, 1966). However, for austenite, grain boundary sliding is dominant at these low strain rates and ductility is reduced as the strain rate is decreased. Similarly, refining the austenite grain size by increasing the flow stress might be expected to have a small detrimental influence on hot ductility but again at these low strain rates the reverse is true and creep considerations dominate rather than recovery mechanisms.

The poor ductility performance of recovered austenite compared to recovered ferrite seems therefore primarily related to the increased ability for crack nucleation in the former. It should also be noted, that in HSLA steels the austenite grain size is always much coarser than the ferrite grain size, and this will again favour the process of grain boundary sliding.

2.4.2 Dynamic recrystallization

The occurrence of dynamic recrystallization was first observed and studied systematically during the creep of Lead (Greenwood and Worner, 1939; Andrade, 1948; Gifkins, 1958). Surveys of work carried out on metals under creep conditions of constant stress or load (Hardwick et al, 1961) and under constant strain rate deformation conditions Jonas et al, (1968) have shown that dynamic recrystallization of initially annealed metals occurs in nickel, copper, gold, γ iron and austenitic steels and high purity α iron, but does not appear to occur in aluminium, zinc, magnesium, tin, low purity α iron or ferritic steels.

In hot working, metals which have a low stacking fault energy give limited dynamic recovery and often show a minimum in ductility in the temperature range close to the hot working range. This minimum in ductility is associated with intergranular failure, This occurs because the limited dynamic recovery gives rise to high flow stresses and work hardening rates preventing the accommodation by lattice deformation of the stress build up at the triple point or grain boundary particles, and intergranular failure by grain boundary sliding occurs.

Ductility does eventually improve as the temperature is raised and frequently this improvement is associated with dynamic recrystallization. Nucleation of dynamic recrystallization occurs at existing boundaries at low

strain rate (Crowther and Mintz, 1986; Roberts et al, 1979). The poorly developed sub-boundaries pin sections of the original boundaries, which bulge out and migrate due to the strain energy difference across the boundary. The introduction of new grains isolates the cracks already formed from the grain boundary, thus inhibiting crack propagation, further crack growth occurs by the capture of a moving grain boundary for a sufficient time for vacancy diffusion and the applied tensile stress to lengthen the crack before the boundary breaks away again. New cracks may also form in the boundaries of the recrystallised grains. Thus under these conditions the grain boundary migration rate may control crack propagation and this may account for the observation that often temperatures have to be higher than those associated with the onset of dynamic recrystallization in order to obtain full recovery of ductility (Wilcox and Honeycombe, 1984; Bernard et al, 1978; Crowther et al, 1987).

It should be noted that it is not always easy to detect the occurrence of dynamic recrystallization from the load/elongation curves. Curves which show dynamic recrystallization are characterised by either an abrupt drop in flow stress or by oscillations of the stress. Unfortunately it is not always possible to determine unambiguously whether dynamic recrystallization has occurred from the curves, particularly at the lower $\dot{\gamma}$ temperature range. Cardoso, (1989) has recently shown from metallographic examinations of tensile samples

quenched immediately after failure, that for coarse grained steels dynamic recrystallization occurs at a temperature 50°C below that detected from the flow stress-curves.

2.4.3 Influence of structure on dynamic recrystallization

During deformation, work hardening and recovery lead to the development of the dislocation and sub-grain structure, but typically dislocations in the sub-grain boundaries remain tangled rather than forming the clean two dimensional network observed in metal in which recovery is more rapid (Jonas et al, 1968). The existence of these higher energy tangled sub-grain boundaries has been shown by Sandström and Lagneborg (1975), to be essential to obtain sufficient stored energy difference to nucleate dynamic recrystallization which occurs at a critical strain, ϵ_c , which is less than the strain at peak stress, ϵ_p as measured from the flow curve.

The relationship between the ϵ_p and ϵ_c is given by Rossard and Le Bon (1975) as:

$$\epsilon_c = a \epsilon_p \dots\dots\dots 2.8$$

Where a = a constant in the range .0.83 -0.67. ϵ_c increases as the initial grain size, d_0 increases (Roberts et al, 1979; Sellars, 1980; Ruibal et al, 1984), and as Z increases (McQueen and Jonas, 1975; Sellars, 1980). Sellars has shown that for steels, a relationship of the form :-

$$\epsilon_p = B d_0^{\frac{1}{2}} Z^P \dots\dots\dots 2.9$$

Where B and p are constants and P is in the range 0.125 to 0.175. At very low stresses, ϵ_c may decrease with increasing Z. (Luton and Sellars, 1969). It is thought that at very low stresses the low dislocation density

requires large strains to provide the necessary stored energy for dynamic recrystallization.

Solid solution alloying reduces the rate of dynamic recovery and hence might be expected to promote dynamic recrystallization. However the rate of grain boundary migration is also reduced by alloying additions and this reduces the rate of dynamic recrystallization. The elements Nb and to a lesser extent V are particularly effective in retarding dynamic recrystallization. Le Bon and Rossard, (1975); Sekine and Maruyama, (1976); Ouchi and Okita, (1982) have found that increasing the Nb addition increases ϵ_p . Weiss and Jonas, (1979) have shown that this effect is due to solute drag on grain boundaries at high strain rates and to the dynamic precipitation of fine NbCN at slower strain rates, which reduce grain boundary migration rates. The nucleation of dynamic recrystallization can be delayed until the dynamic precipitation of NbCN is complete, leading to the characteristic reverse knee of the "P T T" diagram for Nb containing steels. Compared to Niobium steels there are few hot ductility studies on Vanadium and Titanium treated HSLA steels. Irvine et al, (1967) found little or no influence of an addition of 0.15% V or 0.03% Ti on ϵ_p , although these additions retarded grain growth after recrystallization. Cordea and Hook, (1970) observed some retardation of recrystallization in a 0.059% V steel at a temperature below 925°C but the effect was less than that obtained from an 0.011% Nb addition.

Strain rate is also important in influencing ϵ_p . Nucleation of dynamic recrystallization occurs at sub-grain boundaries, and once the nucleus has formed the driving force for growth of the nucleus is the difference in stored energy across the boundary.

At high strain rates, as the nucleus grows, deformation continues and the stored energy is built up in the initially strain free nucleus, reducing the strain energy difference across the boundary. At lower strain rates, the difference in energy across the boundary is greater due to the slower rate of build up of stored energy in the newly recrystallized material and hence recrystallization occurs at lower values of stored energy giving a lower value of ϵ_c .

2.5 FRACTURE MODES RELATED TO THE DUCTILITY TROUGH

The hot ductility curve as shown in Fig. 2.3 can be divided into three regions:-

- 1- The right hand side, the high ductility high temperature region (H D H T)
- 2- The embrittlement region (inter granular fracture)
- 3- The left hand side, the high ductility low temperature region (H D L T)

2.5.1 The right- hand side of the trough (H D H T)

On the right hand side of the trough, the high ductility high temperature region (H D H T) is encountered, and this is usually associated with dynamic recrystallization which leads to an increase in the driving force for grain boundary migration, so that cracks which have initiated are isolated from the prior γ grain boundaries. The high ductility results because growth and coalescence of the cracks is not readily achieved away from the grain boundary. Also the structure is fully austenitic so that there ^{are} ~~is~~ no detrimental ferrite films to cause embrittlement. Furthermore the high temperature encourages less precipitation in the matrix and in the grain boundary.

This mode of fracture is characterised by the appearance of large voids which appear on the fracture surface and these apparently, are not associated with the second phase particles, (Crowther and Mintz, 1986a; Wray, 1981).

These voids are believed to be intergranular cracks which form at an early stage of deformation and become isolated within the grains as a result of grain boundary migration.

2.5.2 Region of embrittlement (inter granular fracture)

This region is characterised by intergranular fracture. Two mechanisms can be responsible:-

1- Grain boundary sliding, which is observed in the single austenite phase and gives rise to smooth fracture facets.

2-Intergranular fracture micro void coalescence due to voiding at the second phase particles at the γ grain boundaries.

The fracture surface can contain both of these mechanisms. Intergranular failure is observed during creep, and as intergranular failure along the γ grain boundaries at low strain rates and strain is also the manner in which the transverse cracks are propagated on straightening, the factors which influence the high temperature intergranular crack nucleation and growth process can be found from a study of the creep literature. Traditionally, intergranular creep defects have been classified as either 'grain edge' or 'r type' (r for rounded) or as 'grain corner' or 'W type' (W for wedge type) (W for wedge cavities) (Evans, 1984). Both types of cavity require grain boundary sliding to nucleate the cavity. The models proposed for the nucleation of 'W type' cracks are illustrated in Fig. 2.8. Calculations have been made to estimate the critical stress required to nucleate a wedge crack. The simpler models assume no matrix relaxation, while more complex models consider the role of thermal activation in

reducing the values of the local concentrated stress. Stroh, (1955) using no matrix relaxation, estimated the critical shear stress for wedge crack nucleation, T_c as:-

$$T_c = \left| \frac{K_s \mu \gamma_f}{(1 - V)d_g} \right|^{\frac{1}{2}} \dots\dots\dots 2.10$$

where V is poisson's ratio, γ_f is the fracture energy, K_s is a constant, d_g is the grain diameter and μ is the shear modulus. Other more sophisticated treatments have shown that wedge crack nucleation requires sliding rates greater than 10^{-9} ms^{-1} (Evans, 1984). Generally, steady state sliding rates are less than 10^{-10} ms^{-1} and this would indicate that nucleation only occurs under high, transient rates of sliding. 'r' type cavity formation also requires grain boundary sliding for cavity nucleation, and one possible mechanism for their formation was proposed by Gifkins, (1956) and is illustrated in Fig. 2.9. In this mechanism, ledges produced by the impingement of slip bands with the grain boundary could lead to the formation of cavities as grain boundary sliding proceeds.

Another possible source of stress concentrations^{ions} at grain boundaries are grain boundary particles. If the stress concentration at such particles is produced by grain boundary sliding alone, the slip distance corresponds to the inter particle spacing. Large applied stresses are

required for particle fracture or particle matrix decohesion. However for the case of intergranular slip impingement against a grain boundary, much smaller applied stresses are required for particle fracture as pile up distances are much greater. In alloys which develop particle free zones (PFZ) adjacent to the grain boundary, particle fracture is much more likely as a large fraction of the specimen strain is concentrated in the PFZ.

It should be noted that the critical stresses required for the nucleation of 'r' type cavities are much lower than those required for 'w' type cavity nucleation, and so 'r' type cavity formation is favoured by low stress, high temperature creep tests, or low strain rate hot workability tests.

Many mechanisms have been proposed to describe the growth of 'r' type cavities, and they can be classified as either cavity growth by deformation mechanism or cavity growth by vacancy diffusion mechanisms. The subject is complex and is dealt with in detail by Evans, (1984). Again particles would be expected to encourage void formation. Creep rupture normally occurs at a strain rate lower than 10^{-4} s^{-1} but the strain rate generally used in the hot tensile test 10^{-3} s^{-1} , has been shown adequate to produce both wedge shaped cracks and 'r' type cavities. Ouchi and Matsumoto, (1982) have observed grain boundary sliding at a strain rate as high

as 10^{-1} s^{-1} in an 0.054 % Nb containing steel strained at 900°C.

2.5.3 Mechanism's of crack formation for steels which have been solution treated

(A) Steels in which no micro-alloying precipitation occurs Plain C-Mn steels having low N and Al levels (0.02-0.04% Al 0.005% N)

a- Micro-Void coalescence fractures.

For steels with C levels $< 0.3\%$, fracture examination of samples which have failed intergranularly reveals that the coarse grain surfaces ($\sim 300 \mu\text{m}$) are covered with cavities (Crowther and Mintz, 1986). Intergranular failure occurs when the temperature is low enough to allow thin films (5 to $20 \mu\text{m}$) of ferrite to form around the γ grain Fig. 2.10. As ferrite is the softer of the two phases, strain concentration occurs round the grain boundary regions and ductile voiding occurs generally at MnS inclusions situated at the austenite grain boundaries. Further reduction in the test temperature rapidly thickens up the ferrite film and ductility fully recovers when in the region of 50% ferrite is present prior to the start of the test. Part of the reason for this improvement in ductility is due to the increased volume fraction of ferrite reducing the strain concentration at the boundaries but probably at least as important is that the relative strength difference between the ferrite and austenite phases becomes less as the temperature is lowered (Wray, 1981) as in Fig. 2.11. The wedge cracks often observed are probably formed by shear displacement of the γ grains along these softer ferrite bands rather than by conventional grain boundary

sliding (Mintz et al 1991).

2.5.4 High carbon steel and C-Mn-Al steels with high Al and N levels.

Intergranular failure in the γ by grain boundary sliding

For these steels, intergranular failure at the high temperature side of the trough is by grain boundary sliding (gbs) in the γ and fracture samples show flat facets with no evidence for micro-void coalescence or ferrite formation (Crowther and Mintz, 1980; Cardoso and Yue, 1989). In the case of the high Al, N steels it is likely that AlN precipitates are formed at the γ boundaries and these pin the boundaries encouraging grain boundary sliding. Reducing the temperature below the Ae_3 will again introduce ferrite giving rise to micro-void coalescence fractures.

Minimum R of A values are very similar, independent of whether the mode of failure is by gbs in the γ or micro void coalescence in the deformation induced ferrite. Hence the change from one type of mechanism to another is not in general accompanied by any discontinuity in the hot ductility curve (Mintz et al, 1991).

2.5.5 Steels in which micro alloying precipitation occurs at the γ boundaries and precipitate free zones (PFZ) are present.

With Nb containing steels, solution treated and cooled to the test temperature, fine matrix precipitation as well as precipitation at γ grain boundaries is present

and frequently PFZ's are observed on either side of the boundaries (500 nm wider) (Mintz et al, 1986). This precipitation is believed to occur during deformation. This situation is then very similar to the thin soft films of deformation induced ferrite surrounding the γ grains and micro-void coalescence fractures are frequently observed (Mintz et al, 1986). In this case the void formation is at the micro-alloying precipitates (NbCN and AlN when Nb and Al are present together). A schematic representation of this fracture process is shown in Fig. 2.12 after Maehara et al, (1984). In these steels, wedge type cracks have been observed, (Crowther and Mintz, 1986). The fine precipitation pins the boundaries allowing cracks formed by gbs to join up. Also intergranular fracture at the high temperature side of the trough shows mixed fracture containing flat facets indicative of gbs as well as the inter-granular micro-void coalescent type of fracture (Crowther and Mintz, 1986). Lowering the temperature increases the amount of intergranular micro-void coalescence until fractures are entirely of this type, and this corresponds to when deformation induced ferrite forms.

2-5-6 The left hand side high ductility low temperature region (H.D.L)

This region starts when the volume fraction of ferrite surrounding the γ , increases giving rise to thicker ferrite films now more uniformly distributed. The strength differential between austenite and ferrite also decreases as the temperature is lowered so that the strain concentration is reduced. Ferrite has a higher stacking fault energy than the austenite and cross slips more readily. Ferrite also has 48 slip planes compared to 12 in γ and therefore dynamic recovery is easier. More deformation can be accommodated by the ferrite so that grain boundary sliding is minimised and high ductility is observed.

2.6 FACTORS INFLUENCING HOT DUCTILITY

There is no more difficult term to define than ductility. Ductility implies the opposite of brittleness i.e. a soft matrix which is readily extended and is easy to fabricate.

Basically, ductility is the ability of material to deform plastically without fracturing (Dieter, 1968). It is recognized that the ductility of a given metal is not a unique property, but rather varies with temperature, strain rate, grain size, precipitation, composition and inclusion content all of which are known to have an important influence on hot ductility.

In this section these variables and their relation to the problem of transverse cracking are reviewed.

2.6.1 Effect of strain rate

At high strain rates, increasing strain rate can lead to reduced ductility, when insufficient time is available for recovery or dynamic recrystallization and fracture is inclusion controlled (Gittins et al, 1981). However, at the lower strain rates relating to the straightening operation, increasing the strain rate improves hot ductility. Figs. 2.13 and 2.14. show the effect of strain rate in the range 10^{-1} to 10^{-4} s^{-1} on hot ductility in the temperature range 700-1000°C (Mintz and Arrowsmith, 1979; Ouchi and Matusumoto, 1982). This effect of strain rate can be very marked, an increase in strain rate by a factor of 10 often increasing reduction of area values by approximately 20%, and often changing the fracture appearance from inter-granular to ductile. Higher strain rates may improve hot ductility for a variety of reasons:-

- 1- Insufficient time is available for the growth of voids formed at precipitates at the grain boundaries (Mintz et al, 1991).
- 2- The amount of the grain boundary sliding is reduced. In particular ϵ_g/ϵ_T decreases with increase in strain rate where ϵ_g = the strain due to the grain boundary sliding and ϵ_T = the total strain to fracture (Ouchi and Matsumoto, 1982)
- 3- The rate of migration of boundaries is increased (Lucke and Stuwe, 1963). Increasing strain rate will produce an increase in the grain boundary migration

velocity V , through the equation of Lucke and Stuwe
,(1963).

$$V = M (C, T) P (C, \dot{\epsilon}, T) \dots \dots \dots 2.11$$

Where M is the grain boundary mobility and includes a term describing the influence of composition C and temperature T , and P is the driving force for grain boundary migration. Although increasing strain rate generally improved hot ductility Maehara and Ohmori, (1984); Yasumoto and Maehara, (1985) have found that decreasing the strain rate from 10^{-1} to 10^{-2}s^{-1} improves hot ductility when unstable fine precipitates are present e.g. Fe Mn sulphides. In this case, lowering the strain rate allows the inclusions to coarsen so that they are no longer able to pin the γ grain boundaries. Even niobium containing steels at the 1.4% Mn level can show improved hot ductility at very low strain rates 10^{-4} to 10^{-6}s^{-1} due to the coarsening of the NbCN (Sakai and Ohashi, 1988).

2.6.2 Influence of grain size on hot ductility

The majority of investigations into the influence of grain size on hot ductility have shown that ductility increases with decreasing grain size for a wide range of metals and alloys including copper (Fleck et al, 1970), alpha brass (Taplin and Whittaker, 1963), austenite in steels (Bywater and Gladman, (1976) and plain carbon steel (Crowther and Mintz, 1986). The beneficial effect on ductility of refining grain size in a creep test is believed to be due to either and/or

- 1- A decrease in the grain boundary sliding rate (Evans, 1969).
- 2- The difficulty in propagating cracks formed on sliding through triple points (Kutumba et al, 1975).
- 3- The crack aspect ratio which controls the stress concentration at the crack tip and will be less in fine grained material, so discouraging crack propagation (Kutumba et al, 1975).
- 4- Reduction in the critical strain for dynamic recrystallization (Sellars, 1979).
- 5- In micro alloyed steel for a given volume fraction of precipitates fine grains will give rise to a reduced grain boundary surface area coverage by precipitation (Fu et al, 1988; Ouchi and Matsumoto ,1982).

Indeed, many hot tensile studies have shown that a coarse

grain size is associated with lower ductility, (Suzuki et al, 1984; Bernard et al, 1978; Offerman et al, 1981). Several other studies have found fine grains to be worse (Weinberg, 1979; Funnell and Davies, 1978; Wray, 1984) and some even concluded that the grain size is not important in influencing hot ductility (Ouchi and Matsumoto, 1984; Carlsson, 1964).

Indeed part of the reason for this contradictory information on the influence of grain size on hot ductility is due to the difficulty in isolating the influence of grain size from that of precipitation. Recent work has tended to examine the influence of grain size on hot ductility for conditions in which no precipitation is present (Crowther and Mintz, 1986). These studies have shown that refining grain size leads to both a reduction in depth and width of the trough as shown in Fig. 2.15. The benefits to ductility from grain refinement, were in part accredited to the form and distribution of the ferrite.

Fu et al, (1988); Crowther and Mintz, (1986) have suggested that for coarse grained material the fall in hot ductility on the high temperature side of the trough corresponds to the temperature at which deformation induced ferrite first forms and it is believed that deformation can raise this to the A_{e3} temperature. In fine grained steels the undeformed A_{r3} temperature is raised closer to the A_{e3} and deformation appears to have

little influence on ferrite formation so that the temperature corresponding to the fall in ductility is related to the A_{r3} (undeformed), and the normal transformation induced ferrite has to encircle the γ to reduce ductility. However recent work by Cardoso (1989), has shown that the thin films of deformation induced ferrite which give rise to the poor ductility are formed just below the A_{e3} even in fine grained steels, and furthermore that the fine grain size increases the volume fraction of deformation induced ferrite produced. The narrow trough in a fine grained steel is then a consequence of the rapid increase in the volume fraction of strain induced ferrite which occurs on lowering the temperature below A_{e3} . Rizio et al, (1988) give a more simple explanation, the maximum strain concentration and ability to link up cracks occurs when a thin continuous ribbon of the softer ferrite phase forms round the γ boundaries. Fine grained material requires a lower temperature for this to occur. The influence of grain size on the minimum depth of the hot ductility trough is illustrated in Fig. 2.16. Included in the figure are the results of Maehara et al, (1985) for C-Mn-Nb-Al steels, in which the grain size had been varied with probably little change in precipitate distribution.

Generally micro alloyed steels show little indication from the hot tensile test that grain size has a significant influence on hot ductility. Ouchi and Matusumoto, (1982) showed that hot ductility of both C-

Mn-Al and C-Mn-Nb-Al steels was independent of austenite grain size in the range 100-300 μm when tested at 900°C. However Mintz et al, (1991) have found that when the precipitation distribution is constant, the changes in hot ductility with grain size are similar to those observed in plain C-Mn steels, Fig. 2.16. Certainly grain size appears to be an important factor in the transverse cracking phenomenon. Schmidt and Josefsson, (1974) have observed that transverse cracks are associated with coarse austenite grains 1 to 3 mm, and this cracking is reduced when these structures are eliminated by the use of a suitable secondary cooling pattern.

2.6.3 Influence of composition on hot ductility

The composition of the steel plays an important role in determining hot ductility.

Work carried out by Suzuki et al, (1981) and (1982) ; Robbins et al (1967) on high purity iron, has revealed no intergranular fracture in the austenite phase. In contrast plain carbon and micro-alloyed steels show embrittlement in this phase (Crowther and Mintz, 1986 a,b). These observations suggest that intergranular fracture is not possible without the presence of some precipitation or second phase particles. Thomas et al, (1986) has drawn attention to the importance of even minor amounts of residual elements on the hot ductility of steels. For micro alloyed steels tested in the temperature range 700-1000°C at a strain rate of 10^{-4} to 10^{-3} s^{-1} intergranular failure may be due to three causes:-

- 1- Nitride and/or carbide forming elements
(precipitates).
- 2- Oxide and/or sulphide forming elements (inclusions).
- 3- Elements with a tendency to segregate to boundaries and weaken them.

2.6.4 Precipitation in steels

The introduction and widespread, use of micro-alloyed steel has greatly influenced steel making production. It has been amply demonstrated that very minor additions of metals such as niobium, vanadium, aluminium and titanium together with a revolutionary vigorous approach to processing, results in steel much stronger and tougher than the plain carbon steels they have replaced.

The main alloying additions niobium, vanadium, and titanium all form stable carbides and nitrides which precipitate in the f.c.c structure. Aluminium is invariably present in these steels and can form a nitride with a hcp structure. Solubility products have been determined for relevant carbides and nitrides in austenite as a function of temperature (Noberg et al, 1968 Narita, 1975) as shown in Fig. 2.17. It is clear that carbides all have a substantially higher solubility than ~~the~~ nitrides, and there are wide variations between the various carbides and nitrides. The solubility of precipitates is also an important factor in determining the rate of coarsening, which in turn influences the effectiveness of particle pinning of the grain boundaries and dislocation arrays. Thus in general terms, the less soluble nitrides should be more resistant to coarsening than the equivalent carbides (Honeycombe, 1987).

2.6.5 The effect of precipitation on the hot ductility

Precipitation has been found to impair hot ductility and a variety of reasons have been given, these being as follows:-

(1) Fine precipitation can pin the γ boundaries allowing time for cracks to join up by grain boundary sliding giving intergranular failure (Mintz and Arrowsmith, 1979; Wilcox and Honeycombe, 1987; Crowther and Mintz, 1986).

(2) The process of recovery and recrystallization is significantly retarded by the addition of small quantities of alloying elements such as Nb, Ti and V (Yasumoto et al, 1982; Luton and Sellars, 1969; Bernard et al, 1978).

(3) Grain refining precipitates encourage void formation under the action of grain boundary sliding either by particle cracking or by particle matrix decohesion (Wilcox and Honeycombe, 1987; Mintz and Wilcox, 1986; Suzuki et al, 1984).

(4) Often as in the case of NbCN there is a matrix precipitation as well as precipitation at the boundaries, and this is accompanied by a precipitate free zone PFZ allowing stress concentration to occur readily along the boundary surrounded by the PFZ (Wilcox and Honeycombe, 1987; Mintz et al, 1986; Maehara et al, 1990).

(5) Matrix precipitation of NbCN observed in Nb micro-alloyed steel concentrates strain onto the grain boundaries and promotes intergranular fracture and low ductility (Bernard et al, 1978; Wilcox and Honeycombe,

1984; Maehara et al, 1990).

Precipitation can be present prior to deformation or can be formed during deformation. It is well known that deformation accelerates precipitation (Le Bon et al, 1975; Akben et al, 1981; Weiss and Jonas, 1980; Vodopivec, 1978). It is believed that this acceleration of precipitation is due to the introduction of favourable nucleation sites by the deformation process. Ouchi and Matsumoto, (1982) were of the opinion that these sites are dislocations and sub-boundaries within the matrix.

Precipitation size and distribution are influenced by whether the precipitation is formed statically prior to test or dynamically during deformation. Investigation into the influence of static and dynamic precipitation have led to the conclusion that for V and Al containing steels, precipitates present before deformation are more detrimental to the hot ductility than those formed during test. In contrast, dynamic precipitation has been shown to be most effective in reducing hot ductility for Nb containing steels (Wilcox and Honeycombe, 1987). Precipitation then occurs rapidly in a finer form both at the γ boundaries and within the matrix (Crowther et al, 1987; Weiss and Jonas, 1980).

Generally its best if the precipitation occurs randomly in the structure (Crowther and Mintz, 1986). Precipitation can be coarsened by decreasing the cooling rate from the solution temperature to the test

temperature and this has been shown to improve ductility in Nb containing steels when it allows formation of the coarse statically precipitated NbCN, reducing the amount of dynamically precipitated fine NbCN (Maehara et al, 1984).

2.6.6 Effect of Nb

Niobium which is very popularly used as a micro-alloying addition in high strength low alloy steels is known to be one of the alloying elements which promotes the hot cracking susceptibility of the ingot or slab. The cause of this cracking was originally attributed to the large inclusion type precipitates of NbCN formed in the centre portion of the ingot (Hannerz et al, 1968).

The effect of Nb content on hot ductility has long been a subject of study due to the high incidence of transverse cracking in continuously cast Nb containing steels. Bernard et al, (1978) found that Nb extends and deepens the hot ductility trough. Similar behaviour has been noted by Suzuki et al, (1982) and Maehara and Ohmori, (1984). Mintz and Arrowsmith, (1979) have also reported again that Nb additions deepen and widen the ductility trough as well increasing the tendency for transverse cracks to form. Their work showed that NbCN precipitates at the austenite grain boundaries encouraging intergranular failure by grain boundary sliding. Maehara et al, (1984) explained that the ductility loss was caused by the dynamic precipitation of carbonitrides such as NbC or AlN both within the matrix and or at the γ grain boundaries, and also by strain concentration within the soft layer along the boundary due to the presence of the precipitation free zones. Crowther and Mintz, (1986) reported that precipitation of NbCN on austenite grain boundaries also encourages grain

boundary sliding, and this was positively confirmed by Ouchi and Matsumoto, (1984).

C-Mn-Nb-Al steels are the most difficult to continuously cast. The combined presence of Al and Nb is very detrimental to the hot ductility because it makes the NbCN precipitation finer and more closely spaced and concentrates the strain onto the grain boundaries, Mintz and Arrowsmith, (1979). Bernard et al, (1978) attributed the ductility trough in Nb containing steels to being due to the retardation of dynamic recrystallization, associated with the Nb addition. They proposed that fracture in these steels occurred before the critical strain for the nucleation of dynamic recrystallization was reached, and supported this argument with metallographic evidence of coarse unrecrystallized austenite grains in the low ductility test temperature range 700 to 1000°C. Wilcox and Honeycombe, (1984) have confirmed this explanation of the ductility trough for C-Mn-Nb-Al steels for which a good correlation exists between the onset of dynamic recrystallization and the recovery of ductility. However for C-Mn-Nb steels they showed that precipitation of NbCN, rather than dynamic recrystallization was the dominant factor controlling hot ductility. Mintz and Arrowsmith, (1979) proposed the more general argument that poor ductilities were associated with low grain boundary mobilities due to the precipitation of NbCN. They showed that fine precipitation was more effective in reducing grain

boundary mobility than coarse precipitation. In agreement with Irvine et al, (1967) they found that increasing the cooling rate from the solution temperature reduced hot ductility by refining the size of NbCN precipitates. Mintz et al, (1986) found that in as cast steels, NbCN was present as a coarse eutectic and coarse MnFe sulphides were located at the inter-dendritic boundary. Reheating the as-cast structure redissolved the coarse eutectics as well as many of the sulphides and on cooling to the test temperature these re-precipitated in a fine form at the γ grain boundary reducing the hot ductility.

2.6.7 Influence of Ti on hot ductility

Ti readily forms a nitride and has been shown to be a very beneficial element to add to steels to improve hot ductility. This beneficial effect has been attributed to a reduction in the amount of N available to form NbCN (Ouchi and Matsumoto, 1982) or AlN (Coleman and Wilcox, 1985). Ti combines preferentially with N at high temperatures (close to the solidus) and on cooling after melting precipitates randomly as a TiN stable compound leaving less or no nitrogen available for the subsequent precipitation of the finer more detrimental nitrides of Al or Nb. Part of the benefit of the Titanium addition can also be related to a refinement of the γ grain size. Also Titanium can modify the sulphide inclusions and so, influence hot ductility (Luyckx et al, 1970; Hilty and Farrell, 1974; Bank and Gladman, 1979; Pickering, 1989). Recent work by Mohamed, (1988) indicates that Ti additions may have only a limited benefit to the hot ductility of as cast C-Mn-Nb-Al steels, as grain refinement is then absent. Some benefit from the removal of AlN might however be expected.

Yasumoto et al, (1985) and Turkdogan, (1987) have reported that transverse cracking is reduced when steels have $<0.0045\%N$ and Ti is in the range of 0.015 to 0.02% wt. Turkdogan, (1987) has suggested that Titanium additions to the melt reduce the transverse cracking by effectively coarsening the Nb and V precipitates making them ineffective in influencing the ductility. This

occurs by the TiN particles acting as nucleating sites for Nb and V precipitation at high temperature, so that less NbCN or VCN can precipitate out at lower temperatures in a fine detrimental form at the γ grain boundaries.

2.6.8 Effect of Al

In the steel works, Aluminium is often used for the deoxidation and grain refining of steel. While Aluminium deoxidation confers many benefits in terms of steel cleanliness and improved strength and toughness through the grain refining action of AlN, certain detrimental aspects of alumina inclusions preclude the use of aluminium in certain cases. Desai, (1959) and Biggs, (1959) have found a significant relationship existing between the incidence of ingot panel cracking and the Al content of the steel, the incidence of cracking increasing as the Al content increased. Woodfine and Quarrel, (1960); Wright and Quarrel, (1962) have found poor ductility associated with AlN precipitation at the austenite grain boundaries, Hasebe, (1972) has reported the same result. Portevin, (1962) also found a ductility trough in the region 800-1000°C and this was associated with the precipitation of aluminium nitride. He noted that the maximum drop in ductility occurred at a temperature when the aluminium nitride had almost redissolved and suggested that local aluminium enrichment had taken place which caused ferrite to appear at temperatures well into what would normally be regarded as the temperature range for fully austenitic structures to be present. Other workers have found difficulty in confirming Portevin's view of the role of aluminium in influencing ductility. The general consensus of opinion is that it is the AlN precipitated at the γ boundaries

which influences ductility. Funnell and Davies, (1978) have obtained evidence that suggests that the size of aluminium nitride particles has an important influence on hot ductility. This can be seen from Fig. 2.18 taken from their work, in which they examined two steels containing similar amounts of nitrogen precipitated as AlN, one in a fine form and the other coarse. The finer particle distribution gave the worst hot ductility. Vodopivec, (1973); Bernard et al, (1978); Ouchi and Matsumoto, (1982) have also found that coarse AlN particles have no effect on hot ductility whereas fine precipitation reduces ductility dramatically.

For cooling rates simulating continuous casting, most studies have found no influence of Al on hot ductility for steels of low Al and N levels. In low N steels, the Al levels have to be high ($>0.07\%Al$) in order for AlN to precipitate out. This is because AlN precipitates very sluggishly on solution treating and cooling to the test temperature. Obviously the level of Al and N present in the steel is important, the higher the solubility product, the greater being the driving force for precipitation. Cardoso and Yue, (1990) used high aluminium steels and found in the steel containing 0.005% N increasing the soluble aluminium from 0.026 to, 0.085% favours AlN precipitation at austenite grain boundaries, thus extending the embrittlement to the single phase austenite range.

In contrast, Al (even in relatively small amounts) deepens and widens the trough in Nb containing steels as

can be seen in Fig. 2.19 (Mintz and Arrowsmith, 1979; Wilcox and Honeycombe, 1984; Ouchi and Matsumoto, 1982; Bernard et al, 1978). Precipitation of AlN in addition to NbCN at γ grain boundaries has been given as the explanation. However Mintz and Arrowsmith, (1979) found that the impairment of hot ductility with increase in Al content was not due to precipitation of AlN but to the production of a finer more effective precipitation of NbCN.

2.6.9 Effect of vanadium

Vanadium has been added to steel for about 80 years as a means of increasing the yield strength. Its effect as a secondary hardening element is well known and it can be seen in Fig. 2.20 that it has only a slightly detrimental effect on the hot ductility of steels compared with that exhibited by Nb and Al additions. Crowther et al, (1987) attributed this behaviour to the fact that V(CN) precipitates mainly as a random precipitation within the matrix whereas Nb and Al when it does precipitate, precipitates at the γ grain boundaries. Additions of Al can reduce the detrimental affect of V (Coleman and Wilcox, 1985). They explain this by the prevention of VN precipitation, due to the preferential formation of AlN. Mintz and Arrowsmith, (1980) believe that V acts in a similar way to Nb but has a reduced effect because of the higher solubility of VN in austenite.

refines the grain size which would result in a reduction in the critical strain E_c for dynamic recrystallization. Also, increasing the Mn content encourages precipitation within the matrix rather than more detrimentally at the γ boundaries (Lankford, 1972). Crowther and Mintz, (1986) found that the finer the sulphides are at the boundaries, the more detrimental they are, presumably because the smaller the inter-critical distance between the particles, the easier it is for a crack to link up. Yasumoto, (1985) found that when very fine MnFe sulphides are present prior to heat treatment they are able to grow during low strain rate testing leading to improved hot ductility. Mintz et al, (1986) have shown that reduction of σ_a in the temperature range 750-1000°C, remains constant for hot rolled steels having S levels in the range of 0.001 to 0.022 wt%. They suggest that it is the amount of S taken back into solution and precipitated at the austenite grain boundaries prior to deformation which controls the hot ductility. Turkdogan et al's, (1955) solubility data indicates that the maximum solubility of S at 1330°C for steels with 1.4% Mn, having pure MnS inclusions is very low ~0.001%. Thus it is possible that the amount of the MnS precipitated at the boundaries will be very low and independent of S level, provided the total S level is >0.001%

Adding (Ca, Ce, La) could be beneficial to hot ductility, and this is attributed to the reduced S levels associated with the formation of CaS, or rare earth sulphides (Coleman and Wilcox, 1985). These workers have reported

that Ca or Ce additions can produce crack free continuously cast slab due to the removal of sulphides from the austenite grain boundaries.

2.6.11 Influence of carbon

Carbon is one of the elements which has received much attention in recent years. Mintz and Crowther, (1986a) have investigated the hot ductility behaviour for plain carbon steels in the temperature range 700 to 1000°C. They found that raising the carbon level from 0.04 to 0.28% caused the trough to move bodily to lower temperature in agreement with the observed change in transformation temperature. However Suzuki et al, (1984) have noted that the trough is deepened as well. Failure was shown to be by strain concentration in the softer ferrite phase enveloping the austenite grains, causing void formation at MnS inclusions with gradual crack linkage leading to intergranular failure. However raising the carbon above 0.28% was accompanied by a change in the fracture mode from being transformation controlled to being controlled by grain boundary sliding in the austenite phase. Mohamed, (1988) reported that for C-Mn-Al steels, raising the carbon level from 0.056% to 0.15% C, moves the hot ductility curves to lower temperature in accord with the changes in A_{e3} and A_{r3} temperature Fig. 2.21. Aluminium has been shown not to influence the hot ductility of these steels because AlN is not able to precipitate out and is not observed. It is therefore reasonable to assume that the behaviour for C-Mn-Al steels should be identical to that given by plain C-Mn steels. Mintz and Crowther, (1986a); Hannerz, (1985) showed that increasing C improved hot ductility

for C-Mn-Al steels and Suzuki et al, (1984) found the same result for an Aluminium free steel.

For C-Mn-Al-Nb steels, Mohamed, (1988), found that increasing the C level from a low level 0.04 to 0.1% deepened and widened the trough, but further increase in C content had little effect, Fig. 2.22. There was little influence of C content on the position of the trough, as here the ductility is controlled by precipitation of NbC. Ouchi and Matsumoto, (1982); Maehara et al, (1985) have also found that hot ductility is insensitive to carbon level between 0.05 to 0.3%C in Nb containing steels.

2.6.12 Other elements

P is one of the elements which has the greatest tendency to segregate between growing dendrites during solidification. Fuji et al, (1975); Brimacombe and Sorimachi, (1979) have shown that P can lead to internal cracks in continuously cast slab.

Mintz and Arrowsmith, (1979) have reported a small influence of P improving the hot ductility of C-Mn-Nb steels and this is believed to be due to P segregation to austenite grain boundaries preventing NbCN from precipitating. However, Ouchi and Matsumoto, (1982) have reported that P levels between 0.004 and 0.026% have no influence on the hot ductility of C-Mn-Nb-Al steels.

Cu Additions of copper to steel have been practiced for more than 30 years and provide good weathering properties and resistance to atmospheric corrosion (Le May et al, 1984). However, it is less well recognized that a Cu addition to steel, as well as providing improved corrosion resistance, can make a significant contribution to the mechanical properties of steel. Cu containing HSLA steels have been developed which provide excellent strength and toughness at a relatively low cost.

The detrimental effect of Cu on the hot ductility of steel is exhibited in two forms. First, it can give rise to hot shortness in the bulk of the steel. Secondly it can have a particularly adverse influence on the surface properties after reheating for hot working. Copeland and Howe, (1975) have studied methods of avoiding surface hot

shortness by preventing the precipitation of the Copper-rich phase. Their approach was to add silicon to the steel and encourage the formation of molten fayalite (2FeOSiO_2) at the surface. They reported that addition of Si in the furnace atmosphere will prevent molten copper-rich phases from forming on heating above $1205.^\circ\text{C}$. Q Gittins, (1977) showed that increasing the O content reduces the hot ductility by increasing the volume fraction of oxide inclusions. Chang, (1972) showed that the tensile ductility of a cast Nickel-base superalloy, Rene 80, at temperatures close to 850°C was severely reduced after prior exposure in air at 980°C , but an inert atmosphere exposure did not produce similar embrittlement.

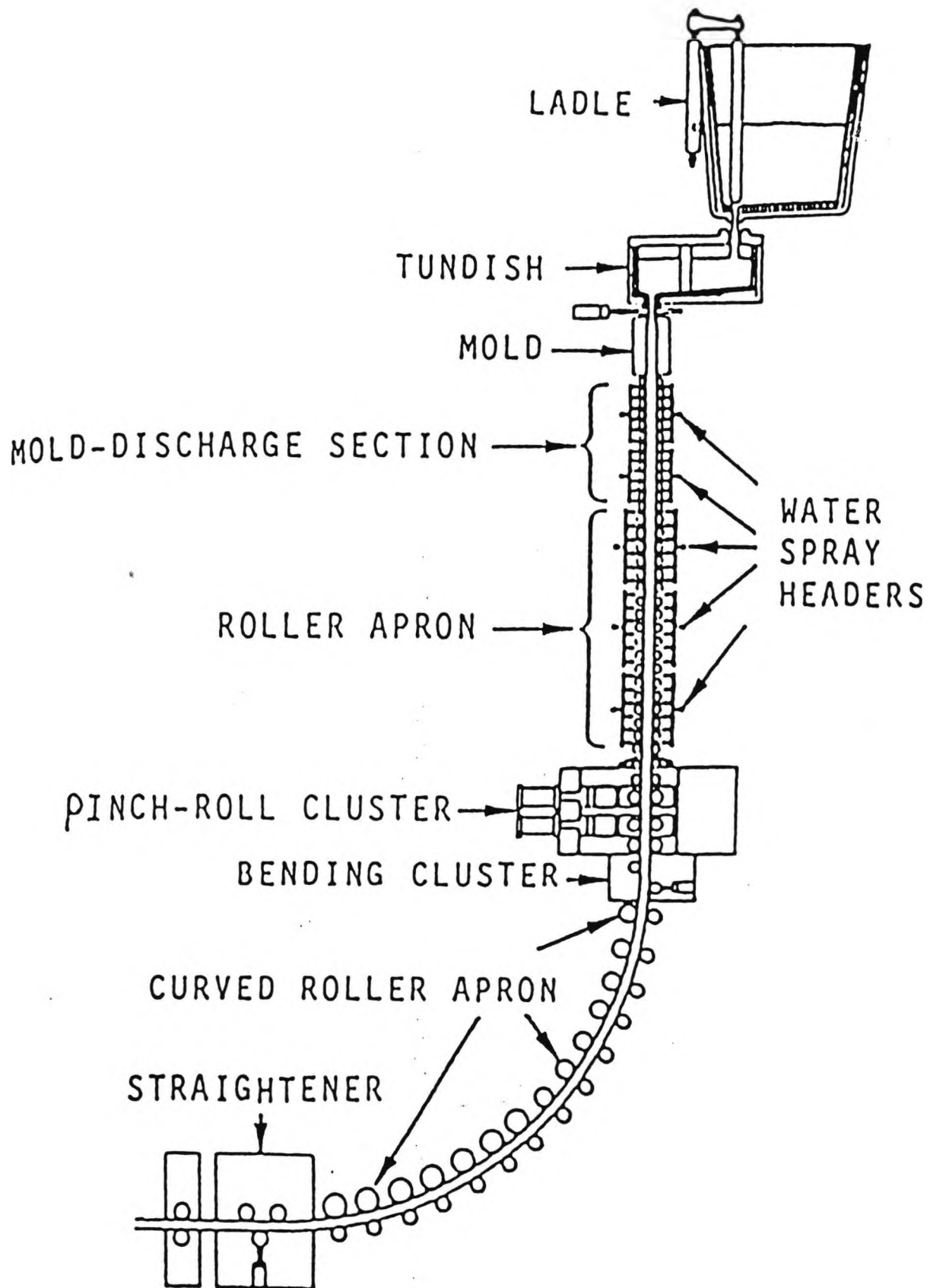


Fig. 2.1 Profile of Gray slab caster
 (After Lankford, 1972).

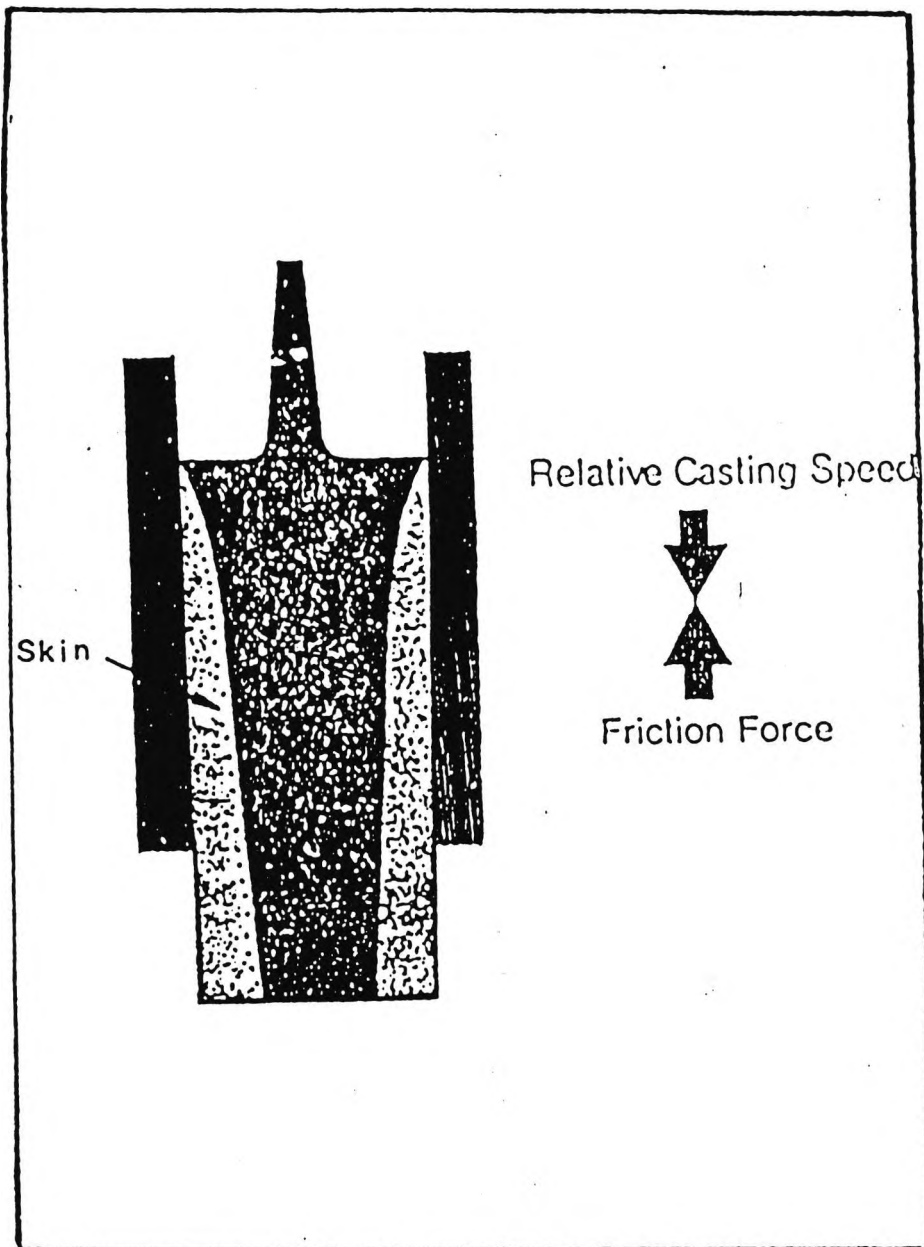


Fig. 2.2 Schematic representation of friction force and tensile force on the skin surface. (After Linkford, 1972).

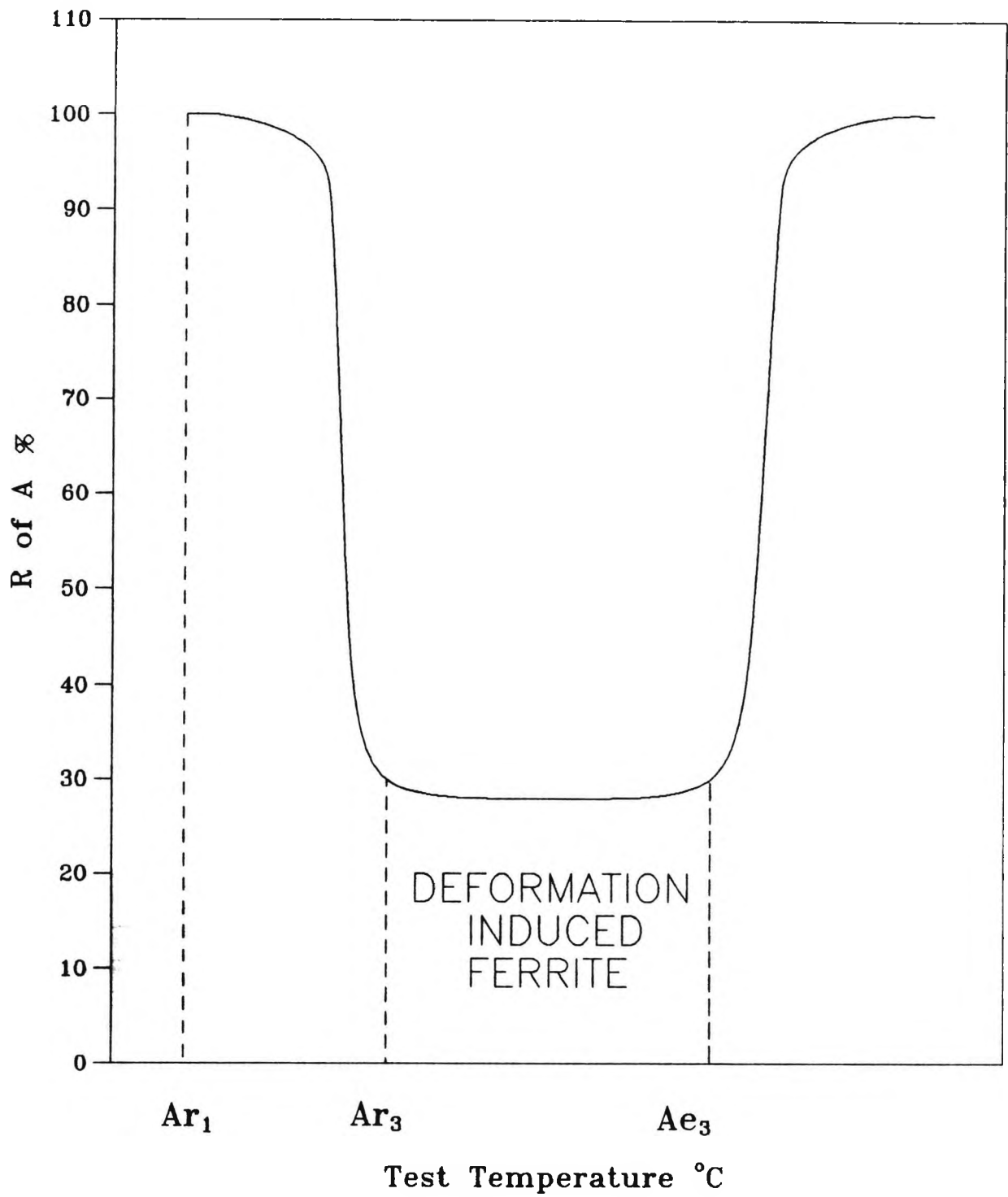


Fig. 2.3 Ductility trough controlled by phase transformation in coarse grained steels (grain size 200 μm). (After Mintz et al 1991).

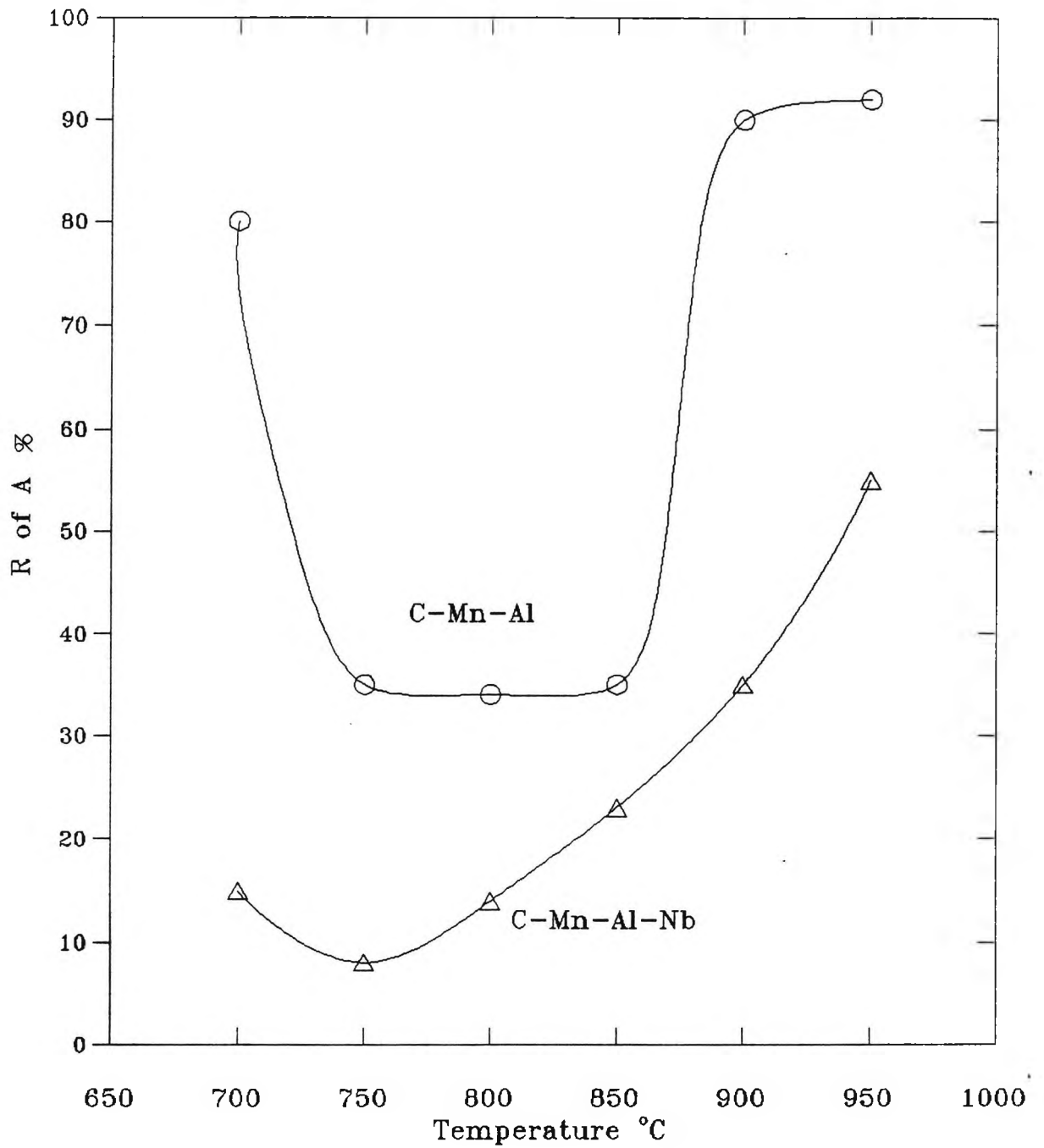


Fig 2-4 Hot ductility for Al and Nb containing steels (After Mintz and Arrowsmith, 1979).

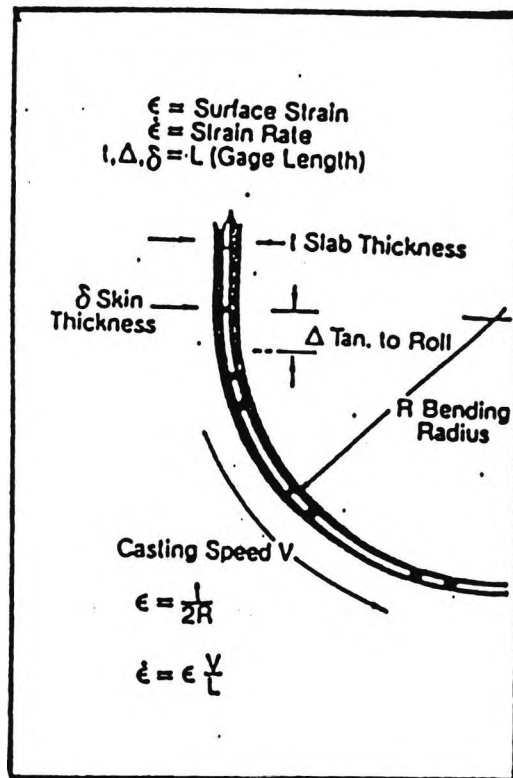


Fig. 2.5 Surface strain and strain rate resulting from bending (After Lankford, 1972).

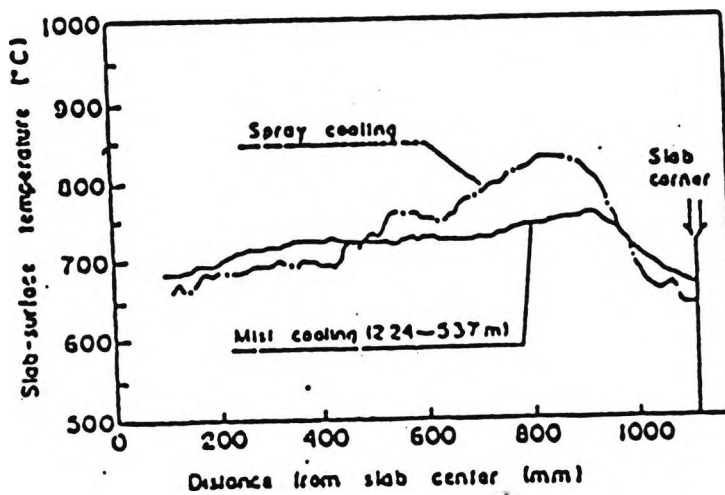


Fig. 2.6 Comparison of temperature distribution between mist cooling and spray cooling. (After Kawasaki et al., 1987).

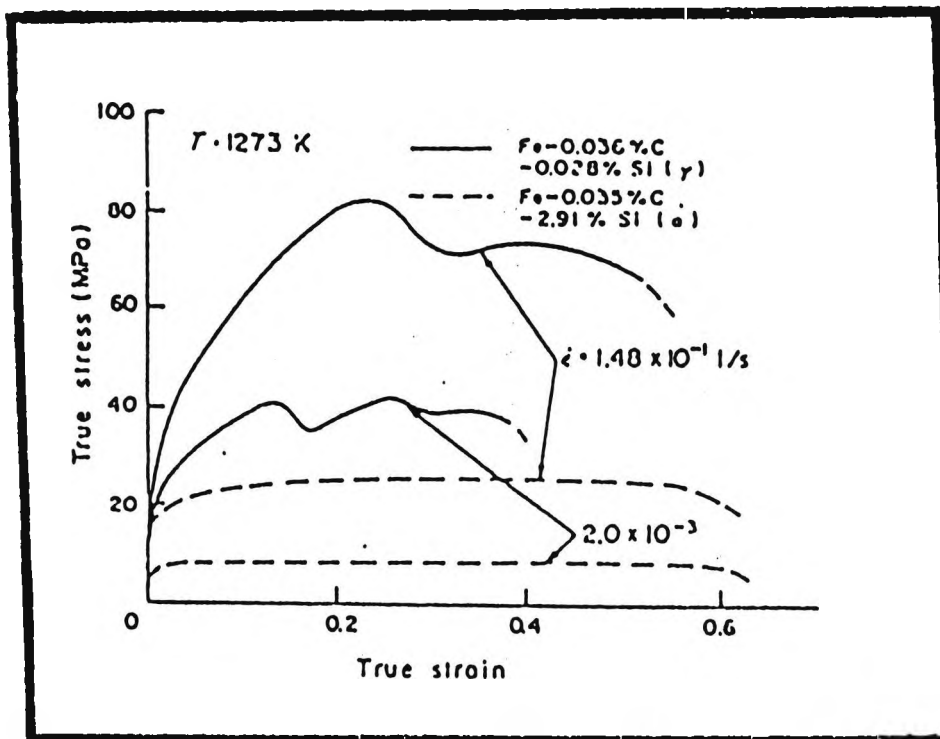


Fig. 2.7 Stress strain curves for a plain carbon and a 2.91% silicon steels tested at 1000°C (After Sakai and Ohashi., 1981).

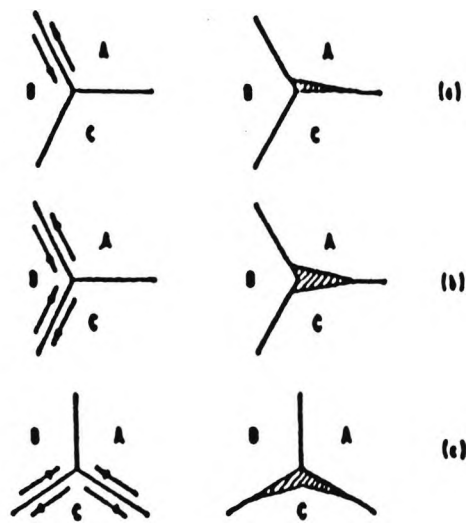


Fig. 2.8 Schematic Models showing the formation of wedge cracks due to grain boundary sliding. The arrows indicate a sliding boundary and the sense of translation. (After Chang and Grant, 1956).

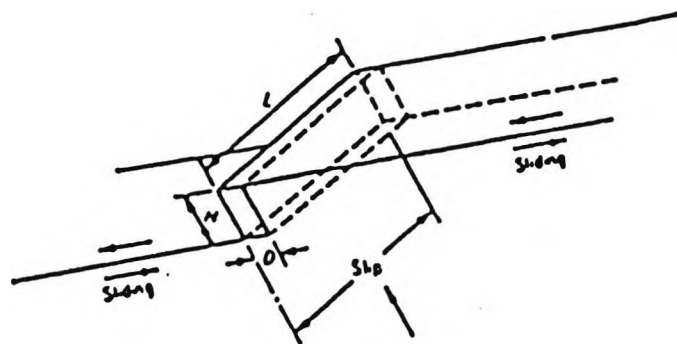


Fig. 2.9 Mechanism for void formation at grain boundary ledge. (After Gifkin, 1959).

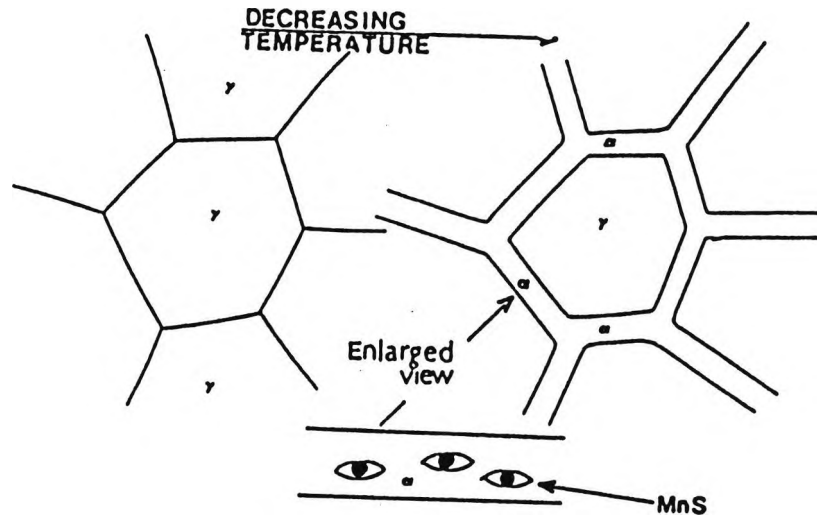


Fig. 2.10 Schematic diagram showing the mechanisms for transformation induced intergranular failure. (After Mintz et al 1991).

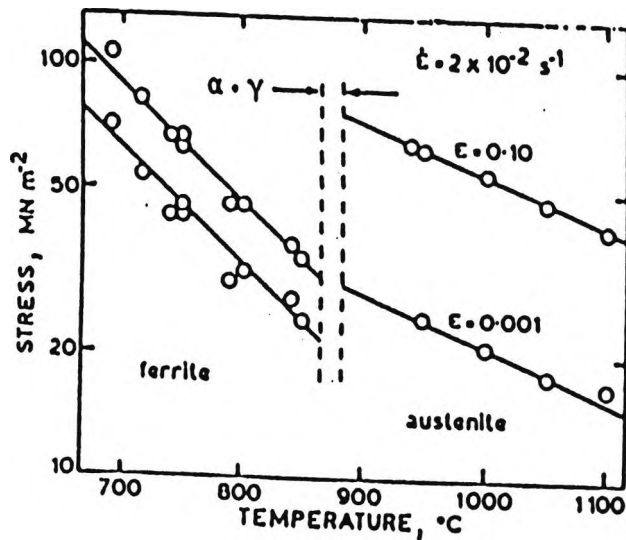


Fig. 2.11 Flow stress at strains of 0.001 and 0.100 for a 0.005% C steel, illustrating difference in strength, temperature dependence, and work hardening rate for α and γ (After Wray., 1981).

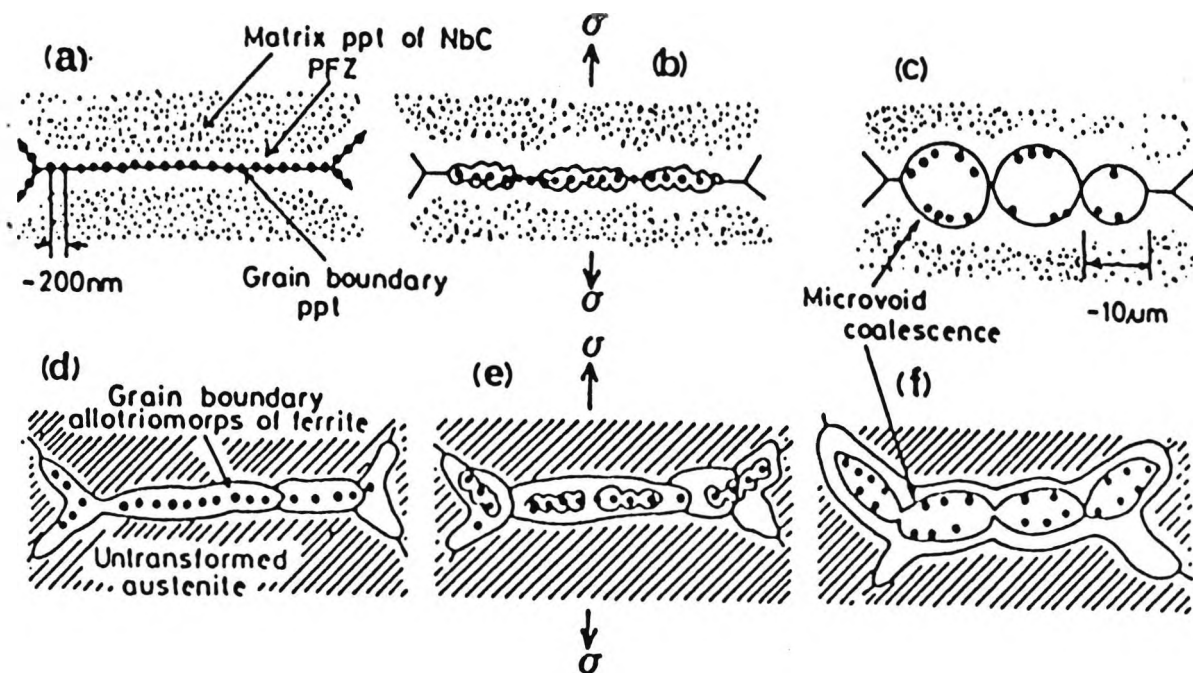


Fig.2.12 Schematic illustrations showing intergranular microvoid coalescence of niobium-bearing steels by deformation in (a)-(c) the low temperature austenite region and (d)-(f) the α - γ duplex phase region. (After Maehara and Ohmori 1984).

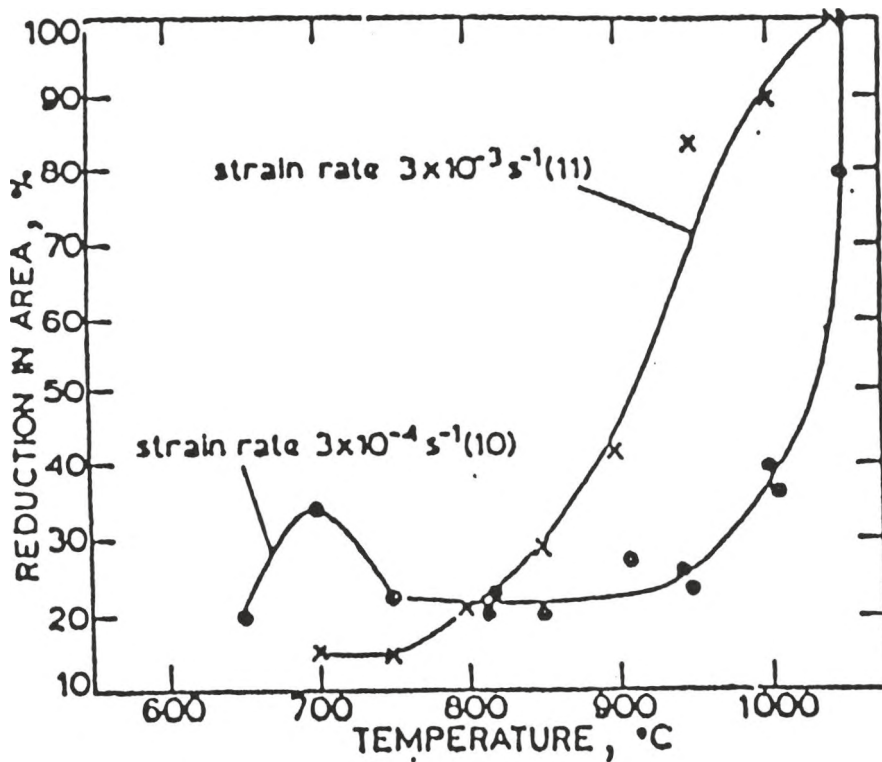


Fig. 2.13 Influence of strain rate on the hot ductility of C-Mn-Al-Nb steel. (After Mintz and Arrowsmith, 1979).

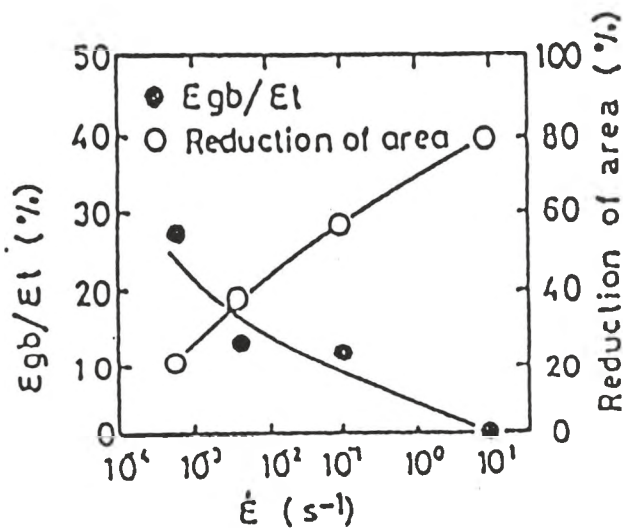


Fig. 2.14 The effect of strain rate on hot ductility and grain boundary sliding in a C-Mn-Nb-Al steel. (After Ouchi and Matsumoto, 1982).

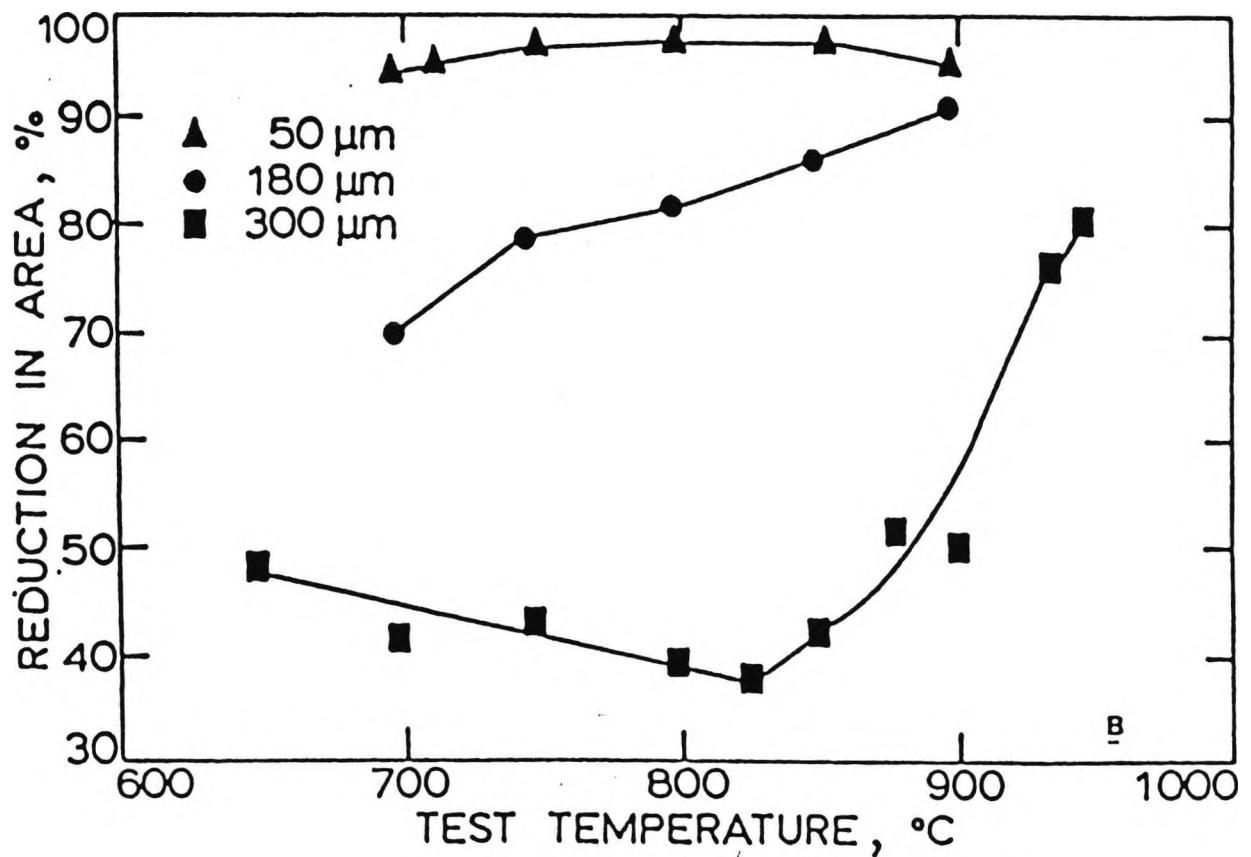
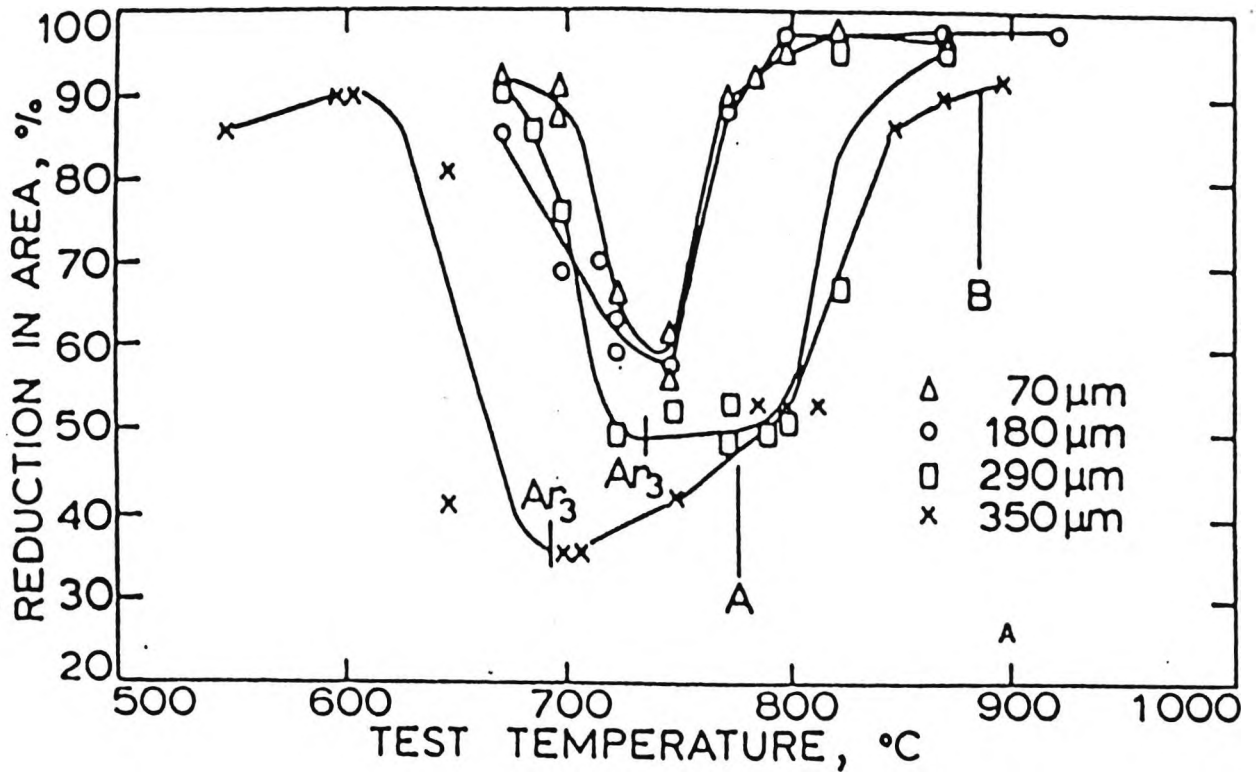


Fig. 2.15 Effect of grain size on the hot ductility of plain C-Mn steels. (A) for 0.19% C and (B) for 0.65% C steel. (After Crowther and Mintz, 1986).

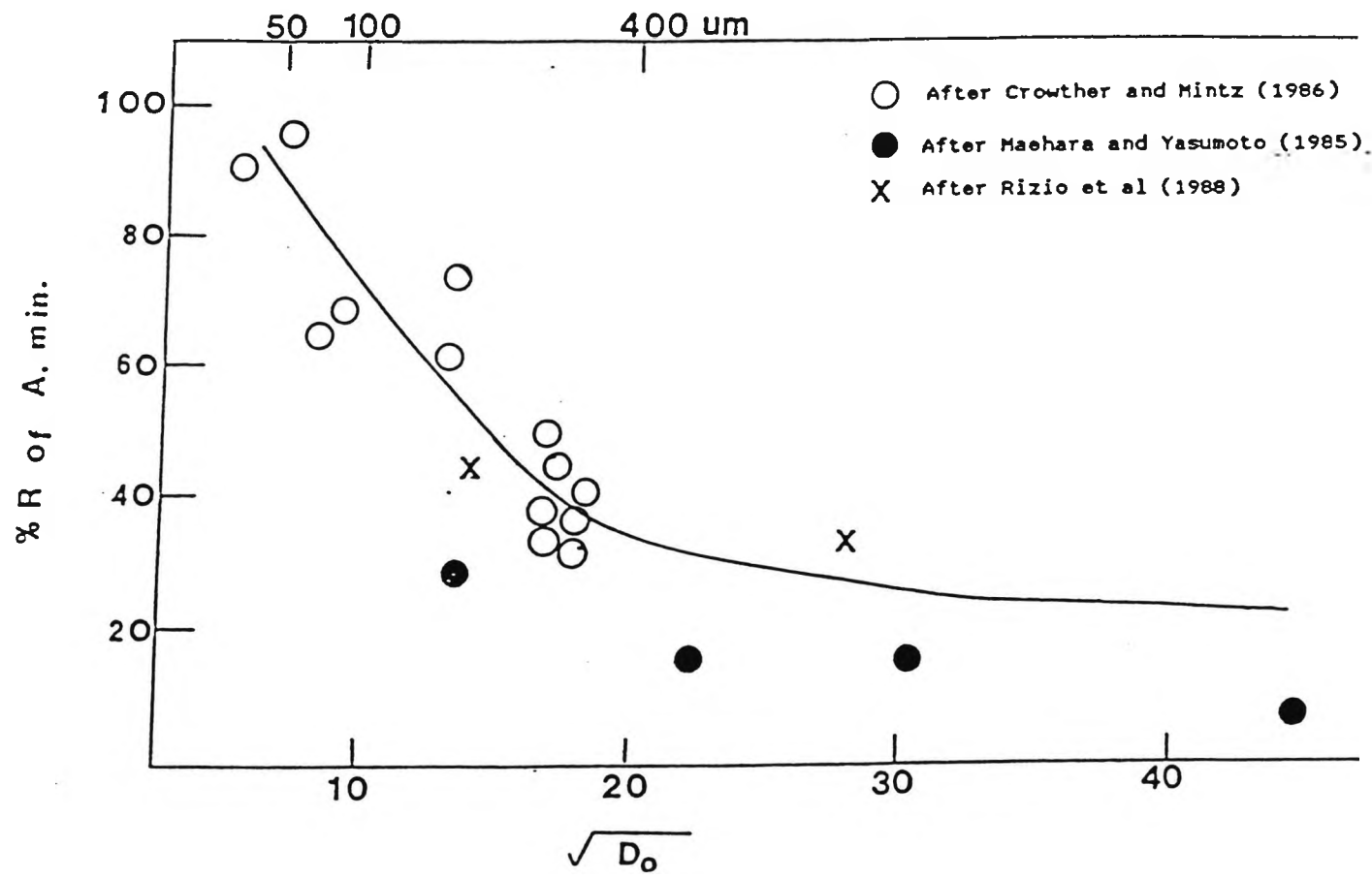


Fig. 2.16 The influence of D_0 (the initial grain size) on the minimum R.of A. value.
(After Mintz et al, 1991).

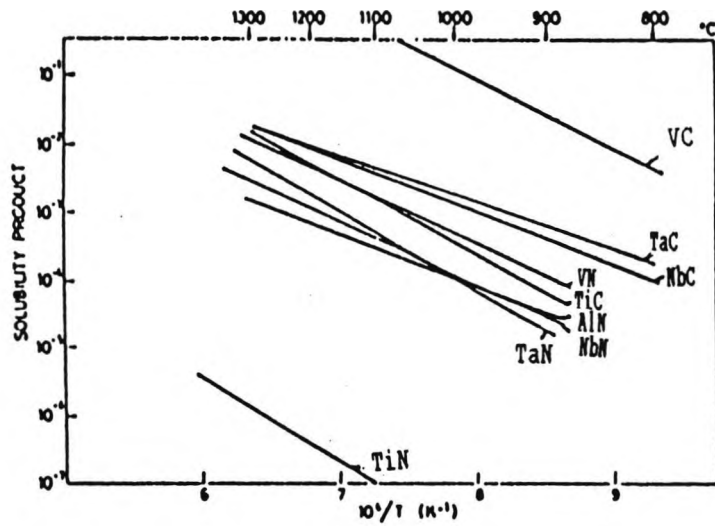


Fig. 2.17 Solubilities of carbides and nitrides in austenite. (After Narita, 1975).

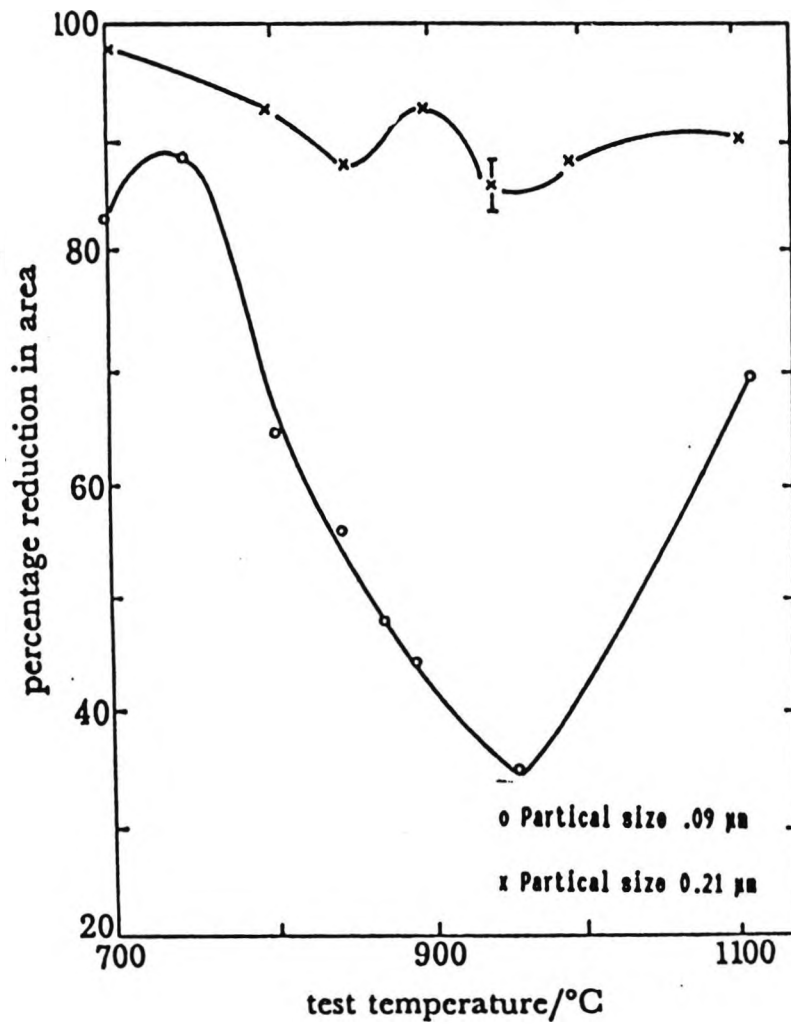


Fig. 2.18 Hot brittleness due to AlN precipitation (After Funnell and Davies, 1978).

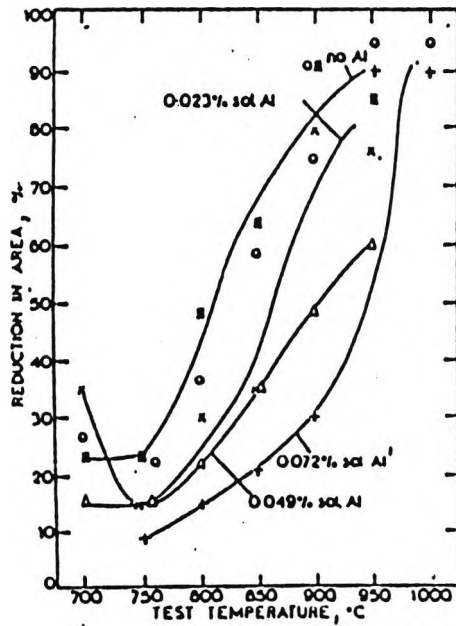


Fig 2.19 Influence of soluble Aluminium on the hot ductility of C-Mn-Nb-Al steels (After Mintz and Arrowsmith, 1979).

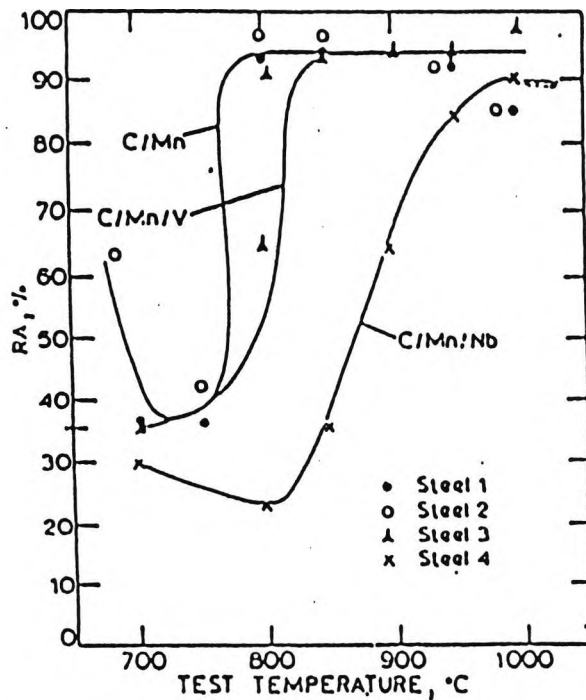


Fig. 2.20 Hot ductility curves for different microalloy steels, showing the effect of V (after Mintz and Arrowsmith, 1980).

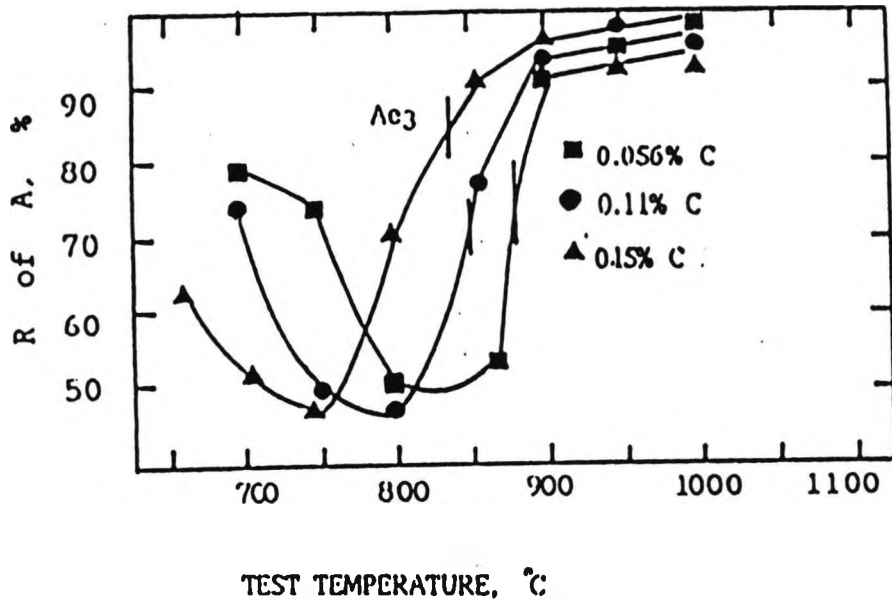


Fig. 2.21 Hot ductility curves for the Al containing steels examined with different carbon levels (After Z.Mohamed, 1988)).

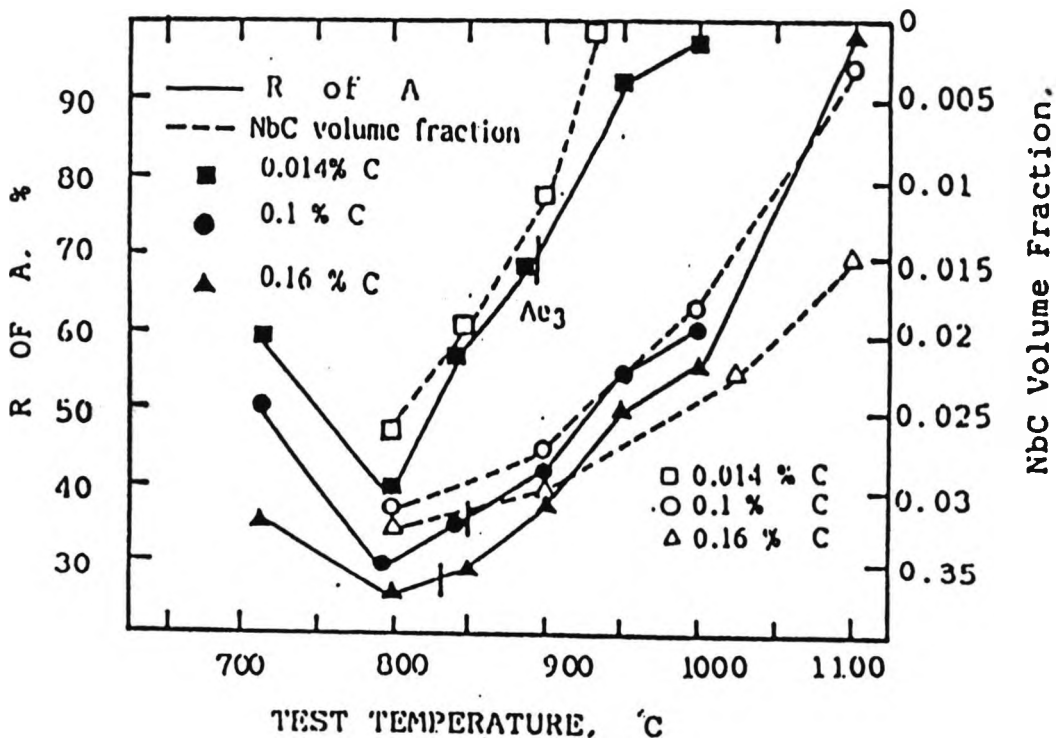


Fig. 2.22 Hot ductility curves for Nb containing steels with different carbon levels (After Z.Mohamed, 1988)).

CHAPTER 3

EXPERIMENTAL TECHNIQUES

3 EXPERIMENTAL TECHNIQUES

3.1 INTRODUCTION

The tensile test is the most commonly used measure of metal properties. The two characteristics that determine the forming properties of a material are its resistance to plastic flow (strength) and its ductility. The first determines the size of the equipment needed for the forming operation, whereas the second determines the maximum allowable deformation without risk of fracture. With high cost materials such as stainless steel and high temperature alloys, suitable data on strength, ductility and structure must be available to decide on the optimum working schedules.

3.2 Methods for studying hot ductility

An important feature of hot ductility tests is that they should give information on strength and ductility over a wide range of strain rate, strain and temperature. Many tests have been used to determine ductility under hot working conditions, but the only ones capable of providing quantitative information on fracture behaviour are the torsion test, impact test and tensile test. The first two of these tests have been used to simulate hot rolling processes, for which it is necessary to apply high strain rates and large strains. The tensile test is not suitable for such work, because of the difficulty in obtaining high strain rates, and in applying a large strain before sample

necking begins. However, the hot tensile test has proved very popular in the study of transverse cracking.

The common engineering measurements of ductility obtained from tension tests are :-

- 1- The elongation between two points along a fixed gauge length at the fracture.
- 2- The reduction in area of the cross sectional area of the specimen at fracture.

Uniform elongation can be a useful measure of fracture strain if little or no necking has occurred, as sometimes happens with brittle, intergranular fractures. However, it is not a suitable parameter for comparing the wide range of ductility levels which occur when the test temperature is varied over a wide range. Total elongation at fracture comprises components of uniform elongation, and elongation due to necking. The values of these two components are a complex function of test temperature, strain rate, composition and microstructure. This makes comparison of total elongation measurements over, for example a wide range of temperatures, difficult, since at different temperatures, identical elongation measurements may be made from samples having different fracture geometries, and hence different fracture strains. Nevertheless Wilcox and Honeycombe, (1984) have used this as a measure of ductility and it can give useful information as to the role dynamic recrystallization has in influencing ductility.

The majority of researchers have used the R.of A. values to provide quantitative information on fracture

strain at the point of fracture, as this measurement is irrespective of sample fracture geometry. This fracture strain ϵ_f , is related to the initial cross sectional area A_0 , and final cross sectional area, A_1 , by:-
$$\epsilon_f = \ln (A_0/A_1)$$

One of the principle disadvantages of the simple tensile test is that of the difficulty in maintaining a constant true strain rate as straining proceeds. As straining proceeds in a tensile test using a constant cross head speed, true strain rate at the point of fracture initially falls, as the sample elongates uniformly, but rises rapidly as heterogeneous deformation commences, and most of the strain is concentrated in the neck. A potential disadvantage of the tensile test is the hydrostatic stress state set up in necked sample. Such ^a stress state can have a strong effect on increasing the rate of growth and coalescence of voids nucleated at inclusions within the specimen. Despite these potential drawbacks, the simple hot tensile test using a constant cross head speed has proved quite adequate for hot ductility studies aimed at simulating the continuous casting process.

In the present study, hot tensile tests using constant cross head speed have been used. Two different hot tensile tests were used, and are described and compared in section 3-3. The metallographic techniques used to study precipitation are described in section 3.4.

3.3 Hot tensile tests

3.3.1 Induction heating tests

To enable rapid changes in sample temperature, and also to enable specimens to be cast in situ the tensile testing equipment used consisted of an Induction furnace and a Hounsfield Tensometer. The equipment is shown schematically in Fig 3.1. The heating section was a large induction generator connected to copper coils, which were wrapped around a silica glass tube. The tube was supported by the grips of the tensometer in which the specimen was placed. The tube consisted of two glass pipes at right angles to each other. The main pipe, as has been stated previously, contained the argon gas envelope, necessary to prevent oxidation. The second pipe was connected to an argon gas bottle and allowed the constant replenishment of the gas envelope as well as creating a back pressure in the tube to prevent the external atmosphere from entering. An Argon flow rate of 4 Litre /min. was utilised during heating and testing, but this was increased to 20 Litre/min. after fracture to ensure that the rate of cooling was high enough to prevent any significant precipitation taking place between the test and room temperatures.

The temperature was measured, using a platinum/platinum- 13% rhodium thermocouple connected to a desk top potentiometer. Standard tables were used to convert the potentiometer reading from milli volt to degree

Celsius. The thermocouple was placed inside the specimen through the axial 2 mm hole in the specimen, via the tensometer grip, the tip of the thermocouple coming to rest in the centre of the specimen. A ceramic covering was placed over the thermocouple to protect it during the test. Tests were performed at two strain rates, 2.10^{-3}s^{-1} in the case of melting and $1.3.10^{-3}\text{s}^{-1}$ in the case of heating up to 1330°C . The induction coil provided a zone of uniform temperature, 22 mm in ^{the} case of melting and 30 mm on heating up to solution temperature and cooling to the test temperature

In each case, any sample which failed outside the zone of uniform temperature was discarded. Repetition of 5 tests gave a standard deviation of 3% about the mean reduction in area values of 45%. The sample used in the test is shown in Fig 3.2, having a diameter of 7.93 mm and 70 mm in length.

3.3.2 Instron tests

The second piece of tensile test equipment used was an Instron model 1026 equipped with a split platinum wound furnace, illustrated in Fig. 3.3. The tensile samples, having a diameter of 5.04 mm and gauge length of 25.4 mm are shown in Fig 3.4. Temperature control was maintained by means of a Pt 13% Rh thermocouple connected to a purpose build Isoheat temperature controller unit, capable of maintaining fixed heating and cooling rates. The thermocouple was attached to the surface of a dummy sample,

and the temperature controller indicated that it was 13°C higher than the actual sample. Test temperatures were therefore taken to be the surface temperature, i.e. 13°C less than the reading on the temperature controller. Samples were nickel plated prior to test and enclosed in a loosely fitting glass tube as described by Crowther, (1986). An argon gas flow was established so as to prevent both oxidation and decarburization.

3.3.3 Measurement of Reduction in Area

To obtain reduction in area values from fractured tensile samples the fractured ends were examined under a Vickers Projection Microscope, and measurements of the diameter at fracture to nearest 0.1 mm were taken. Reduction in area values were then calculated, assuming that the cross section of the fractured samples remained circular

3.4 CARBON EXTRACTION REPLICA PREPARATION

The principle of the replica technique is to transfer the surface topography of the solid body to a thin film so that it may be observed in the microscope by transmission. Samples for replication were first prepared by grinding and then polishing to $1/4 \mu\text{m}$ followed by etching with 2% nital. The sample is then repolished, etched very lightly and then cleaned ultrasonically for 1 min. A carbon film was evaporated onto the prepared surface at a pressure of 10^{-4} torr. The thickness of the film should be 20 Å for optimum extraction. To judge the thickness of the film it is useful to place a clean glass slide with a drop of oil on it on a piece of white paper alongside the specimen. Since the carbon will not form a film on the oil droplet, the whiteness of the paper continues to show through the droplet during evaporation. When the colour of the carbon film is golden yellow, the film is approximately at the required thickness. Non conductive laquer was then applied onto the mounting disk to define the area to be examined. The carbon film was then scribed into 3 mm squares. The replica was removed by immersion in 1 to 10% HCl, depending on the coarseness^{ne} of the precipitates. After polishing a very light etch, 1% HCl was used, to reveal the fine particles, while the coarser were revealed by deep etching in 10% HCl. The replicas were then washed in distilled water, and finally collected on 4 mm copper grids. In the case of the replicas taken directly from the fracture surface, a carbon film was deposited directly onto the

fracture surface and removed with 10% HCl. Replicas were examined using a JEOL. 100 TEM microscope operating at 60 KV. The microscope was equipped with an EDAX X-ray analysing system, capable of identifying elements with an atomic number greater than 11. The system was therefore, not capable of analysing for C and N and hence could not distinguish between carbide and nitride precipitates. The smallest spot size available was 50 nm in diameter. Some work was also carried out at Jeol House using a JEOL 2000 FX, which could identify precipitates as fine as 1 nm and analyse for C and N. Precipitate sizes were measured directly from the negatives. To calculate a mean precipitate diameter, assuming spherical precipitates, at least 200 measurements were taken from 3 separate replicas from the same sample. For any particular steel, these measurements were based on approximately 200 particle counts taken from different grain boundary regions, and from different replicas. Such measurements although not providing absolute measurements of grain precipitate distributions, are adequate for making comparisons between different steels.

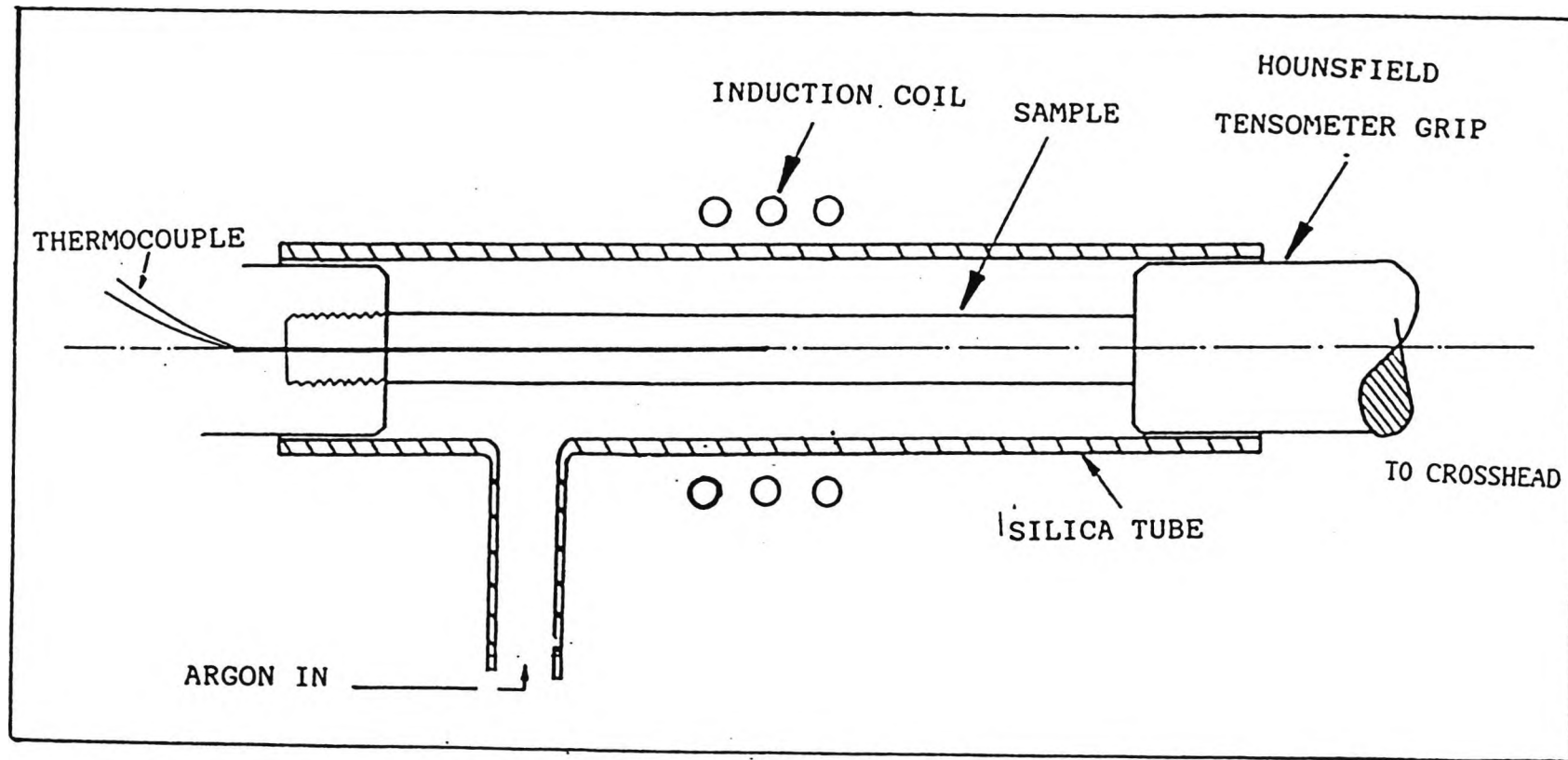


Fig 3.1 Schematic illustration of induction heating equipment for high temperature tensile testing.

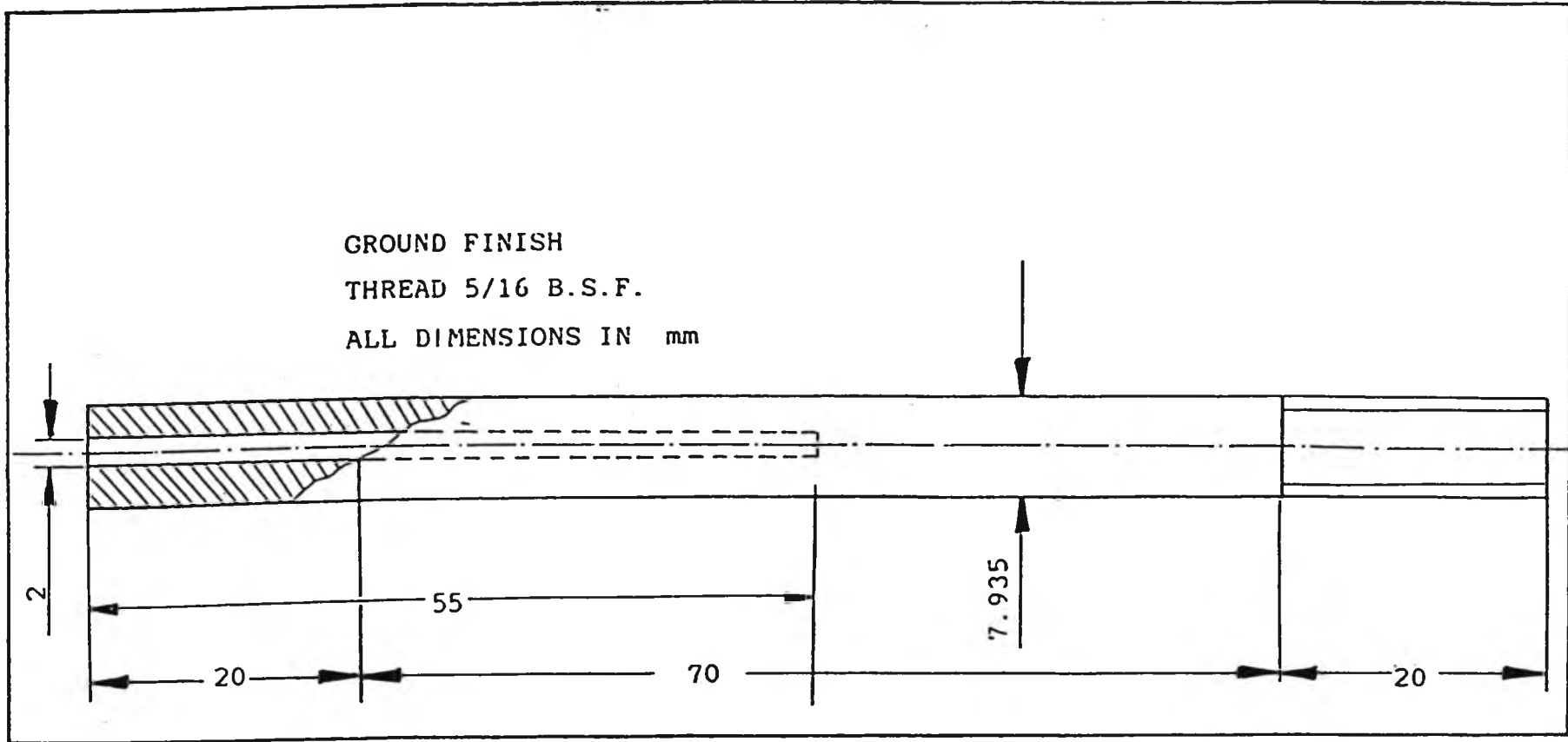


Fig 3.2 Induction test specimen

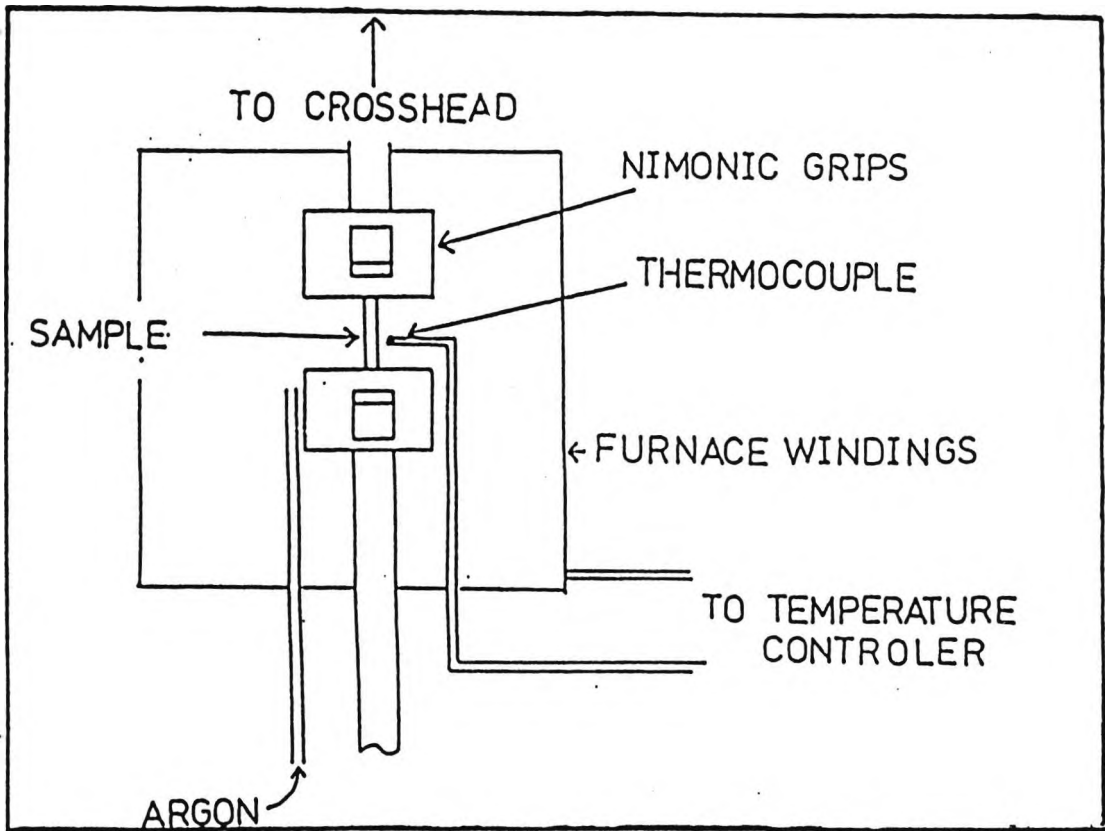


Fig 3.3 Schematic illustration of Instron high temperature testing equipment

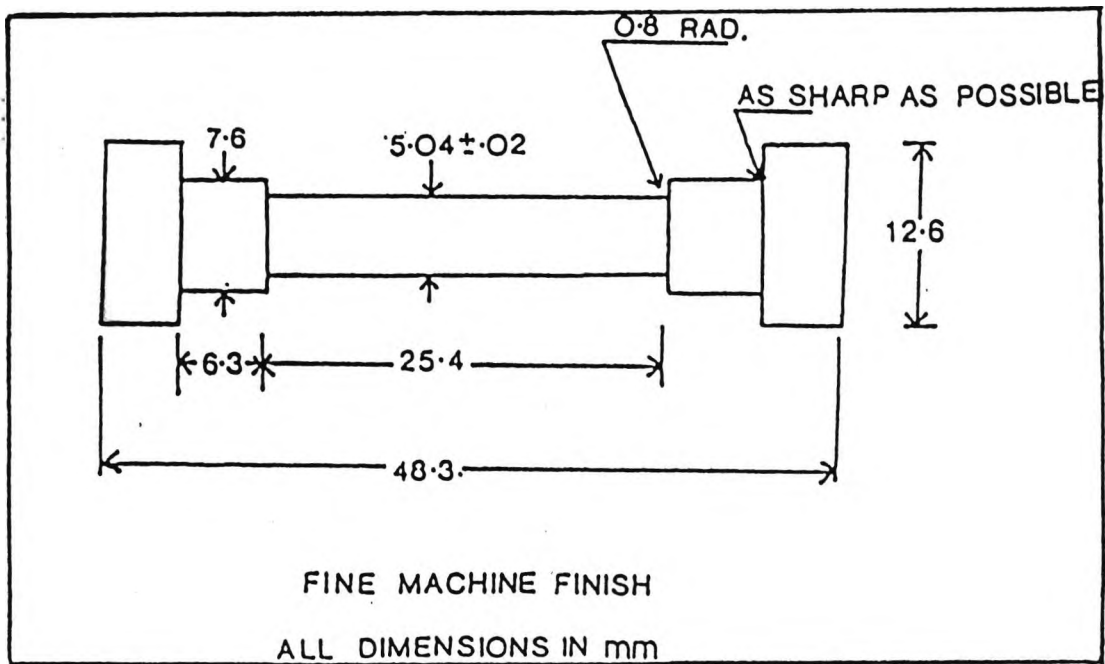


Fig 3.4 Instron test piece

CHAPTER 4

EFFECT OF CALCIUM ON THE HOT
DUCTILITY OF STEELS.

4.1 Introduction

4.1.1 Ductility at room temperature.

It is well known that the presence of inclusions has a deleterious effect on ductility. In general ductility decreases with increase in the volume fraction of sulphide or oxide inclusions (Coward et al, (1976). Calcium has been added to steels since 1930 as part of general steel processing to reduce S levels. Rare earth additions-(not examined in the present exercise)-which act in a similar manner to Ca have also been extensively used commercially to modify sulphides and improve fracture toughness.

Banks and Gladman, (1979) have reported that the addition of cerium and calcium successfully modified the initial morphology of sulphide inclusions to an isolated globular form and also decreased their plasticity.

The demand for High Strength Low Alloy [HSLA] steels with higher levels of cleanliness, toughness and formability has resulted in the use of Ca additions. Although it is an expensive technique improved ductility occurs by these additions (Tipnis et al, 1973). Pircher and Klapdar, (1977) have used a technique for successfully deoxidizing and desulfurizing steel by injecting calcium compounds into the ladle with an immersion lance after tapping. The calcium reaction lowers the dissolved sulphur and oxygen in the steel.

Most of the reaction products rise from the molten steel into the slag, so that steels which ^{with} $<0.001\%$ S can be

produced. Hilty and Ferrel, (1974) have also reported that adding 88 ppm Ca to a steel containing 0.005% S eliminated the pure MnS inclusions, forming instead hard spherical calcium oxy-sulphides which do not elongate on rolling and hence do not reduce the through-thickness ductility.

4.1.2 Ductility at high temperature

Although Ca additions improve ductility at room temperature, little attention has been given to use this element to improve high temperature ductility. Paul et al, (1982) reported that calcium and rare earth additions improve hot ductility mainly because of the formation of fine, none deformable inclusions. Yamaguchi et al, (1979) have also reported that additions of calcium give superior hot ductility, the depth of the ductility trough being reduced. Crowther and Mintz, (1986 d) and Crowther et al, (1987) have shown that Ca additions to C-Mn-Al steels improve hot ductility, and the hot ductility is no longer sensitive to the direction samples are taken from in the plate. In their work, samples were heated from room temperature to the test temperature prior to testing rather than solution treating and cooling to the test temperatures.

Recently Mohamed, (1988) has shown that the calcium treatment of steel also improves the hot ductility for samples cooled to test temperature after first solution treating. This treatment is more akin to the process route

for continuous casting, and is therefore of particular interest.

This improvement in hot ductility in Ca containing steels is believed to be due to the reduced amount of sulphur able to redissolve and precipitate in a fine form at the new austenite grain boundaries produced on solution treating. The smaller number of sulphide inclusions present at the boundaries will allow an earlier onset of dynamic recrystallization and will offer less sites for micro-voiding.

However, this improvement has so far only been examined after heating directly to the test temperature or cooling down from a solution temperature of 1330°C. This chapter extends this work to the commercially interesting treatment of melting samples and cooling them down to the test temperature.

4.2 Experimental

4.2.1 As cast steels

The steels were vacuum melts supplied in the hot rolled state, rolled to 12 mm thick plates. The compositions of the steels examined are given in Table. 4.1. Steels (A), (B), and (C) were Al containing steels with different levels of S. In this group, steel (A) had been Ca treated. Steels (D), (E), (F) and (G) were Nb containing steels with different S levels. In this group steels (D) and (E) had been Ca treated.

Tensile samples having a length of 110 mm and diameter 7.94 mm (as in chapter 3) were machined from the plates with their axis parallel to the rolling direction. They were placed inside silica tubes with an 0.2 mm diametrical clearance. A 2 mm diameter hole was drilled from one end of each sample to the mid-length of the sample, so the thermocouple could be inserted, Fig. 4.1.

The samples were heated by induction heating as described in (chapter 3), so that approximately 22 mm of the length of the mid length position could be melted. The molten region was contained in the tolerance fitted silica sheath which in turn was surrounded by a further silica tube through which argon could be circulated to prevent oxidation occurring. Samples were melted, held for 5 minutes then cooled down at a cooling rate of 100°C/min to the required test temperature range 750-1100°C. The test pieces were held for 5 min and strained to fracture using a

strain rate of $2 \times 10^{-3} \text{ s}^{-1}$.

4.2.2 Melted and reheated steels

In addition to examining the hot ductility directly after casting, steels (A), (B), and (C) were reheated after melting to 1330°C held for 5 minutes and then cooled to test temperatures in the range 750 to 1000°C using the same cooling rate and tested to failure using the same strain rate, as used in section 4.2.1

Fracture surfaces from all the broken tensile samples were examined using a JEOL T100 Scanning Electron Microscope, operating at 25 KV. Carbon extraction replicas were prepared from a section approximately 1 mm behind the fracture surface and examined using a JEOL 100 TEM transmission electron-microscope operating at 60 KV as in section 3.3.

4.3 RESULTS

The curves of percentage reduction in area against test temperature in the range 750-1000°C are given in Figs. (4.2) to (4.11).

4-3-1 Hot ductility of C-Mn-Al steels in the as cast state, steels directly cast and cooled down to the test temperature

The hot ductility was found to be improved when Ca was present in the steel, as can be seen in Fig. 4.2 where steel (A) is the Ca containing steel and steel (C) is a similar Ca free steel, see Table. 4.1.

In the case of steel (C), (low S Ca free), the ductility started to fall from 950°C and reached a minimum of ~35%. Steel (A), (Ca containing), gave the better ductility over the temperature range 700-900°C with a minimum R. of A. value of 40% at 800°C. It should be noted that steel (A), (the Ca containing steel), had a higher S level than steel (C), (Ca free) yet had the better hot ductility.

The high S, Ca free steel gave the worst ductility of the three steels examined. At 850°C, the Ca free high S steel (B) gave an R of A value of 38%, while steel (A), the Ca containing steel, gave ~60% R.of.A Fig. 4.2.

4.3.2 Hot ductility of C-Mn-Nb-Al steels.

Steels directly cast.

As before, it can be seen from Fig. 4.3 that the Ca containing steels give the better hot ductility. The ductility for all steels started to fall around 1000°C reaching a minimum at temperatures in the range 800 to 900°C. The minimum ductilities for the Ca free steels, (F) and (G), were ~30%, and 35% for the Ca containing steel (D). However, the Ca containing steel gave considerably better hot ductility in the temperature range 900 to 1000°C when compared to the Ca free steels.

The influence of niobium in reducing the ductility on as cast steels is clearly shown in Fig. 4.4

4.3.3 Melted and reheated C-Mn-Al Steels

Samples heated up to 1330°C after melting and cooling to the test temperature.

Solution treating the low S as cast steels (A), (Ca containing) and (C), (Ca free) improved hot ductility, probably because the grain size had been considerably refined by the solution treatment, but steel (A), (the Ca containing) steel gave the better hot ductility, see Figs. 4.5 and 4.6. In contrast for the high S steel, (B), the hot ductility was worse after solution treatment and the curve was shifted towards higher temperatures, as in Fig. 4.7. This may be related to its much higher sulphur level (0.012% S wt) as will be discussed later.

4.3.4 Dynamic recrystallization

The stress - total elongation curves for the steels examined are shown in Figs. 4.8 to 4.11. For the as-cast C-Mn-Al, Ca containing steel (A) fluctuations in the flow curves at test temperatures $\geq 900^{\circ}\text{C}$ were observed. These fluctuations arrowed in the figures are similar to those associated with dynamic recrystallization (Wilcox and Honeycombe, (1984).

The onset of dynamic recrystallization occurred earlier in the Ca containing steel C-Mn-Al steel than in Ca free low S steel. Dynamic recrystallization occurred at $\geq 900^{\circ}\text{C}$ and $\geq 950^{\circ}\text{C}$ for the as-cast Ca containing and Ca free steels respectively and at $\geq 875^{\circ}\text{C}$ and $\geq 900^{\circ}\text{C}$ for the as-cast reheated Ca containing and Ca free steels respectively. Dynamic recrystallization appeared delayed in the high S, Ca free, steel (B) particularly for the as-cast reheated condition, the onset of dynamic recrystallization being $\geq 950^{\circ}\text{C}$ and $\geq 1000^{\circ}\text{C}$ for the as-cast and as-cast reheated condition respectively.

All this behaviour tends to suggest that S is in some way preventing dynamic recrystallization from occurring.

As expected the Nb containing steels showed delayed dynamic recrystallization and this was again most marked for the Ca free steel, (1000 and 1050°C respectively for Ca containing and Ca free).

4.4 FRACTOGRAPHY

4.4.1 SEM examination

SEM examination of the fracture surface of samples from the calcium free as cast Al containing steels exhibited intergranular micro void coalescence, usually associated with the second phase particles, as the main fracture mode. This is illustrated in Fig. 4.12. Dendritic separation which was observed in small areas of these samples was attributed to microshrinkage during solidification as in Fig. 4.13. Small spherical sulphide inclusions were observed on the dendritic nodules. These sulphides were not present when the steel was reheated to 1330°C after melting as illustrated in Fig. 4.14.

Intergranular fracture due to grain boundary sliding was also observed in the as cast calcium free Al containing steels when the samples were tested at 900°C, the fracture surface appearing flat as in Fig. 4.15.

In the as cast Al-Ca containing steels the fracture surface at low ductility values was mainly intergranular ductile voiding as in Fig. 4.16.

The fracture surface of these steels also contained some regions of interdendritic failure (about 20% coverage) as seen in Fig. 4.17. No evidence of intergranular failure was observed in the as-cast reheated Ca containing steel, ductile rupture being the main mode as in Fig. 4.18

At temperatures in the region of 800°C, the fracture surface of the as cast Nb steels with or without calcium, was a mixture of intergranular microvoid coalescence and intergranular decohesion as in Fig. 4.19. The intergranular fracture due to grain boundary sliding in the austenite is shown more clearly in Fig. 4.20.

4.4.2 METALLOGRAPHY

In the polished samples of the calcium free C-Mn-Al steel, steel (B) (melted and reheated) which had the higher S level (0.012% wt.S), sulphide inclusions were observed to be arranged in lines Fig.4.21 These are probably situated at the γ grain boundary and may inhibit grain boundary movement. In contrast for the calcium containing, melted and reheated samples, fewer sulphide inclusions were noted as shown in Fig. 4.22

4.4.3 TEM examination

Examination of carbon extraction replicas taken from the transverse sections of the tensile samples close to the fracture (~1 mm behind the fracture surface) revealed that a few isolated precipitates of AlN were present in all the steels examined. However, in the as cast Nb containing steels there is a fine precipitation of NbCN at the grain boundaries as well as in the matrix Fig. 4.23 The precipitation patterns were similar for both Ca containing and Ca free steels. Fig. 4.24 shows the NbCN precipitation at sub-grains boundary in the as cast Nb containing steel. In addition to the fine NbCN precipitation, a coarse NbCN eutectic was also found in these steels, Fig. 4.25.

In the as cast Ca containing steels only a few MnFeCaS, Fig.4.26 inclusions were found, while in the Ca free steels many MnFeS inclusions were found as in Fig.

4.27. In the melted and reheated steel (B), there were fine sulphide inclusions, in the matrix as well as in the grain boundaries, Fig 4.28. These sulphides were generally fine $MnFeS$, but MnS and CuS inclusions were also identified.

4.5 DISCUSSION

4.5.1 As cast condition

It can be concluded from all the results that the presence of calcium in the steel in all cases improves the hot ductility. Although calcium additions generally give both modified sulphides and lower total S levels, the better hot ductility is not a consequence of the generally lower S levels. For example, the Al containing steel, steel (A) and steel (C) have similar total S levels, but the Ca containing steel (A), has the better hot ductility in the as cast state, Fig. 4.2. Also for the C-Mn Nb-Al steels Fig 4.3 directly cast and cooled to the test temperature, steel (D) and (F), have similar low S levels, but again, steel (D), the calcium containing steel, has the better hot ductility Fig 4.3.

Modification of the inclusions is not likely to be the explanation for the improvement in the hot ductility shown by calcium containing steels because MnS inclusions are themselves spherical in shape even in the Ca free steel as seen in Fig 4.21. There is also no significant difference in grain size between the calcium containing and calcium free steels. The grain sizes are all ~1000 μ m, so this can not be used to explain the difference in the hot ductility, Table. 4.2.

The improvement of the hot ductility when Ca is present is most likely related to the smaller amount of

sulphur available to precipitate out during cooling at the interdendritic boundaries which later become the γ grain boundaries. It can be seen in Figs. 4.2 and 4.3 that an increase in the sulphur level, shifts the ductility trough towards higher temperatures, and this may be because the fine sulphide (<50 nm) particles Fig. 4.28, restrict dynamic recrystallization, and the more that are present the higher is the temperature for dynamic recrystallization.

Dynamic recrystallization is first observed at 900°C for the C-Mn-Al, (Ca containing steel), and 950°C in (Ca free steels) as shown in Figs. 4.8, 4.9 and 4.10. For the Nb containing steels, again the onset of dynamic recrystallization occurred 50°C higher in the Ca free steel Fig. 4.11. It is likely that these sulphides will segregate to the interdendritic boundaries during solidification and precipitate at the γ grain boundaries during cooling to test temperature.

Because of the difference in the C levels between the C-Mn-Al and the C-Mn-Nb-Al steels, it is difficult to define precisely the influence of niobium on the as cast hot ductility. However, comparison of steels with similar sulphur levels with and without niobium, Fig 4.4 showed that Nb is detrimental to the hot ductility. This contrasts with the work of Guo et al, (1988), in which no influence of Nb on hot ductility of as-cast samples could be found for a niobium addition of 0.04%. However, in their work

this may have masked the detrimental influence of NbCN precipitation on hot ductility.

4.5.2 As cast and reheated condition

Again, calcium can be seen to improve the hot ductility, compare curve for steel (A) Fig 4.6 with those for the calcium free steels, (B) and (C), Fig 4.7. The as-cast hot ductility was improved when steels (A) and (C) were solution treated, the grain size being reduced from ~1000 μm to ~400 μm .

In contrast, for steel (B) which had the highest S level 0.012% S wt, the hot ductility after solution treatment was worse Fig. 4.7 even though grain refinement occurred, the curve being shifted towards a higher temperature with a slightly lower minimum ductility.

The reason for this behaviour is probably because the sulphides produced in as cast state are not pure MnS but MnFeS (Mintz et al, 1986). On reheating, ductility is controlled by the amount of S which can redissolve at 1330°C and precipitate in a fine detrimental form at the γ grain boundaries when cooled to the test temperature. The amount of S which goes back into solution at 1330°C is very much dependent on the purity of the sulphides and the Mn and S level of the steel. For pure MnS inclusions, a steel with 1.4% Mn would according to Turkdogan's et al solubility data, (1955) allow 0.001% S to go to back into solution at 1330°C and this would be available to precipitate out at the γ ^{ole} boundaries in a fine form on cooling to the test temperature so influencing the hot ductility. As all the steels in the present exercise have >0.001% S, provided the sulphides are pure MnS, the same

amount 0.001% S would redissolve at 1330°C and precipitate on cooling giving the same hot ductility. This clearly is not the case. One of the steels, steel (A), has calcium present and this will severely reduce the amount of S able to redissolve and precipitate out. This steel gives the best hot ductility Fig. 4.5. The other two steels have no calcium present, but the sulphides are not MnS, but MnFeS and therefore, more S than 0.001% S will go back into the solution. Previous work by Mintz et al, (1986) indicates that 0.005% S is likely to redissolve in this type of steel. Hence more S will go back into solution for steel (B) than for steel (C), and this probably accounts for the poor ductility of steel (B) , Fig 4.2. The increased precipitation of fine sulphides in steel (B) on cooling to the test temperature Fig. 4.28 may also act in a similar way to NbCN and delay the onset of dynamic recrystallization to higher temperatures as shown in Fig. 4.10.

4.5.3 Hot-rolled and solution treated steels, cooled directly to test temperature.

To complete the story, it is necessary to examine the influence of Ca on the same steels after solution treating and cooling to test temperature. This work was carried out by Mohamed. (1988) but his results are given here again for completeness.

It can be seen in Figs. 4.29 and 4.30 that for hot rolled and solution treated steels the addition of calcium is beneficial to hot ductility. The R. of A. values are probably better than those obtained after directly casting because of the smaller grain size produced on solution treating (grain size after solution treatment was ~400 μm compared to 1000 μm after direct casting). As before adding calcium reduced the amount of S which goes back into solution at 1330°C and reprecipitates at the new γ boundaries formed on cooling to the test temperature. The sulphide inclusions in the calcium containing steel are more likely to be CaMnS rather than pure MnS and hence, the solubility of these sulphides at 1330°C will be much lower than for MnS. It is recommended that the Ca/S ratio should be 2:1 to obtain a modified calcium rich oxy-sulphide. In these laboratory casts, the Ca/S was 1:1, so that some of the sulphides will be CaMnS. This would mean that at 1330°C a greater amount of S is soluble than is given by the CaS solubility product. Nevertheless the amount of S able to redissolve at 1330°C will be very much less than when calcium is not present.

4.6. CONCLUSIONS

Calcium treatment improves the hot ductility in steels both directly cast and cooled to the test temperature, as well as after solution treating and cooling to the test temperature. This is due to the total sulphur being reduced by the calcium treatment, so that there are a fewer sulphides at the interdendritic grain boundaries which on cooling subsequently become the γ grain boundaries. The lower volume fraction of sulphides at the boundaries reduces grain boundary sliding and voiding in the boundary regions.

Reheating to the solution temperature after casting also generally results in improved hot ductility due to grain refinement. However, in the higher sulphur calcium free steel (0.012% wt S) this was not the case, the ductility trough shifting towards higher temperatures. This arises because impure MnFeS inclusions are present allowing more S to go back into solution than given by the equilibrium solubility data. This excess S probably reprecipitates at the γ grain boundary leading to enhanced grain boundary sliding and cavitation. The very fine sulphides observed also probably act in the same way as NbCN delaying the onset of dynamic recrystallization to higher temperatures.

Table 4.1

Composition of Steels Examined wt.%

Code	Type	C	Mn	Si	P	S	Nb	Al	N	Ca
Steel A	C-Mn-Al-Ca	0.065	1.42	0.46	0.007	0.004		0.042	0.0066	0.0040
Steel B	C-Mn-Al	0.056	1.46	0.42	0.007	0.012		0.034	0.0075	
Steel C	C-Mn-Al	0.110	1.42	0.32	0.011	0.002		0.038	0.0038	
Steel D	C-Mn-Nb-Ca	0.086	1.41	0.53	0.007	0.005	0.025	0.041	0.0048	0.0040
Steel E	C-Mn-Nb-Ca	0.100	1.35	0.41	0.015	0.003	0.023	0.035	0.0060	0.0026
Steel F	C-Mn-Nb	0.098	1.41	0.30	0.009	0.007	0.031	0.040	0.0042	
Steel G	C-Mn-Nb	0.100	1.39	0.42	0.007	0.010	0.026	0.036	0.0075	

Table 4.2

Grain size μm of steels examined

Code	Type	Solution treated	As-cast	As-cast reheated
Steel A	C-Mn-Al-Ca	500	1010	500
Steel B	C-Mn-Al	290	800	280
Steel C	C-Mn-Al	300		300
Steel D	C-Mn-Nb-Ca	440	880	
Steel E	C-Mn-Nb-Ca	400		
Steel F	C-Mn-Nb	500	840	
Steel G	C-Mn-Nb	490	800	

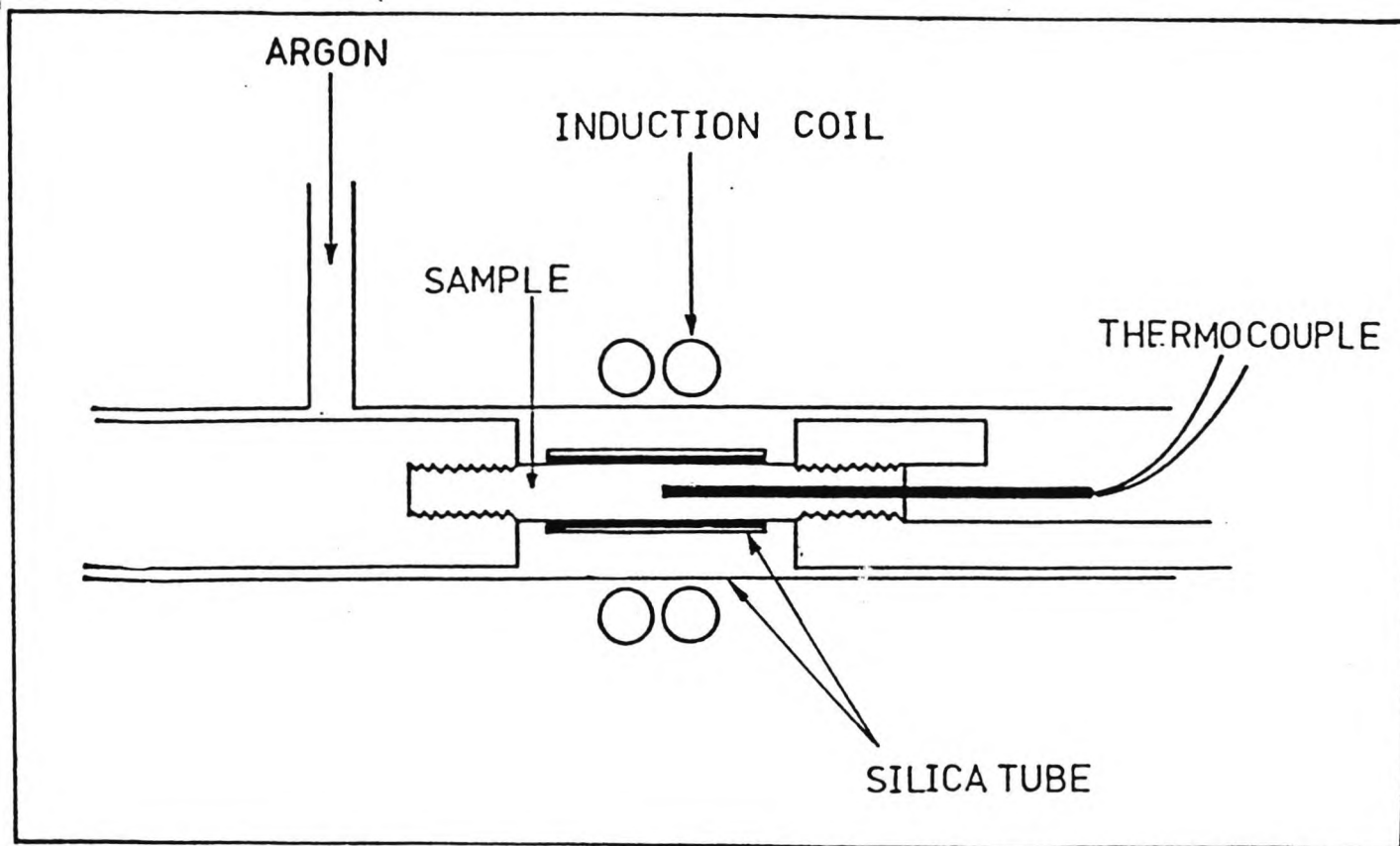


Fig. 4.1 Experimental arrangement for measuring hot ductility in as-cast condition.

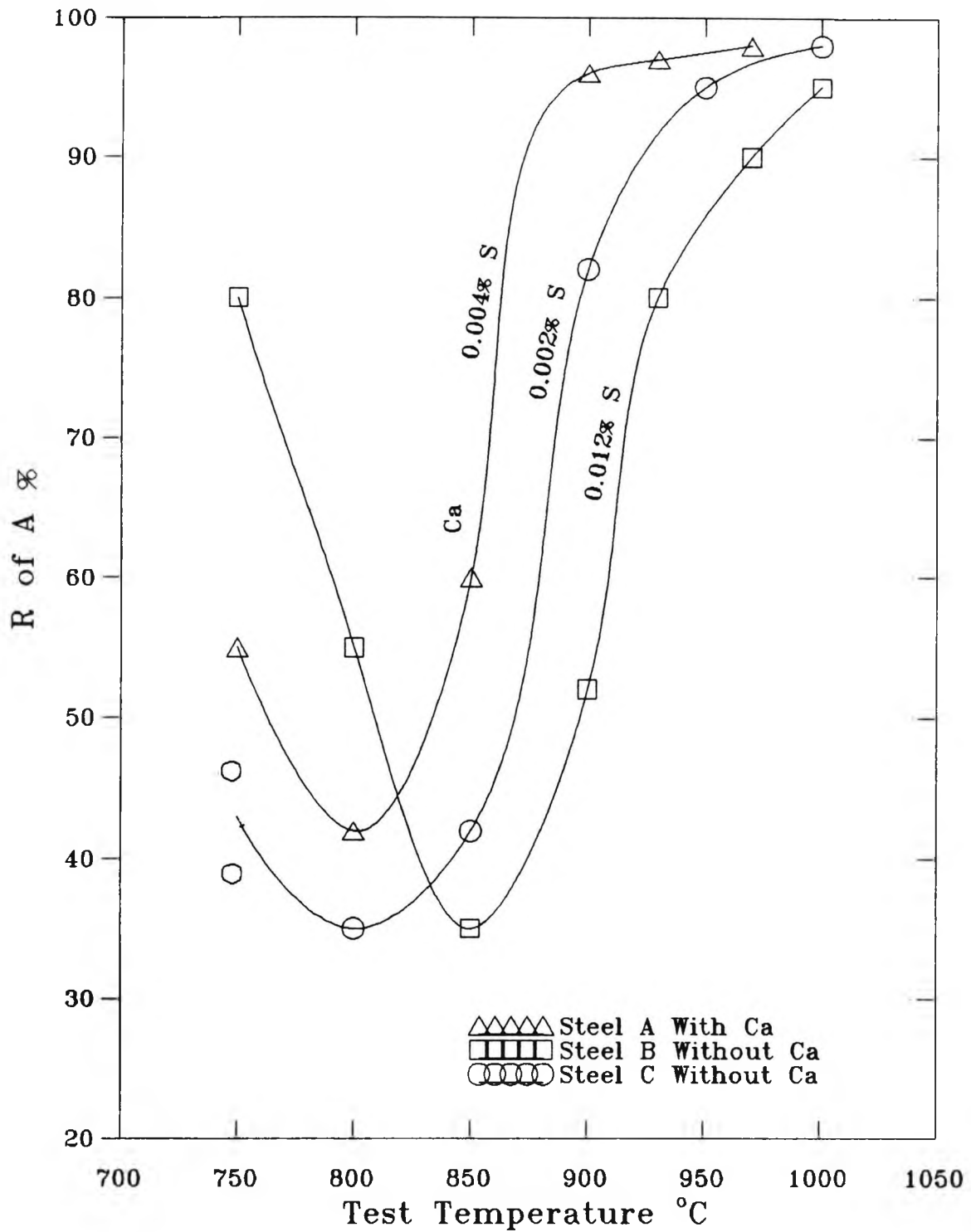


Fig 4.2 Hot ductility curves for the C-Mn-Al steels with and without calcium. Steels directly cast and cooled to test temperature.

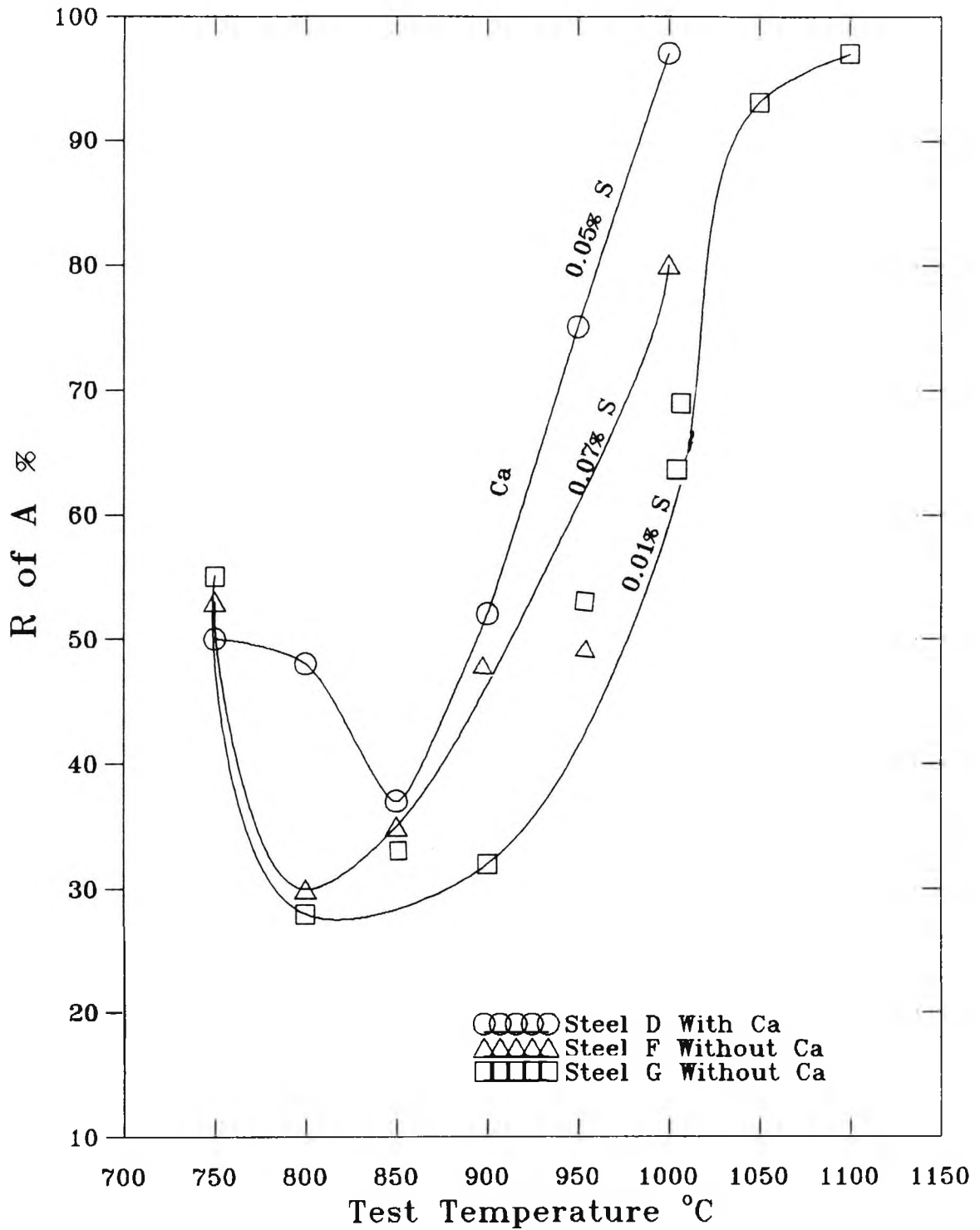


Fig 4.3 Hot ductility curves for the C-Mn-Nb-Al steels with and without calcium. Steels directly cast and cooled to test temperature.

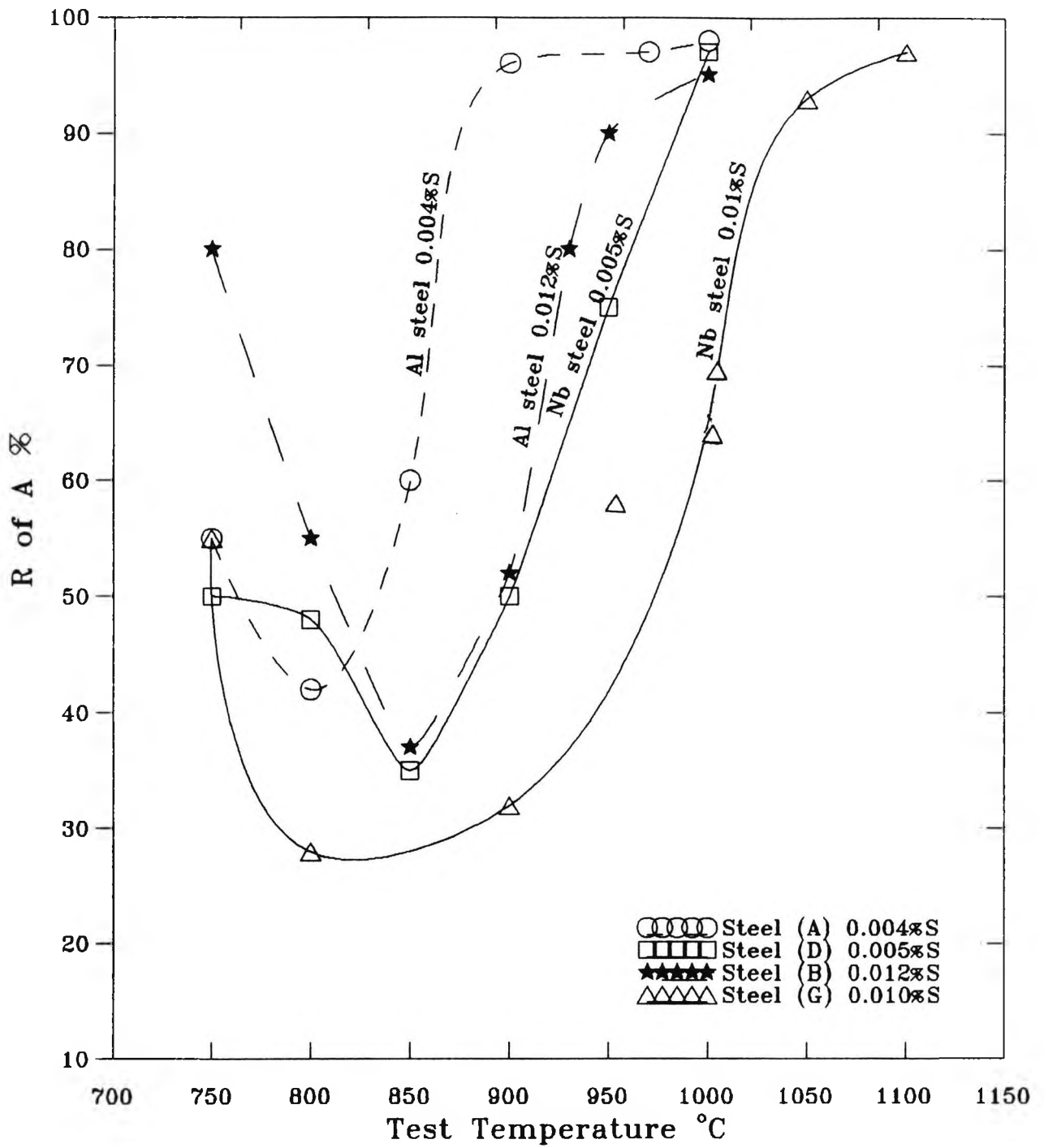


Fig 4.4 Hot ductility curves for C-Mn-Al and C-Mn-Nb-Al steels at two S levels.

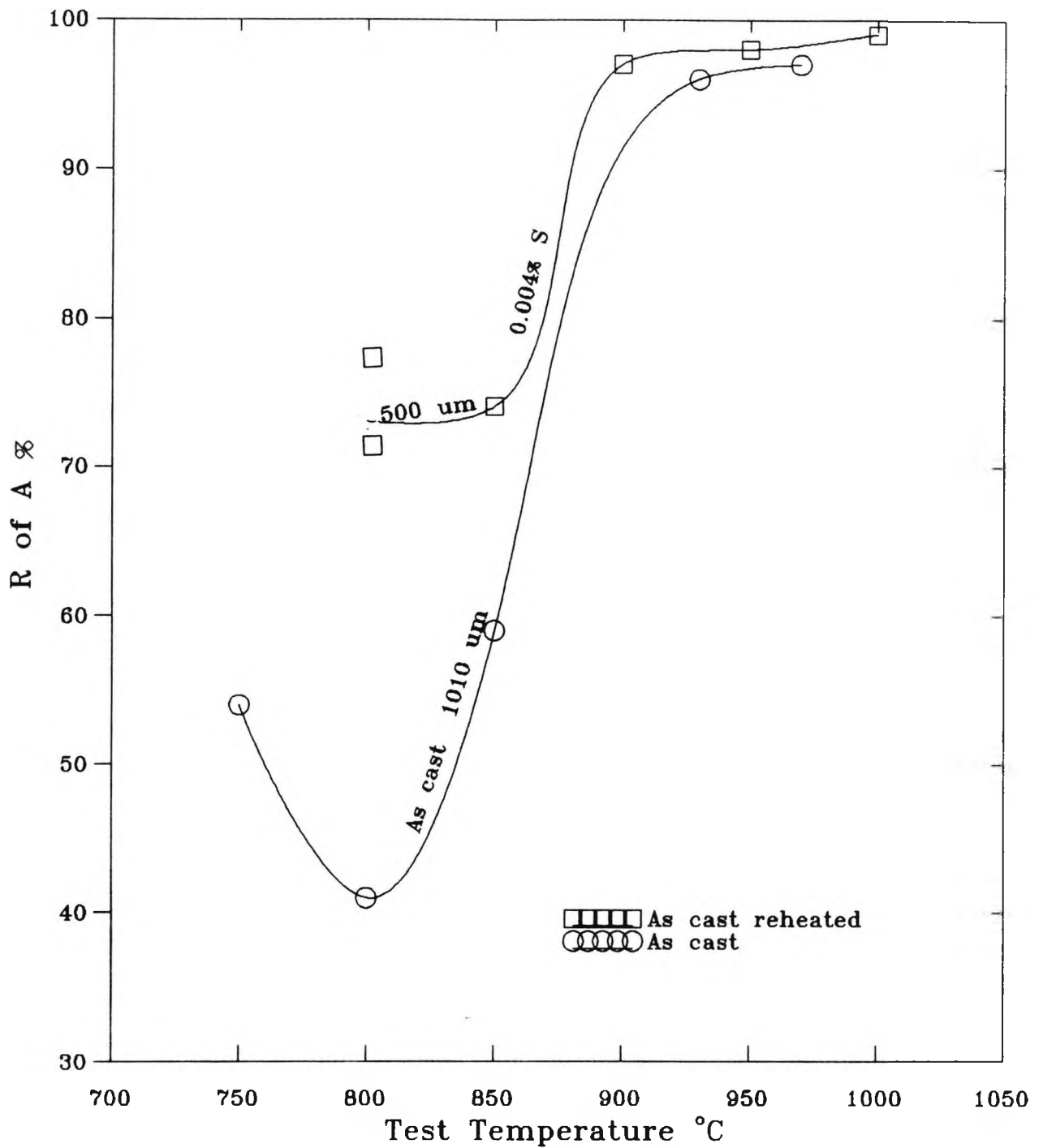


Fig. 4.5 Hot ductility curves for the calcium treated C-Mn-Al steel, steel (A) after casting, and casting followed by reheating.

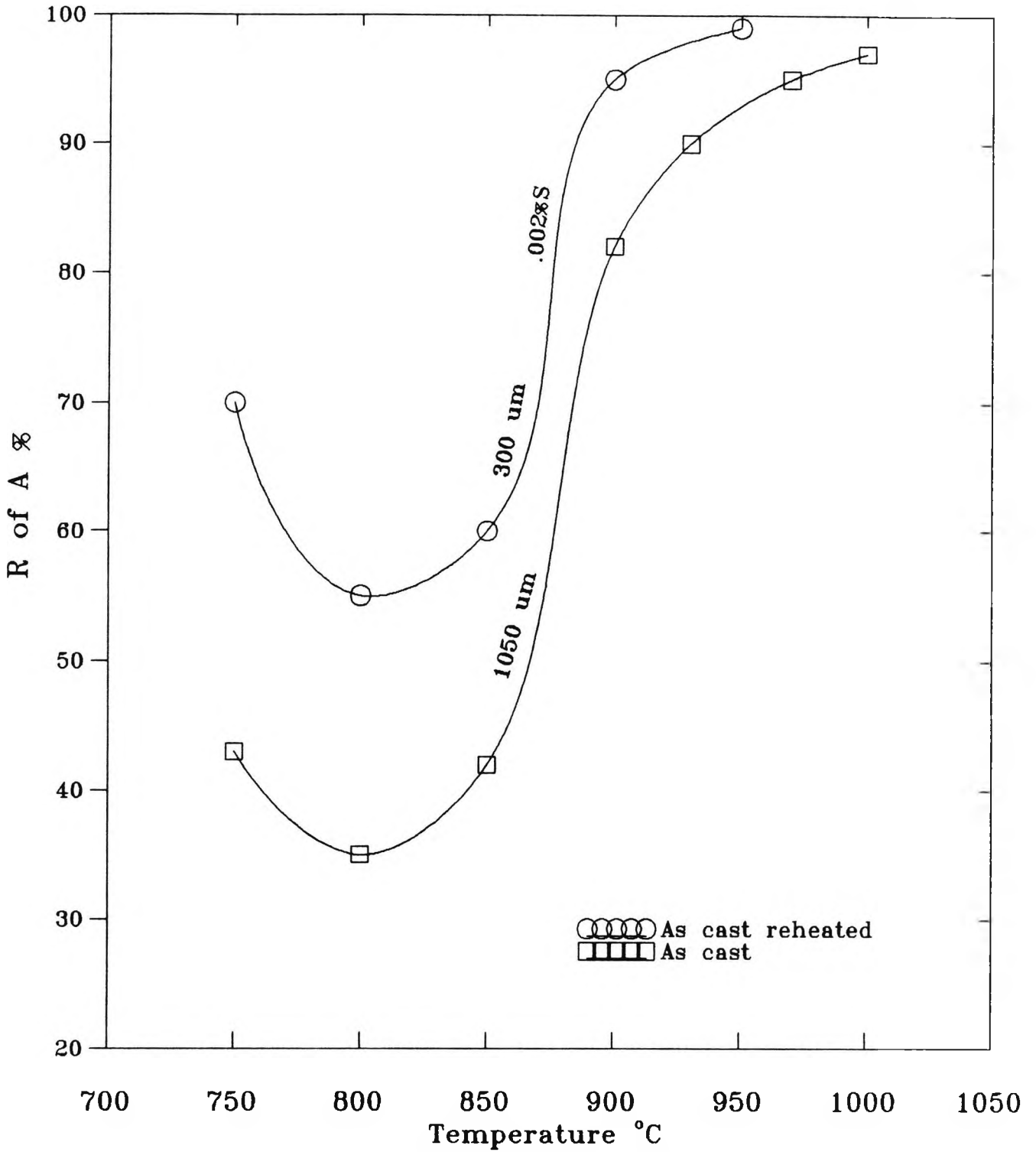


Fig. 4.6 Hot ductility curves for as cast and as cast reheated C-Mn-Al, Steel (C).

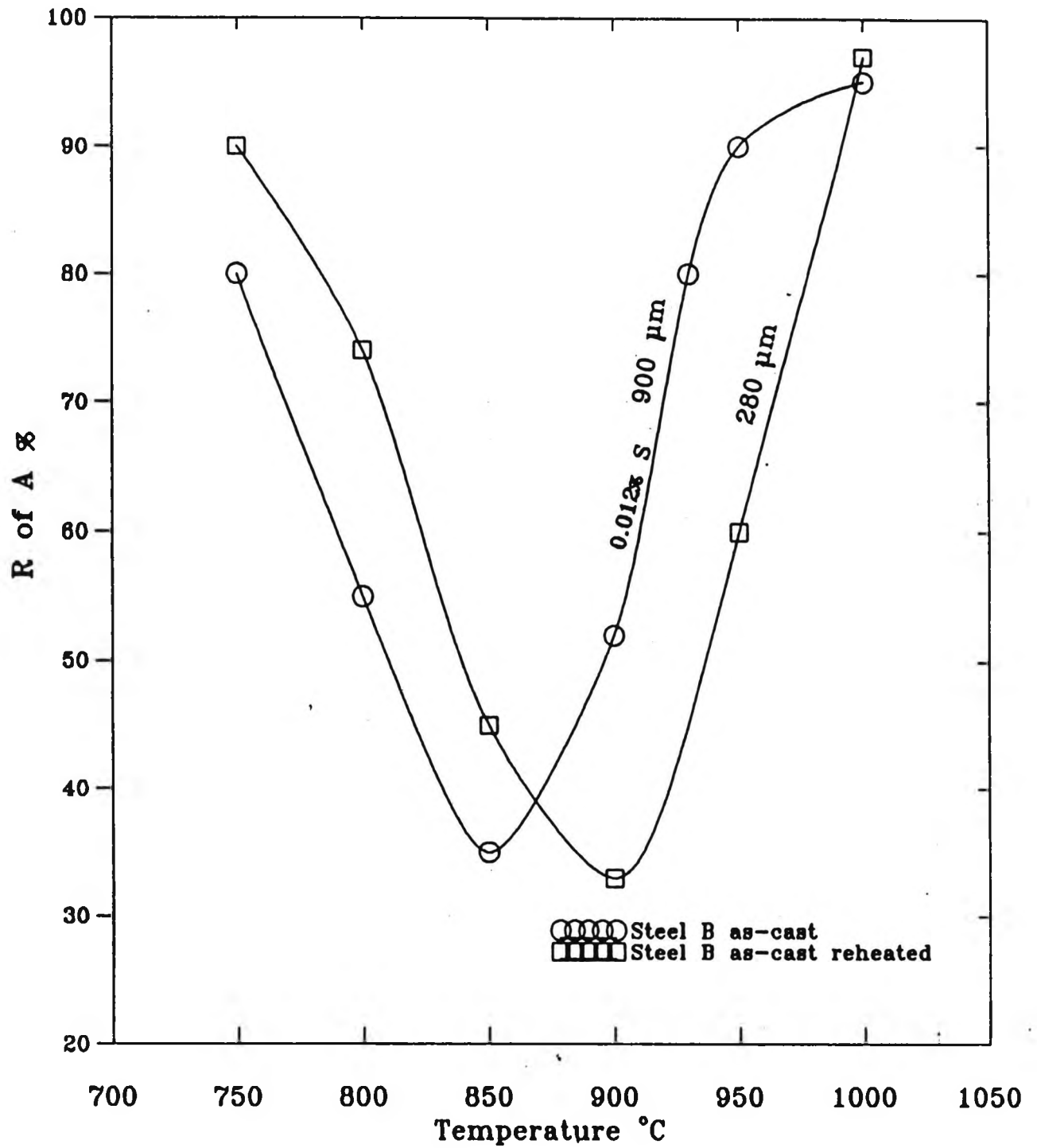


Fig. 4. 7 Hot Ductility curves for as-cast and as-cast reheated C-Mn-Al, steel B.

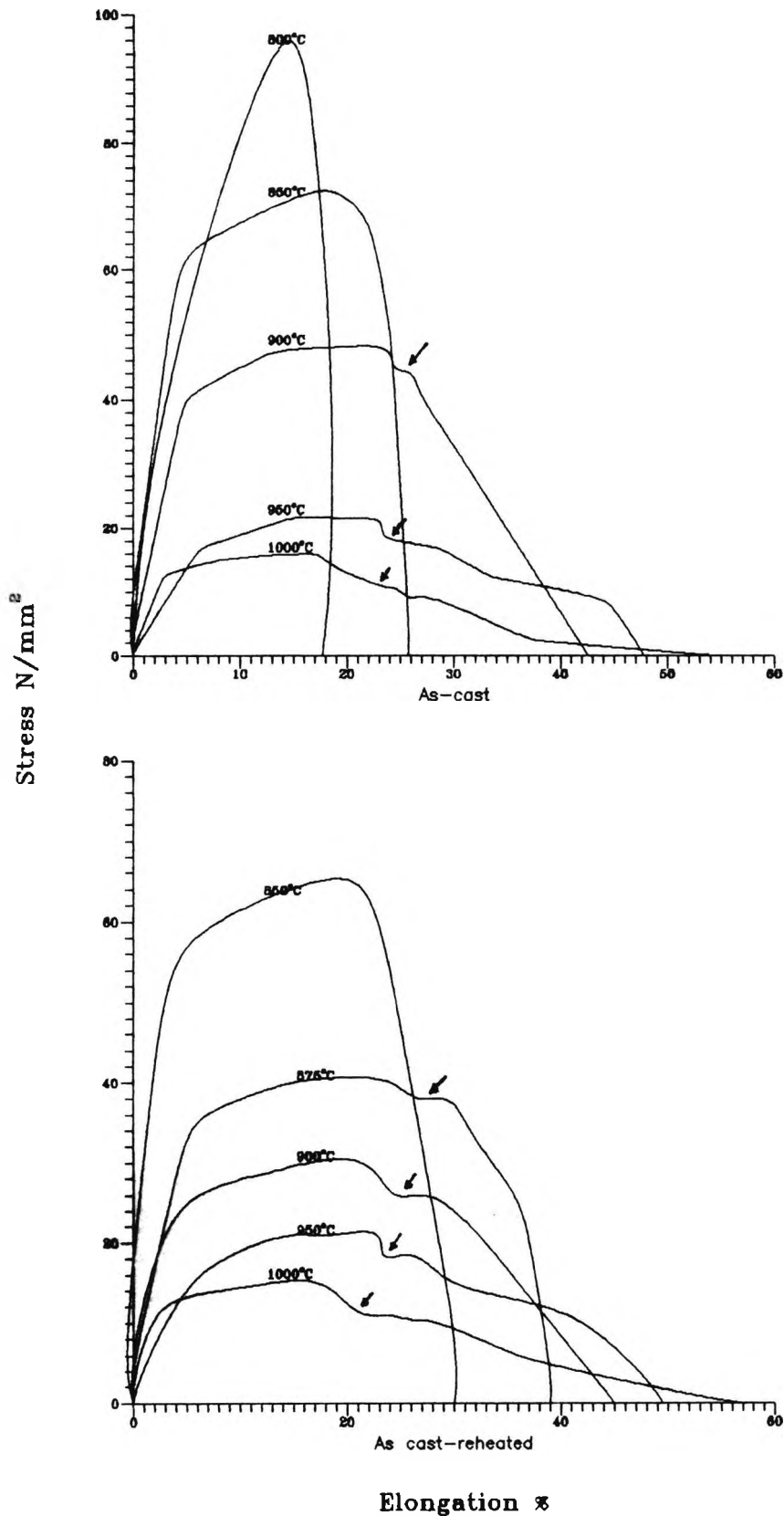


Fig. 4.8 Stress/Elongation curves for Ca Containing C-Mn-Al steel (A). (Arrows indicate dynamic recrystallization).

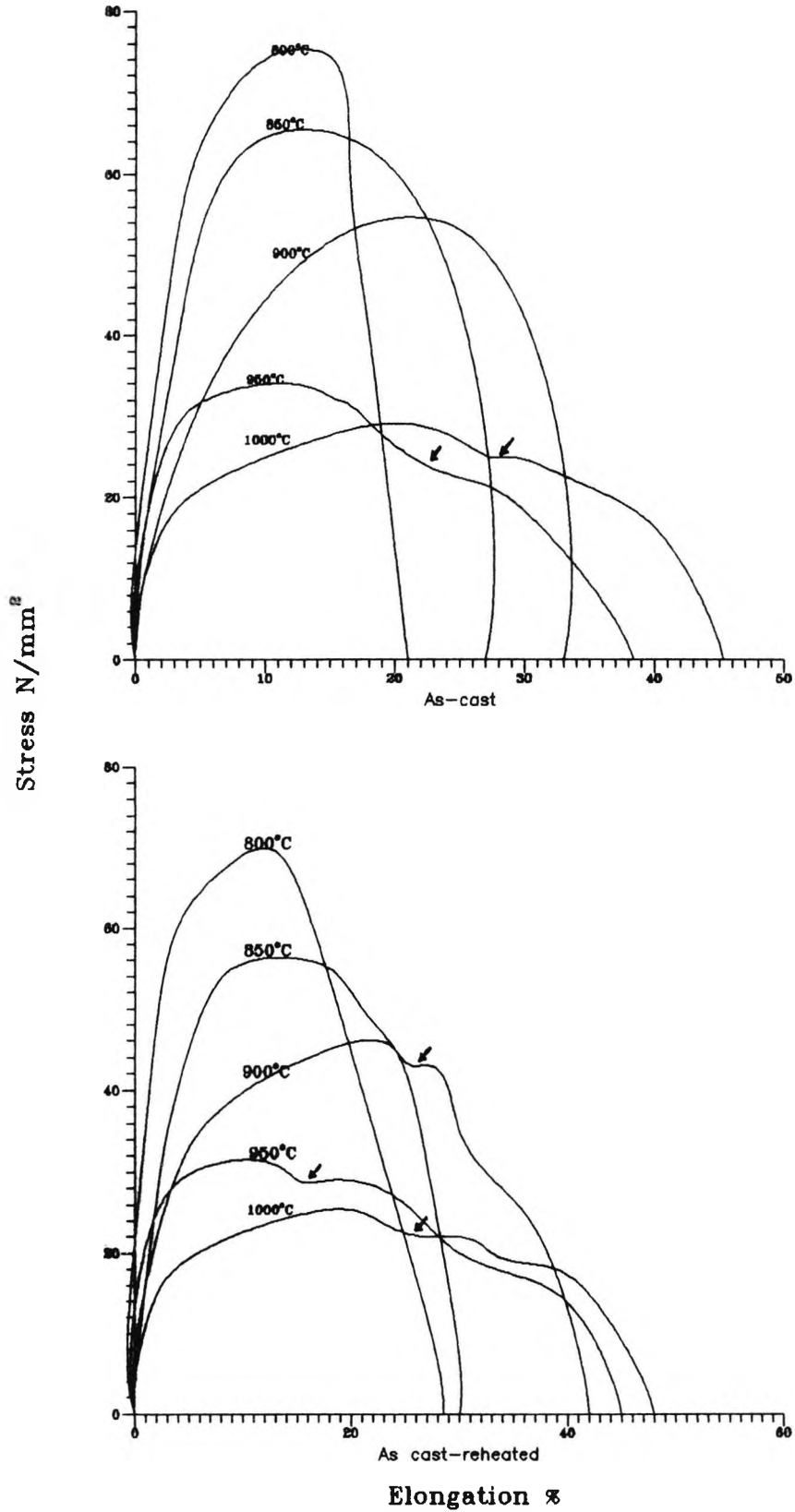


Fig. 4.9 Stress/Elongation curves for Ca free C-Mn-Al steel (C).
 (Arrows indicate dynamic recrystallization).

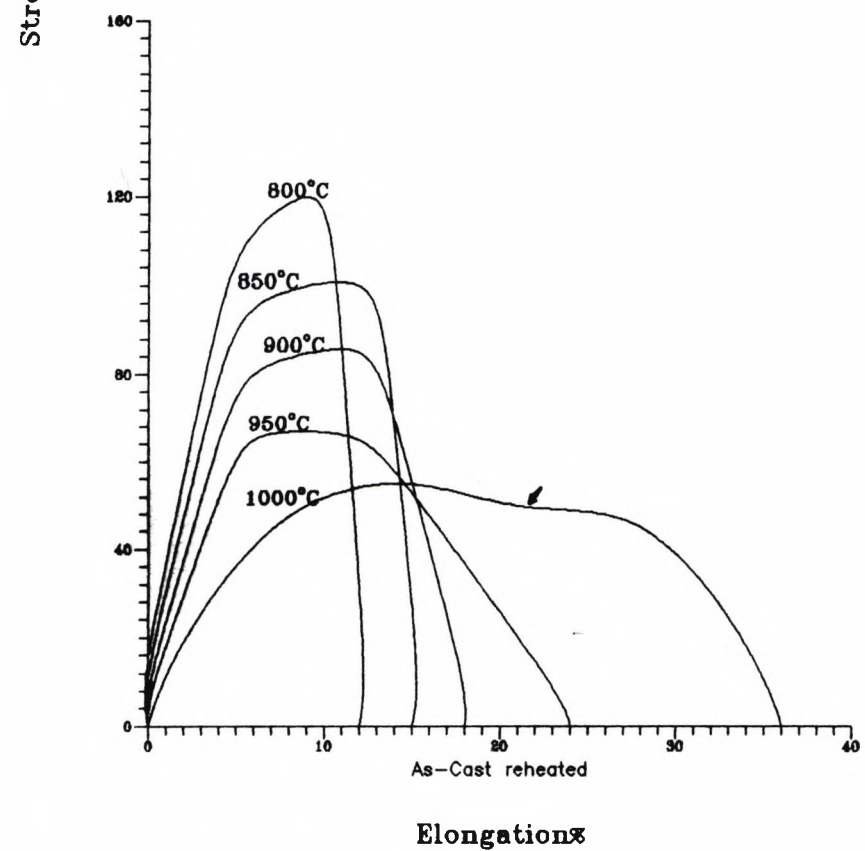
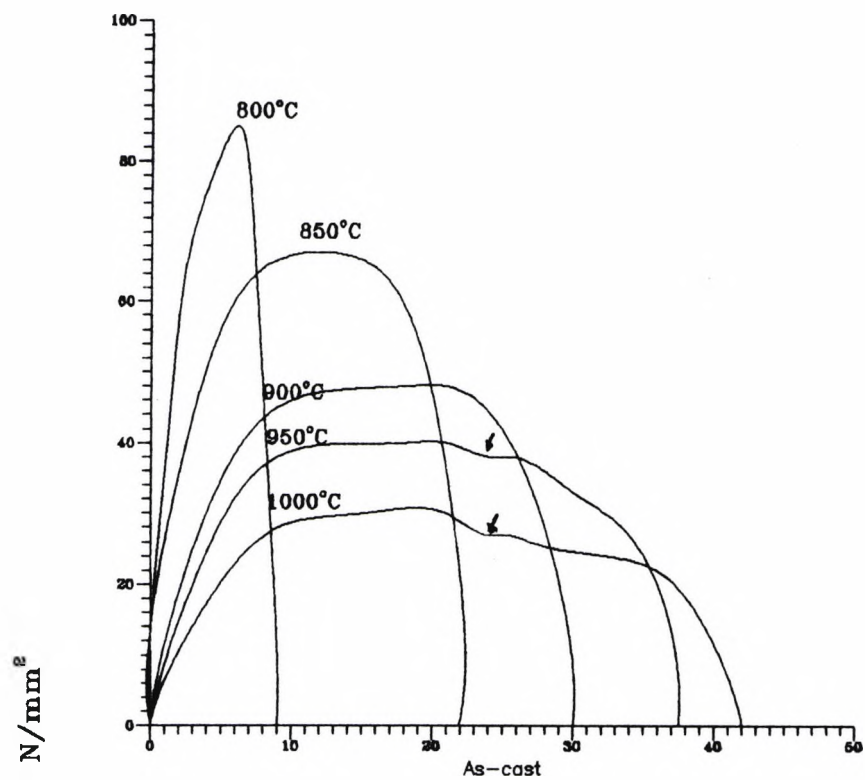


Fig 4.10 Stress/Elongation curves for Ca free High S, C-Mn-Al steel (B).
(Arrows indicate dynamic recrystallization).

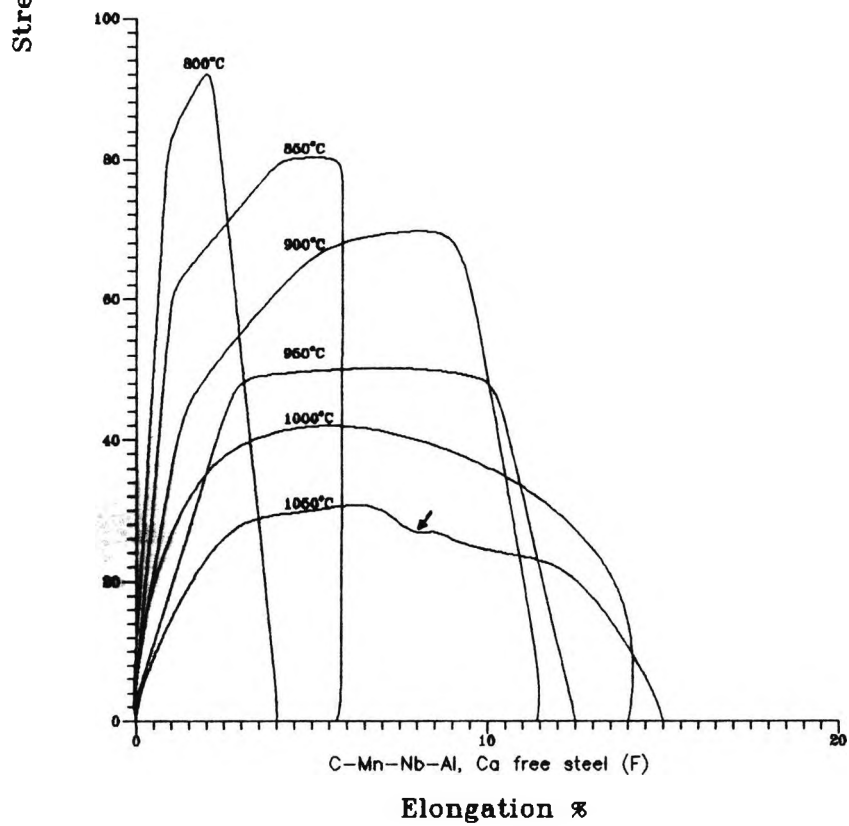
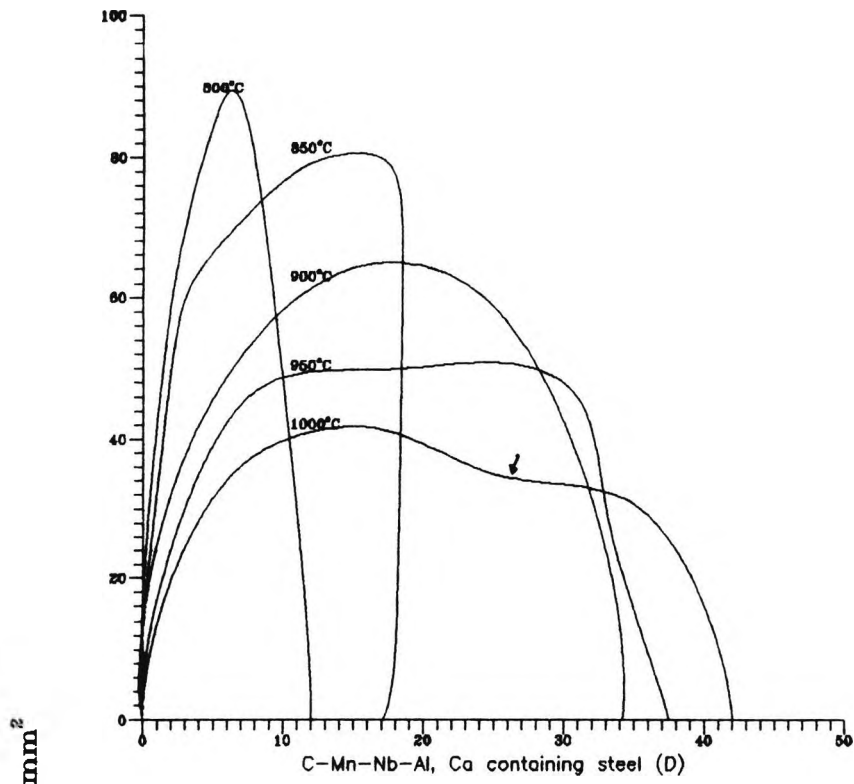


Fig 4.11 Stress/Elongation curves for as-cast C-Mn-Nb-Al steels.
(Arrows indicate dynamic recrystallization).

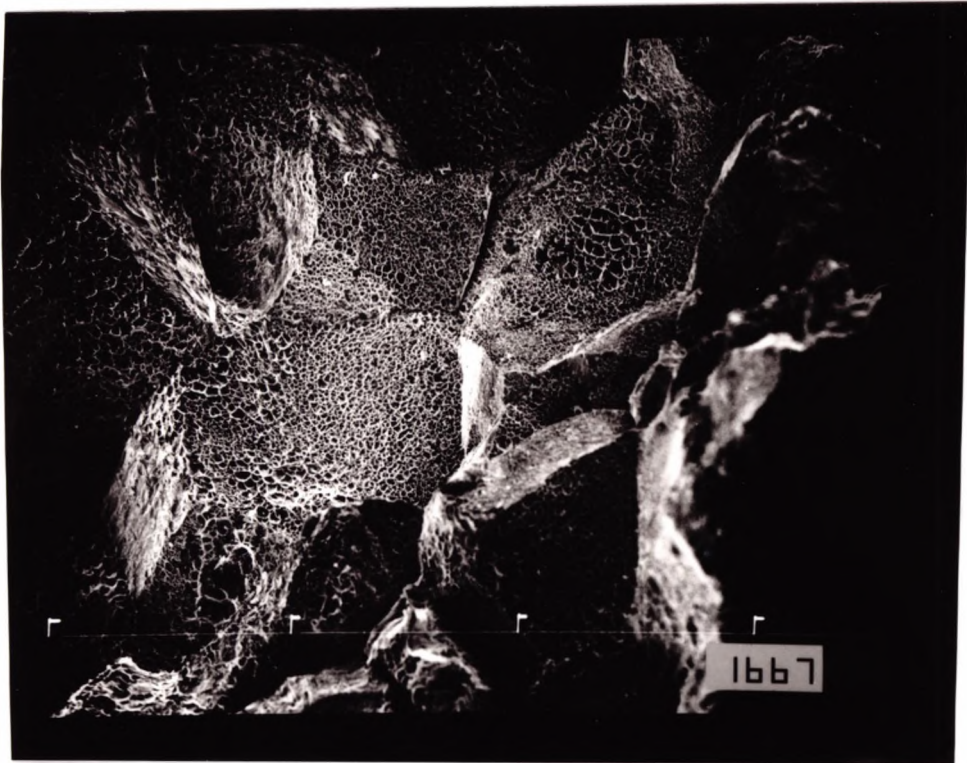


Fig. 4.12 Fracture surface of as-cast C-Mn-Al steel tested at 900°C showing intergranular micro-void coalescence and intergranular decohesion (steel C).

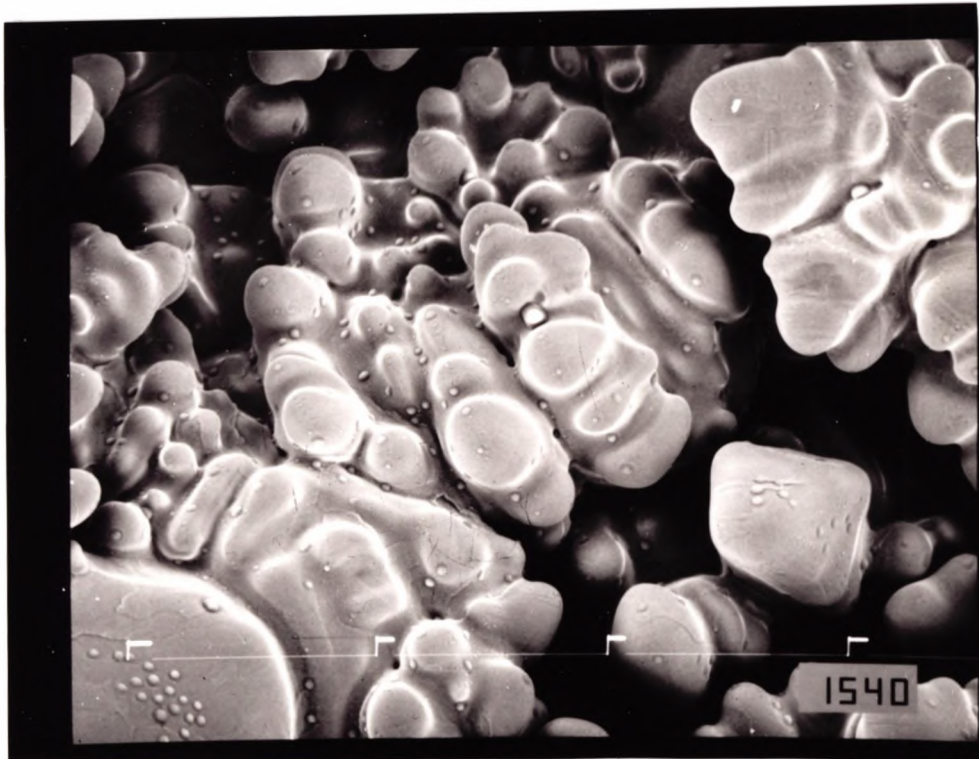
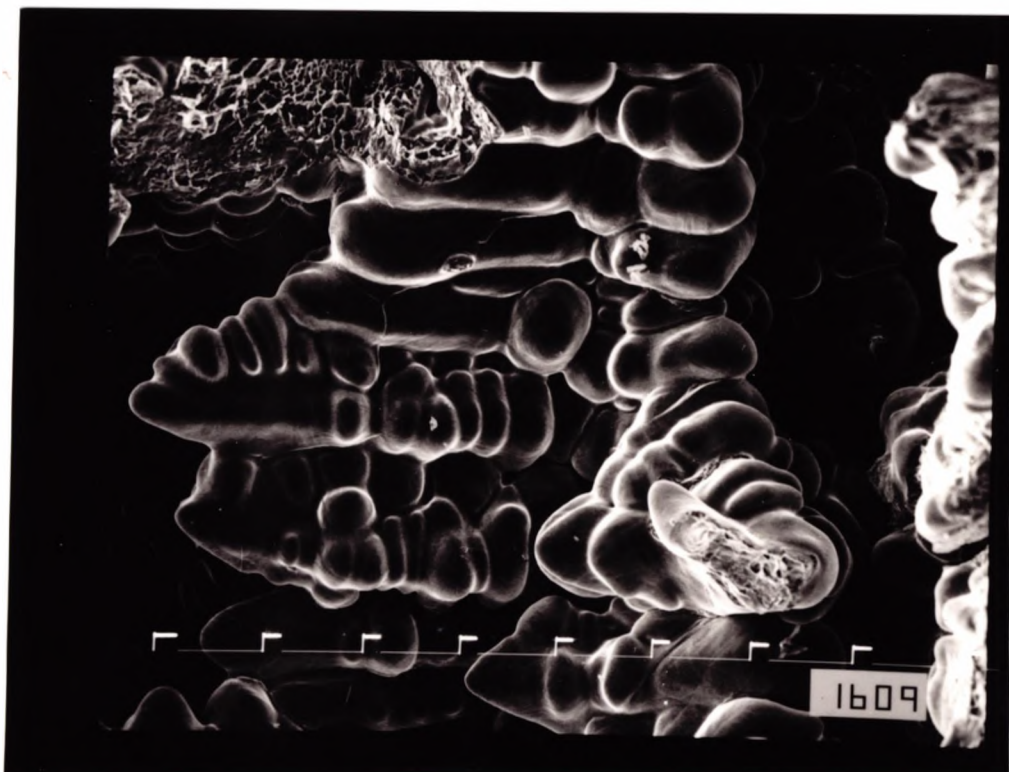
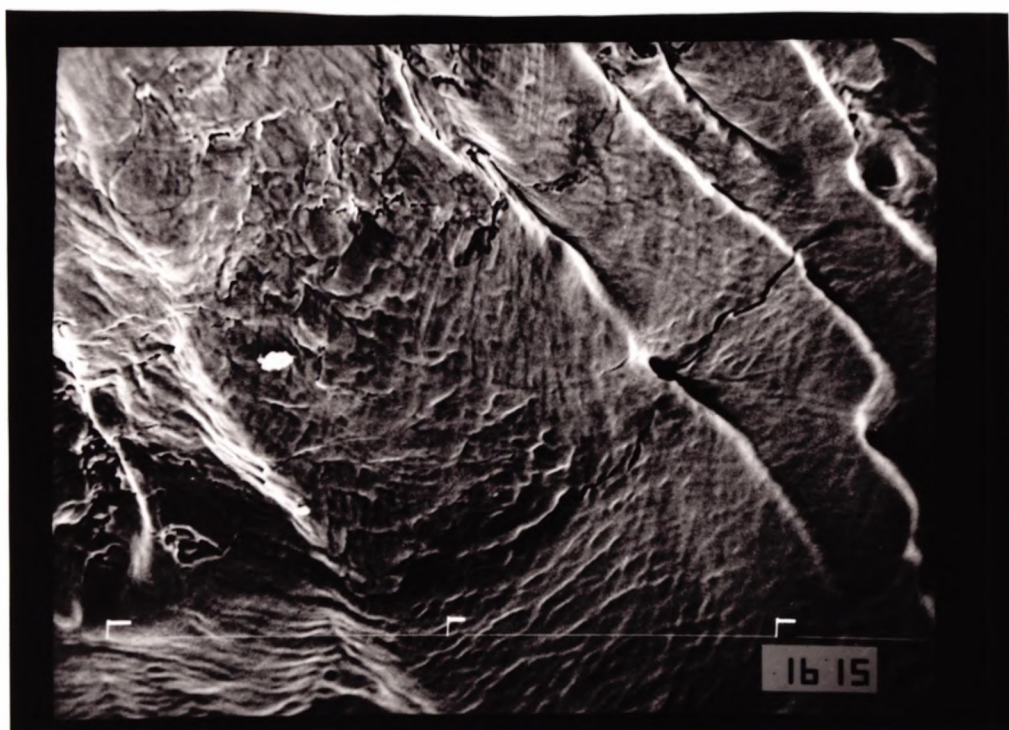


Fig. 4.13 Typical dendritic region found on fracture surface of as-cast C-Mn-Al steel, steel (C), tested at 750°C.



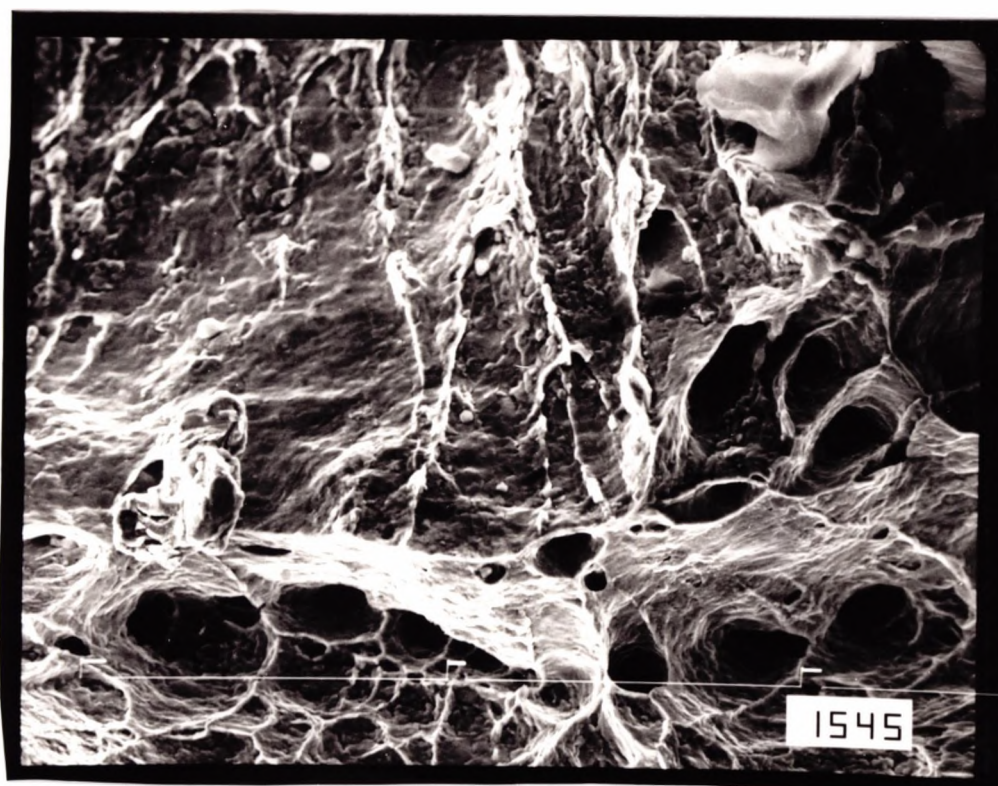
66 μm

Fig. 4.14 Dendritic failure in C-Mn-Al steel as-cast and reheated and tested at 800°C, steel (C).



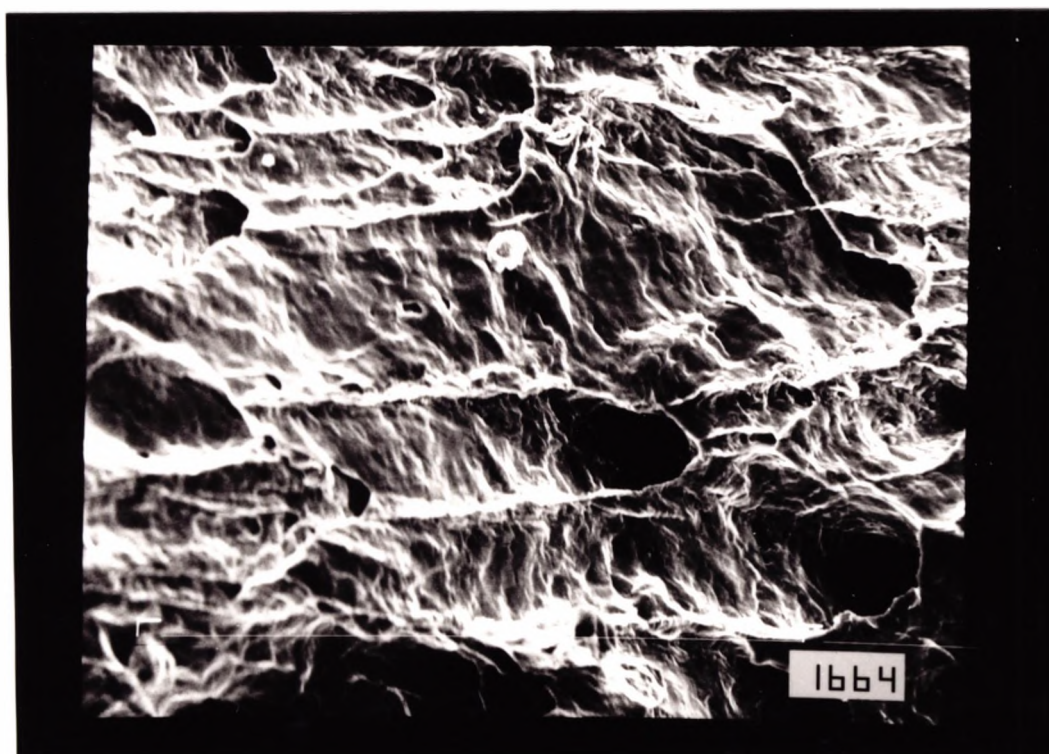
20 μm

Fig. 4.15 Fracture surface of as-cast C-Mn-Al steel showing grain boundary sliding, steel (B) tested at 900°C.



20 μm

Fig. 4.16 Ductile mixture of interdendritic and ductile voiding fracture observed in C-Mn-Al-Ca steel (A) tested at 850°C.



20 μm

Fig. 4.17. Interdendritic fracture in as-cast calcium containing steel (A), tested at 850°C.

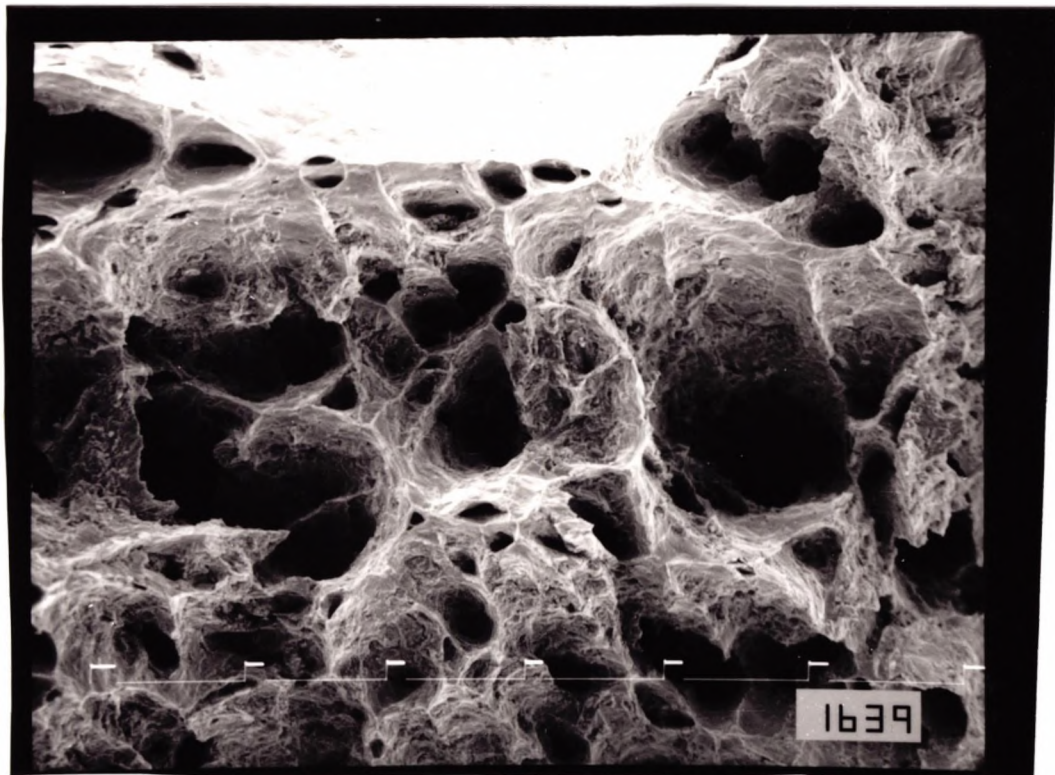


Fig. 4.18 Fracture surface of as-cast reheated C-Mn-Al-Ca steel (A) showing high temperature ductile rupture fracture, steel tested at 850°C.

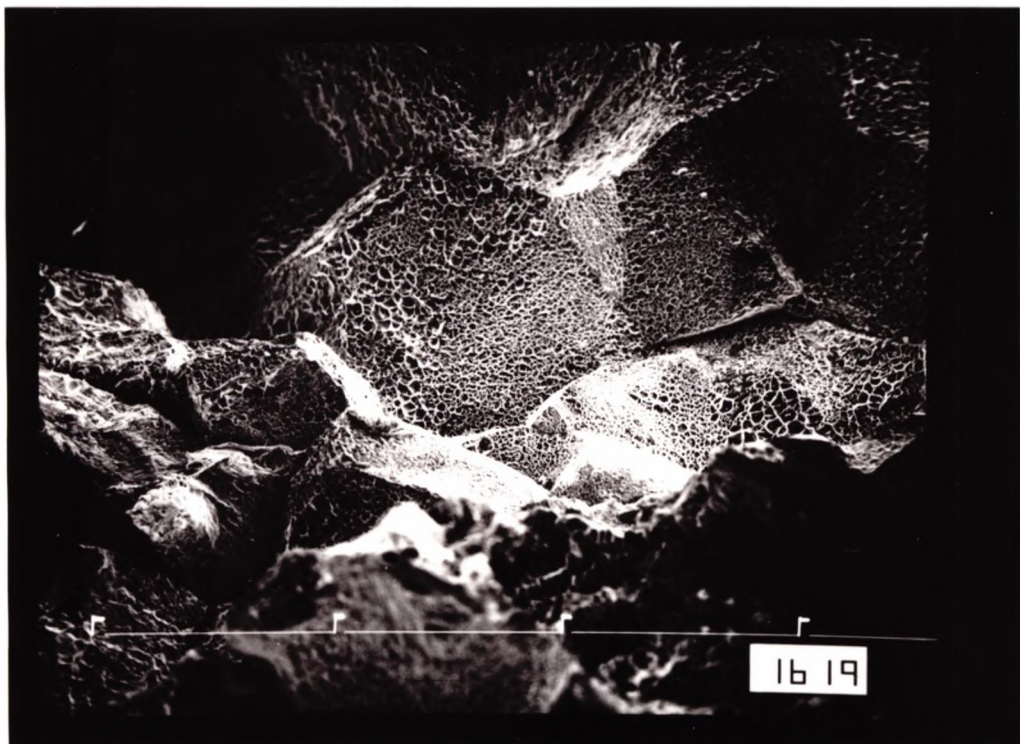
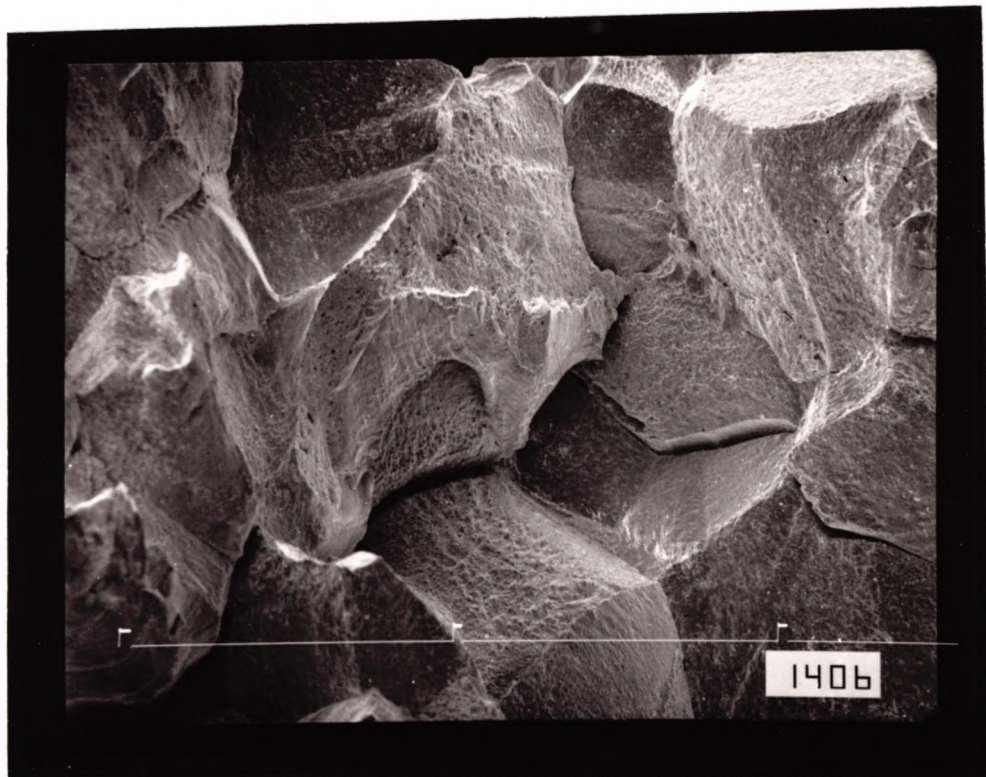
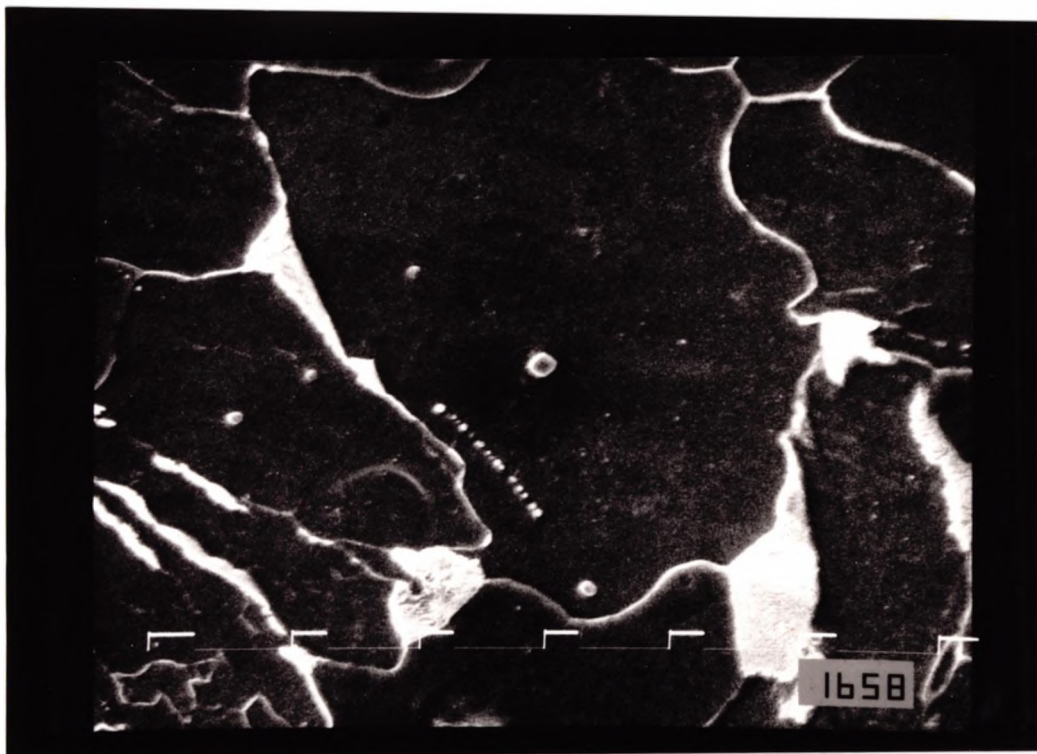


Fig. 4.19 Fracture surface of as-cast C-Mn Nb-Al steel (D) tested at 800°C. Showing a mixture of intergranular micro-void coalescence and intergranular decohesion.

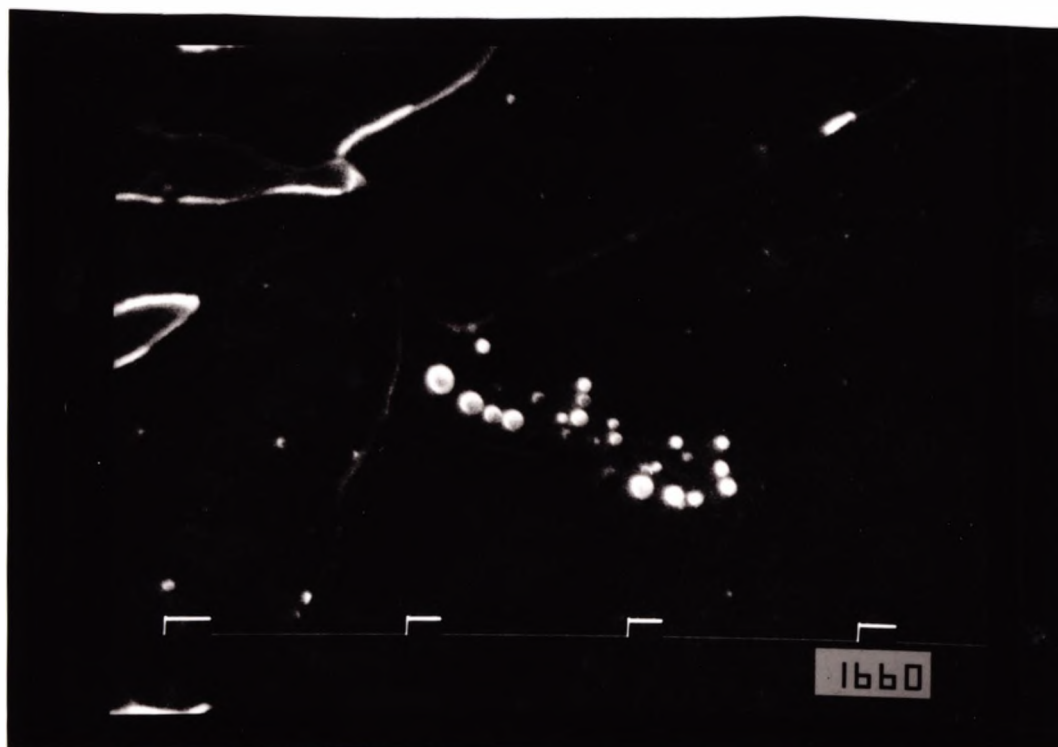


100 μm

Fig. 4.20 Fracture surface of the Ca containing as-cast C-Mn-Nb-Al steel (D) tested at 800°C, showing intergranular fracture due to grain boundary sliding.

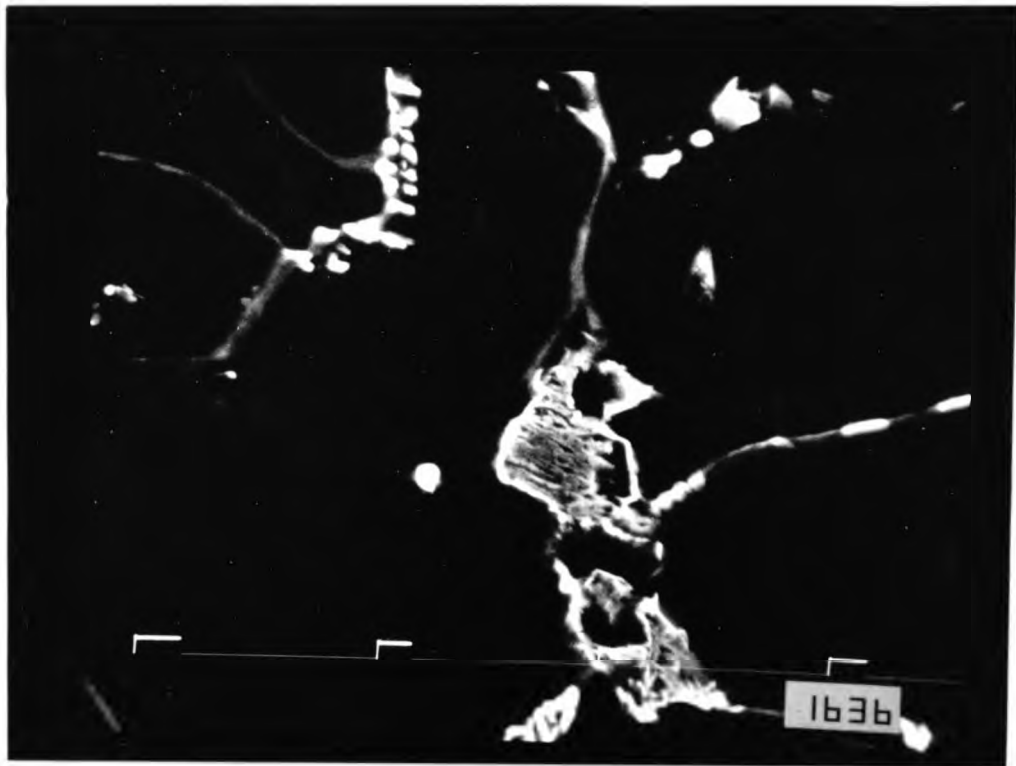


5 μm



3 μm

Fig. 4.21 Sulphide inclusions found in C-Mn-Al steel. The steel was as-cast and reheated, and tested at 900°C, (steel B).



3 μm

Fig. 4.22 Isolated inclusions in Ca containing steel, in as-cast reheated conditions, steel (A), tested at 900°C.

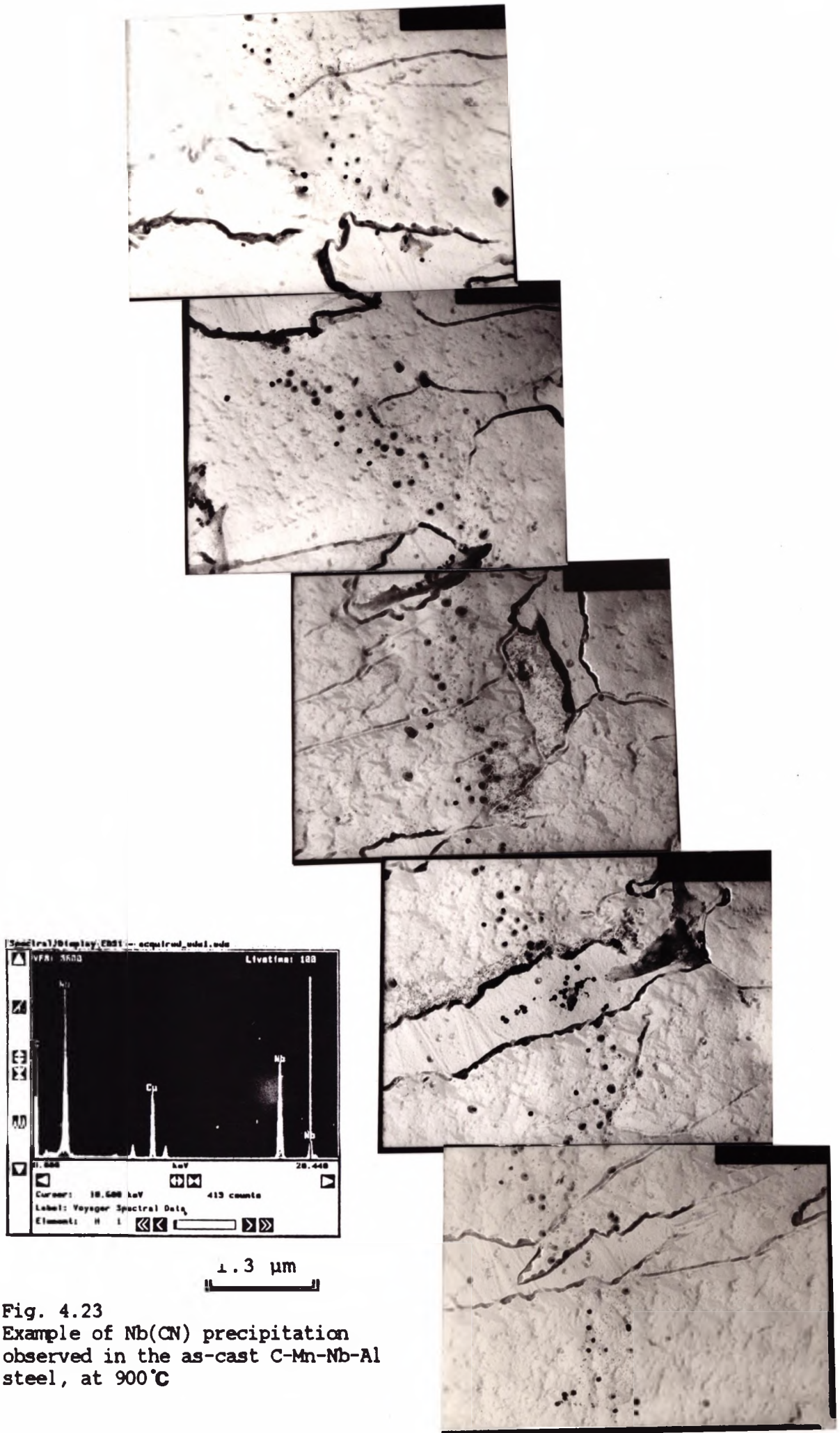
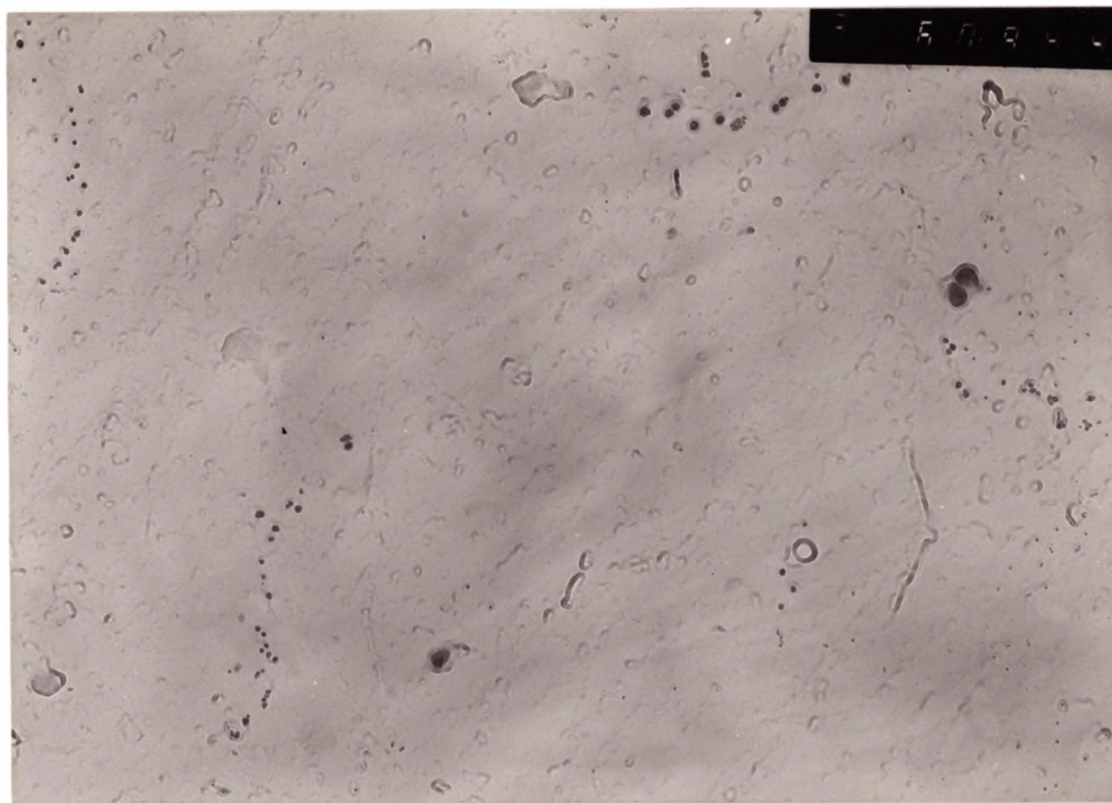


Fig. 4.23
 Example of Nb(CN) precipitation
 observed in the as-cast C-Mn-Nb-Al
 steel, at 900°C



0.5 μm

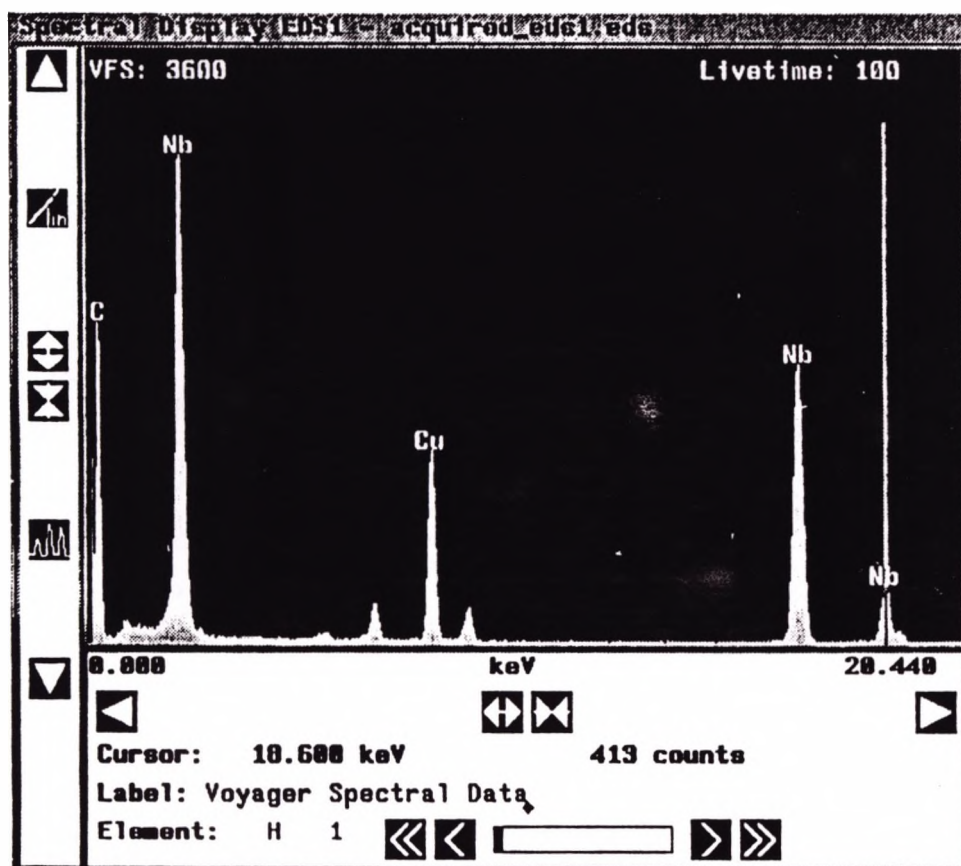
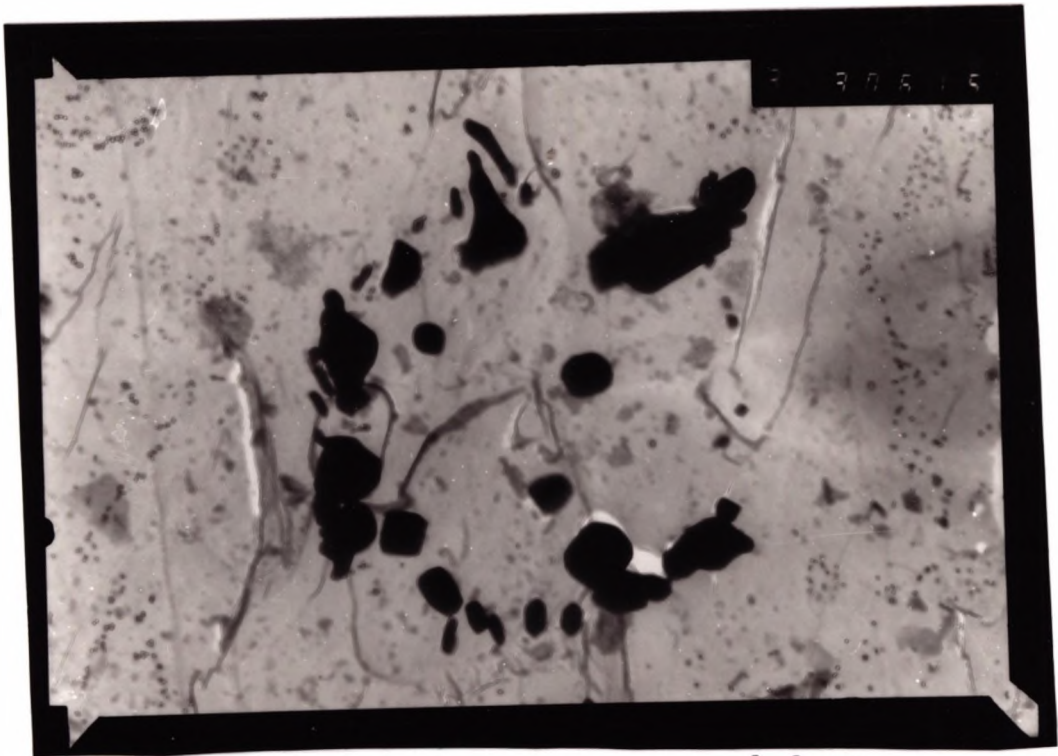
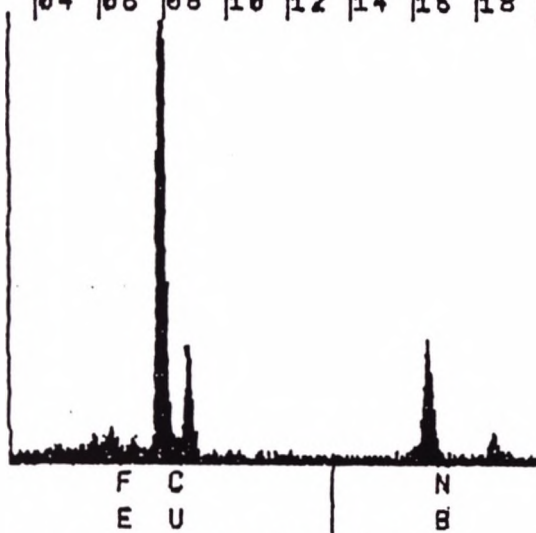


Fig. 4.24 Nb(CN) observed at sub-boundaries in the Ca treated steel, steel E tested at 800°C.



1.2 μm

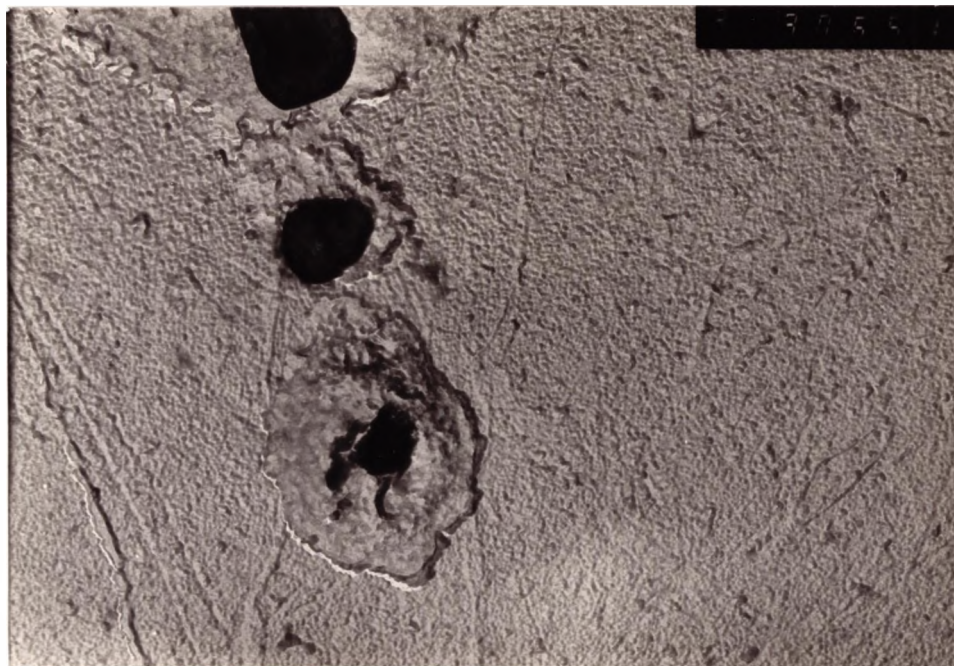
30-APR-90 03:46:58 EDAX READY
 RATE: 19CPS TIME: 4LSEC
 00-20KEV: 10EV/CH PRST: OFF
 A: B:
 FS= 1086 MEM: A FS= 100
 |04 |05 |08 |10 |12 |14 |16 |18 |20



CURSOR (KEV)=13.440

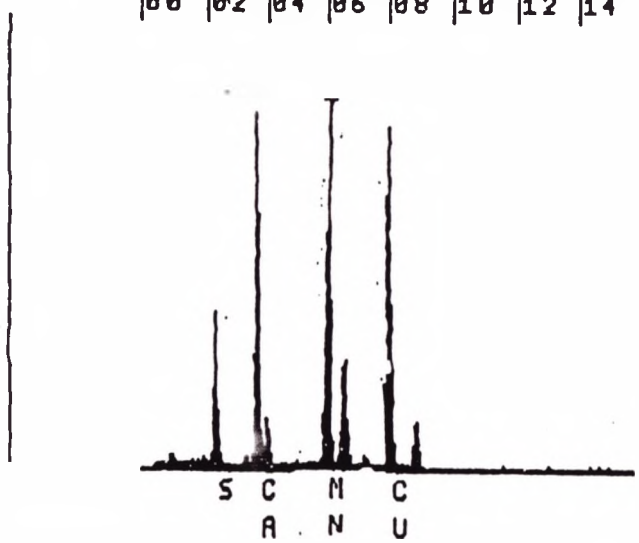
EDAX

Fig. 4.25 NbCN eutectic observed in the Ca treated steel, steel (G) tested at 900°C.



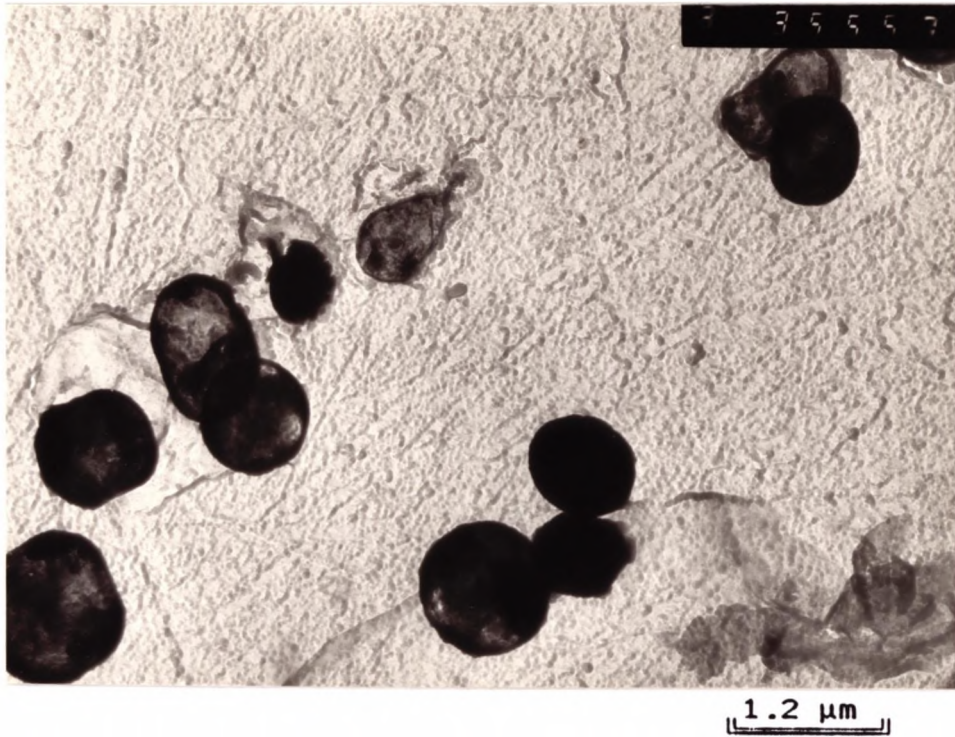
1.3 μ m

09-MAY-90 07:17:11 PEAK IDENT
 RATE: 2185CPS TIME: 104LSEC
 00-20KEY: 10EV/CH PRST: OFF
 A: B:
 FS= 2433 MEM: A FS= 200
 |00 |02 |04 |06 |08 |10 |12 |14



CURSOR (KEY)=06.160 EDAX

Fig. 4.26 CaS inclusions observed in the as cast steel A, tested at 900°C.



22-JAN-90 12:03:21 EDAX READY
 RATE: 103CPS TIME: 37LSEC
 00-20KEY: 10EV/CH PRST: OFF
 A: B:
 FS= 200 MEM: A FS= 200
 |02 |04 |06 |08 |10

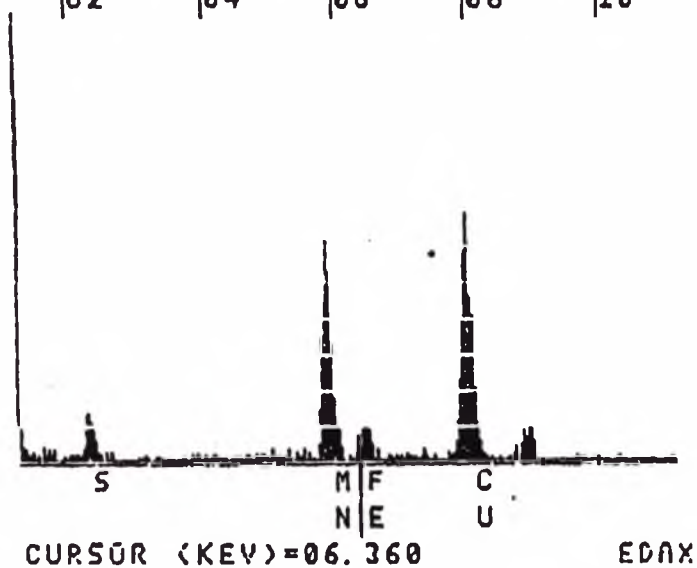
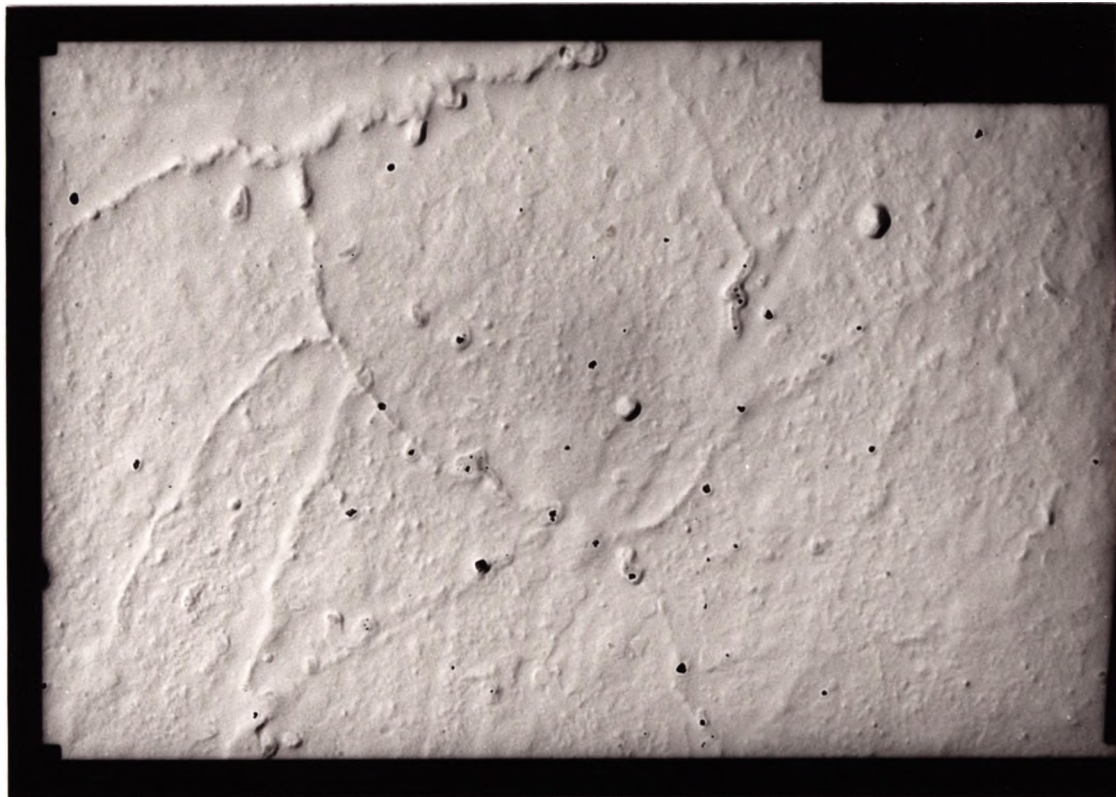


Fig. 4.27 MnFeS inclusions found in as-cast steel (B), tested at 900°C.



1.2 μm

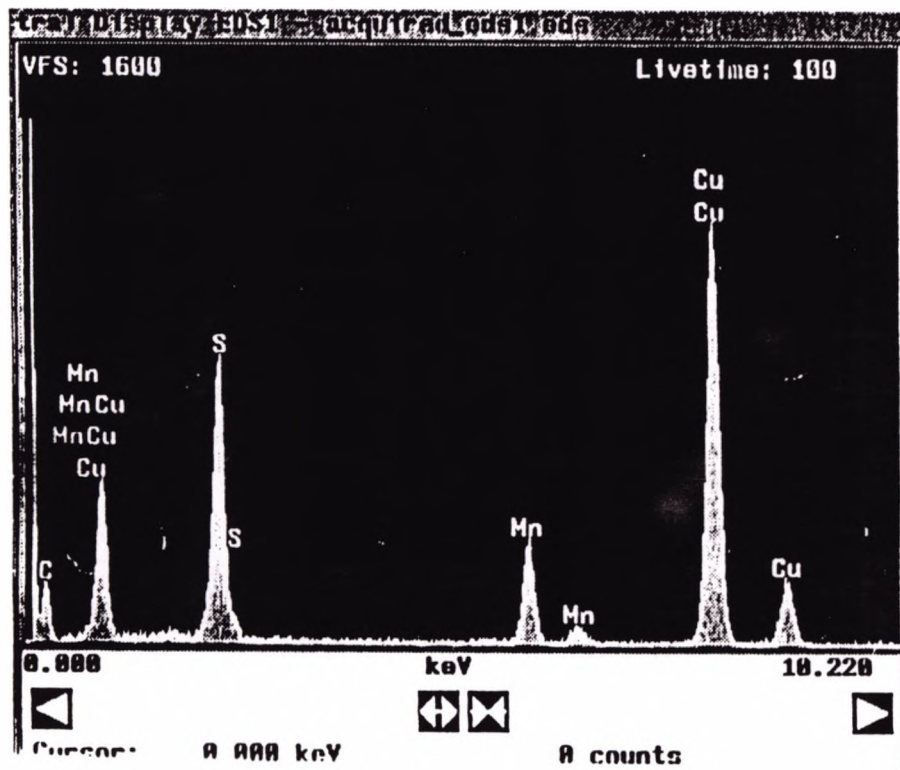


Fig. 4.28 Fine sulphide inclusions found in as-cast and reheated steel (B), tested at 800°C.

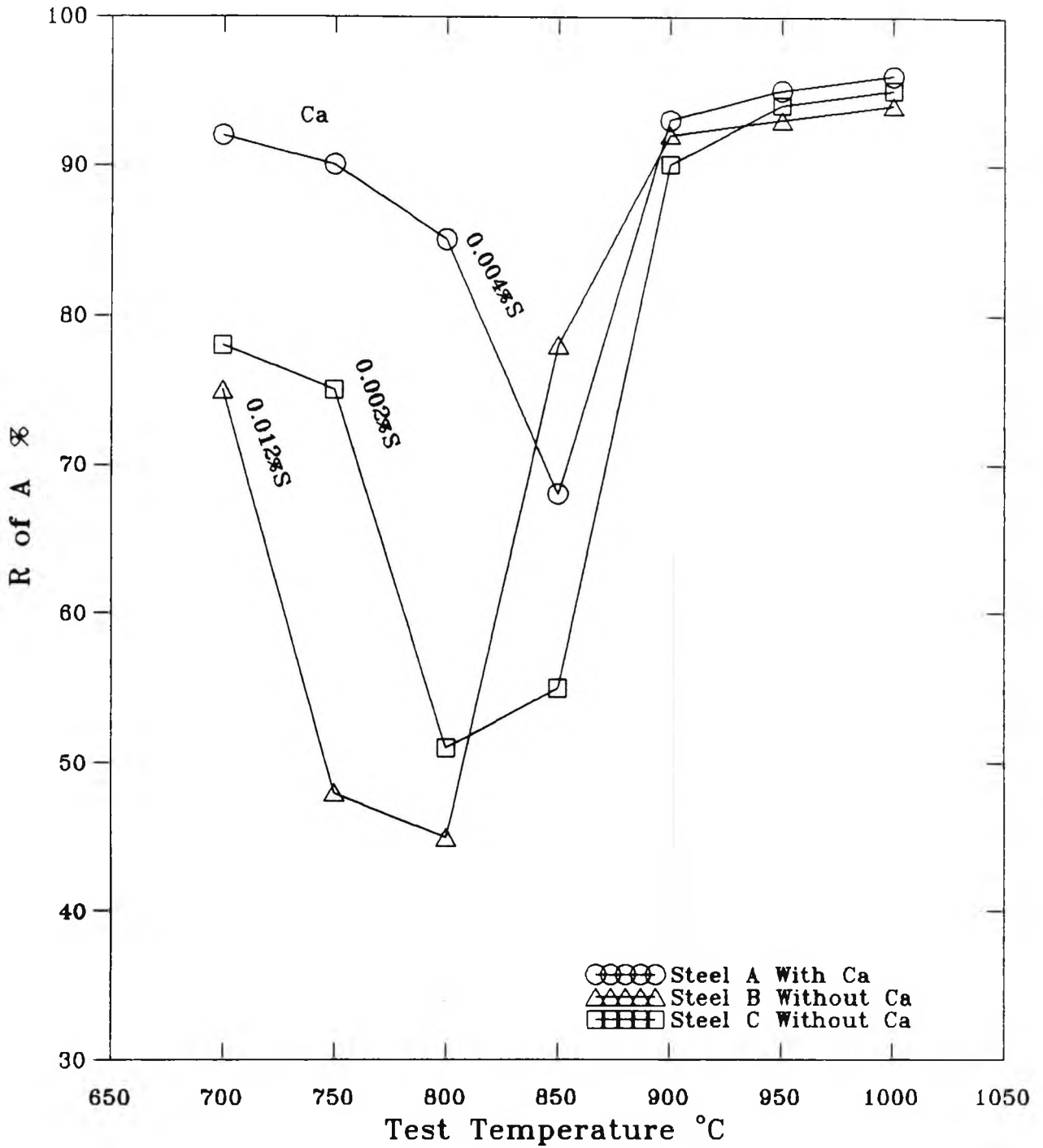


Fig 4.29 Hot ductility curves for the C-Mn-Al steels with without calcium. Steel solution treated and cooled to the test temperature. (After Mintz et al 1989).

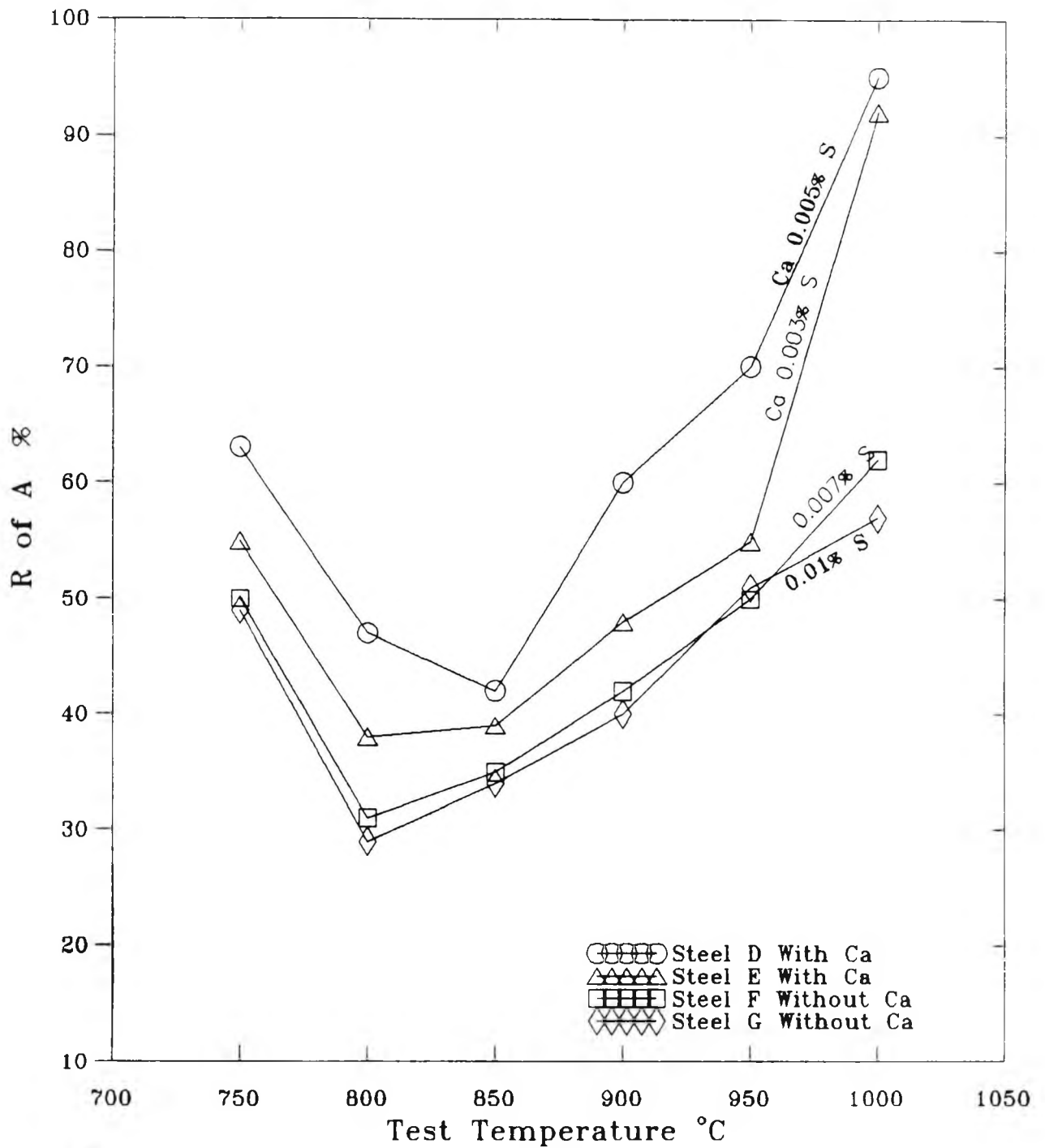


Fig. 4.30 Hot ductility curves for the C-Mn-Nb-Al steels with and without calcium. Steel solution treated and cooled to the test temperature. (After Mintz et al, 1989).

CHAPTER _____ 5

THE INFLUENCE OF S AND Nb ON THE
HOT DUCTILITY OF AS CAST STEELS.

5.1 INTRODUCTION

Micro alloying steels (particularly Nb-Al steels) generally have deeper and wider troughs than found in plain C-Mn steels. There have been numerous investigations into establishing the cause of this behaviour. Mintz and Arrowsmith, (1979) and Wilcox and Honeycombe, (1980) have shown that this marked fall in ductility is a result of precipitation generally Nb(CN) and also occasionally AlN, at the γ grain boundaries.

The majority of tensile testing has been carried out under conditions in which the steel after processing is reheated above the solution temperature of the micro-alloying steel precipitates ($\sim 1300^\circ\text{C}$) and then cooled to the test temperature in the range 700 to 1300°C . Cooling conditions are chosen to be similar to those encountered during continuous casting and the strain rate for the tensile testing is chosen to approximate to that undergone at the surface of the strand when it is straightened ($3 \cdot 10^{-3} \text{ s}^{-1}$). These conditions, are of course, very different from those experienced during continuous casting. The thermal cycling (i.e the rise and fall in temperature) which occurs as the strand moves between the rolls introduces thermal stresses and precipitation patterns which are not produced in the simple tensile test. Also the presence of columnar grains at the slab surface which could aid the propagation of the cracks, and the segregation of elements such as P and S to the

interdendritic boundaries are not re-produced in the simple tensile test.

Recent work by Mintz et al, (1986) found that the hot ductility for C-Mn-Nb-Al steels after casting is better than after hot rolling and solution treatment, They suggested that in as-cast tensiles, the Nb precipitates in a coarse form as a eutectic, so there is less Nb available to precipitate in a fine detrimental form at the γ grain boundaries on cooling to the test temperature. Major differences can therefore exist between as-cast material and solution treated steel and these differences will influence the hot ductility.

Two elements which can emphasize this difference in behaviour are S and Nb. For example, Mintz et al, (1986) found there was no influence of S on hot ductility for plates heated to the solution temperature, whereas it can be seen from chapter (4) that adding Ca to the as-cast steel which removes S improves hot ductility. Guo et al (1988) have also shown that the S is detrimental to as-cast hot ductility causing both a deepening and a shifting of the ductility trough to higher temperatures.

Again Nb additions are well known to increase the tendency for transverse cracks to form, (Mintz and Arrowsmith, 1979; Hannerz, 1985; Ouchi and Matsumoto, 1982). There ^{are} ~~is~~ however some conflicting ideas about the effect Nb has on as-cast hot ductility. Guo et al, (1988)

have found little influence of Nb up to 0.04% although higher additions were detrimental to the hot ductility. This contrasts with the result in chapter (4) which shows small Nb additions are detrimental to both as-cast and solution treated steels, the latter condition giving the worst ductility.

The aim of this chapter is to obtain a clearer understanding of the importance of S and Nb on the hot ductility of as-cast C-Mn-Nb-Al steels. Such information is required because it is the C-Mn-Nb-Al grades of steel which are most prone to transverse cracking.

5.2 EXPERIMENTAL

The steels were supplied as vacuum melts and hot rolled to 12 mm thick plate. The compositions of all steels examined are given in table 5.1.

Tensile samples having a length of 70 mm and diameter 7.94 mm were machined from the plates with their axis parallel to the rolling direction. Details of the tensile samples and melting technique can be found in chapter 4.

Samples were melted at 1540°C for 5 minutes, re-solidified and cooled to the required test temperature in the range 750°C to 1000°C. The cooling rate to the test temperature was 100K/min. After reaching the test temperature, the samples were held for 5 minutes, and then strained using a strain rate of $2 \cdot 10^{-3} \text{ s}^{-1}$.

Carbon extraction replicas were taken close to the fracture surfaces (~1 mm) and examined using both a JEOL 100KV TEM and a JEOL 2000FX Mark 2.

γ grain sizes were determined prior to deforming. Also evidence for dynamic recrystallization was sought from optical micro-structural observations on fractured samples. Fractured surfaces were examined using a JEOL T100 SEM.

5.3 RESULTS

5.3.1 Hot ductility curves

The hot ductility curves of reduction in area against test temperature are given in Fig. 5.1.

The calculated Ae_3 temperature using Andrew's, (1965) formula was approximately the same for all steels, close to 850°C and these temperatures have been marked on the curves.

All the steels show a marked ductility trough but the low Nb, low S, steel (A) gave the better hot ductility. The temperature for minimum ductility was 800°C for all steels. The minimum R.of.A value was 25% in the high Nb, high S, steel (C) compared to 35% in the low S, Nb free, steel (A).

Increasing the S level was found to deepen and widen the trough in both the Nb free steel (D) and Nb containing steel (C).

The high S high Nb, steel (C) showed the worst hot ductility in the temperature range 850°C to 950°C.

5.3.2 Stress/Elongation curves

The load v elongation curves for the four steels are given in Fig. 5.2. The occurrence of dynamic recrystallization can be detected from these curves, either by an abrupt drop in the flow stress or by the oscillations in the flow stress. It would appear from these curves that the temperature for the dynamic recrystallization was 900°C

for the low S Nb free steel, (A), 950°C for both the low S Nb steel, steel (B) and high S Nb free, steel (D), and 1000°C for the high S high Nb, steel (C) as in Fig. 5.2.

5.3.3 Metallography

The austenite grain size for all steels tested was approximately 1.3 mm. Evidence for deformation induced ferrite was found in all steels examined as shown in fig 5.3 and 5.4. for steels (C) and (D).

Metallographic examination of fractured samples from these steels close to the point of fracture confirmed that the lowest temperature for the onset of dynamic recrystallization was about 50°C lower than the temperature obtained from the tensile flow curves Fig. 5.2 in agreement with Cardoso, (1989), as shown in Fig 5.5.

Fracture surfaces at low ductilities were a mixture of interdendritic and intergranular failure. as in Fig. 5.6 Intergranular failure was in turn a mixture of intergranular micro-void coalescence, characteristic of inclusion controlled failure as in Fig. 5.7, and intergranular decohesion, characteristic of failure due to grain boundary sliding, Fig. 5.8. The former is evidenced by the ductile dimples on the fracture surface and contain sulphide inclusions, Fig. 5.9 the latter by the flat, featureless facets Fig 5.8. .It was noted that in a few regions dendrites were also observed as in Fig. 5.10. The last of these occurs as a result of micro shrinkage during

solidification. Examination of these areas gives useful information as to the inclusion distribution. Small spherical sulphide inclusions were observed on the dendrite nodules. Fig 5.10 These particles were also revealed on the polished surface of sectioned fractured samples, Fig. 5.11. Interdendritic failure was also present characterised by elongated granular areas, Fig 5.12

5.3.4 Replica examination

Examination of carbon extraction replica revealed that only very occasionally were AlN precipitates found in any of the steels examined. This is in agreement with previous work by Crowther et al, (1987).

In Nb free steels, (A) and (D) coarse MnFeS were found at the interdendritic boundaries Figs. 5.13 and 5.14. and a very fine matrix precipitation of Fe-Oxysulphide was also often present near the boundaries. Raising the S level increased the volume fraction of both the coarse sulphide and the fine matrix Fe-Oxysulphides. These fine Fe-oxysulphide precipitates are shown in Figs. 5.15 and 5.16

In the Nb containing steels (B) and (C), extensive Nb(CN) was found to be present in a fine form in the matrix, Figs 5.17 and at the prior γ grain and sub-boundaries Figs. 5.18 and 5.19. Some of the precipitates were found to be Nb(CN) which had precipitated out on the MnFeS inclusions as in Fig 5.20. Coarse Nb(CN) eutectics were also observed, Fig 5.21. Also coarse MnFeS eutectics were observed in the high sulphur steels, Fig. 5.22.

5.4 DISCUSSION

5.4.1 Hot ductility behaviour of C-Mn-Al Steels.

It is clear from the present results that reducing the sulphur level in as-cast C-Mn-Al steels improves hot ductility (steels A and D in Fig. 5.1). Intergranular failure in C-Mn and C-Mn-Al steels has been shown to be generally transformation induced, Crowther and Mintz (1986), and occurs when a thin film of ferrite forms around the γ grain. As the ferrite is the softer of the two phases strain concentration takes place in this film causing voiding round the MnS inclusions situated at the boundaries. Thus an increase in sulphur content will increase the volume fraction of sulphides at the γ boundaries and would be expected to encourage intergranular failure. The thin films of ferrite which form have been shown to be deformation induced and form at temperatures up to the Ae_3 , Crowther and Mintz, (1986). Ferrite formed prior to test in coarse grained steels also forms thin films, (Crowther and Mintz, 1986; Maki et al, 1985) and is likely to be effective in producing intergranular failure, but lowering the temperature below the Ar_3 (undeformed), soon introduces large volume fractions of ferrite reducing the strain concentration at boundaries giving rise to improved ductility. The trough extends from the Ae_3 to 20°C to 30°C below the Ar_3 (Mintz et al, 1991).

In the present instance the calculated Ae_3 temperature

from Andrew's formula, (1965) are similar for all steels- (850°C) and most of the drop in ductility has occurred above the A_{e3} temperature for steels (B), (C) and (D), when the steels are fully austenitic. One possibility to account for this may be that, for as-cast steels, the calculated A_{e3} temperature cannot be used because equilibrium is not maintained at the γ boundaries as intense segregation of elements such as Nb and Al to the dendritic boundaries probably occurs on solidification Turkdogan, (1987). For example, Edwards et al, (1982) have suggested that Al segregation to the boundaries in as-cast steels can raise the A_{e3} temperature there, so that thin films of ferrite form at temperatures much higher than would be normally expected. Unfortunately, the cooling rate after fracture was not fast enough to freeze in the micro-structure at the test temperature, so this possibility could not be examined.

However, even in conditions where no significant segregation of alloying elements has taken place, it is possible to obtain low ductility intergranular failure in the austenite, and failure is then primarily due to grain boundary sliding (Crowther and Mintz, 1986). Again, in chapter (4) there is evidence for S influencing this failure mechanism but how it does so is less clear.

Osinloku et al, (1985) have reported that S segregates to the boundaries and weakens them. Although S does segregate, when a tensile stress is imposed, Nachtrab and Chou, (1986) could find no co-relation between this segregation and the intergranular failure of C-Mn-Al and C-

Mn-Nb-Al steels.

Another more plausible explanation has been suggested by Coleman and Wilcox, (1985) that the fine precipitation of AlN or Nb(CN) pins the boundaries allowing grain boundary sliding to occur and the coarser sulphide inclusions encourage voiding at the boundaries enabling cracks formed by grain boundary sliding to enlarge and link up. In this case it is the sulphides at the boundaries which control intergranular failure in the austenite. For example, for hot-rolled, high Mn steels (1.4% Mn) heated to 1330°C and cooled to the test temperature no influence of S on hot ductility could be found for steels having S levels in excess of 0.002%, Mintz et al, (1986). This arises because, prior to heating, the sulphides are not generally located at the γ boundaries and the amount of S about 0.001%S, which re-dissolves at 1330°C and which controls the subsequent precipitation at the boundaries is very small. Thus, provided the S content is >0.001%, the same amount of S always goes back into solution and re-precipitates in a fine form on cooling to the test temperature. In contrast, in as-cast steels, it is the total S content which is important because the S precipitates at the interdendritic boundaries which later become the γ boundaries. Furthermore, in these as-cast coarse grained steels, dynamic recrystallization is difficult so that very fine precipitation at the boundaries is not needed to prevent the boundaries from migrating, and cracks formed by grain boundary sliding are allowed to develop unhindered.

A further possibility exists in the present examination in that fine Fe-oxysulphides have been observed and behaviour may then be similar to Nb containing steels. Although the discussion has been centred on C-Mn-Al steels, it is clear from Fig. 5.1, that removing the S and or Nb from C-Mn-Nb-Al steels also gives rise to very similar improvements in ductility, and this will be discussed next.

5.4.2 Influence of Nb on hot ductility

It is also clear from Fig. 5.1 that Nb is detrimental to ductility when steels are compared at the same S level. For Nb containing steels, intergranular failure in the high temperature range is invariably by grain boundary sliding in the γ phase, as discussed before in chapter 2. Recent work by Crowther et al, (1986) found that Nb is less detrimental to the hot ductility in the as-cast condition than in the solution treated state. This arises because in the as cast state a large amount of Nb precipitates in a coarse eutectic form, so that the amount of Nb available to precipitate dynamically in a fine detrimental form at the γ boundaries on cooling to the test temperatures will in consequence be much reduced. In addition in the solution treated condition the sulphides in the matrix are able to partially re-dissolve particularly if they are Mn Fe sulphides and the additional S taken back into solution at 1330°C is also able to re-precipitate in a finer form at the γ boundaries.

Mintz and Mohamed, (1989) found for solution treated steel, that the fall in hot ductility in the range 800 to 1000°C corresponded well with the increasing precipitation of NbC predicted from equilibrium solubility calculations, Fig 5.1. These calculations were based on the assumption that the precipitation is so rapid during tensile deformation that it conforms to equilibrium conditions.

Equally good correspondence can be found for the higher S containing steel in this exercise if it is assumed that a

large proportion (~50%) of the Nb is precipitated as the eutectic in a coarse ineffective form prior to testing in the temperature range 800°C to 1000°C, Fig 5.1 (i.e. the Nb level is taken to be 0.015% in the calculations).

The solubility equation for the NbC derived by Irvine et al, (1967) has been chosen for the calculations, although it is appreciated that the precipitate is not NbC but Nb(CN). This simple approach has been found to give good agreement with the experimental results (Mohamed and Mintz, 1989). This equation is:-

$$\log [\text{Nb}] \cdot [\text{C}] = (-6770/T) + 2.26 \quad 5.1$$

Where T is the absolute temperature K

As a sample calculation for a temperature of 1000°C

$$[\text{Nb}] \cdot [\text{C}] = K_s$$

Where K_s is the solubility product and from equation (5.1)

this is 8.749×10^{-4} at 1000°C

To calculate how much C is out of solution (X) combined with Nb the following equation can be used

$$[\text{Total Nb} - 7.75X][\text{Total C} - X] = 8.749 \times 10^{-4}$$

Atomic weight of Nb and C are 93 and 12 respectively.

Hence for NbC there is Wt per cent, 7.75 times as much Nb than C.

Total Nb has been taken as 0.015% and total C is .0.10%

Hence $X = 8.39 \cdot 10^{-4}$ at 1000°C

$$\begin{aligned} \text{Wt per cent of NbC present} &= 7.75 X + X \\ &= 8.75X \end{aligned}$$

as ρ for NbC = 7.6 g/cm³

and ρ for Fe = 7.87 g/cm³

The volume fraction NbC present at 1000°C = $8.75X \cdot \rho_{\text{Fe}} / \rho_{\text{Nb}}$.

The volume fraction NbC present at 1000°C
= $8.39 \cdot 10^{-4} \cdot 8.75 \cdot 1.04 = 7.3 \cdot 10^{-3}$

5.5 CONCLUSIONS

It has ^{been} shown that both Nb and S are detrimental to the hot ductility of as-cast steels, deepening and widening the trough. Nb is, of course added to give grain refinement and/or precipitation hardening in the finished product. S is an impurity and may be reduced, see chapter 4. It is clear from this exercise that Nb and S have a very similar influence on the hot ductility of as-cast steels and a reduction in S level from 0.016%, to 0.002% is almost equivalent to the removal of Nb from the steel. Fortunately, the S levels in the present day high quality HSLA plate steel are continually being reduced not, however, because of the potential benefits to the hot ductility, but to achieve improvements in fracture toughness so that S levels are now often close to 0.002%.

Table 5.1

Composition of Steels Examined wt, %

Code	C	Mn	Si	P	S	Nb	Al	N
Steel A	0.10	1.37	0.30	0.011	0.002	0.005	0.024	0.0040
Steel B	0.10	1.37	0.31	0.011	0.003	0.031	0.025	0.0033
Steel C	0.10	1.43	0.30	0.010	0.016	0.030	0.029	0.0040
Steel D	0.10	1.41	0.29	0.010	0.016	0.005	0.033	0.0040

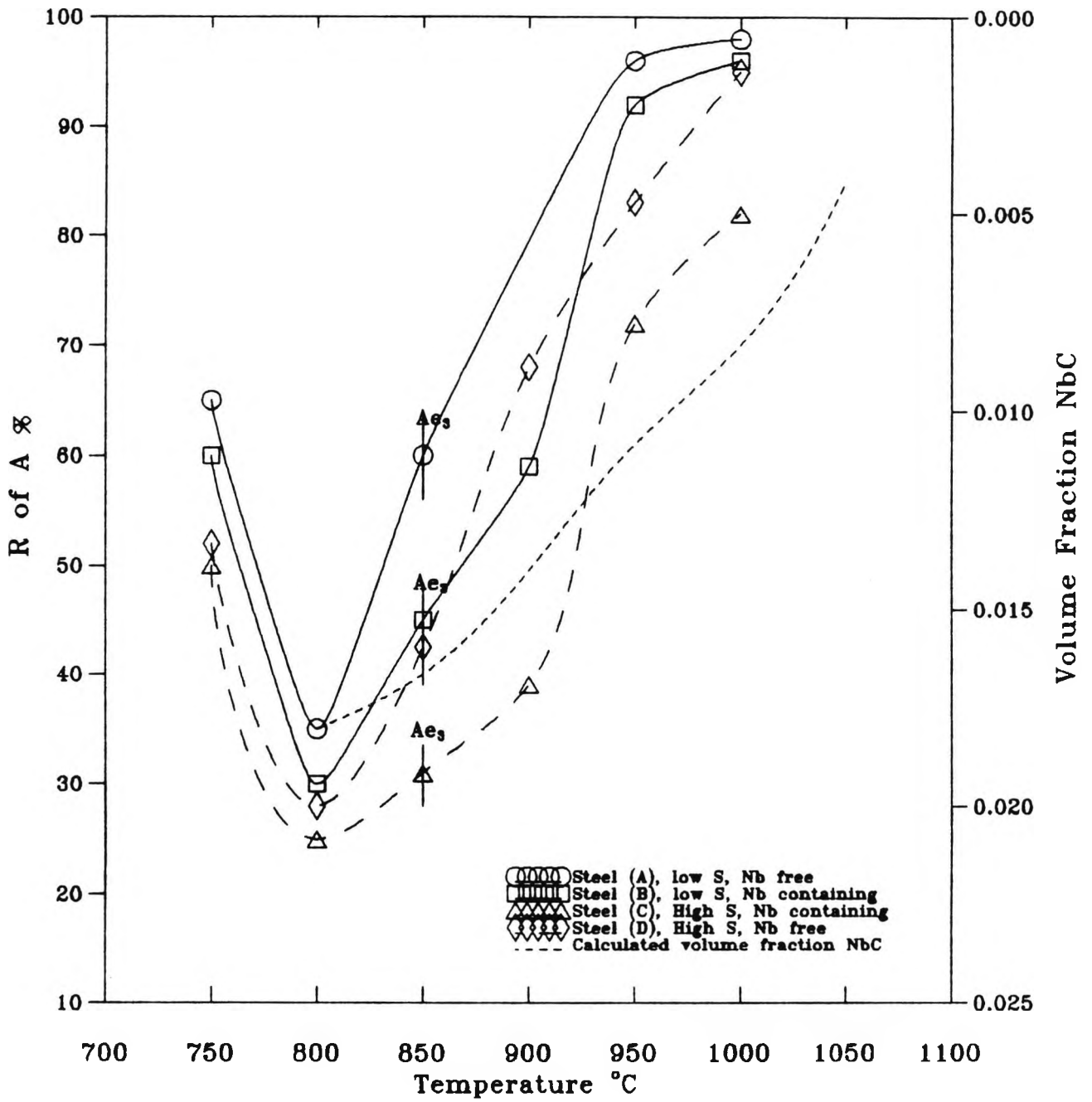


Fig. 5.1 Hot ductility curves for all the steels examined.

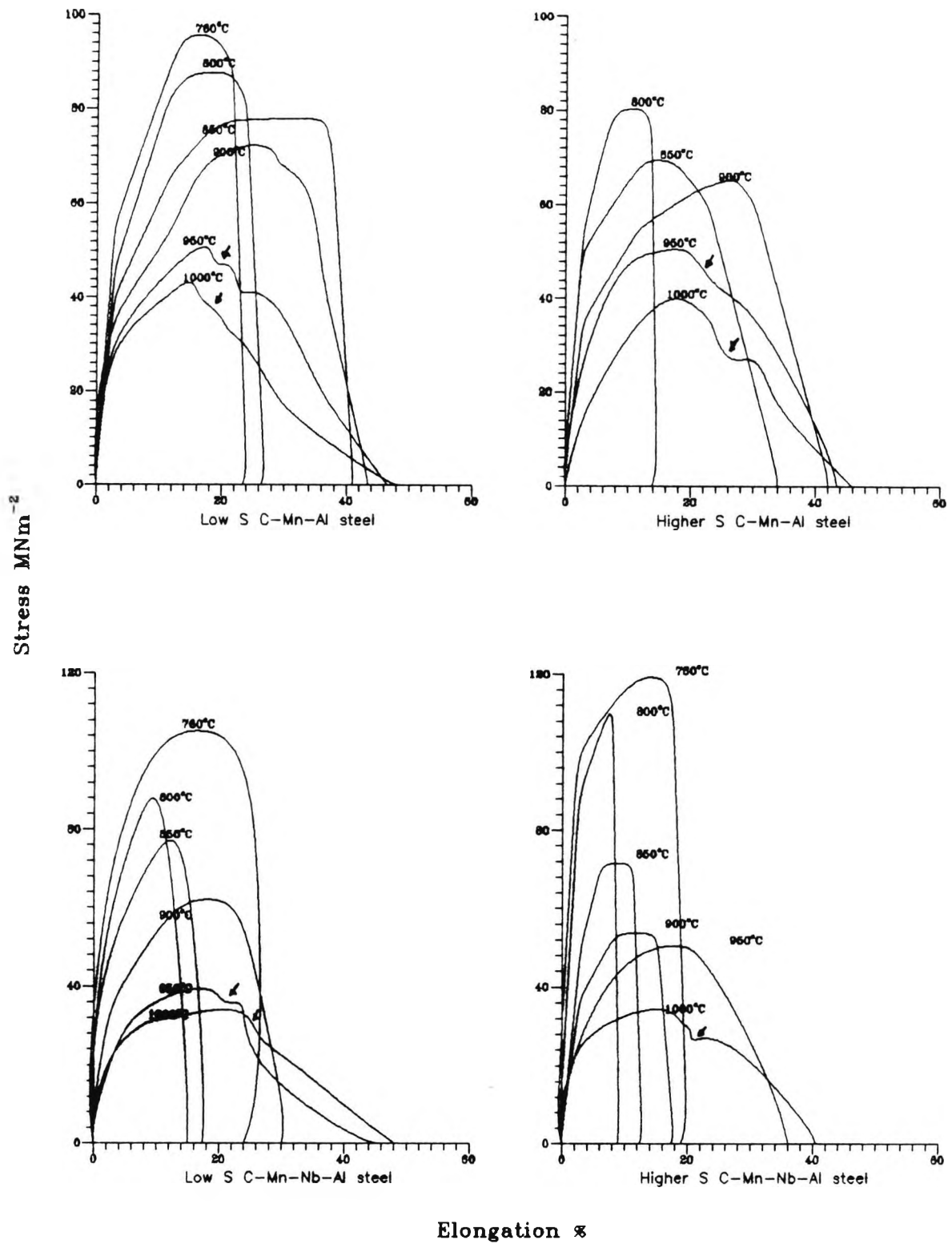
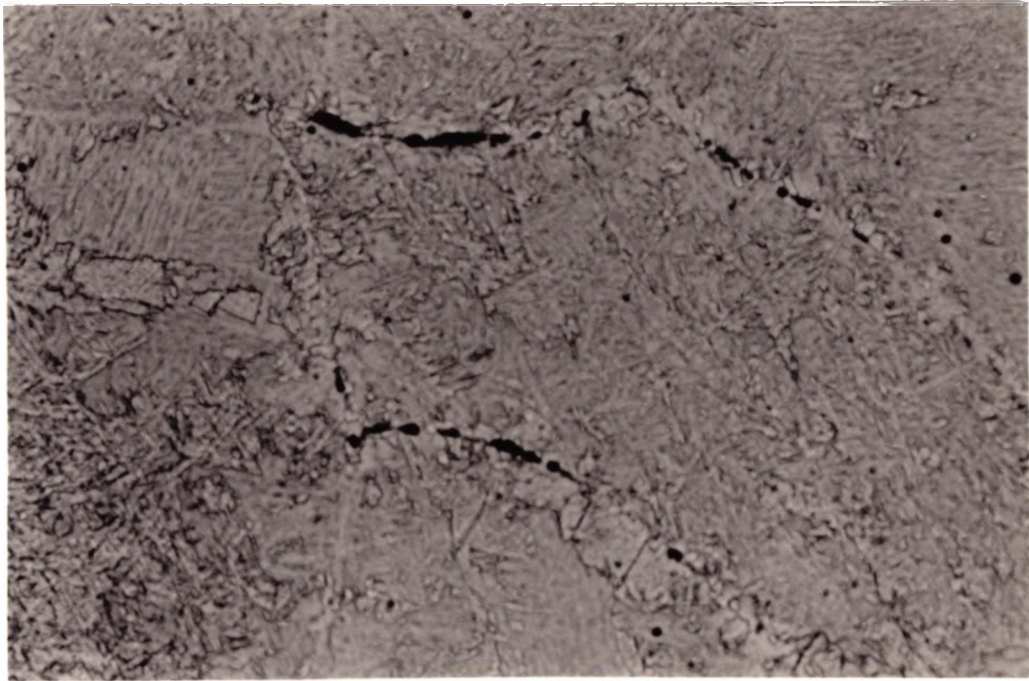


Fig. 5.2 Stress/Elongation curves for all the steels examined.
 (Arrows indicate dynamic recrystallization).



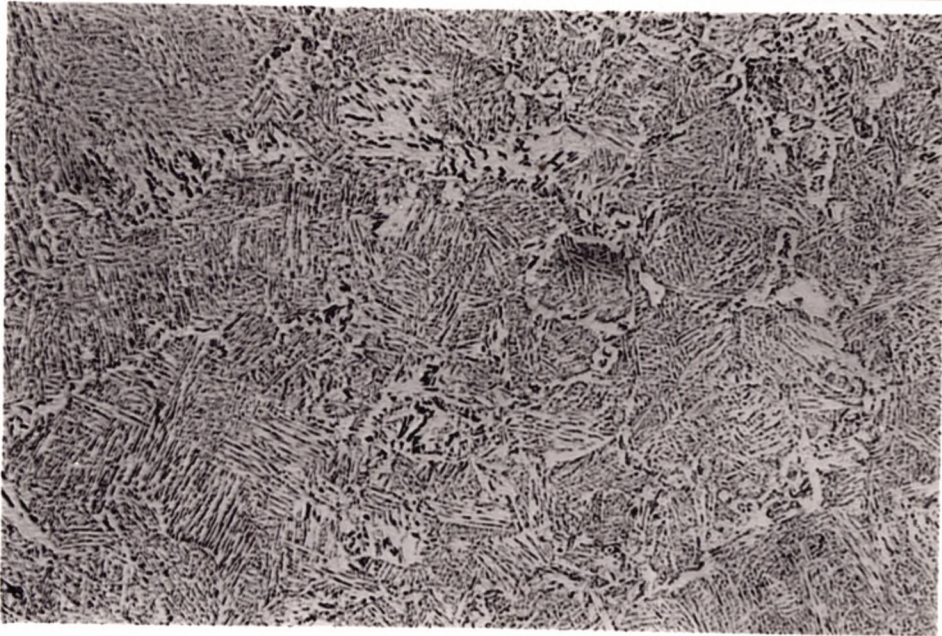
100 μm

Fig. 5.3 Evidence of deformation induced ferrite in low Nb/high S steel (D), tested at 850°C.



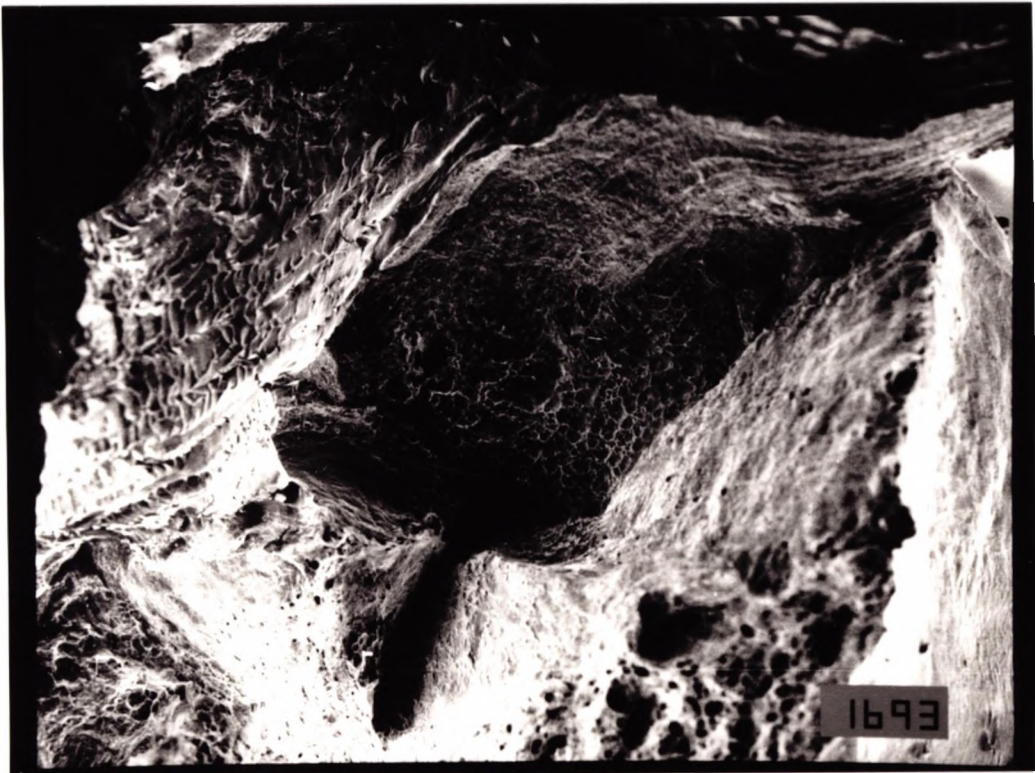
200 μm

Fig. 5.4 Evidence of deformation induced ferrite in high Nb/high S steel (C), tested at 850°C.



200 μm

Fig. 5.5 Evidence of dynamic recrystallization found in steel (D), tested at 900°C.



250 μm

Fig. 5.6 Fracture surface of low S/high Nb, steel (B) showing intergranular micro-void coalescence and intergranular decohesion.

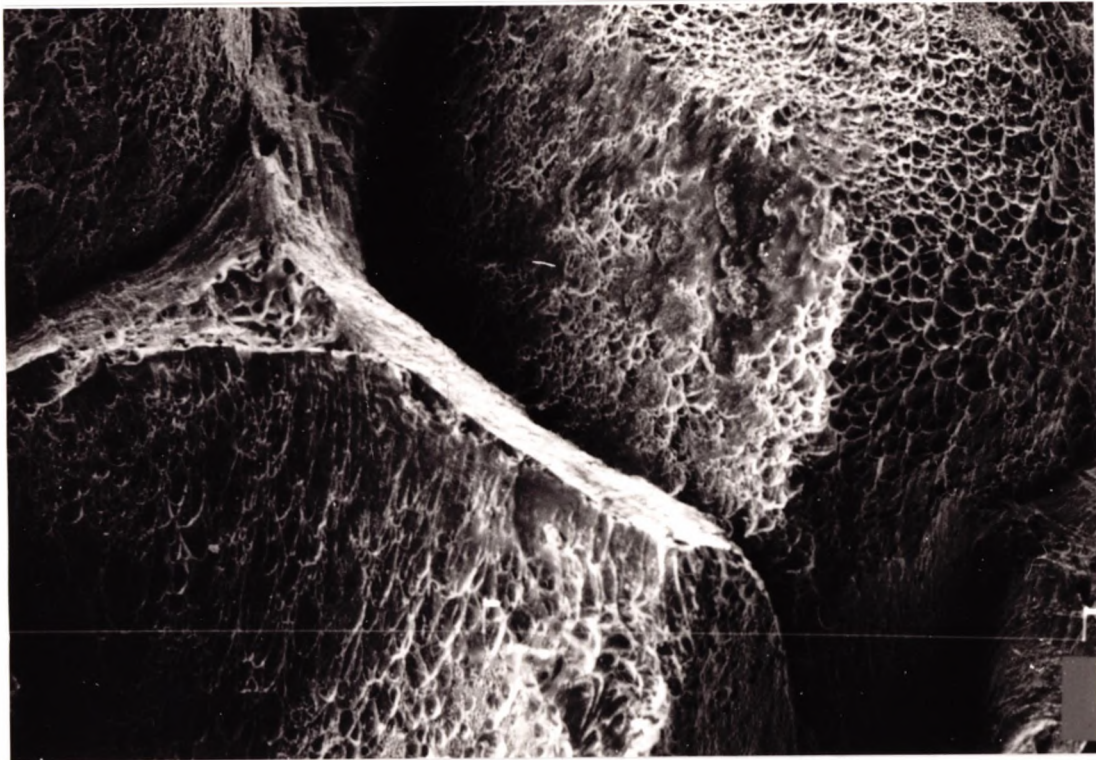


Fig. 5.7 Fracture surface of high S/high Nb steel (C) Showing intergranular micro-voids, steel tested at 800°C.

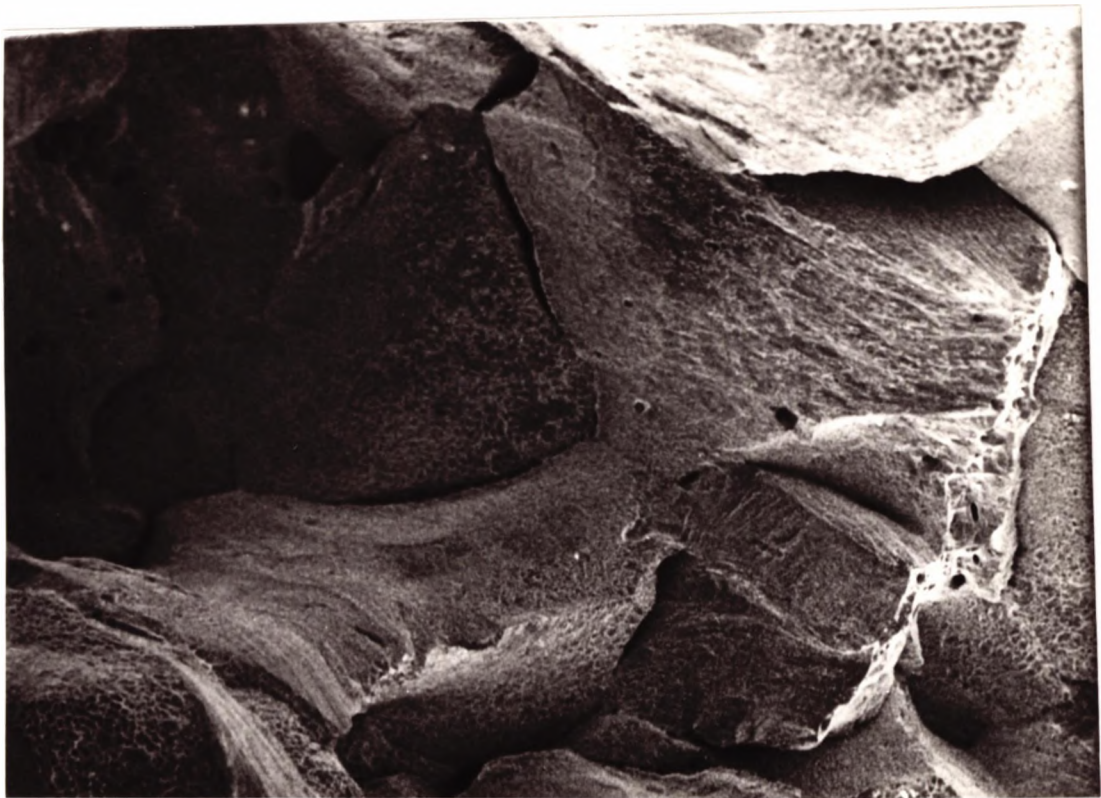
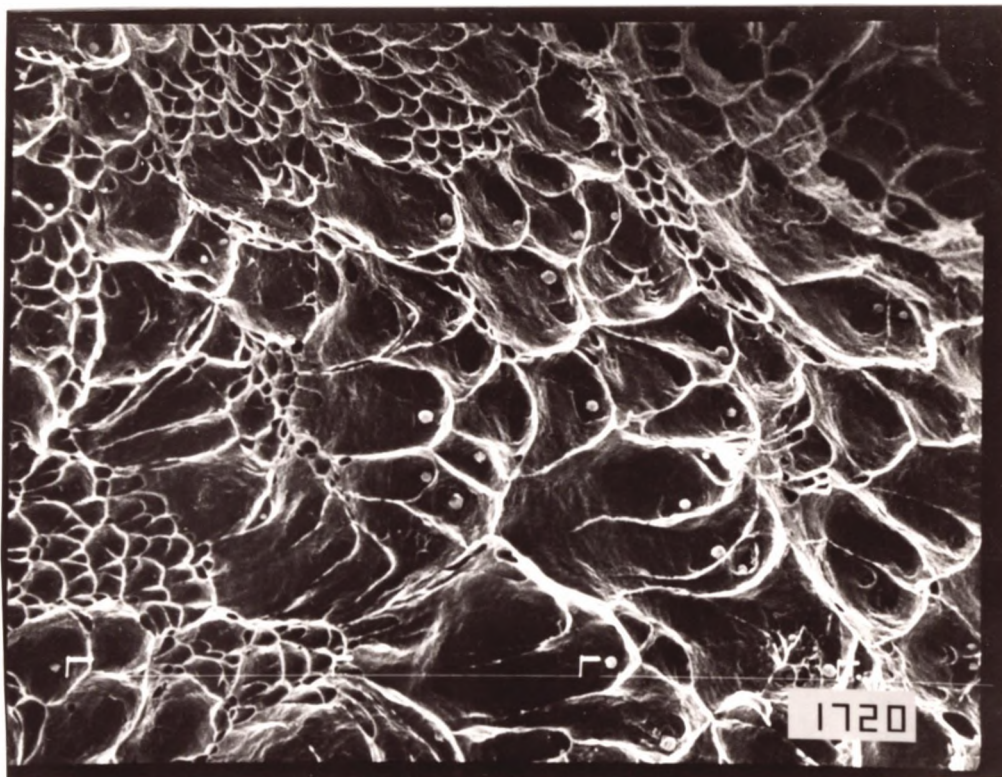
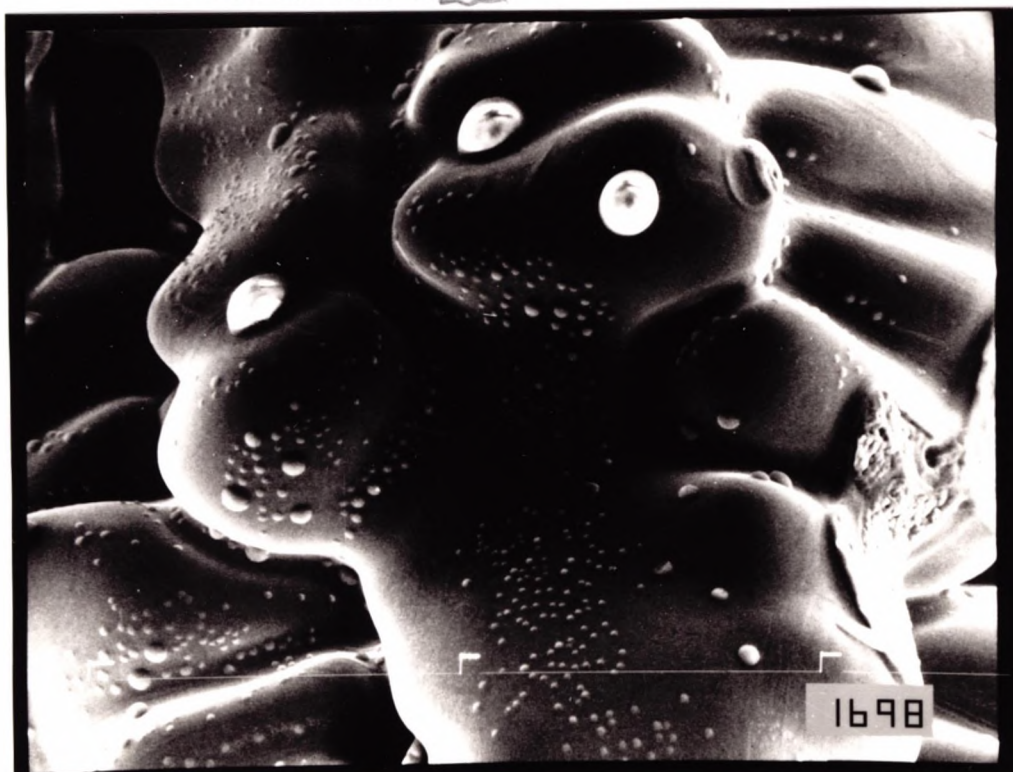


Fig. 5.8 Fracture surface of low S/high Nb, steel (B) Showing grain boundary sliding plus ductile voiding, steel tested at 800°C.



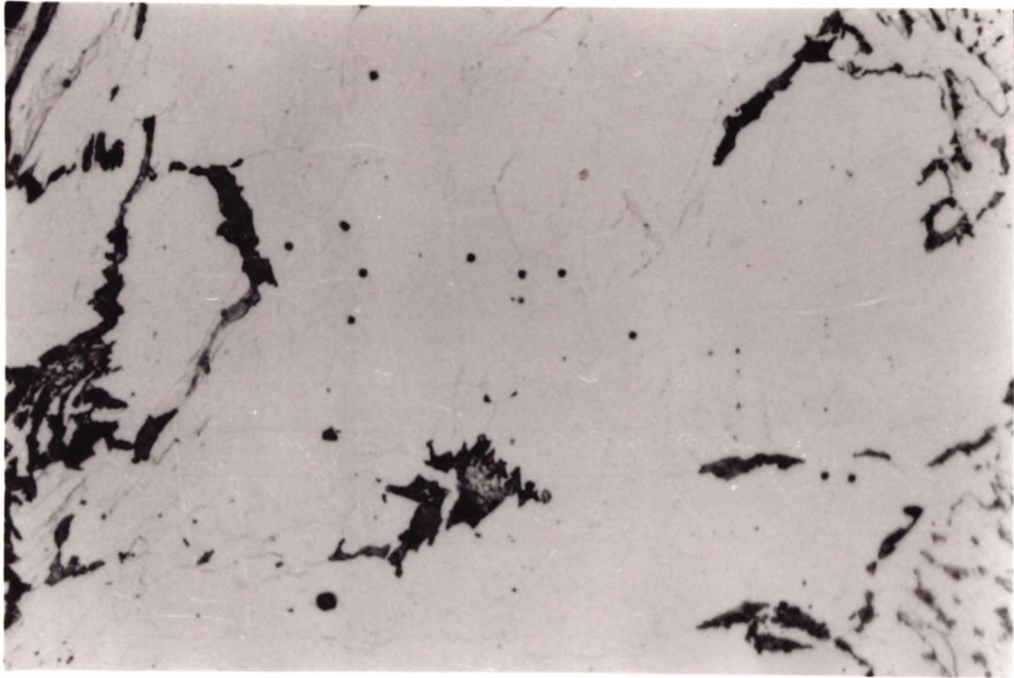
187 μm

Fig. 5.9 Micro-void coalescence around sulphide inclusions observed in high S/Nb steel (C) tested at 800°C.



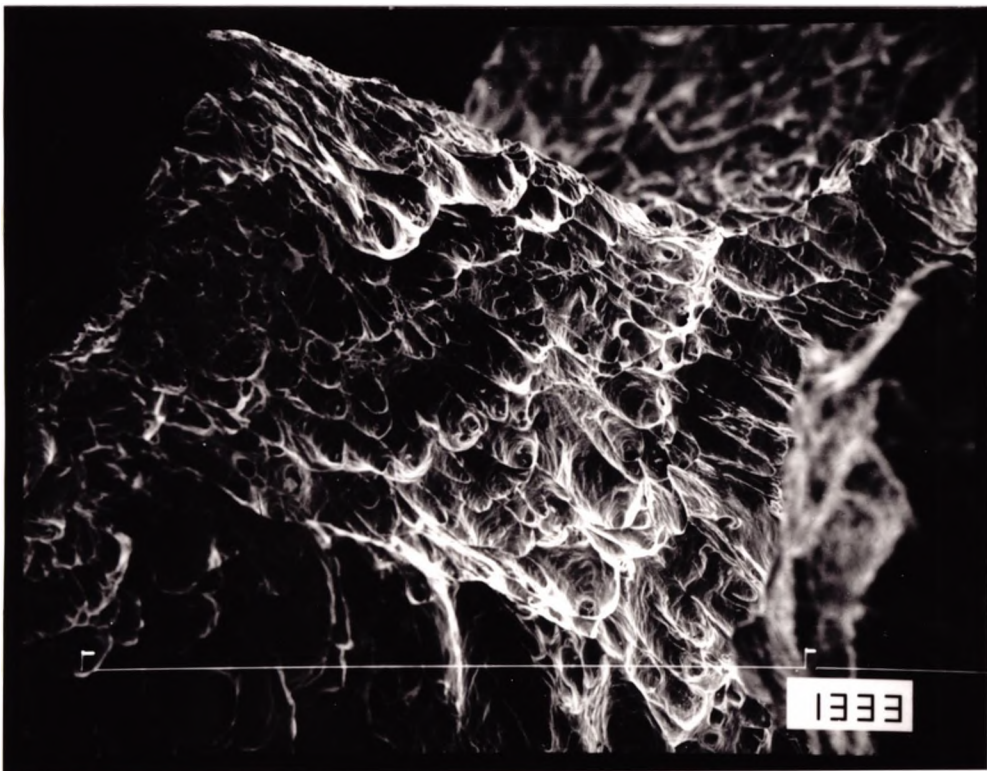
20 μm

Fig. 5.10 Spherical sulphides found on dendrite nodules in High S/Nb steel (C), tested at 850°C.



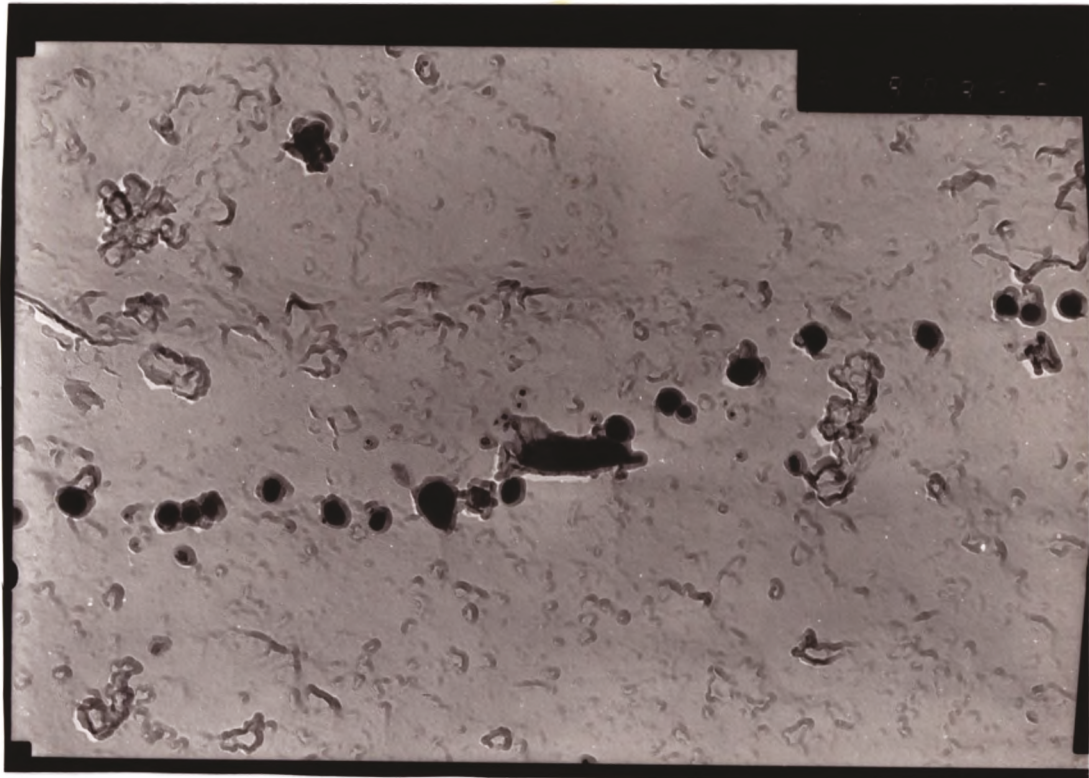
31 μm

Fig. 5.11 Sulphide inclusions found in high S/Nb steel (C). Steel tested at 850°C.



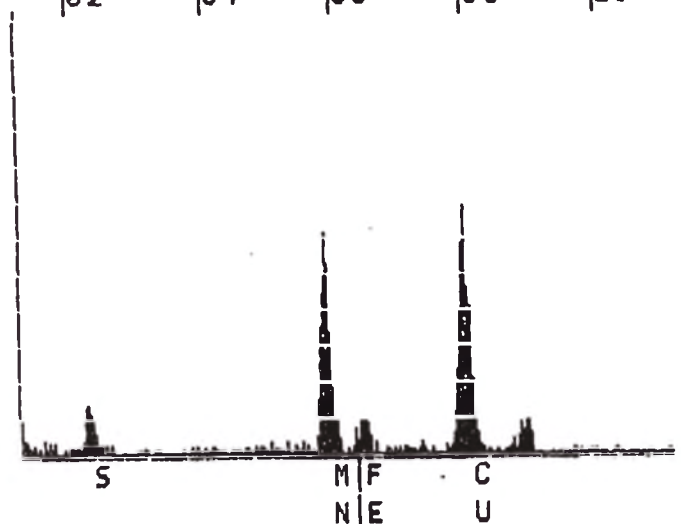
47 μm

Fig. 5.12 Typical interdendritic fracture observed in low Nb high S, steel (D) tested at 850°C.



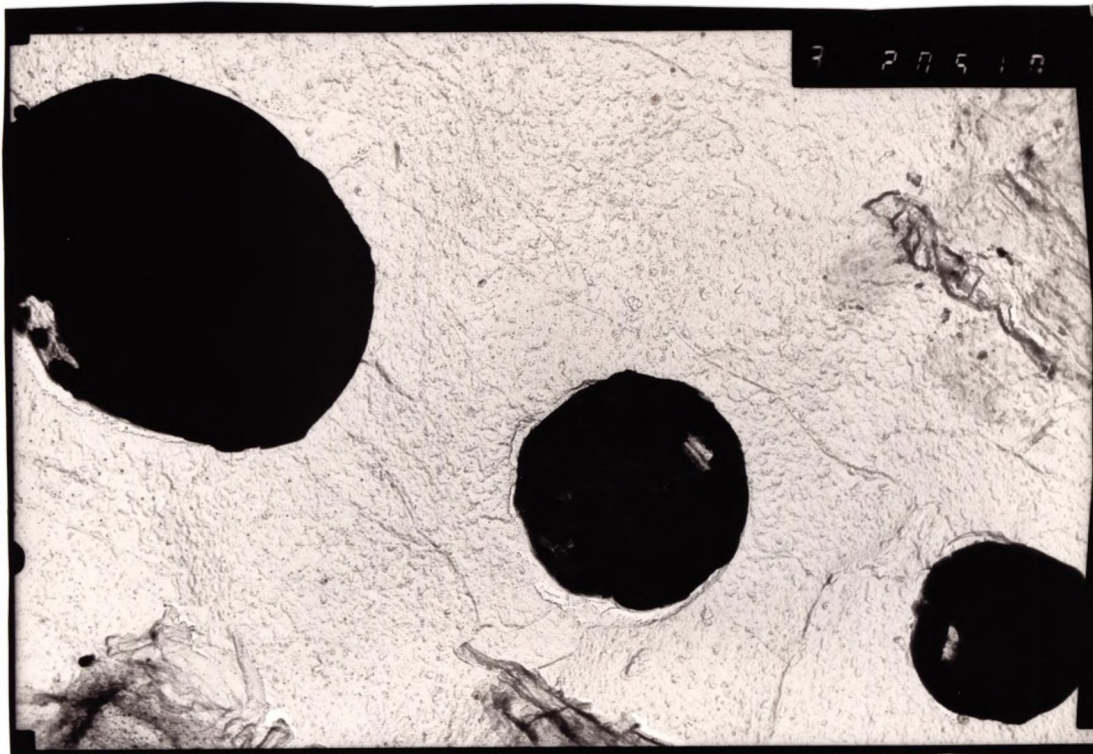
0.35 μ m

22-JAN-90 12:05:21 EDAX READY
 RATE: 103CPS TIME: 37LSEC
 00-20KEY: 10EV/CH PRST: OFF
 A: B:
 FS= 200 MEM: A FS= 200
 |02 |04 |06 |08 |10



CURSOR (KEY)=06.360 EDAX

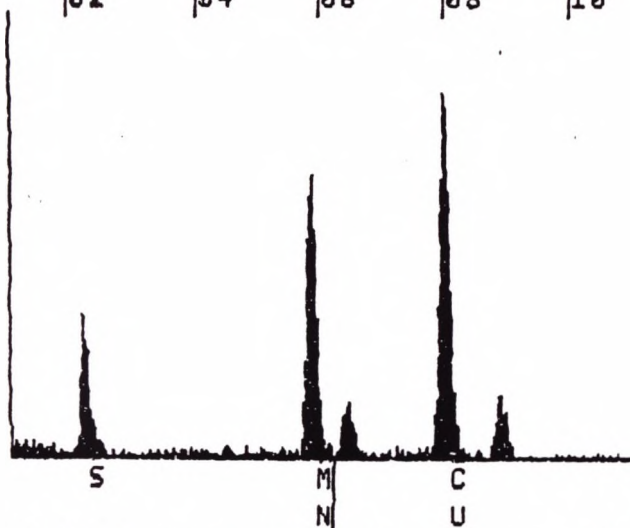
Fig. 5.13 (Mn,Fe)S inclusions present at interdendritic boundaries found in steel (D), steel tested at 900°C.



1.7 μm

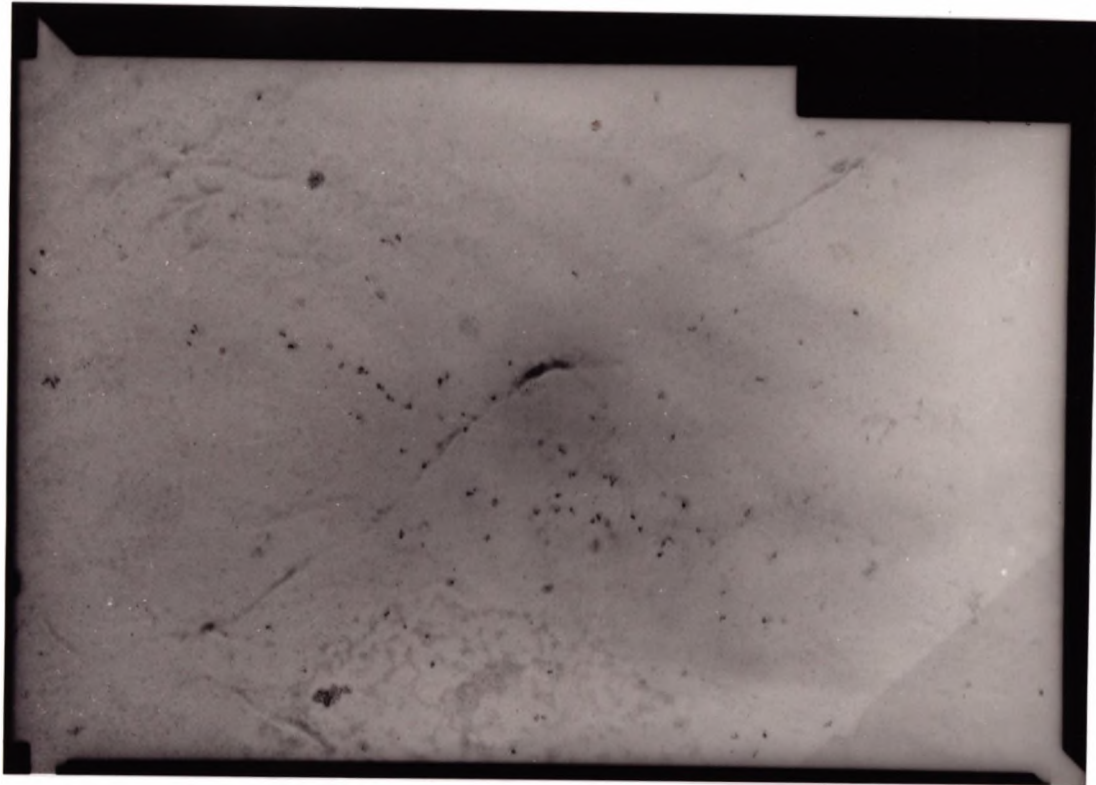
```

04-DEC-89 10:58:09 EDAX STORE
RATE:      1441CPS TIME      22LSEC
00-20KEV: 10EV/CH PRST      OFF
A:         B:
FS=      422   MEM: A   FS=    200
  |02    |04    |06    |08    |10
  
```



CURSOR (KEV)=06.240 EDAX

Fig. 5.14 Very coarse (Mn,Fe)S inclusions found in steel (D), tested at 900°C.



0.35 μ m

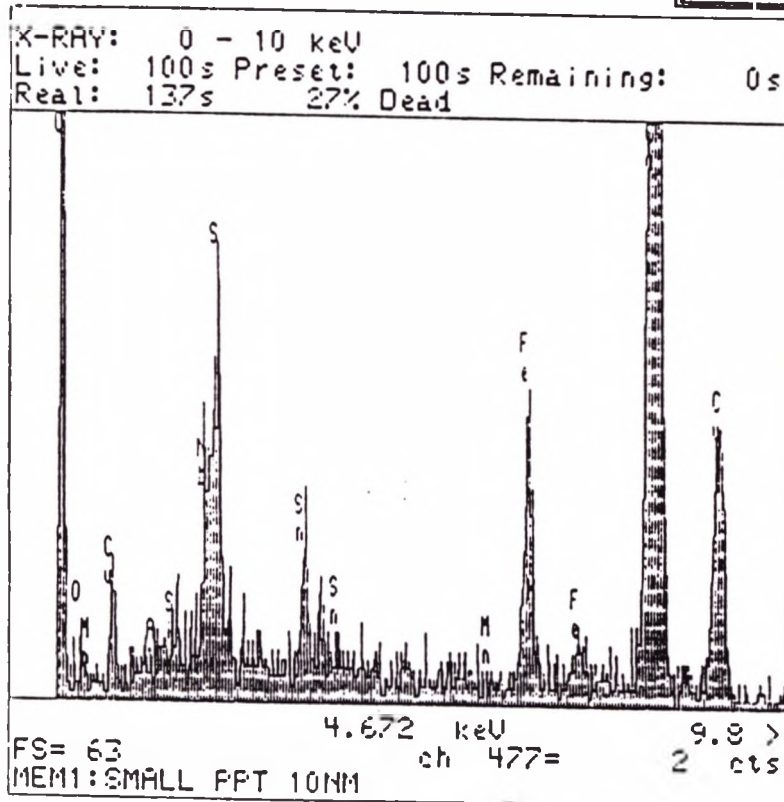
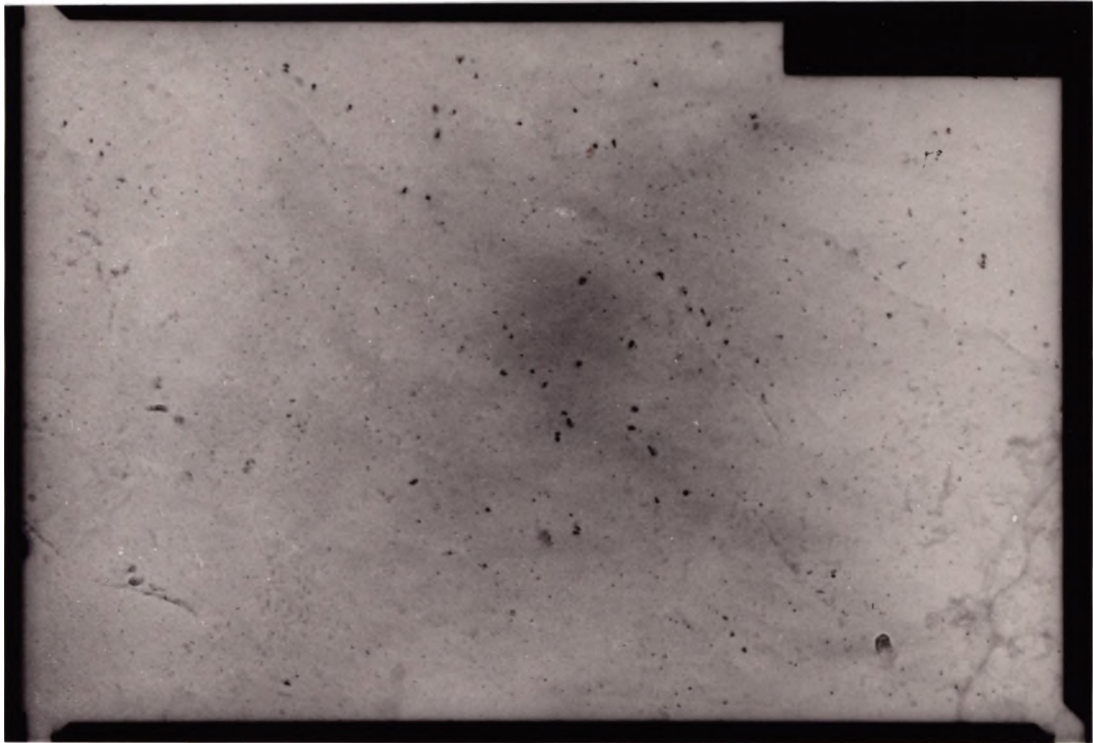


Fig. 5.15 Very fine Fe-oxysulphides found in high S steel, steel (D) tested at 900°C.



0.35 μm

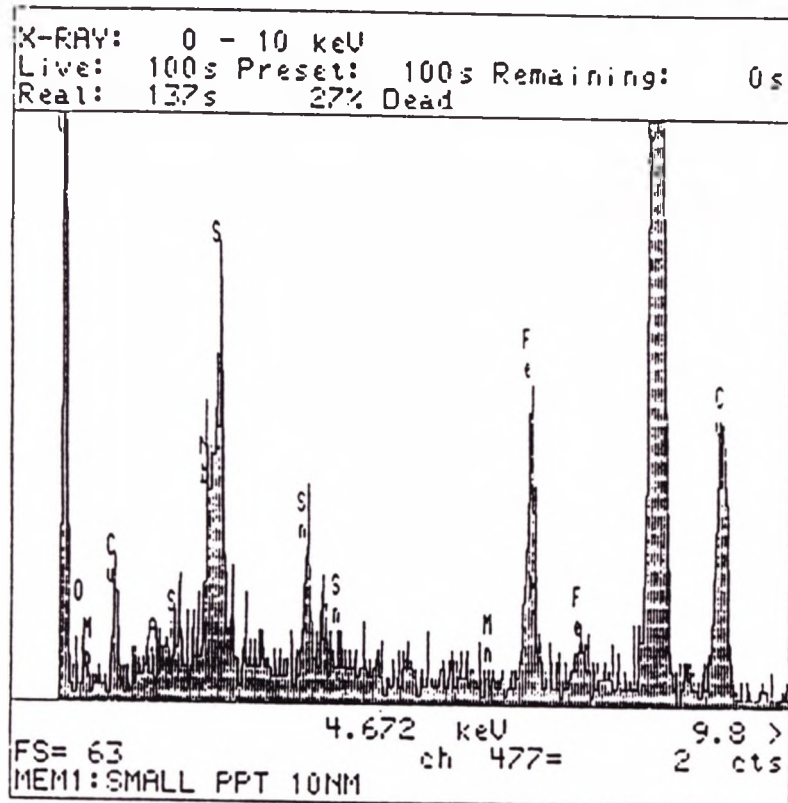
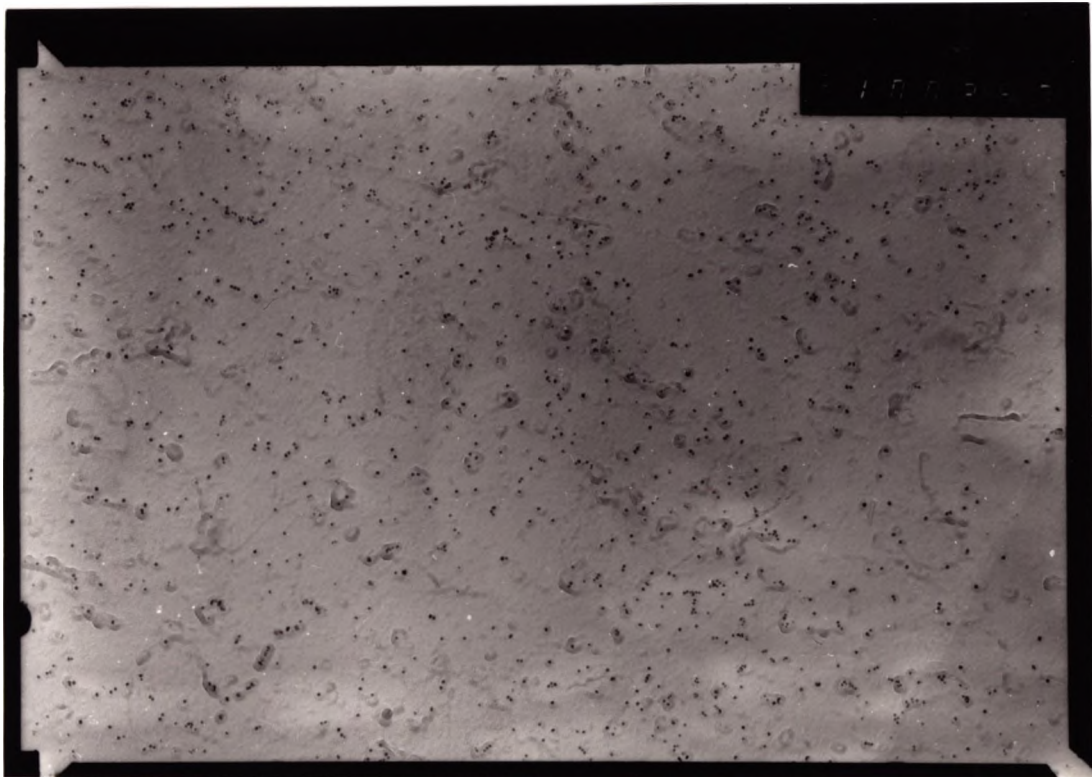
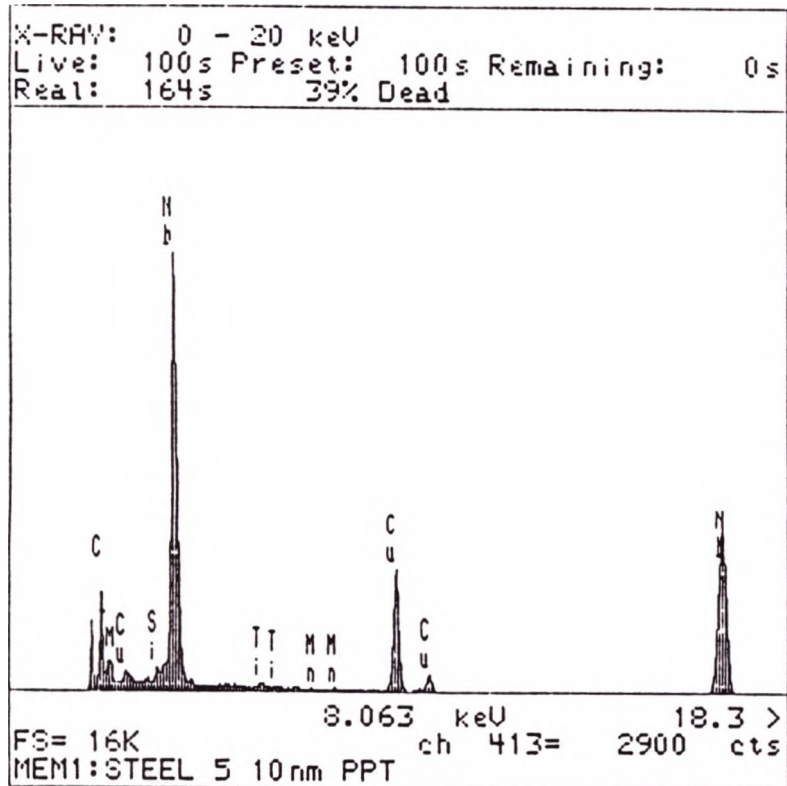


Fig. 5.16 Very fine Fe-oxysulphides found in high S steel, steel (D) tested at 900°C.

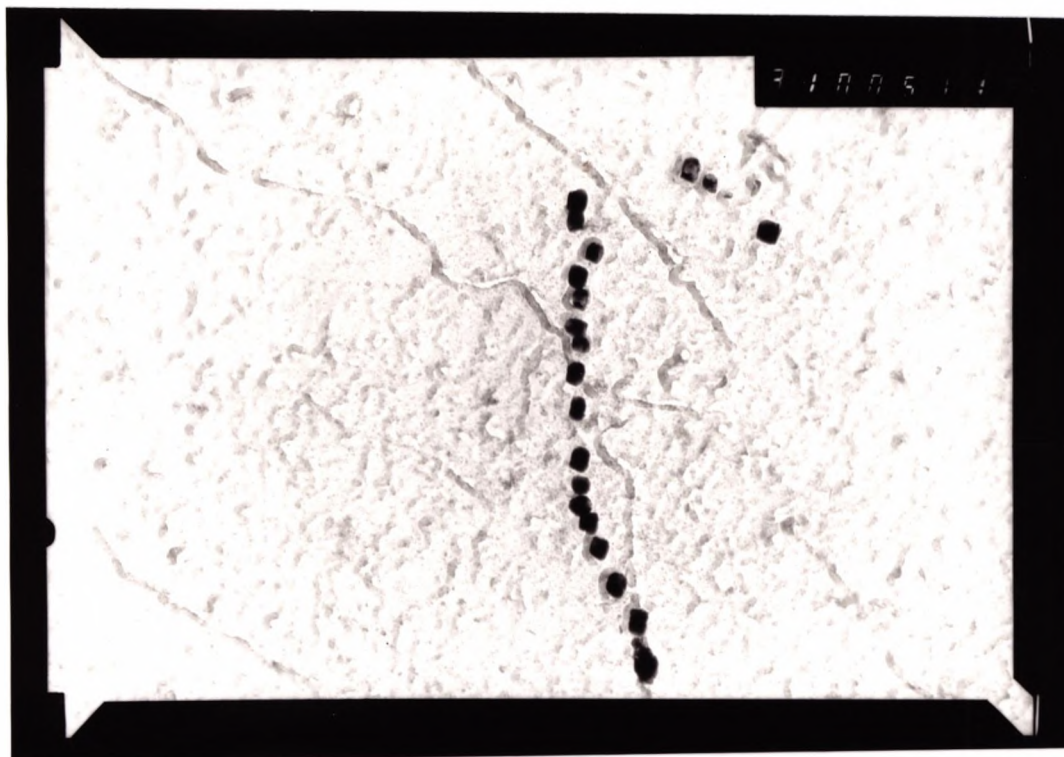


0.35 μm



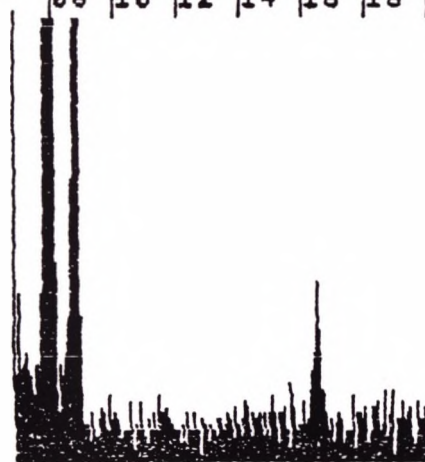
0.35 μm

Fig. 5.17 Very fine Nb(CN) matrix precipitation found in low S high Nb, steel (B), tested at 900°C.



0.35 μm

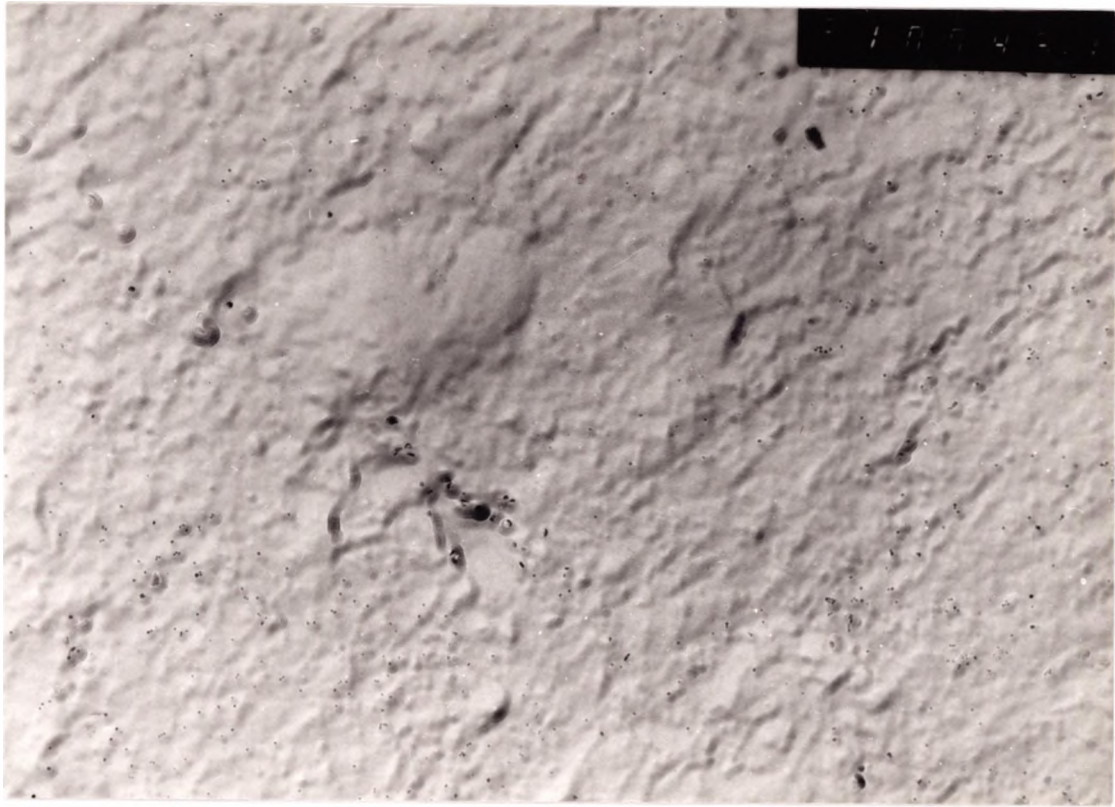
RATE: 328CPS TIME: 13fLSEC
 00-20KEY:10EV/CH PRST: 200LSEC
 A: JW07 B:
 FS= 64 MEM: A FS= 12
 |08 |10 |12 |14 |16 |18 |20



C
U
CURSOR (KEY)=17.120

EDAX

Fig. 5.18 Nb(CN) precipitation in the grain sub-boundary found in high S high Nb, steel (C), tested at 900°C.



0.35 μm

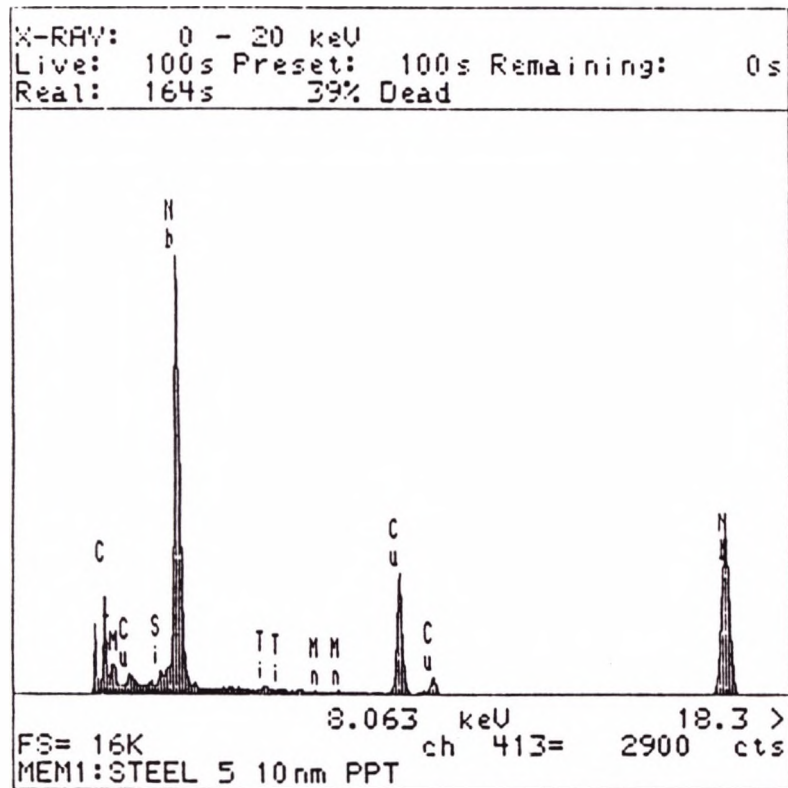
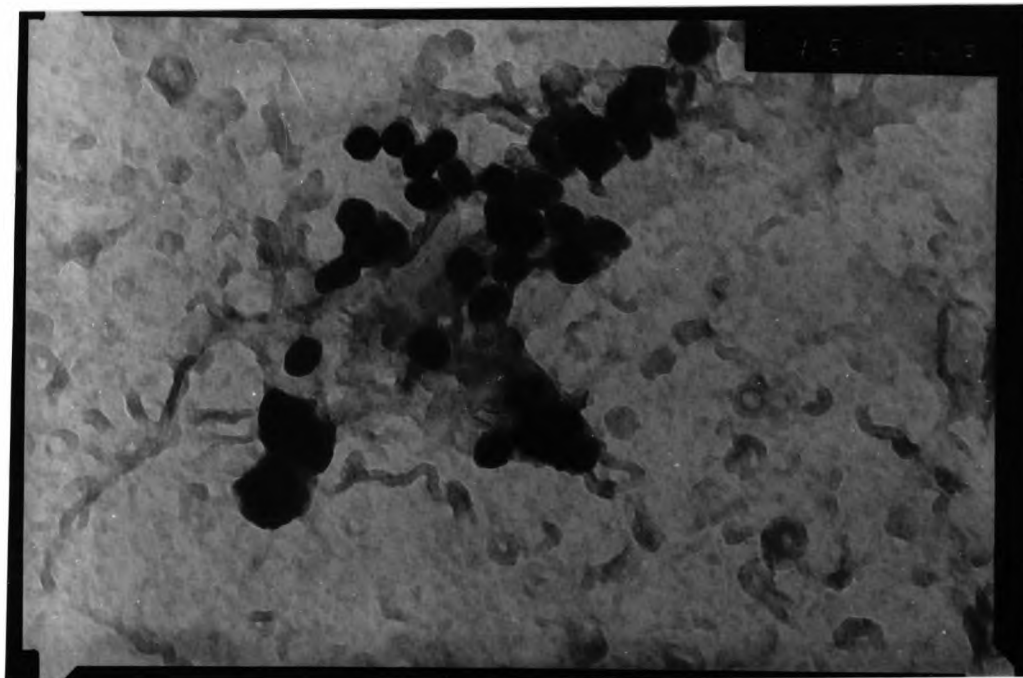


Fig. 5.19 Nb(CN) precipitation in the sub-boundary found in high S high Nb, steel (C), tested at 900°C.



0.35 μm

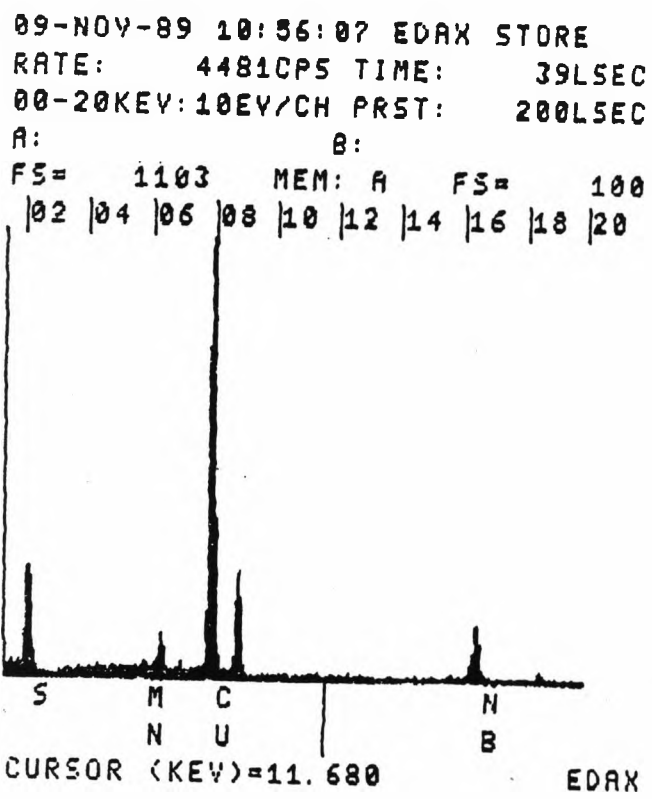
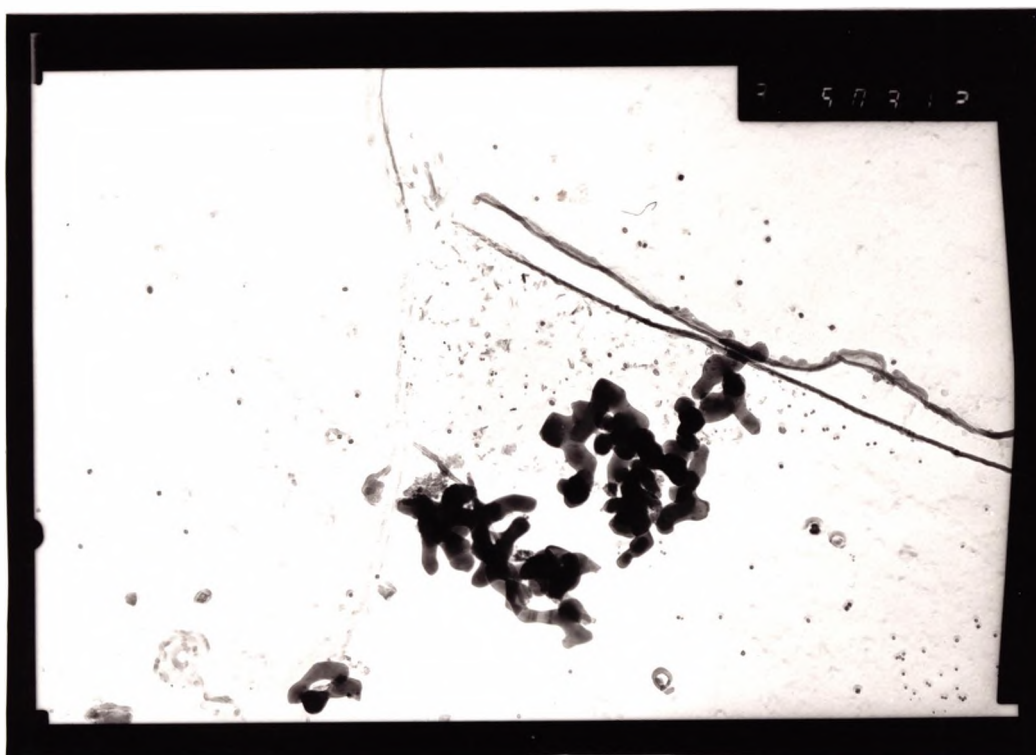
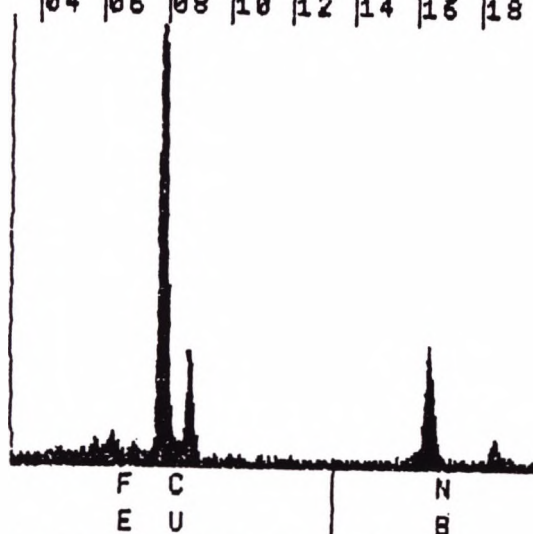


Fig. 5.20 Mixture of Nb(CN) with (Mn,Fe)S found in high S/Nb steel (C), tested at 900°C.



0.35 μm

30-APR-90 05:46:58 EDAX READY
 RATE: 19CPS TIME: 4LSEC
 00-20KEY: 10EV/CH PRST: OFF
 A: B:
 FS= 1086 MEM: A FS= 100
 |04 |06 |08 |10 |12 |14 |16 |18 |20



CURSOR (KEY)=13.440

EDAX

Fig. 5.21 Nb(CN) eutectic found in high S/Nb steel (C), tested at 900°C.

CHAPTER _____ 6

EFFECT OF TITANIUM ON THE HOT
DUCTILITY OF C-MN-AL STEELS

6.1 INTRODUCTION

Titanium is known to be an efficient nitrogen scavenger in killed steel and it is recognized that it can strengthen the steel by either grain refining or by precipitation hardening Samill et al, (1976). Titanium additions are widely used in reinforcing steels used for concrete structures especially in those regions of the world which are vulnerable to earthquakes. It is essential that the reinforcing steel must be capable of accepting a significant amount of plastic yielding and yet not fail by brittle failure. Strain ageing is an obvious danger since it can reduce the ductility and will markedly increase the impact transition temperature. Since nitrogen is the major cause of strain ageing in steel it is clearly desirable to reduce or remove this element completely by the addition of titanium which is one of the strongest nitride formers.

The use of titanium as a micro-alloying addition to steels has increased substantially in the last few years as developments in steel making techniques have made control of the addition more precise. The precipitates of titanium nitride have a low solubility and resist particle coarsening, and hence can be used as grain refiners up to very high temperatures. Their presence has therefore been found useful as a means of refining the grain size of as-cast structures as well as in welding applications where the HAZ can be markedly refined by its addition, more so than any other micro-alloying agent. Yasumoto et al,

(1985); Turkdogan, (1987), have reported that the incidence of transverse cracking is reduced when titanium is added, particularly for the more difficult to cast grades of Nb containing steels. It has been suggested that when titanium is present, coarse Ti rich particles are produced on solidification and these act as nucleation sites for the precipitation of NbC at high temperature so that there is little NbC available for precipitating out in a fine detrimental form at lower temperatures during the straightening operation.

The likelihood of a steel exhibiting transverse cracks on straightening has, in general, been found to relate well to the "Reduction in Area" values (R of A) obtained from the simple laboratory hot tensile test. Ouchi and Matsumoto, (1979); Mintz and Mohamed, (1988) have reported that small Ti additions to steel have resulted in high R of A values being found in the temperature range of the straightening operation (700-900°C), much higher than those obtained when other micro-alloying additions are used. However these tensile tests have invariably been carried out on hot rolled plate, reheated to temperatures in the range 1300°C to 1400°C. Whereas these temperatures are adequate to dissolve Nb(CN) and AlN, and produce a coarse grain size reminiscent of as-cast structure, this is not so for Ti containing steel where small, randomly precipitated Ti particles remain and are able to refine the austenite grain size. Thus the improvement of ductility on adding Ti is related to the finer grain size which may not be present

in the as-cast state. Thus in order to obtain meaningful information from the hot ductility test, concerning the influence of Ti additions on the continuous casting operation, samples must be melted and cooled directly to the tensile test temperature. This chapter has therefore been devoted to examining the effect of Ti on the ductility of as-cast steels.

6.2 EXPERIMENTAL

The compositions of the steels are given in Table 6.1. The steels had approximately the same base composition of 0.1% C and 1.4% Mn. The micro-alloying additions made to the steels were as follows:

-Nb, Ti and Al and

-Nb and Al

The Ti containing steel was a commercially produced steel hot rolled to 40 mm gauge, while the Ti free steel was a vacuum melt supplied in the hot rolled to 12 mm state.

Details of the tensile samples and melting techniques used can be found in chapter (4), page(100). The strain rate chosen was $2 \cdot 10^{-3} \text{s}^{-1}$.

Samples were melted at 1540°C for 5 min, and resolidified and cooled to the required temperature in the range 700 to 1100°C held for 5 min and then tensile tested to failure. Cooling rates to the test temperature were 100 and 25 °C/min.

In addition to the forementioned heat treatments the Ti containing steel was also melted as before then cooled to -300°C followed by reheating to the solution temperature of 1330°C held 5 min, cooled to the test temperature in the range 750 to 1050°C, and held for 5 min prior to tensile testing. Cooling rate in this instance was 100°C/min. Samples given this heat treatment will be referred to in the text as as-cast reheated.

Carbon extraction replicas was also taken close to the

point (~1 mm) of fracture of the low ductility intergranular failed samples and examined using both a JEOL 100KV TEM and a JEOL 2000FX Mark 2. Austenite grain sizes were determined prior to deformation as well as close to the fracture of strained samples using the linear intercept method. Longitudinal sections including the point of fracture were taken from the broken tensile samples and prepared for metallographic examination. Also fracture examinations were carried out using a JEOL T100 SEM.

6.3. RESULTS

6.3.1 Hot ductility curves

Hot ductility curves of R of A against test temperature are given in Figs. 6.1 and 6.2 for the titanium containing steel and titanium free steel respectively. The calculated Ae_3 temperature using Andrew's (1965) formula have been marked on the curves. This temperature was approximately the same, 850°C for the two steels.

For the titanium containing steel, cooled at 100°C/min, Fig 6.1, R of A fell from 80 % at 1000°C and reached its minimum value at 800°C (32%). Reducing the cooling rate to 25°C/min, can be seen to give a marked improvement in ductility over the temperature range 800 to 1000°C.

The reheated as-cast Nb/Ti containing steel, gave the widest ductility trough, the trough extending from 800 to 900°C.

In contrast to the big effect cooling rate has on the ductility of the Ti containing steel, it can be seen from Fig 6.2 that for the Ti free Nb containing steel, there is only a small improvement in ductility on lowering the cooling rate. For both cooling rates the minimum R of A occurred at 800°C, and was 24%.

6.3.2 Stress/Elongation Curves

The stress - total elongation curves for the steels examined are shown in Figs 6.3 and 6.4. The fluctuations in

the flow curve exhibited at the higher temperatures are believed be associated with dynamic recrystallization, (Wilcox and Honeycombe, 1979).

For the Nb/Ti containing steel, dynamic recrystallization was observed at test temperatures of $\geq 900^{\circ}\text{C}$ for both cooling rates of $100^{\circ}\text{C}/\text{min}$ and $25^{\circ}\text{C}/\text{min}$. In the case of the as-cast reheated sample the onset of dynamic recrystallization was delayed to temperatures $\geq 1000^{\circ}\text{C}$, .Fig 6.3.

For the Nb, Ti free steels these fluctuations were observed at $\geq 1000^{\circ}\text{C}$ for a cooling rate of $100^{\circ}\text{C}/\text{min}$ and $\geq 950^{\circ}\text{C}$ for a cooling rate of $25^{\circ}\text{C}/\text{min}$

It should be noted that for the Nb/Ti containing steel the peak stress was higher after reheating than in the as-cast state.

6.3.3 Metallography

Grain sizes in the as-cast state were very coarse ~2 mm and were the same for the two cooling rates, see Table 6.2 . Reheating the as-cast structure refined the grain size Fig 6.5.

Samples quenched after fracture in the temperature range of low ductility showed wedge type cracks due to grain boundary sliding, Figs 6.6 and 6.7. Some evidence for deformation induced ferrite was found in all the steels after quenching from temperatures showing intergranular fracture, Fig 6.8.

6.3.4 Fracture appearance for Nb/Ti and Nb steels

Fracture appearance for both the Nb and Nb/Ti were similar. The fracture surfaces at low ductility were a mixture of interdendritic and intergranular failure, Fig 6.9. Intergranular failure was in turn a mixture of intergranular micro-void coalescence, characteristic of inclusion induced failure and intergranular decohesion characteristic of failure by grain boundary sliding, Fig. 6.10. An example of interdendritic failure is shown in Fig 6.11. Dendrite nodules were also observed occasionally. These are present due to micro-shrinkage. When necking starts to take place the fracture path will seek out such regions. Examination of these regions is useful as information concerning the form and degree of S segregation during solidification is revealed. Due to the low S content of the steel few sulphides were observed on the

nodule surface and only spherical sulphides (2 to 3) μm were present as shown in Fig 6.12. These particles redissolved when the as-cast steel was reheated and were no longer observed on the nodule surface, Fig 6.13.

High temperature ductile rupture was observed in all the samples at high temperature Fig 6.14. This type of failure is characterised by large voids. These probably originate from cracks formed early on by grain boundary sliding which are not allowed to develop due to dynamic recrystallization and elongate out during necking of the sample. When the steel was melted and reheated, the low ductility fracture surface also showed a mixture of interdendritic and intergranular failure, Figs 6.15, 6.16. and 6.17. The interdendritic contribution to the intergranular failure was in the region of 20% of the fracture surface.

6.3.5 Replica examination

Examination of carbon extraction replicas under the TEM revealed there were only a few AlN particles present in the steels and this was independent of the cooling rate. The as-cast Nb/Ti containing steel had both a coarse Ti rich eutectic Fig 6.18 as well as a Nb rich coarse eutectic, Fig 6.19. In this steel a whole range of Nb-Ti containing precipitates were observed having a wide variation in size and composition. The coarser precipitates generally contained a higher percentage of Ti than Nb in accord with them having probably been formed at

high temperature. Finer precipitates were generally Nb rich, as shown in Figs 6.20, 6.21, 6.22, 6.23 and 6.24. These precipitates varied in size and inter-particle spacing see Table 6.3. The Nb/Ti free steel besides having the eutectic precipitation also had considerably more fine Nb(CN) precipitation both at the matrix Fig 6.25 and at the grain boundaries Fig 6.26 and Fig 6.27.

For the Nb/Ti steel reducing the cooling rate had a significant effect on the precipitate distribution as well as their size, the precipitates being coarser with a wider inter-particle spacing, see Figs 6.28, 6.29, and 6.30 and Table 6.3.

For the Ti free steel reducing the cooling rate had only a minor influence in coarsening the precipitation and the very fine matrix precipitation of Nb(CN) was still present in large amounts as in Fig 6.31.

Finally reheating the Nb/Ti steel, resulted in more intense fine precipitation. There was intense precipitation in the matrix as well as at the γ grain boundaries and sub-grain boundaries as shown in Figs 6.32, 6.33, 6.34 and 6.35.

6.4 DISCUSSION

6.4.1 As-cast condition

Ti is added to steels mainly as a grain refining addition and the generally improved hot ductility which has been found in the literature can be regarded as being mainly due to this grain refinement. However in the as-cast situation, no grain refinement occurs on adding Ti and the grain size remains coarse ~2 mm. The grain size was the same independent of cooling rate or the presence of Ti. The explanation for the improved ductility must be therefore related to the differences in precipitation behaviour between the steels. The Nb/Ti free steel showed significant precipitation of fine Nb(CN) in the matrix and at the boundaries and this was little influenced by the cooling rate in the range 25 to 100°C/min. In contrast, the Ti containing steel had a coarser precipitation distribution than the Ti free steel at the higher cooling rate and this coarsened significantly on reducing the cooling rate to 25°C/min, Table 6.3.

It has been shown that finer precipitates particularly when they are in the γ grain boundaries are detrimental to the hot ductility because they encourage grain boundary sliding and cavitation and the more closely spaced the particles are the easier it is for the cracks to link up. On this basis it would be expected that Ti containing steels because of their generally coarser precipitation would give better ductility, particularly at the slow cooling rate, in accord with the present findings. The present results suggest that a Ti addition is mainly beneficial to hot

ductility when the cooling rate during solidification and cooling to the test temperature is slow i.e 25°C/min giving rise to a coarser precipitation with a wider inter-particle spacing, see Table 6.3. This probably occurs as suggested by Turkdogan, (1987) because the Ti can combine with N at high temperatures forming coarse TiN particles which act as nucleation sites for precipitation of Nb at high temperatures, so there is less Nb available for precipitation as the fine detrimental NbC at the lower temperature range of 800 to 1000°C. Turkdogan, (1987) has suggested that Ti additions to the melt reduce transverse cracking by coarsening the precipitation of Nb and V making them ineffective in influencing ductility. To ensure coarsening of the particles Turkdogan, (1987) recommended that the volume fraction of the TiN particles should be kept to a minimum. Commercial cooling rates at the surface of continuously cast strands are often 60°C/min. and the present work indicates that this may be too fast to always obtain the benefit of a Ti addition.

6.4.2 As-cast reheated

The fine grain size produced on reheating would have been expected from previous work to have given improved hot ductility, Crowther and Mintz, (1986 b). However this did not occur on reheating the as-cast Ti containing steel. Although reheating refined the grain size, 2 mm to 180 μm ductility was found to deteriorate. The explanation for this behaviour is that in the as-cast condition as well as a fine NbCN precipitation there is also both a coarse eutectic of NbCN and impure (Mn,Fe)S inclusions. However on reheating to solution temperature these coarse eutectics are able to redissolve and thus increase the amount of Nb and S which is able to precipitate out in a fine form on cooling to test temperature. This more extensive fine precipitation at the boundaries and within the matrix encourages voiding and grain boundary sliding at the boundaries as well as delaying the onset of dynamic recrystallization. Ductility is therefore reduced even though the grain size is refined. These observations are in agreement with other studies by Mintz et al, (1986); Mintz and Mohamed, (1988).

6.5 CONCLUSIONS

- 1- Ti is not able to grain refine in the as-cast state. The grain size for the Ti free and Ti containing steel steels in the as cast state were the same ~2 mm.
- 2- The as-cast grain size was found to be independent of cooling rate in the range 25 to 100°C/min.
- 3- When the cooling rate was 100°C/min the hot ductility of the Ti containing is slightly better than that obtained for the Ti free steel.
- 4- In contrast for a slower cooling rate 25°C/min a marked improved in ductility occurred when Ti was present. The ductility markedly improved because the precipitation was found to be coarser.
- 5- A **change** in cooling rate from 100 to 25°C/min had little influence on the ductility of the Ti free steel. Precipitation remained fine at both cooling rates.
- 6- Reheating the as-cast steel refined the grain size but led to a wider ductility trough. This is believed to be due to the solution treatment allowing more Nb and S to redissolve and be

available for precipitating in a fine detrimental form on cooling to the test temperature.

Table 6.1

Composition of Steels Examined wt, %

Code	C	Mn	Si	P	S	Al	Nb	N	Ti
Steel A	0.115	1.48	0.33	0.019	0.004	0.023	0.023	0.008	0.02
Steel B	0.11	1.54	0.32	0.015	0.004	0.035	0.029	0.009	—

Table 6.2

Austenite grain size for the steels examined
at the two Cooling rates in(μm)

Steel	Cooling rate	Grain size μm
Steel A as-cast	100°C/min	2,000
	25°C/min	2,000
Steel A as-cast reheated	100°C/min	180
Steel B	100°C/min	2,000
	25°C/min	2,000

Table 6.3

Precipitates observed in the grain boundaries and in the matrix for the steels examined.

measurements were made on 100 particles at 850°C

Code	Cooling rate	Grain boundary precipitation			Matrix precipitation	
		Type	Average Size nm	Inter-particle spacing nm	Average Size nm	Inter-particle spacing nm
Ti steel	As-cast 100°C/min	NbCN*	15	30	10	17
		TiN*			90	540
	25°C/min	NbCN	50	35	30	350
	As-cast reheated 100°C/min	NbCN	15	30	10	15
		TiN			85	900
Ti free steel	As-cast 100°C/min	NbCN	15	30	10	17
	As-cast 25°C/min	NbCN	25	40	12	17

* Coarse particles have been taken as TiN and fine particles as Nb(C) for the Ti containing steel
Analysis indicates that these particles are often mixed Ti/Nb particles.

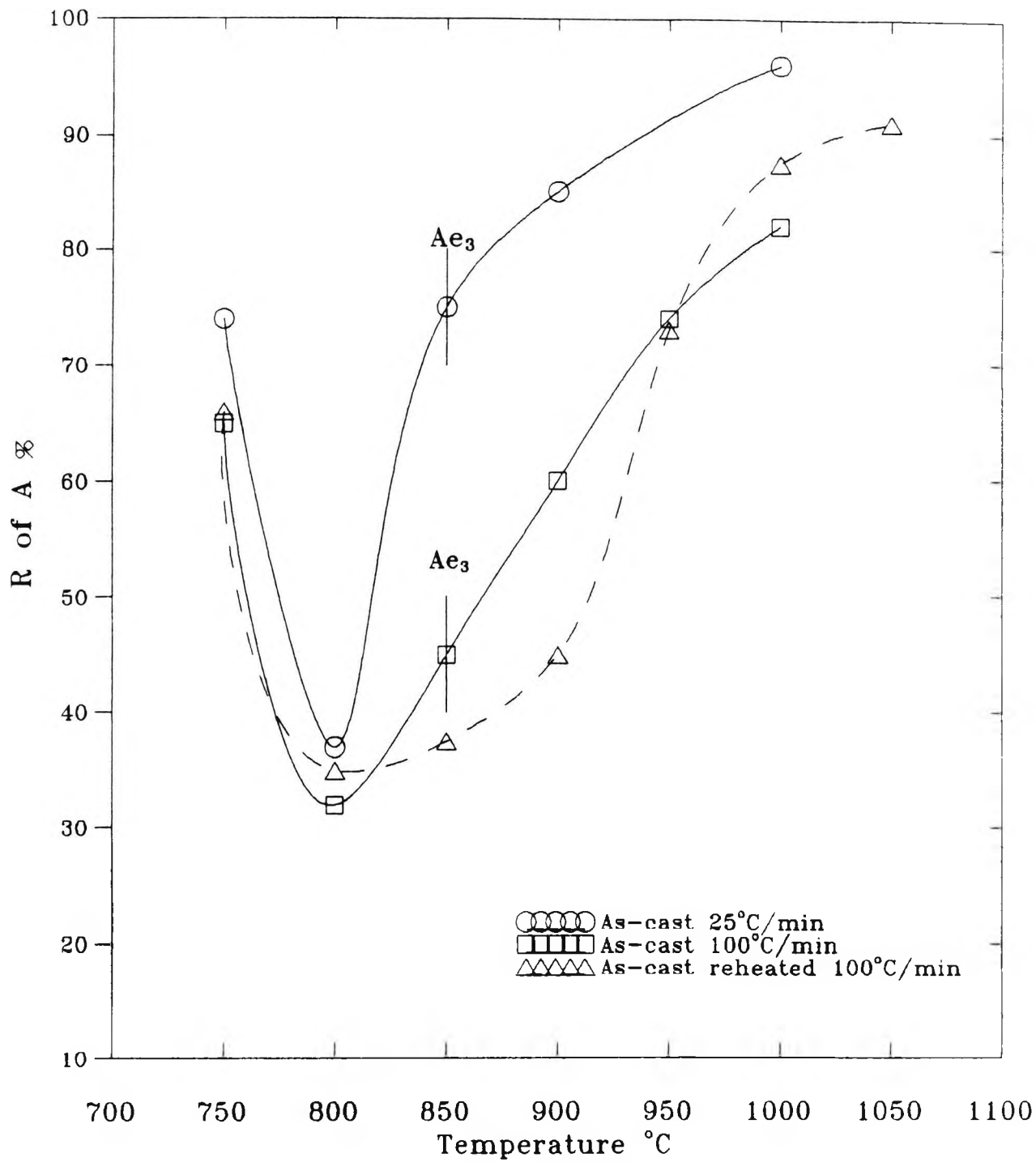


Fig. 6.1 Hot ductility curves for Nb-Ti steels

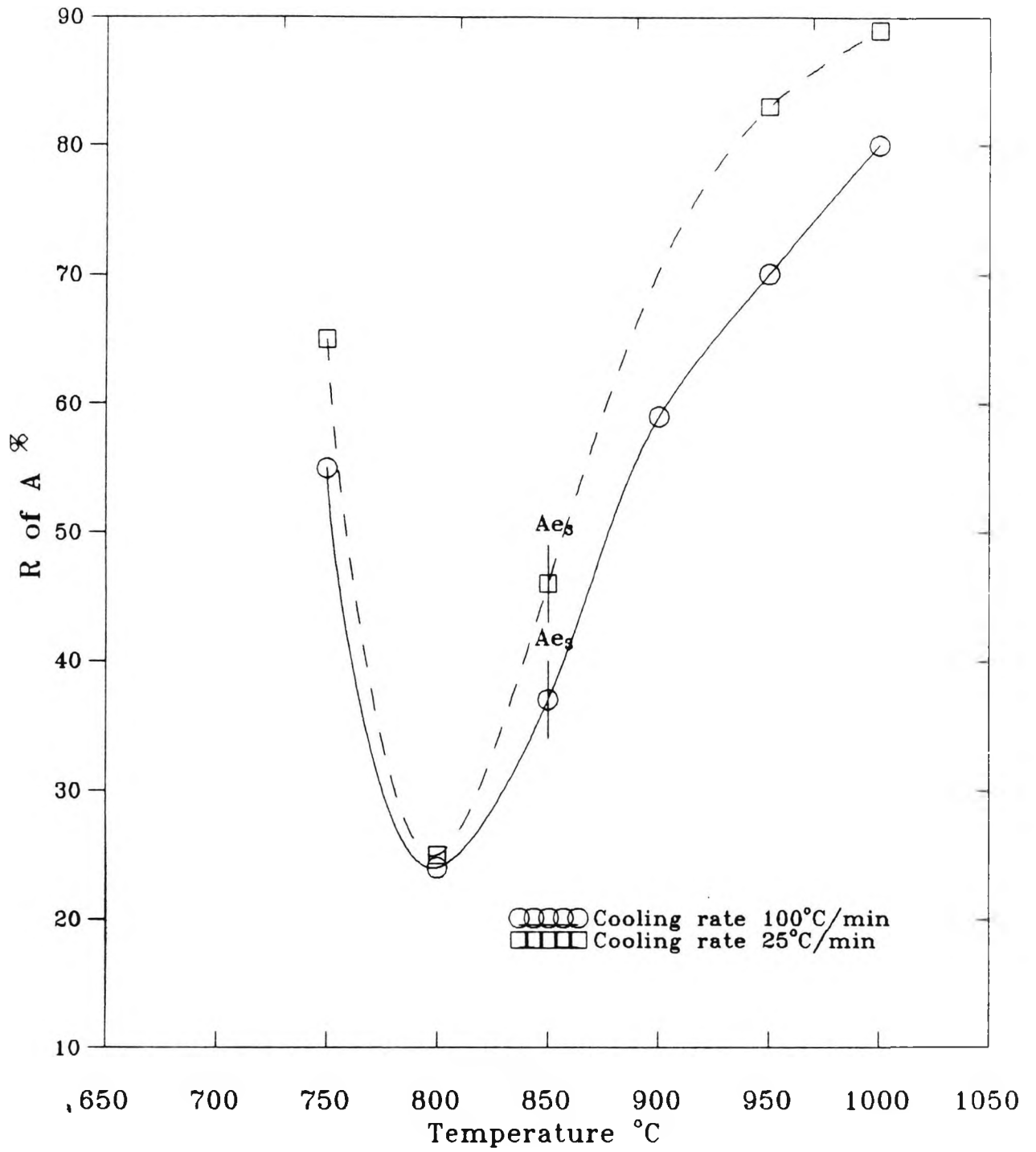


Fig. 6.2 Hot ductility curves for Nb containing steel.

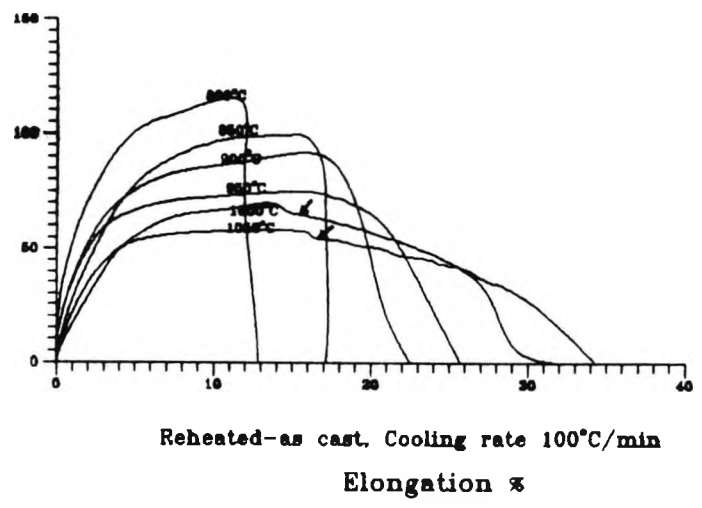
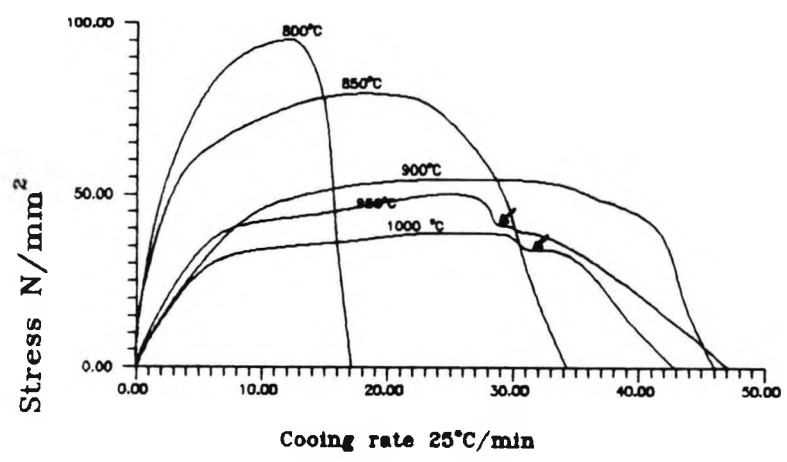
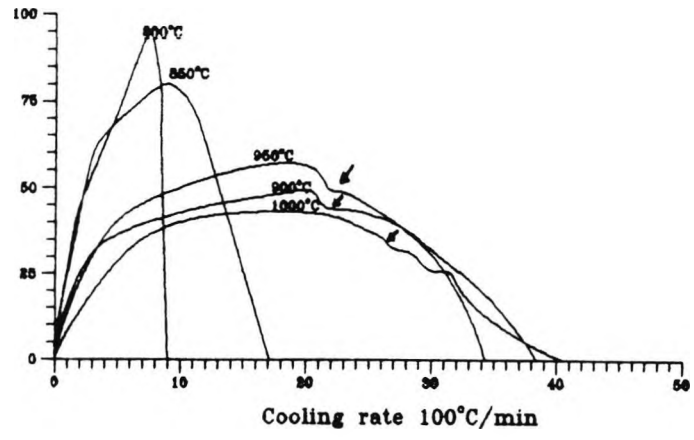


Fig 6.3 Stress/Elongation curves for Ti containing steel.
 (Arrows indicate dynamic recrystallization).

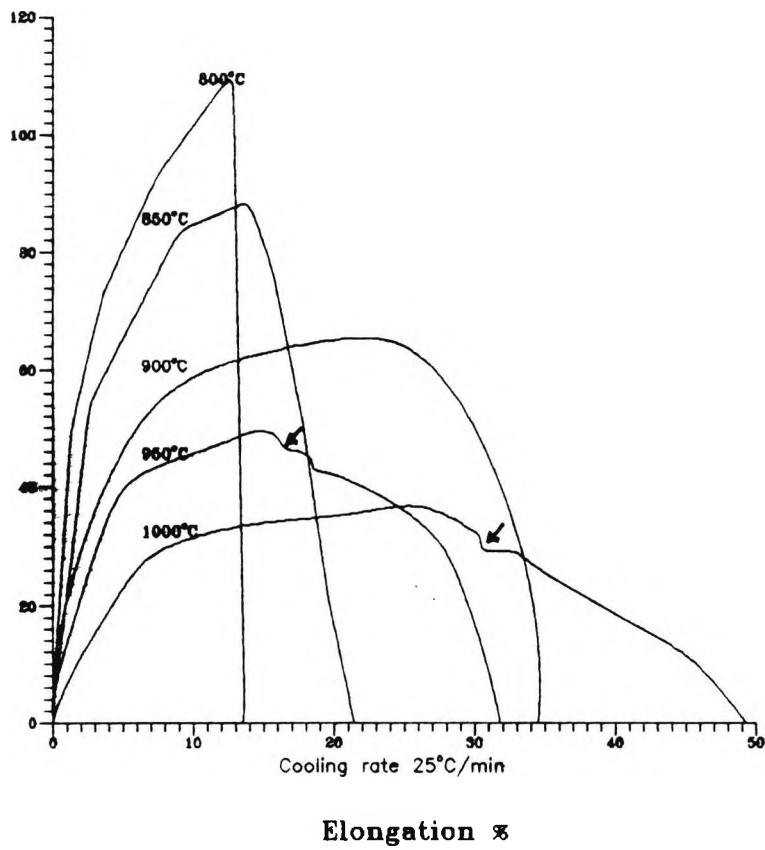
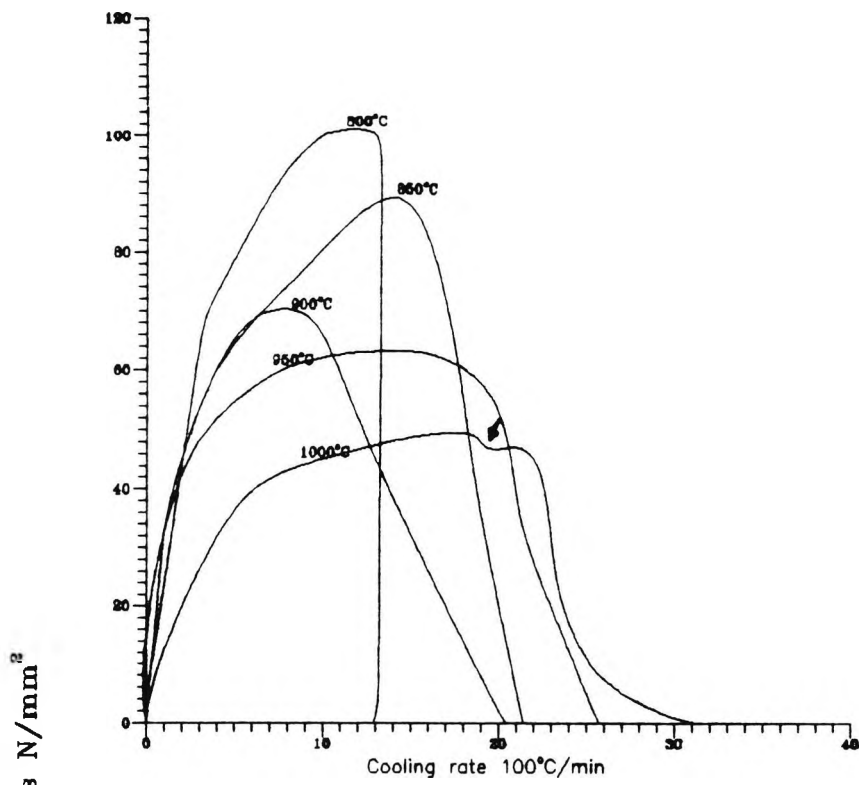
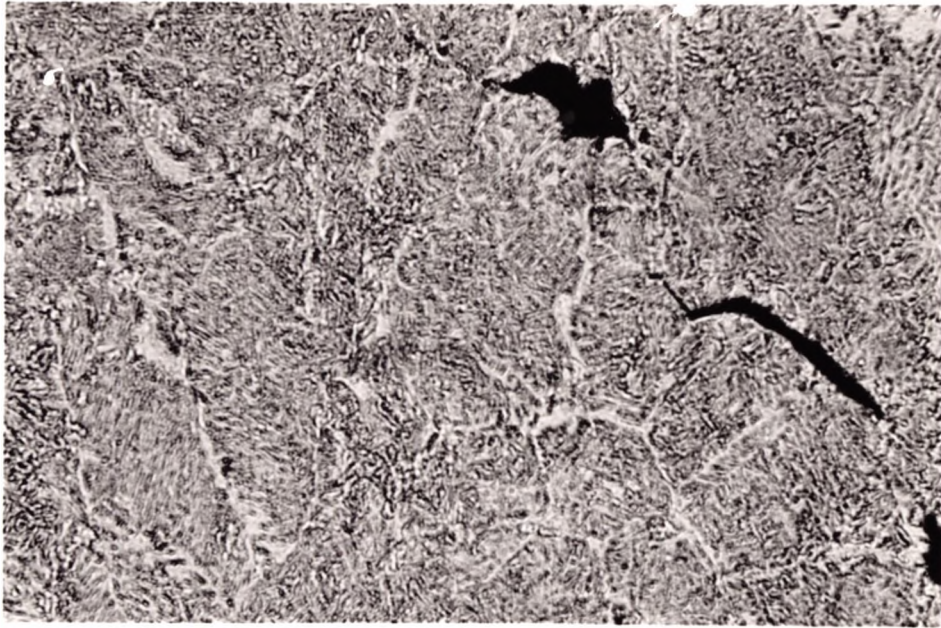
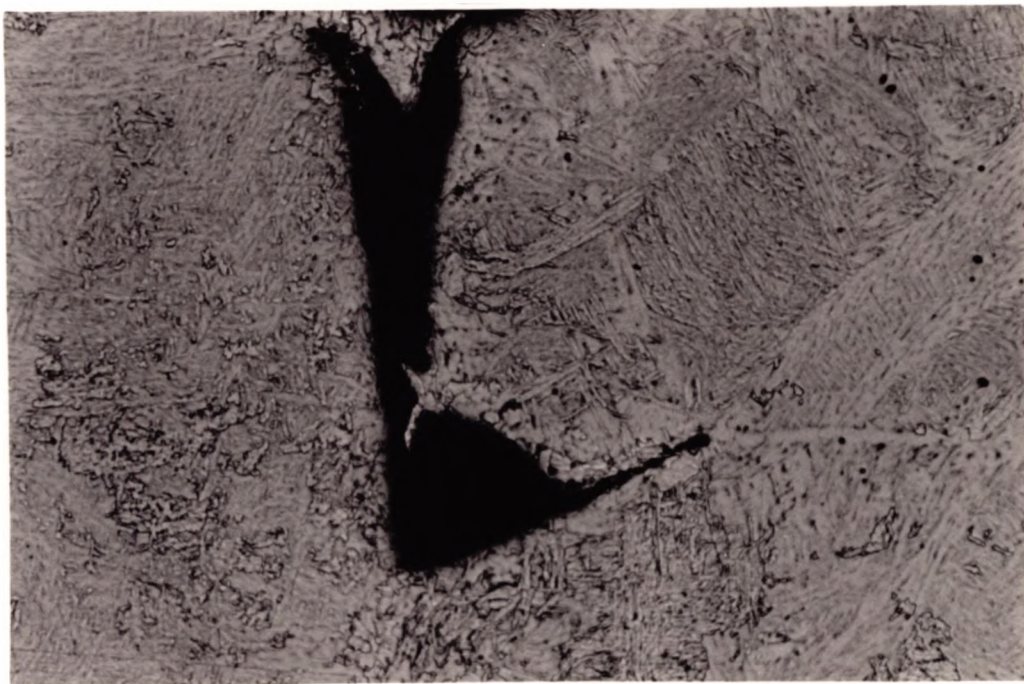


Fig 8.4 Stress/Elongation curves for the Ti free steel.
(Arrows indicate dynamic recrystallization).



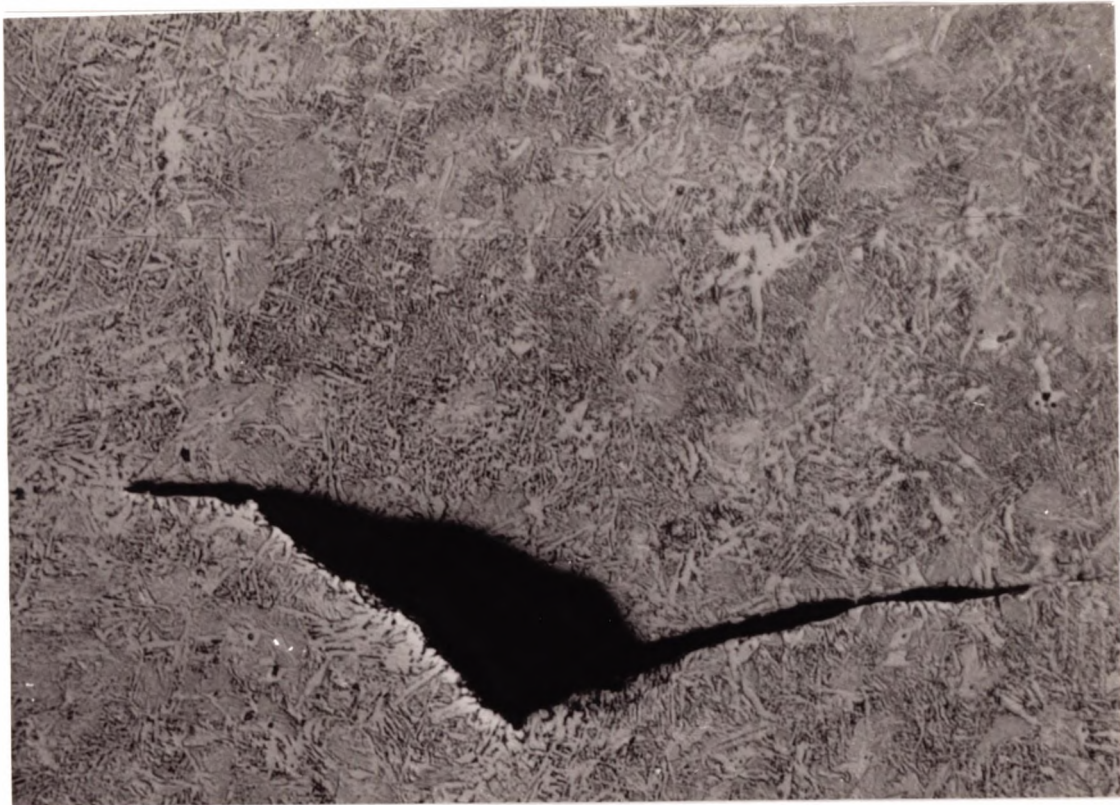
200 μm

Fig. 6.5 Fine grain structure in as-cast reheated Ti containing steel, tested at 800°C. Cooling rate 100°C/min.



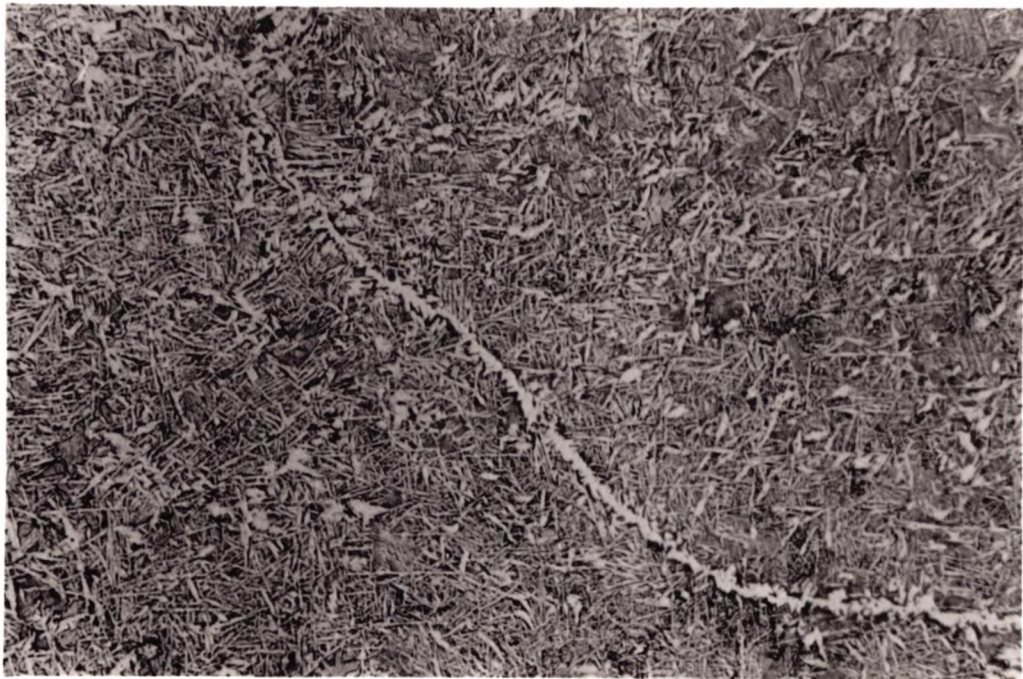
200 μm

Fig. 6.6 Typical wedge type crack found in Ti containing steel tested at 850°C, cooling rate 100°C/min.



200 μm

Fig. 6.7 Typical wedge type crack found in Ti as-cast steel tested at 850°C, cooling rate 25°C/min.



100 μm

Fig. 6.8 Evidence of deformation induced ferrite in the as-cast Ti free steel tested at 850°C. Cooling rate 100°C/min.



Fig. 6.9 Fracture surface of as-cast Ti steel, tested at 850°C, showing a mixture of inter granular microvoid coalescence and intergranular decohesion (R of A 47%).

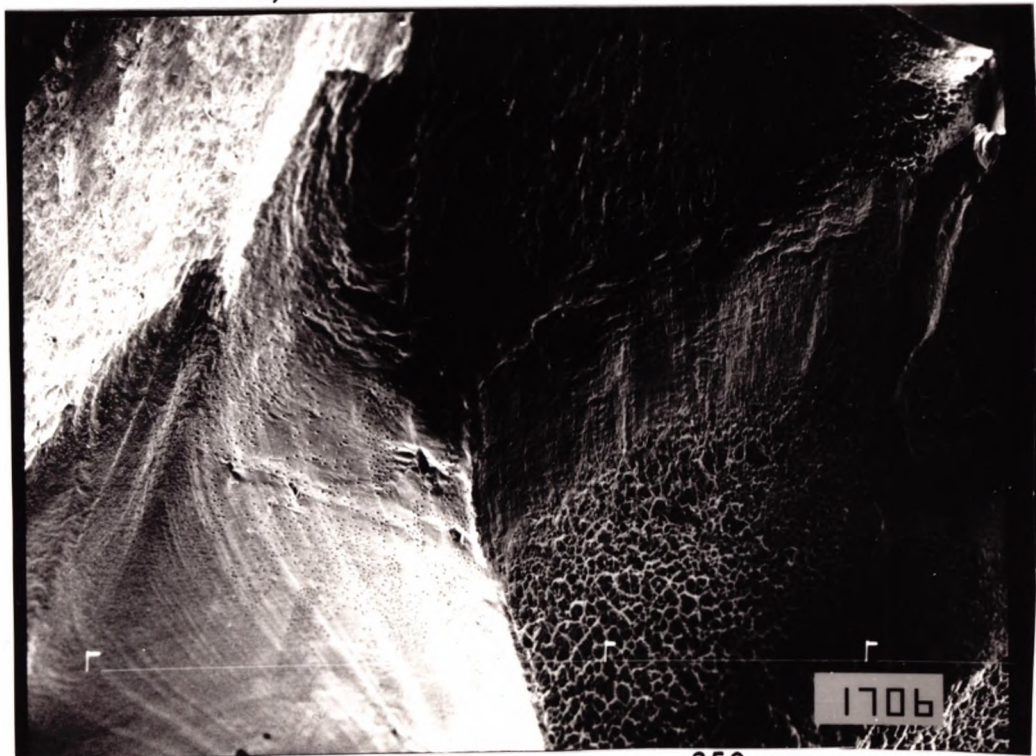
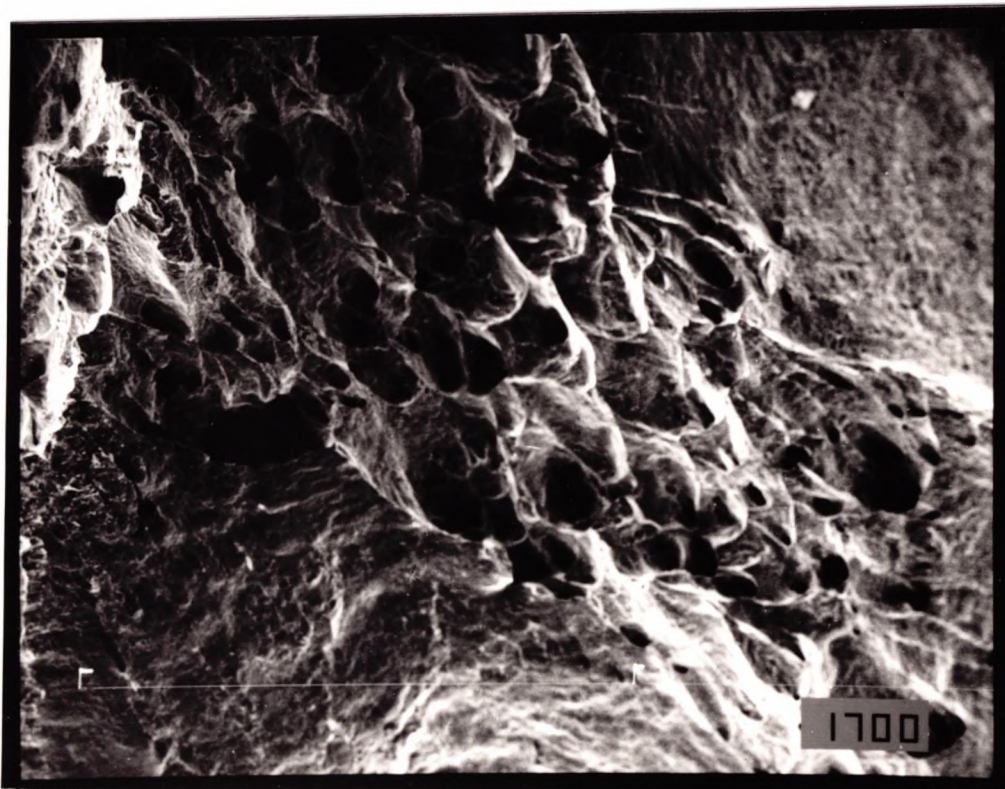


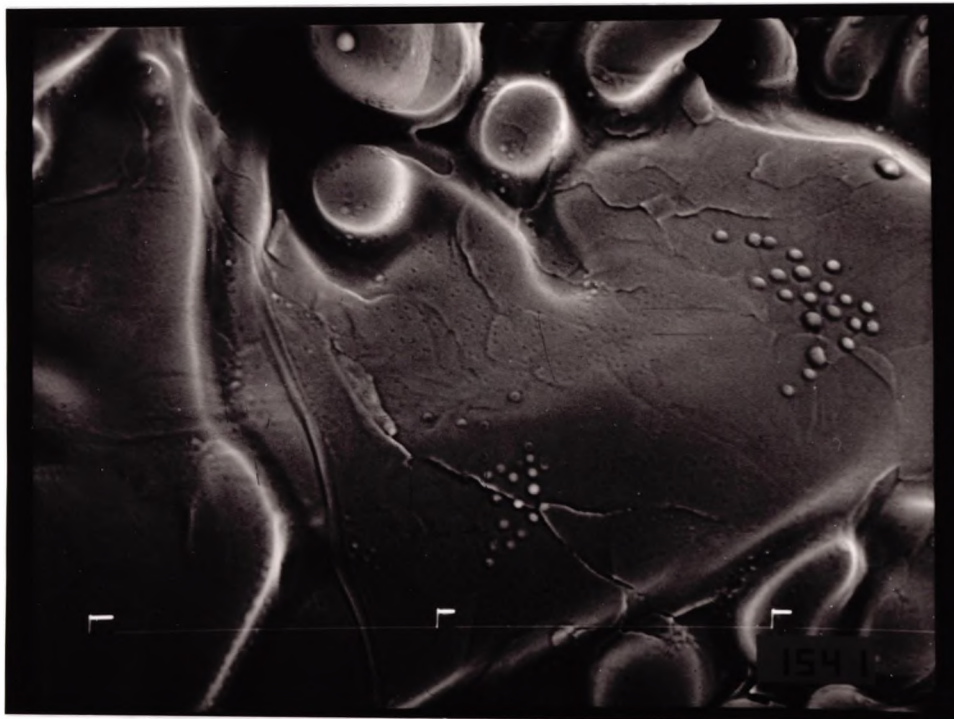
Fig. 6.10 Fracture surface of as-cast Ti containing steel tested at 850°C, showing evidence of grain boundary sliding. (R of A 38%) cooling rate 25°C/min.



1700

133 μm

Fig. 6.11 Interdendritic failure observed in Ti free steel tested at 900°C. (R of A 63%). Cooling rate 25°C/min.



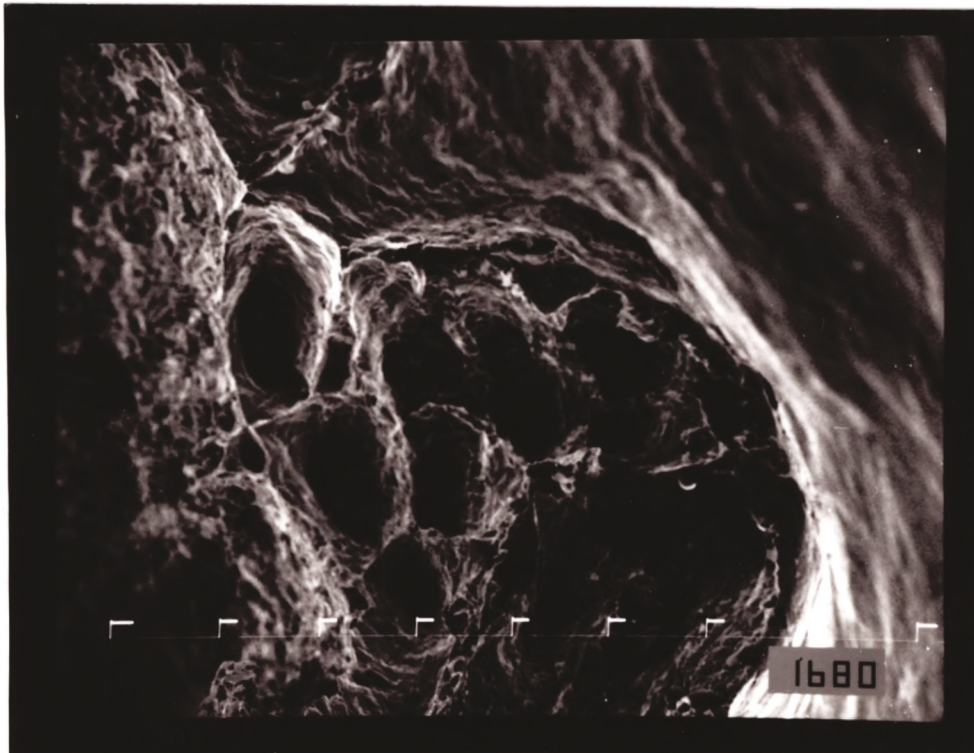
20 μm

Fig. 6.12 Fracture surface of as-cast Ti containing steel tested at 850°C, showing isolated dendritic region with spherical MnS inclusions on the nodule surface. Cooling rate 100°C/min.



66 μm

Fig. 6.13 Dendritic regions found in the as-cast reheated Ti containing steel tested at 850°C. Cooling rate 100°C/min.



50 μm

Fig. 6.14 Typical high temperature rupture fracture in Ti containing steel, tested at 950°C, (R of A 74%). Cooling rate 100°C/min.



Fig. 6.15 Fracture surface of as-cast reheated Ti containing steel tested at 900°C showing a mixture of intergranular micro-void coalescent, intergranular decohesion failure and interdendritic failure. (R.of.A 40%). Cooling rate 100°C/min.

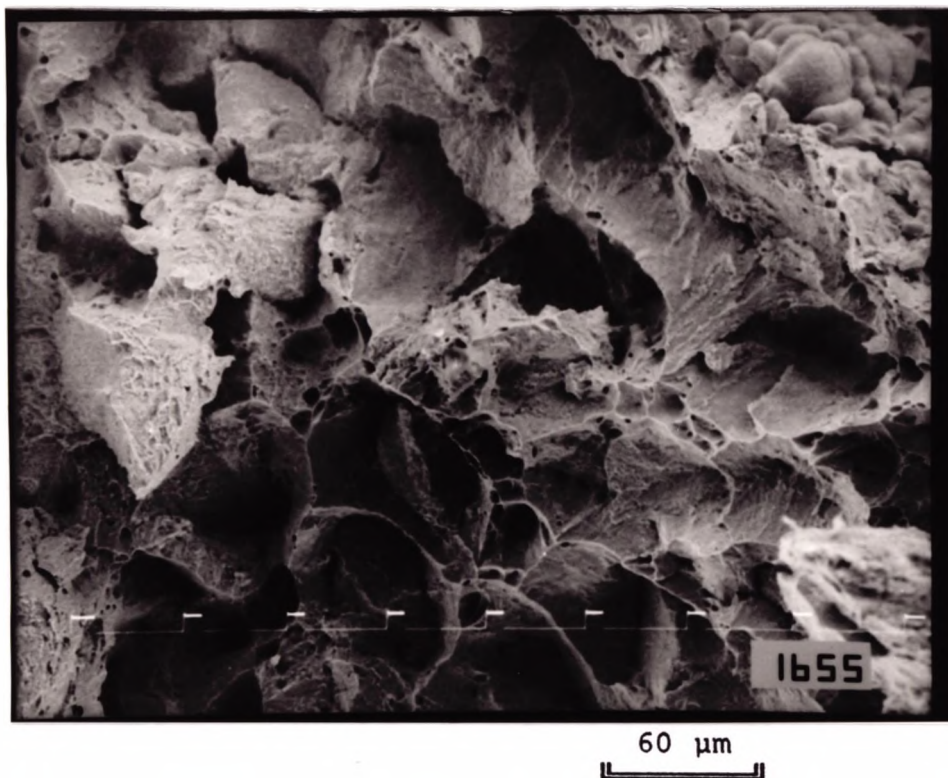
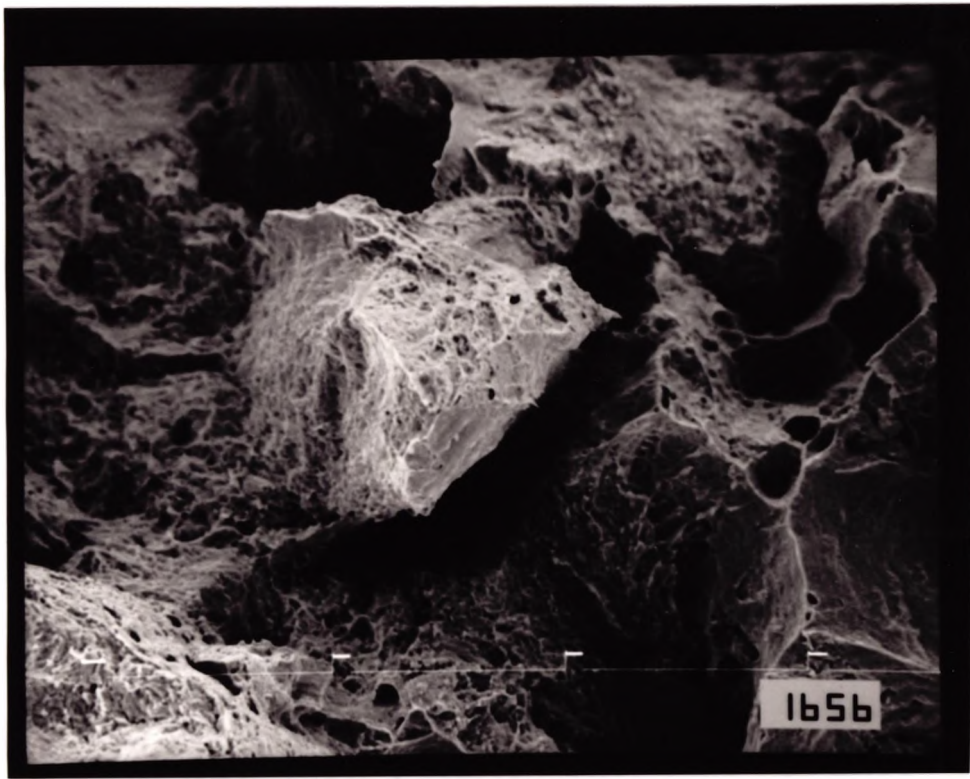
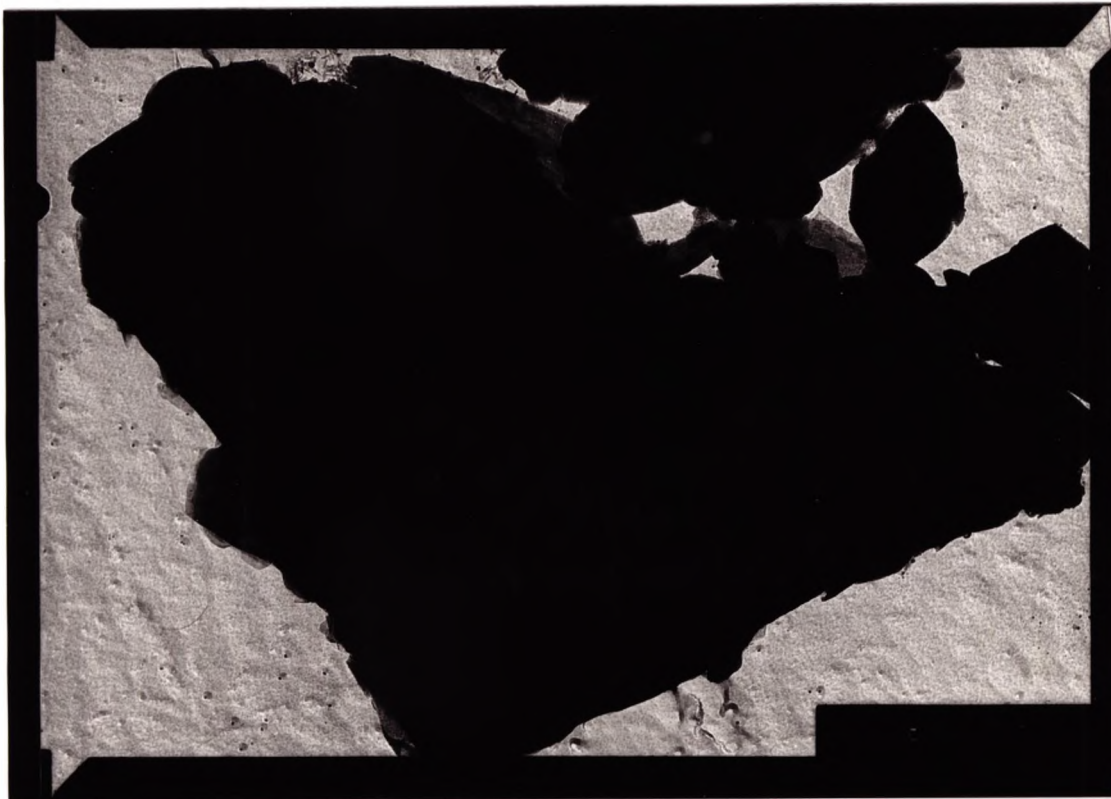


Fig. 6.16 Fracture surface of as-cast reheated Ti containing steel, tested at 900°C showing a mixture of intergranular micro-void coalescence and interdendritic failure (R.of.A 40%). Cooling rate 100°C/min.



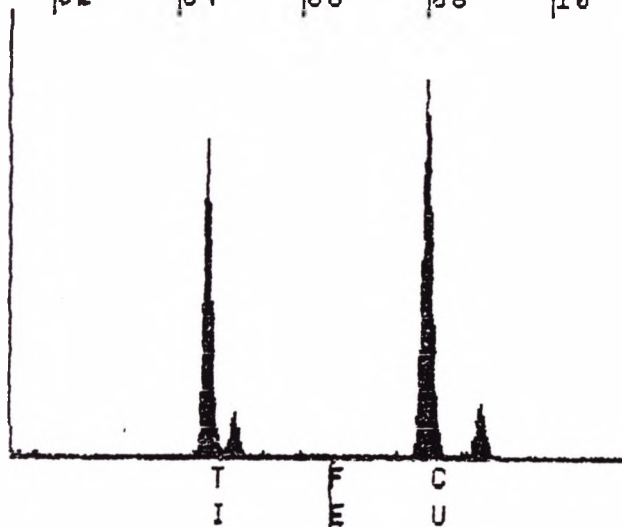
30 μm

Fig.6.17 Fracture surface of as-cast reheated Ti containing steel, tested at 900°C showing a mixture of intergranular micro-void coalescence and intergranular decohesion. R.of.A 40%). Cooling rate 100°C/min.



0.5 μ m

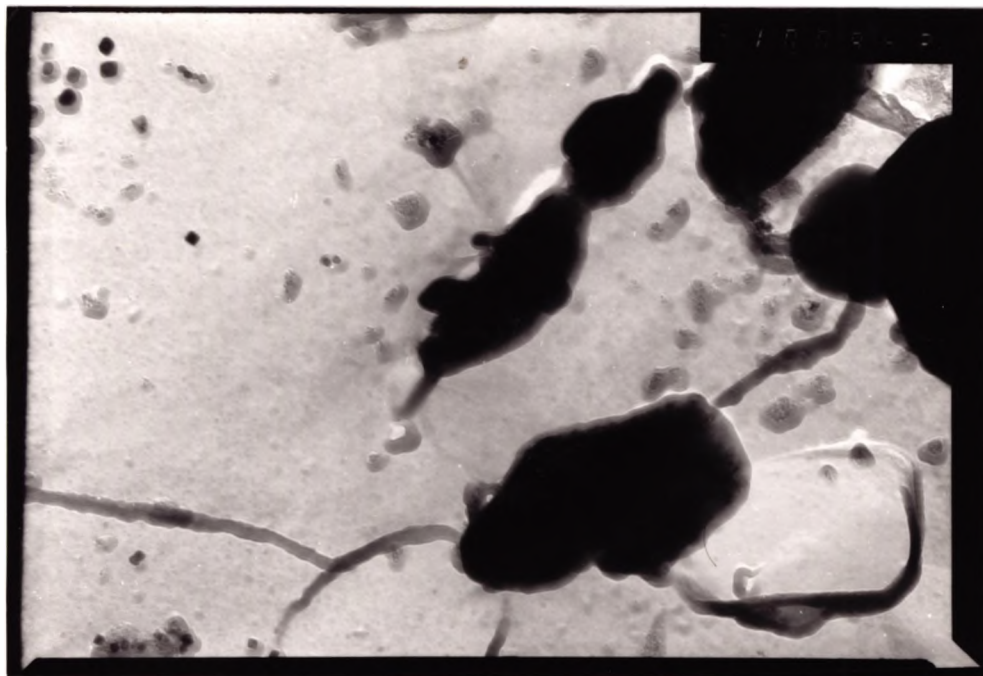
30-OCT-89 03:03:43 EDAX READY
 RATE: 53CPS TIME: 200LSEC
 00-20KEY: 10EV/CH PRST: 200LSEC
 A: B:
 FS= 1273 MEM: A FS= 200
 |02 |04 |06 |08 |10



CURSOR (KEV)=06.480

EDAX

Fig. 6.18 Ti eutectic found in the Ti containing steel tested at 1000°C, cooling rate 100°C/min.



0.36 μm

10-APR-90 15:23:27 PEAK IDENT
 RATE: 160PS TIME: 13LSEC
 00-20KEV: 10EV/CH PRST: OFF
 A: B:
 FS= 50 MEM: A FS= 50
 |00|02|04|06|08|10|12|14|16|18|20|22|24|26|28

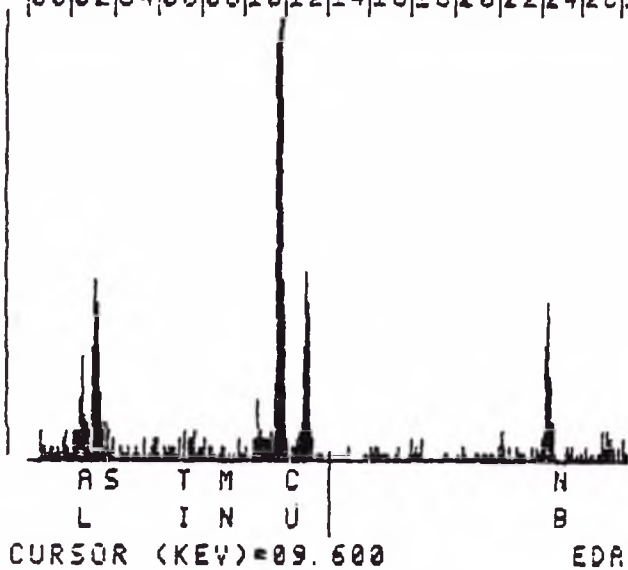
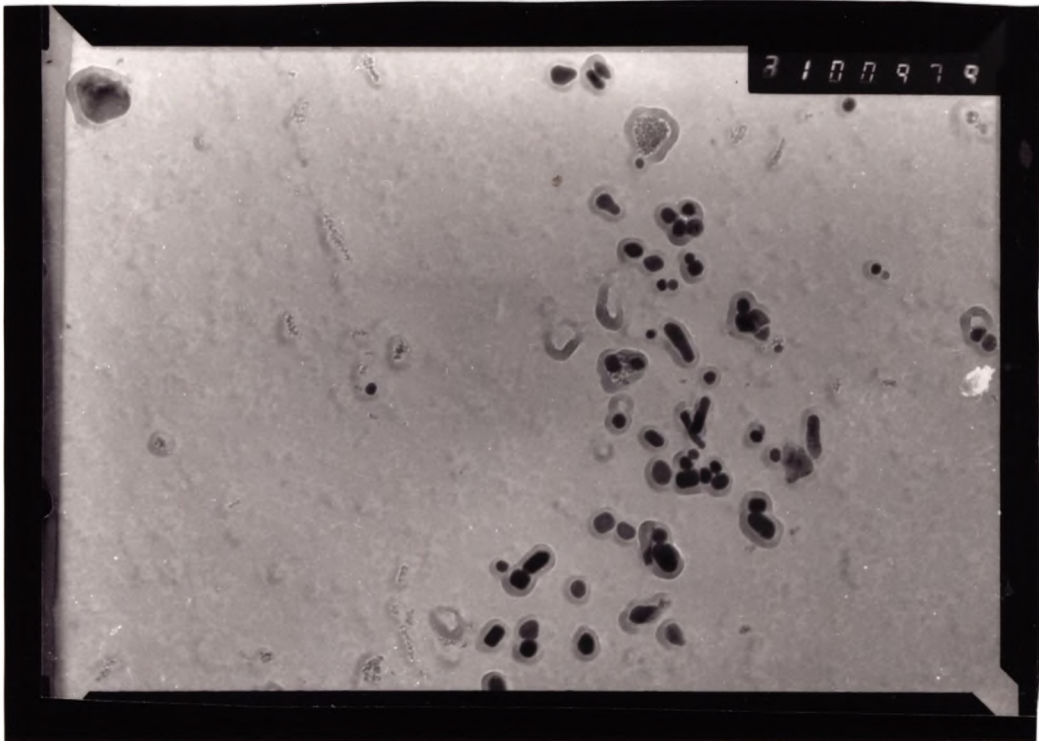
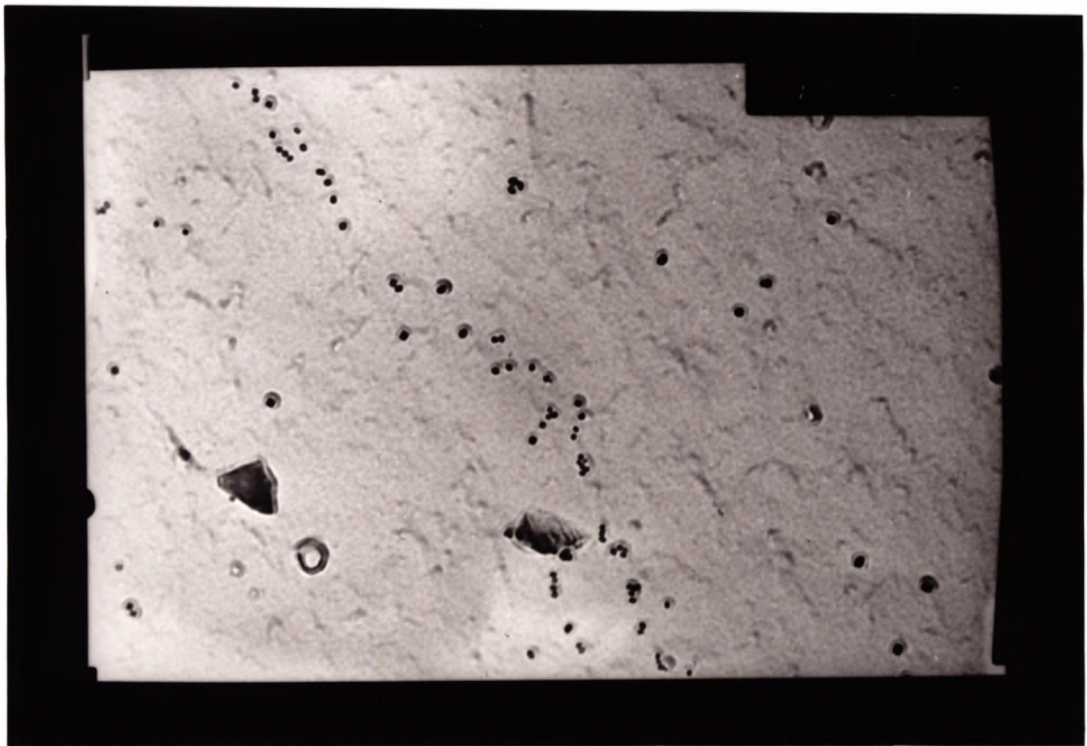


Fig. 6.19 Nb rich eutectic observed in Ti containing steel tested at 1000°C, cooling rate 100°C/min.



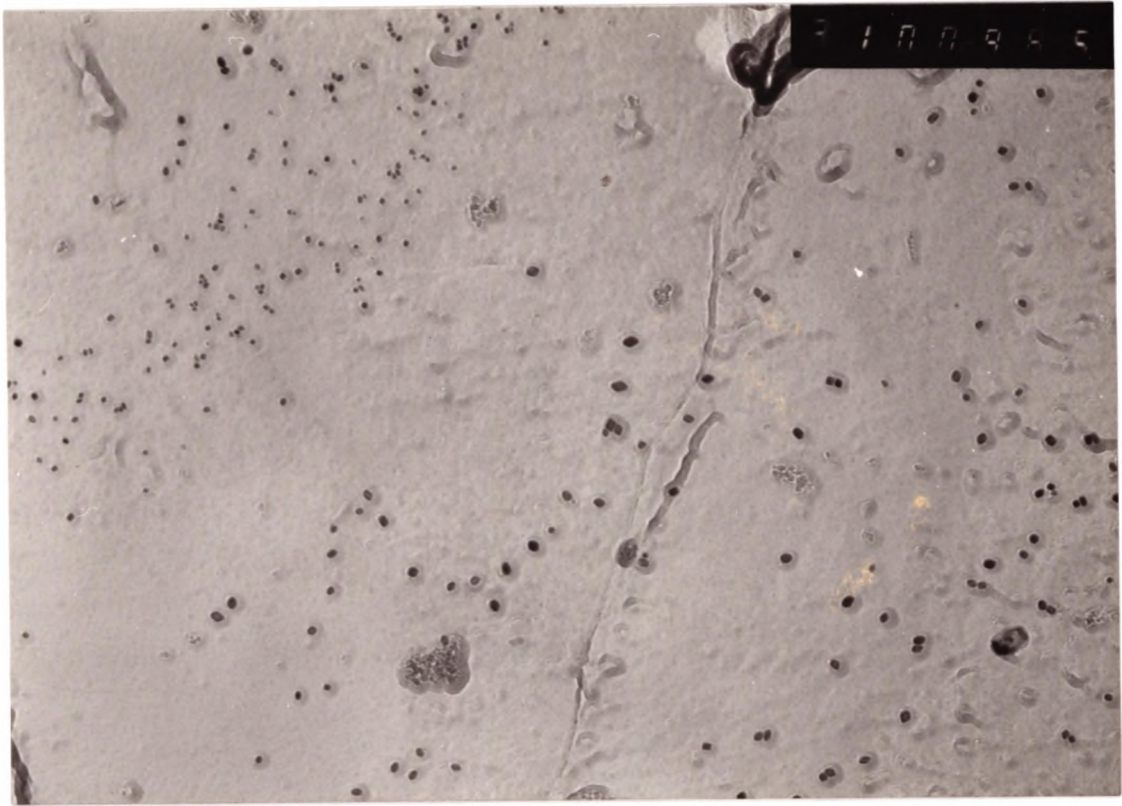
0.35 μm

Fig. 6.20 Coarse Nb rich precipitation found in the Ti containing steel, tested at 1000°C, cooling rate 100°C/min.



0.35 μm

Fig. 6.21 Fine Nb(CN) precipitation found in the Ti containing steel, tested at 850°C, cooling rate 100°C/min.



0.35 μm

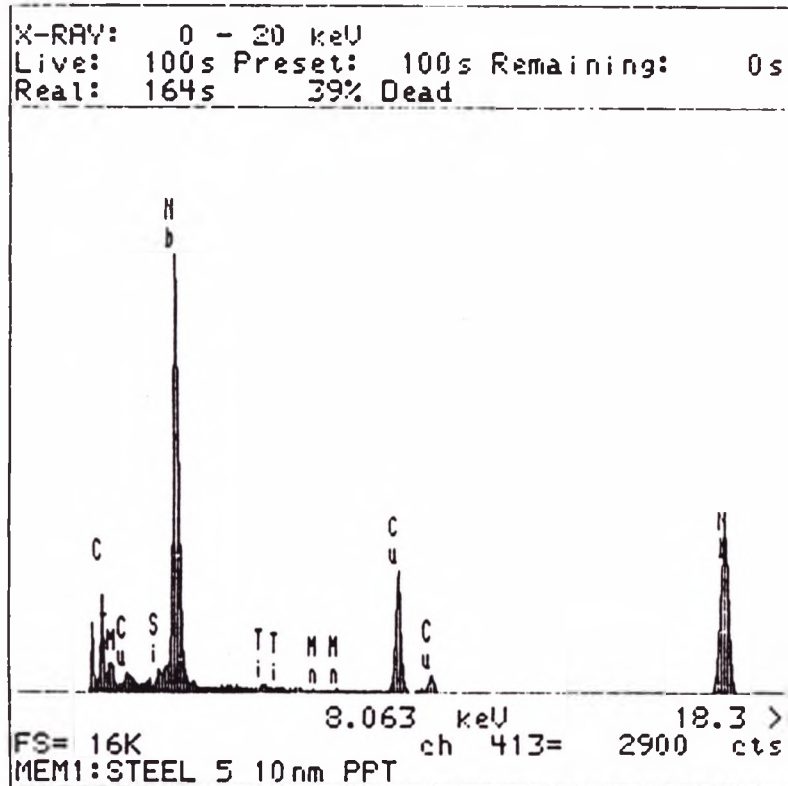
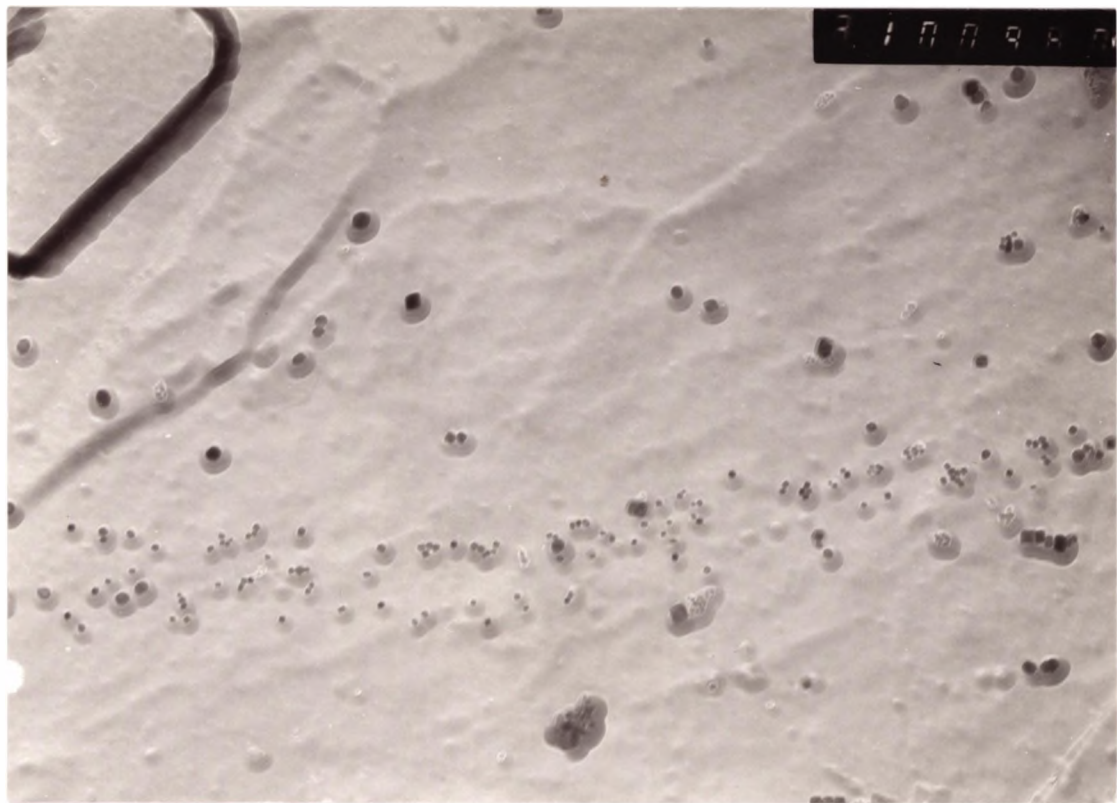


Fig. 6.22 Fine Nb(CN) precipitation found in Ti containing steel tested at 850°C, cooling rate 100°C/min.



0.35 μm

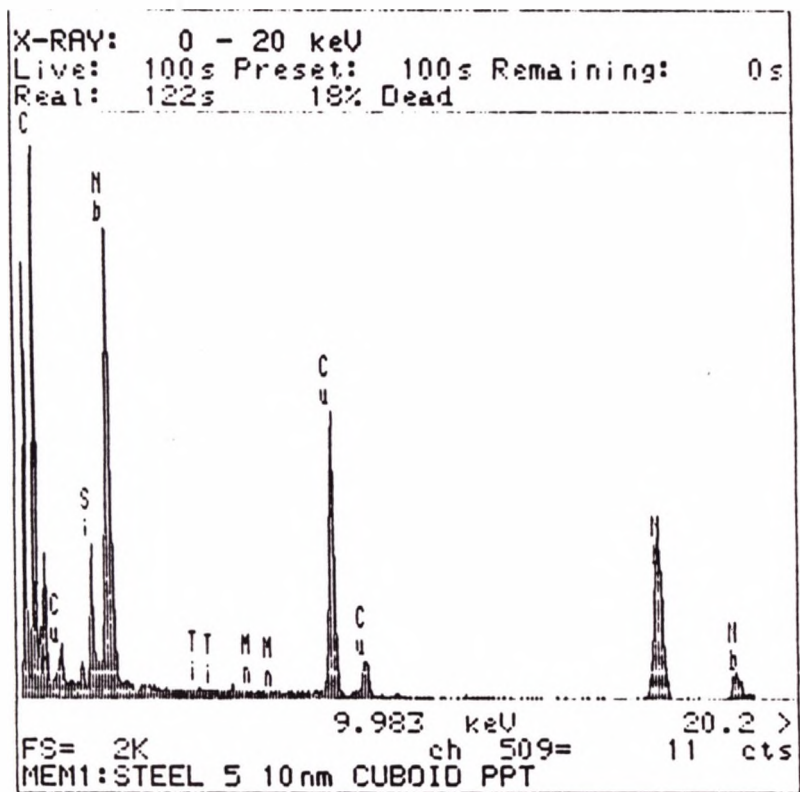
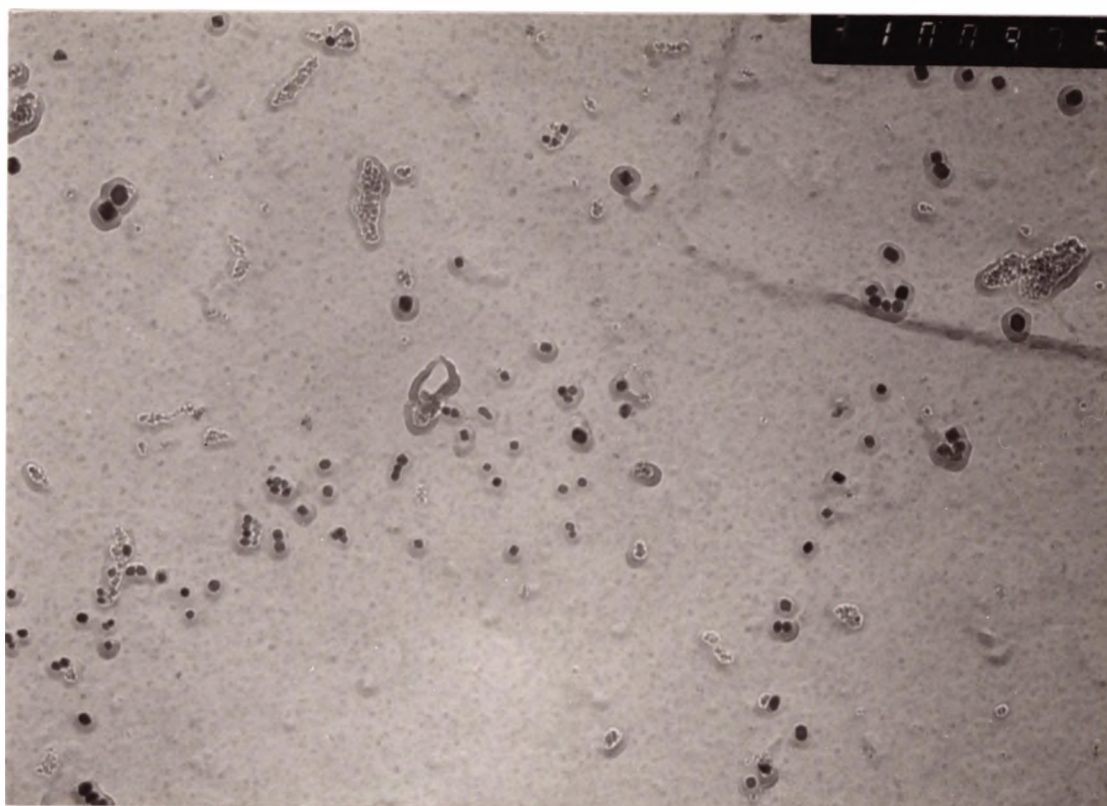


Fig. 6.23 Fine Nb(CN) precipitation found in Ti containing steel, tested at 850°C, cooling rate 100°C/min.



0.35 μm

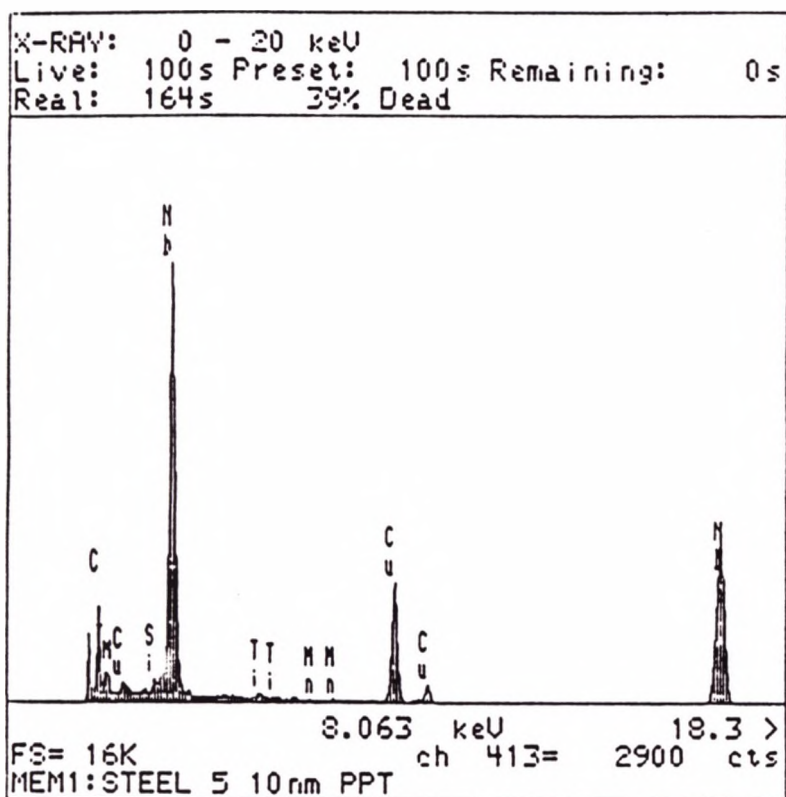
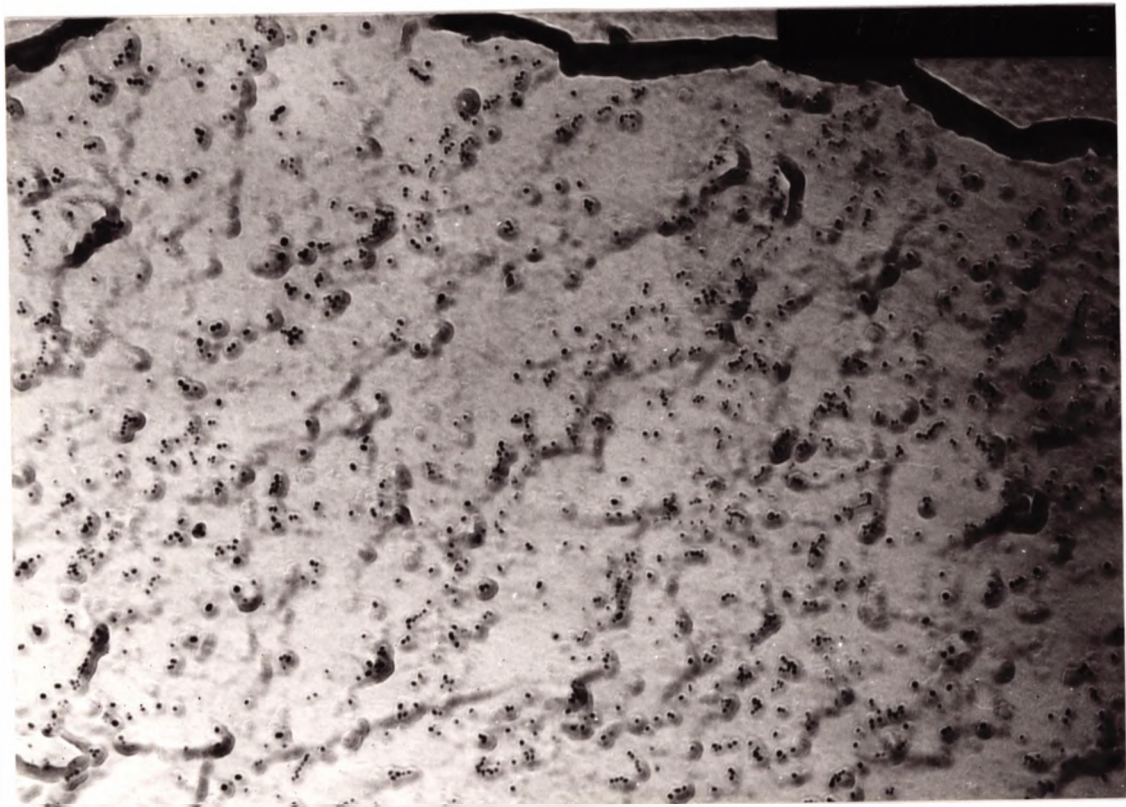


Fig. 6.24 Fine Nb(CN) precipitation found in the Ti containing steel, tested at 850°C. Cooling rate 100°C/min.



0.35 μm

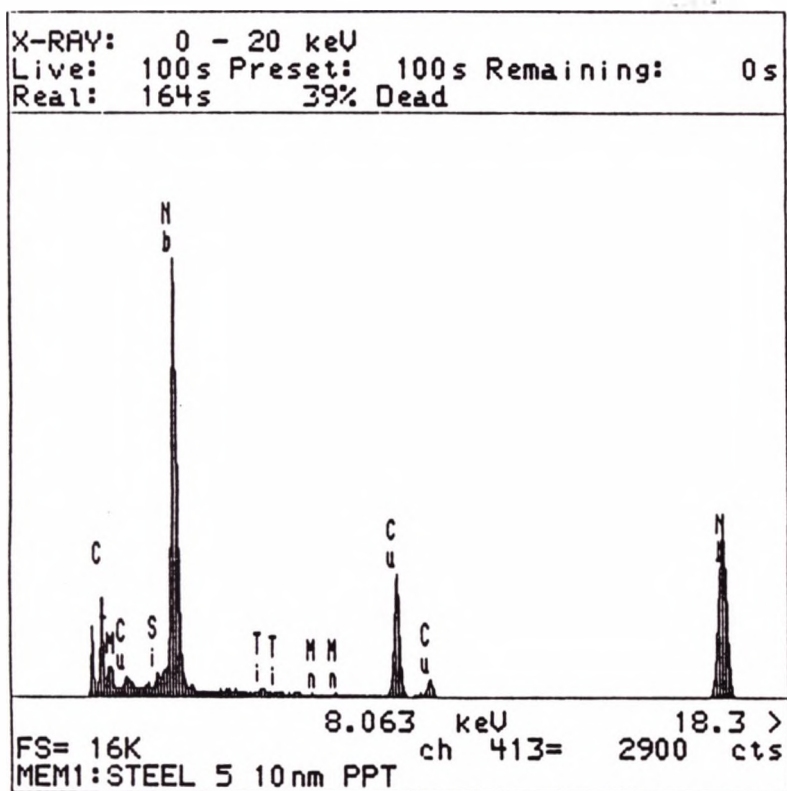
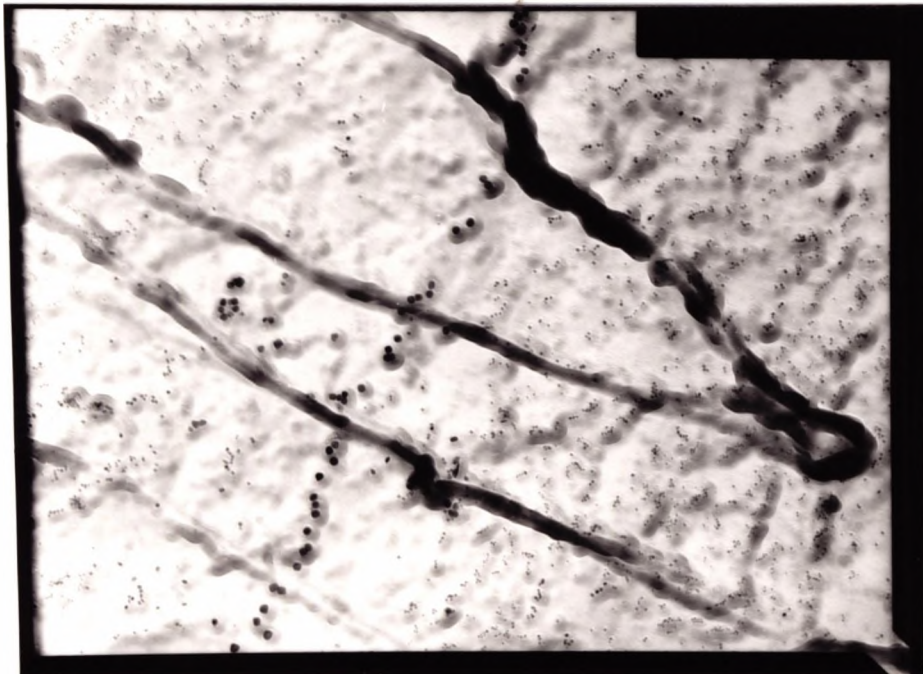


Fig. 6.25 Fine Nb(CN) precipitation found in Ti free steel , tested at 850°C, cooling rate 100°C/min.



0.35 μm

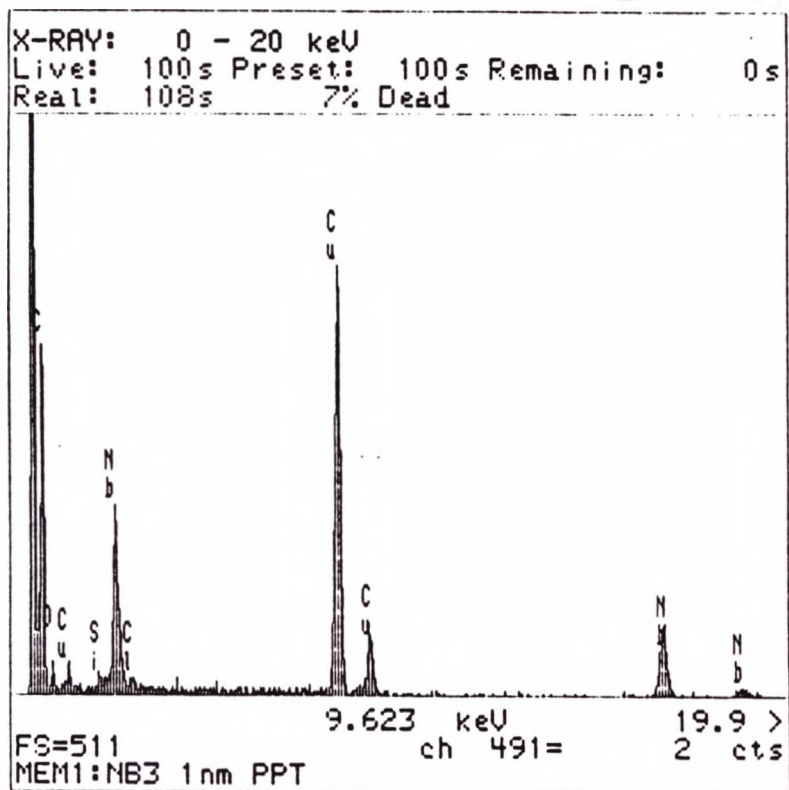
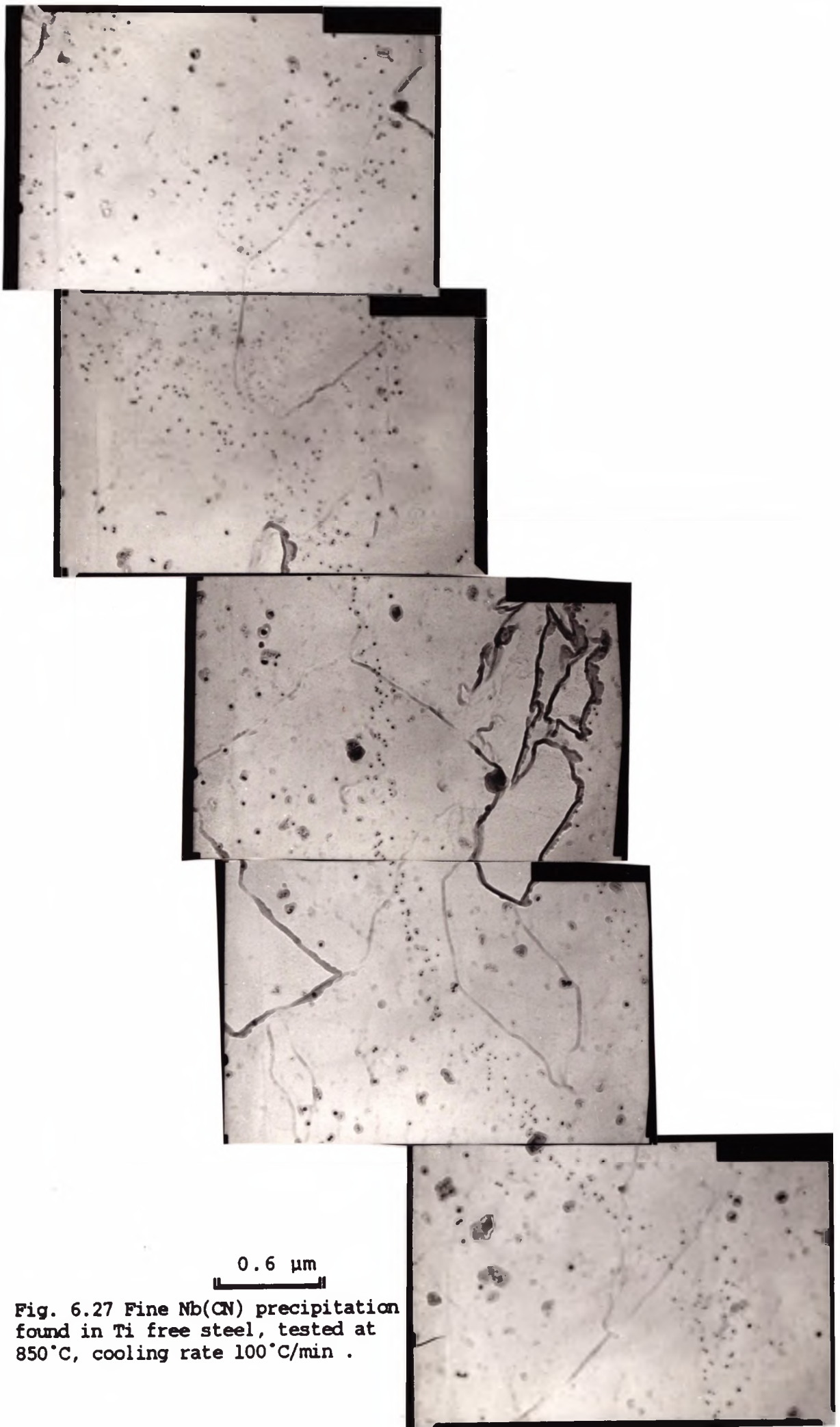


Fig. 6.26 Fine Nb precipitation found in Ti free steel, tested at 850°C cooling rate 100°C/min.



0.6 μm

Fig. 6.27 Fine Nb(CN) precipitation found in Ti free steel, tested at 850°C, cooling rate 100°C/min .

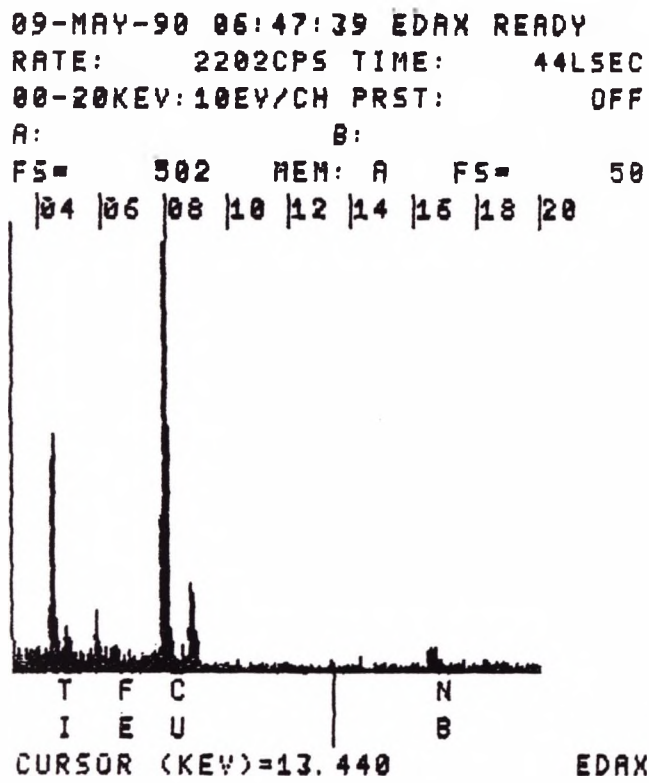
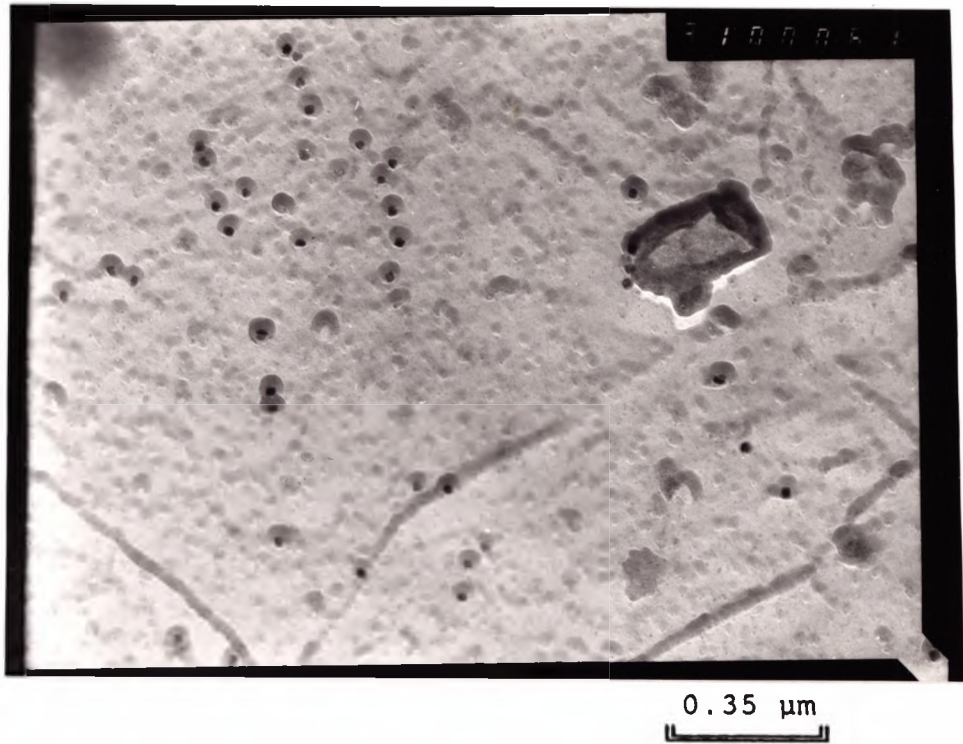


Fig. 6.28 Nb and Ti precipitation found in Ti containing steel tested at 850°C, cooling rate 25°C/min.

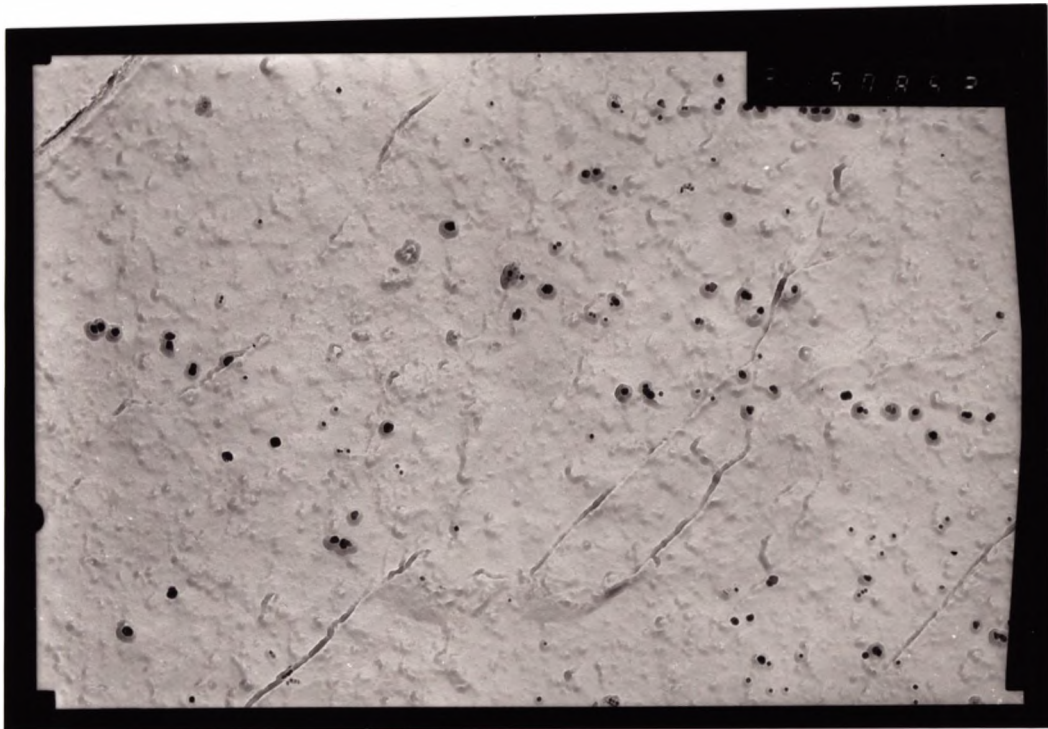


Fig.6.29 NbC precipitation found in Ti containing steel, tested at 850°C, cooling rate 25°C/min.

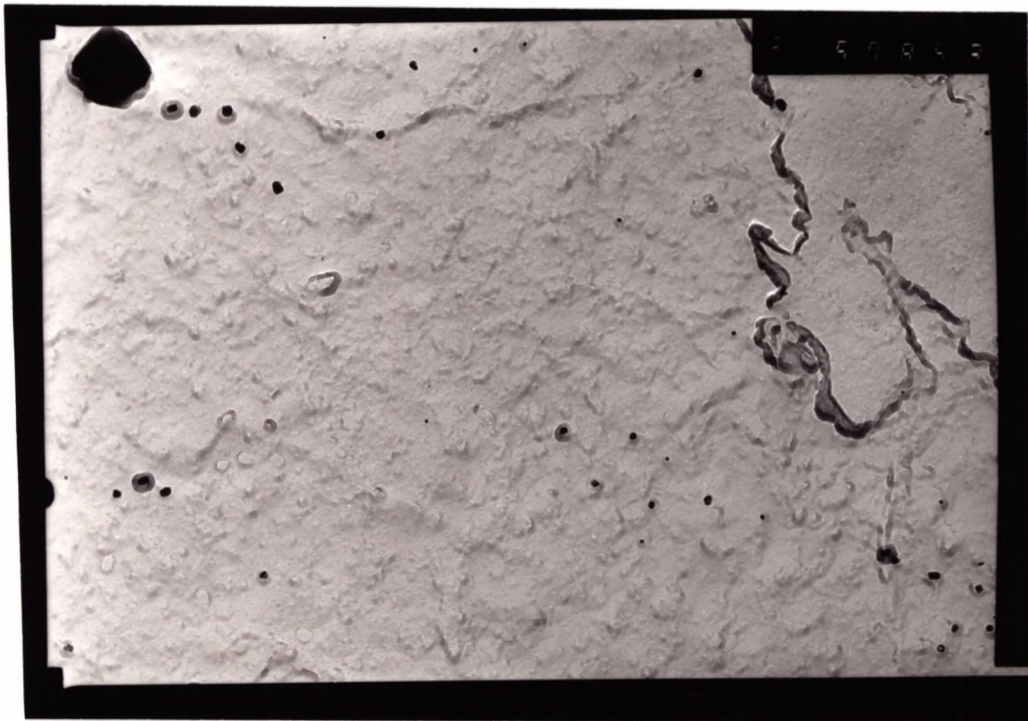
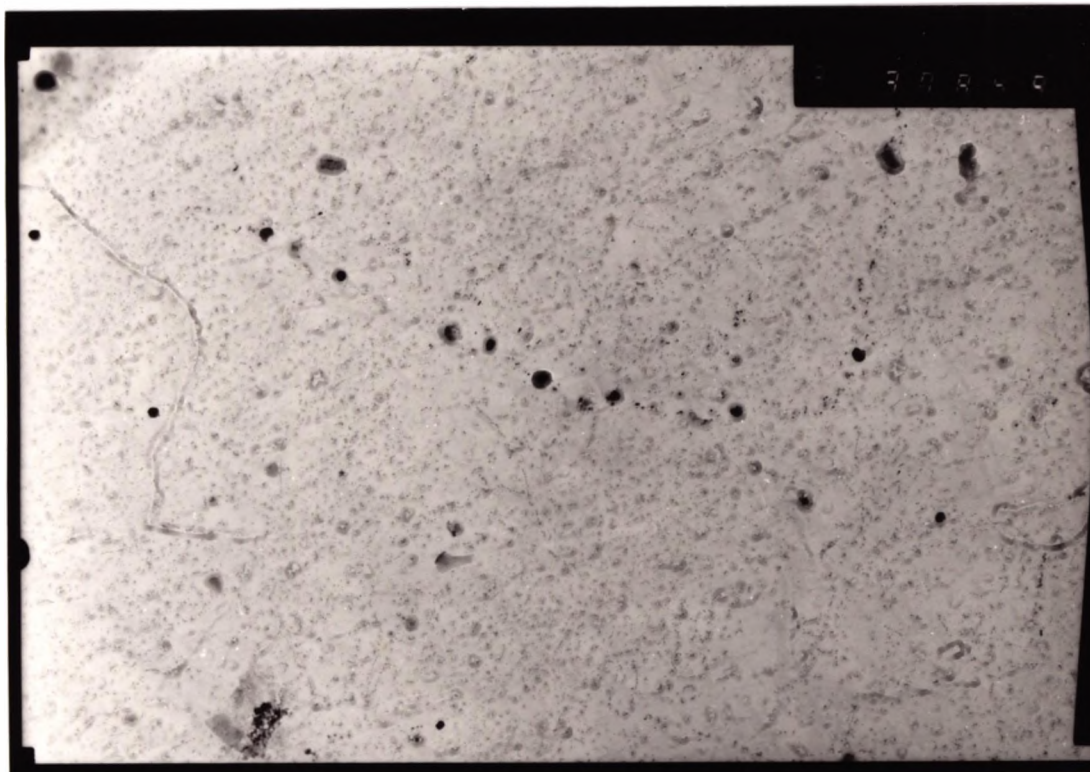
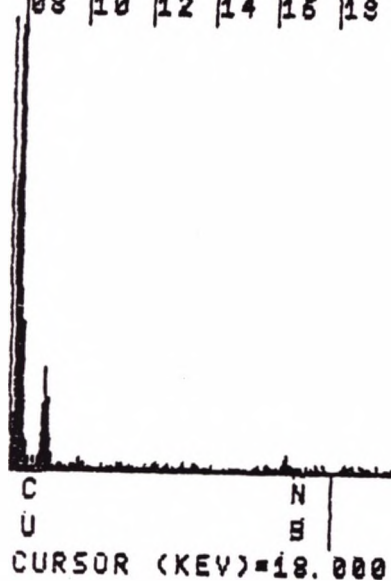


Fig.6.30 Nb and Ti precipitation found in the Ti containing steel, tested at 850°C, cooling rate 25°C/min.



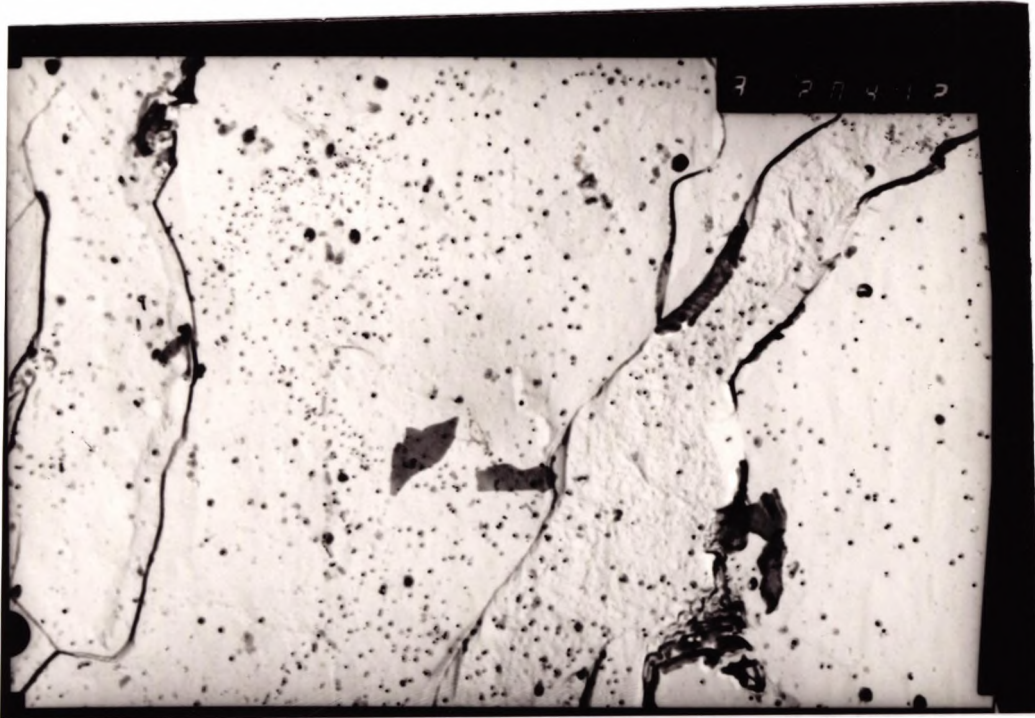
1.1 μm

15-FEB-90 06:17:05 EDAX READY
 RATE: 1350CPS TIME: 111LSEC
 00-20KEV:10EY/CH PRST: 200LSEC
 A: B:
 FS= 382 MEM: A FS= 100
 08 |10 |12 |14 |16 |18 |20



EDAX

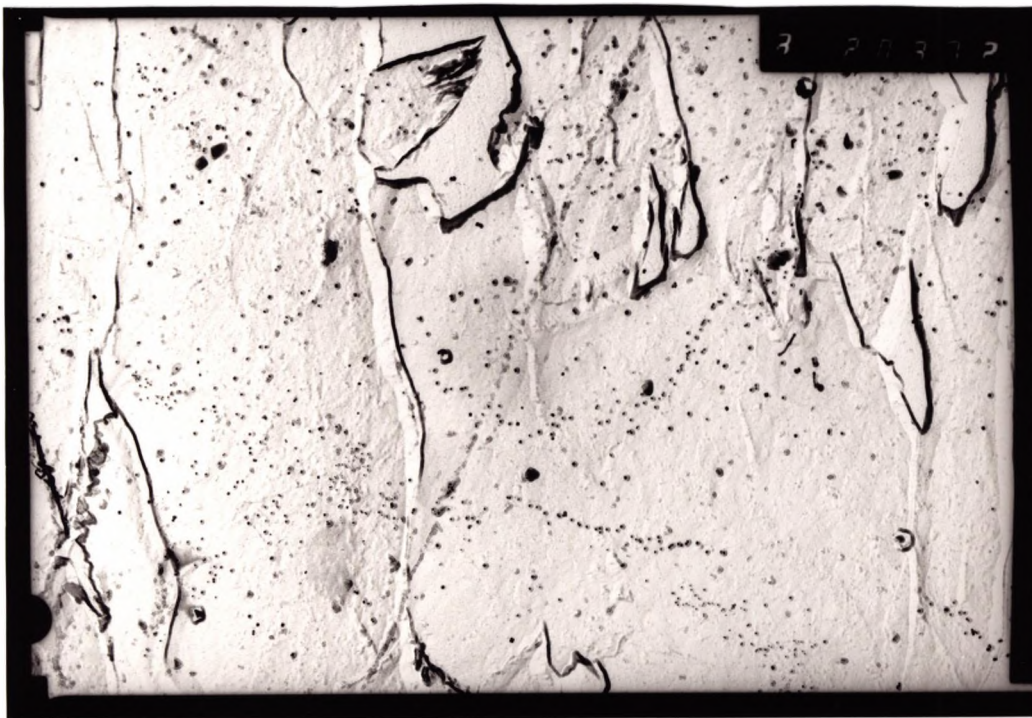
Fig.6.31 Nb precipitation found in Ti free steel, tested at 850°C, cooling rate 25°C/min.



1.8 μm



Fig.6.32 Nb and Ti precipitation found in as-cast reheated Ti containing steel, tested at 850°C. Cooling rate 100°C/min.



1.8 μm



Fig.6.33 Nb and Ti precipitation found in as-cast reheated Ti containing steel, tested at 850°C. Cooling rate 100°C/min.

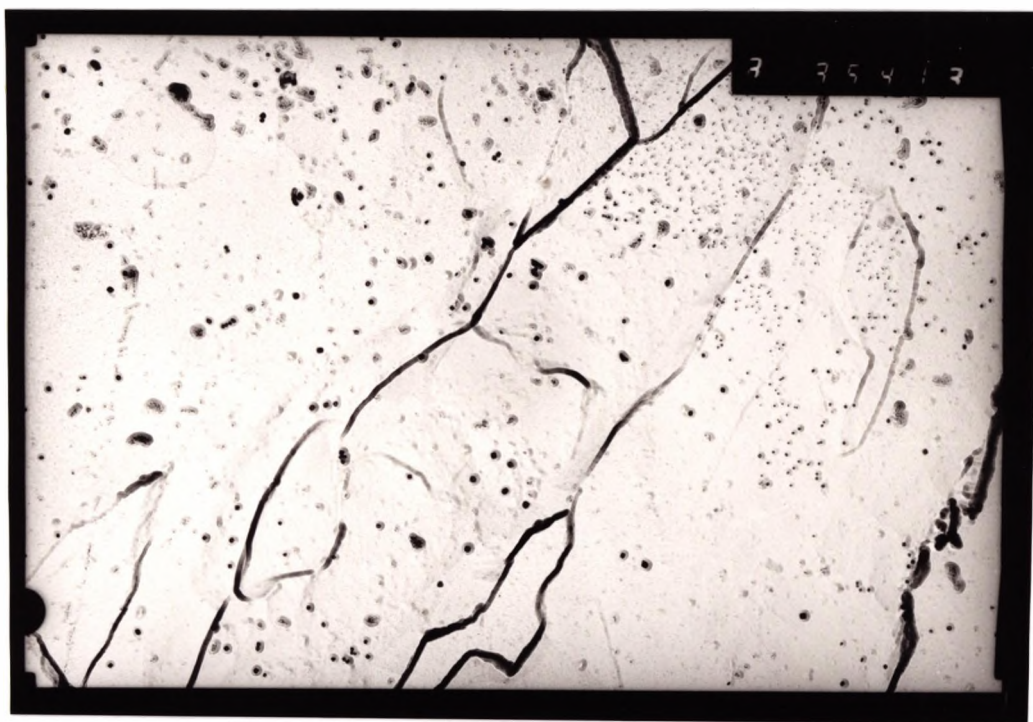


Fig. 6.34 Nb and Ti precipitation found in as-cast reheated Ti containing steel, tested at 900°C. Cooling rate 100°C/min.

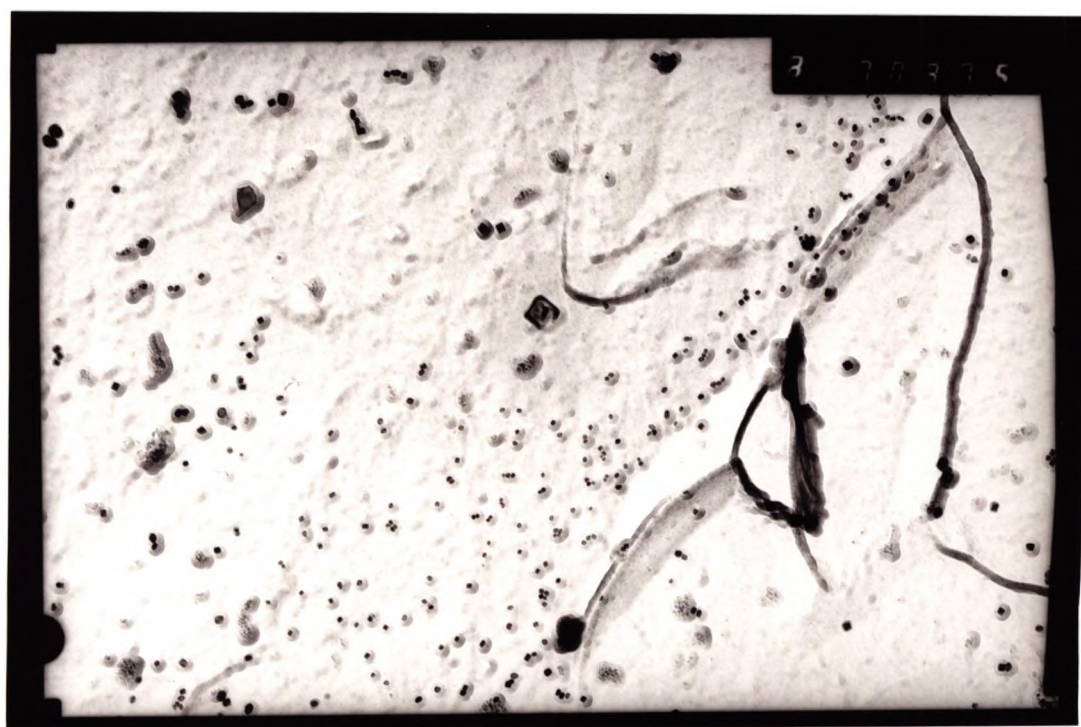


Fig.6.35 Nb and Ti precipitation found in as-cast reheated Ti containing steel, tested at 900°C. Cooling rate 100°C/min.

CHAPTER.....7

EFFECT OF Ti AND C ON THE HOT
DUCTILITY OF C-MN-AL STEELS

7.1 INTRODUCTION

In the last few years considerable interest has been shown in the hot ductility of micro-alloyed steels, particularly the C-Mn-Al-Nb grades which have been found difficult to continuously cast (Brimacombe and Sorimachi, 1977). It has been found from laboratory hot tensile tests in the temperature range 700-1000°C that the ductility trough is due to Nb(CN) precipitation at the γ grain boundaries, (Mintz and Arrowsmith, 1979; Wilcox and Honeycombe, 1980). However, this precipitation also has a marked effect in delaying the onset of dynamic recrystallization by restricting the boundary movement, and allowing cavitation processes to develop leading to intergranular failure.

However, ductility troughs are also observed in the absence of micro alloying elements (Ouchi and Mastumoto, 1982; Suzuki et al, 1982; Mintz and Arrowsmith, 1980).

In this case, the fall in ^{the}ductility trough is believed to be due to the onset of the γ to α transformation causing strain concentration in the softer ferrite which envelopes round the austenite grains. Increasing the C level will reduce the transformation temperature, and should therefore cause the ductility curve to move bodily to lower temperatures and this has been observed by a number of investigators (Crowther and Mintz, 1986; Suzuki et al, 1984; Mintz and Mohamed, 1989).

Unfortunately data for the influence of C on the hot

ductility of as-cast steels is lacking. This chapter, studies the effect of both carbon and titanium on as-cast hot ductility. Ti was included for examination because Mintz, (1980) had noted that in commercially produced Ti containing casts made at the 0.08% C level the as-cast grain size at the strand surface was finer than that exhibited by commercially produced Ti free casts made at the peritectic C level 0.16% in which coarser columnar grains were present. It was not clear whether this behaviour was due to the difference in C content or the presence of Titanium.

7.2 EXPERIMENTAL

C-Mn-Al steels with the same base composition (1.5% Mn, 0.35% Si) at two different C levels 0.05% C, and at the peritectic C level of 0.15% C, were chosen for examination. Both Ti free and Ti containing steels, 0.02% Ti, were examined and the full compositions are given in Table 7.1. The steels were laboratory air melts hot rolled to 12 mm thick plate.

Longitudinal tensile sample having a length of 70 mm and diameter of 7.94 were machined from the plates with their axis parallel to the rolling direction. The same technique as used in chapter (4) has been used for tensile testing the samples. The Samples were melted at 1540°C for 5 min, resolidified and cooled at 60°C/min to test temperature in the range 750-1000°C held for 5 min and then strained to failure at a rate of 2.10^{-3}s^{-1} .

Austenite grain sizes were obtained prior to deformation on quenched samples using the linear intercept measurement on both transverse and longitudinal sections. Measurements from the two sections were similar and the average has been taken as the γ grain size.

Carbon extraction replicas were taken from a cross-section taken close to the fracture surface for samples giving low ductility values. Carbon extraction replicas were also taken directly from the fracture surface. The precipitates extracted were analyzed using the EDAX attachment, and semi-quantitative analysis obtained using the EDAX programme SW.9100 version 2.3.

Examination of the fracture surface was carried out using a JEOL T100 scanning microscope operating at 25 KV.

7.3 RESULTS

7.3.1 Hot ductility curves

The curves of reduction in area against test temperature are given in Figs 7.1, 7.2, 7.3. and 7.4. All the steels show a marked ductility trough. At the 0.05% C level, the reduction in area values fell from 95% to about 25% and 37% at 850°C for the Ti free and Ti containing steels respectively as shown in Fig. 7.1.

The Ti steel gave a small improvement in ductility over the Ti free. Ductility was fully recovered when the temperature was further lowered to 750°C.

At the 0.15% C level, the ductility started to fall at 900°C and reached a minimum of 23 and 28% R.of.A for Ti free and Ti containing steels at the temperature of 800°C, Fig 7.2. The major effect of increasing the carbon levels was to shift the hot ductility curves to lower temperature, Fig 7.3 and 7.4 for Ti free and Ti containing steels respectively. Raising the C level from 0.05% to 0.15 caused the ductility trough to move to lower temperatures by approximately 50°C. Again the hot ductility for the Ti containing steel was slightly better. Ductility fully recovered for all steels examined when the test temperature was further lowered to 750°C.

7.3.2 Stress/Elongation curves

The stress/total elongation curves for all the steels examined are shown in Figs 7.6 and 7.7. The fluctuations in the flow curves at test temperature $>900^{\circ}\text{C}$ were observed

for all C levels examined. These fluctuations are arrowed in the figures.

7.3.3 Metallography

The γ grain size was the same and coarse ~ 1.5 mm for all steels examined. i.e the Ti addition was not able to grain refine in the as-cast state. The γ grain size was also found to be independent of the C content.

Evidence for deformation induced ferrite was found for all steels tested at test temperatures close to the minimum ductility temperature on the hot ductility curves, Fig. 7.8.

Wedge type cracks formed by grain boundary sliding were frequently observed, Fig 7.9.

In accord with the minor differences in the hot ductility behaviour of Ti Containing steels, and Ti free steels, no difference was noted in their fracture appearance. Fracture at low ductility tended to be mainly of the micro-void coalescence mode, Fig 7.10. Second phase particles were often associated with these microvoids, Fig 7.11. Intergranular decohesion was also observed Fig.7.12 characterised by flat austenite grain facets as well as high temperature rupture, Fig 7.13. At high temperature, ductile rupture was observed this being shown by large voids on the fracture surface apparently not associated with second phase particles. As in previous work isolated regions containing dendrites were observed. Because of the higher S levels in these steels lines of many coarse, angular Mn(Fe)S inclusions 2 to 6 μm long could be seen which probably mark regions where a number of dendrites meet Fig. 7.14. Smaller spherical inclusions 2 μm in cross

section were observed on the nodule surface.

7.2.3 Replica Examinations

Only a few AlN precipitates were noted in the steels examined. The Ti containing steels contained randomly distributed Ti rich precipitates as in Fig 7.15, 7.16 and 7.17.

Replicas taken directly from the fracture surfaces showed some very coarse Ti and Al rich particles in the Ti containing steel, Fig 7.18 and some Al rich particles in the Ti free steels, Fig 7.19.

7.4 DISCUSSION.

7.4.1 Influence of Ti on hot ductility.

In the present as-cast study only a very limited benefit to the hot ductility occurred on adding Ti. This small improvement in ductility was present at both C levels, 0.05 and 0.15% C. This contrasts with the large influence Ti has on hot ductility when steels are heated to 1330°C and tested in the temperature range 1000 to 700°C (Mintz et al, 1980). In the latter instance Ti can grain refine. Finer grain sizes improve ductility because they make it more difficult for cracks to propagate by increasing the number of triple points, which the cracks have to surmount, as well as reducing the stress concentration associated with a crack.

In the as-cast situation the grain size was the same and coarse ~1.5 mm, independent of the presence of Ti. Ti has no effect in the as-cast state, because on melting, all the Ti particles go back into solution and precipitation takes place just after solidification, when they are unable to control grain size. A coarse structure is therefore produced which is no different from that found in Ti free steels. The very small improvement in ductility observed on adding Ti, may in this instance, be due to the removal of nitrogen as aluminium nitride.

Mintz et al, (1991) have suggested that the solubility product has to be in the range of 3.10^{-4} for aluminium nitride to start precipitating out and the high N level in

the present steels combined with moderate soluble Al levels bring the solubility products close to this value. Also segregation of Al and N to the boundaries is likely to be high in as-cast steels making AlN precipitation more likely. If AlN is able to precipitate then having Ti present should considerably reduce the amount of AlN precipitated, as the Ti will remove most of the N from solution as a TiN precipitation.

AlN is likely to be more detrimental to ductility than TiN because it is precipitated at the γ grain boundaries rather than randomly in the matrix.

Although these results indicate little benefit to the hot ductility on adding Ti to a C-Mn-Al steel, care must be taken in translating these results to the continuous casting operation. The cyclic rise and fall in surface temperature by impingement of the water sprays on the strand as it moves between the rolls is known to encourage precipitation, so that a marked detrimental grain boundary precipitation of AlN may occur under these conditions. Whereas this cyclic rise and fall in temperature is unlikely to influence the hot ductility curves for Ti containing steels, it may have a pronounced influence on the curves for Ti free steels where widening and deepening of the trough is noted (Cardoso and Yue, 1989).

7.4.2 Influence of C on the hot ductility.

Because there is only a very small amount of AlN precipitation in these steels intergranular failure will not be associated with grain boundary sliding in the austenite. The steels are likely to behave like plain C-Mn steels in which the trough obtained is related to the onset of the γ to α transformation (Mintz et al, 1991).

In these steels on lowering the test temperature transformation takes place from γ to α and a situation is reached in which a thin film of ferrite (5 to 20 micron) is formed surrounding the austenite grain boundaries. As the ferrite is the softer of the two phases, the deformation becomes concentrated in these thin films. Voiding occurs at the MnS inclusion situated at the boundaries as with normal ductile failure.

Maki et al (1985); Crowther and Mintz, (1986 b); Mintz et al (1990) have reported that the ferrite responsible for the thin film is deformation induced and forms at temperatures up to the Ae_3 . Ductility recovers on the low temperature side of the trough just below the Ar_3 temperature when the normal transformation induced ferrite is formed prior to test, in a sufficient volume fraction to distribute the strain more uniformly. Hence raising of the C level will lower the transformation temperature and shift the ductility curves to the lower temperatures as is observed in Figs 7.3 and 7.4. Using Andrew's formula, (1965) to calculate the Ae_3 temperatures, the high C steel has an Ae_3 of 870°C and the 0.05% C steel an Ae_3 of 830°C .

reasonably close to the observed change of 50°C.

A widening of the trough also occurs as the carbon level rises from 0,05 to 0.15% Fig 7.3. The reason for this is also probably related to the transformation behaviour. If the width of the trough is taken as the difference between the Ae_3 and Ar_3 temperatures, then it can be seen from Crowther and Mintz's work on plain C-Mn steels, in which the steels were heated to 1330°C prior to cooling to the test temperature, that this difference increases at least up to a carbon level of 0.35%, Fig 7.5. The cause of this widening is presumably due to the lowering of the Ae_3 temperature with increase in C content, reducing the diffusion rate and slowing down transformation under non-equilibrium conditions.

The present results indicate that even though the width of the trough is reduced as the C content decreases, lower C levels do not guarantee better hot ductility than higher C steels. It can be seen in Fig 7.3 and 7.4 that the test temperature or straightening temperature is also important in dictating whether lower C steels have the better ductility. If straightening is carried out at a temperature of 850°C, the higher C steel has the better hot ductility, while at 800°C the lower C steel has the highest R of A ductility values.

Care again must, however, be exercised in transferring these results directly to the continuous casting operation. There is evidence to indicate that at the peritectic composition, 0.15% C, a composition range which seems to

favour transverse cracking, coarse columnar grains are produced at the surface of a continuously cast slab while at lower and higher carbon contents this does not occur and the grain size is finer (Maehara et al, 1985). Lower temperatures refine the as-cast grain size by having the δ ferrite phase present while higher temperatures refine the grain size by having the liquid phase present. It is possible these columnar grains ~~which~~^{will} give rise to poor ductility.

In the present investigation, coarse columnar grains were not produced at the peritectic composition. This arises because the cooling conditions in the small tensile samples are very different from those experienced at the surface of the slab. Heat transfer in the small tensile is mainly conduction along the length, not from the surface as in continuously cast material, and solidification is more rapid.

Maehara et al, (1985) have also suggested that the coarser grain size present in the peritectic range should lead to poor hot ductility. However although coarsening the grain size will reduce the ductility, as already mentioned, the major influence of grain size on R of A values occurs in the grain size range 20 to 300 μm , (Crowther and Mintz, 1986). The γ grain size in continuously cast slab will always be $>500 \mu\text{m}$, even at the lower and higher C ranges and it is unlikely that coarsening the grain size further would have such a major effect on hot ductility. It is possible, however, that a columnar grain structure can give very deep cracks at the slab surface if the boundary

regions are weak, as has been indicated by recent work of Harada et al, (1990) which suggests that transverse cracks are associated with intense P segregation, this being introduced by the mould oscillations causing liquid high in segregates to be entrapped between the solidifying dendrites near the surface. This work also indicated the entrapment did not occur to the same extent with the low carbon steels, again perhaps due to the absence of columnar grains, at the slab surface.

Thus neither the dendritic structure nor the segregation patterns, encouraged by the mould oscillation, can be simulated in the hot tensile test. Nevertheless, there is no doubt that C will influence the transformation behaviour and care should be taken in adjusting the secondary cooling conditions to give the optimum hot ductility at the straightener.

7.5 CONCLUSIONS

1- Ti had only a small influence in improving the hot ductility at the two C levels examined 0.05 and 0.15%. This small improvement was probably due to the Ti removing some of the N from solution as TiN and preventing the more detrimental AlN from precipitating out as the temperature was lowered to the temperature range 1000°C to 700°C.

2- Raising the C level was found to move the ductility curve troughs to lower temperatures, in agreement with previous work, (Crowther and Mintz, 1968; Mintz and Mohamed 1988). This would be expected as the troughs are controlled by the presence of deformation induced ferrite which forms in the temperature range between the Ar_3 and Ae_3 . The trough was found to widen with increase in C level and this can also related to changes in transformation temperature.

3- Grain size was coarse at both the C levels examined and not influenced by the Ti addition.

Although these results have important commercial implications for continuous casting practice, care must be taken in applying the result directly as the casting and cooling conditions used in the hot tensile test are very different from those applied during the commercial operations.

Table 7.1

Composition of Steels Examined wt.%

<u>Code</u>	<u>C</u>	<u>Mn</u>	<u>Si</u>	<u>P</u>	<u>S</u>	<u>Al</u>	<u>N</u>	<u>Ti</u>
Steel 1	0.051	1.51	0.37	0.015	0.010	0.04	0.0094	—
Steel 2	0.051	1.51	0.38	0.014	0.009	0.03	0.0094	0.02
Steel 3	0.14	1.57	0.36	0.015	0.010	0.04	0.009	—
Steel 4	0.15	1.56	0.36	0.015	0.010	0.04	0.0094	0.018

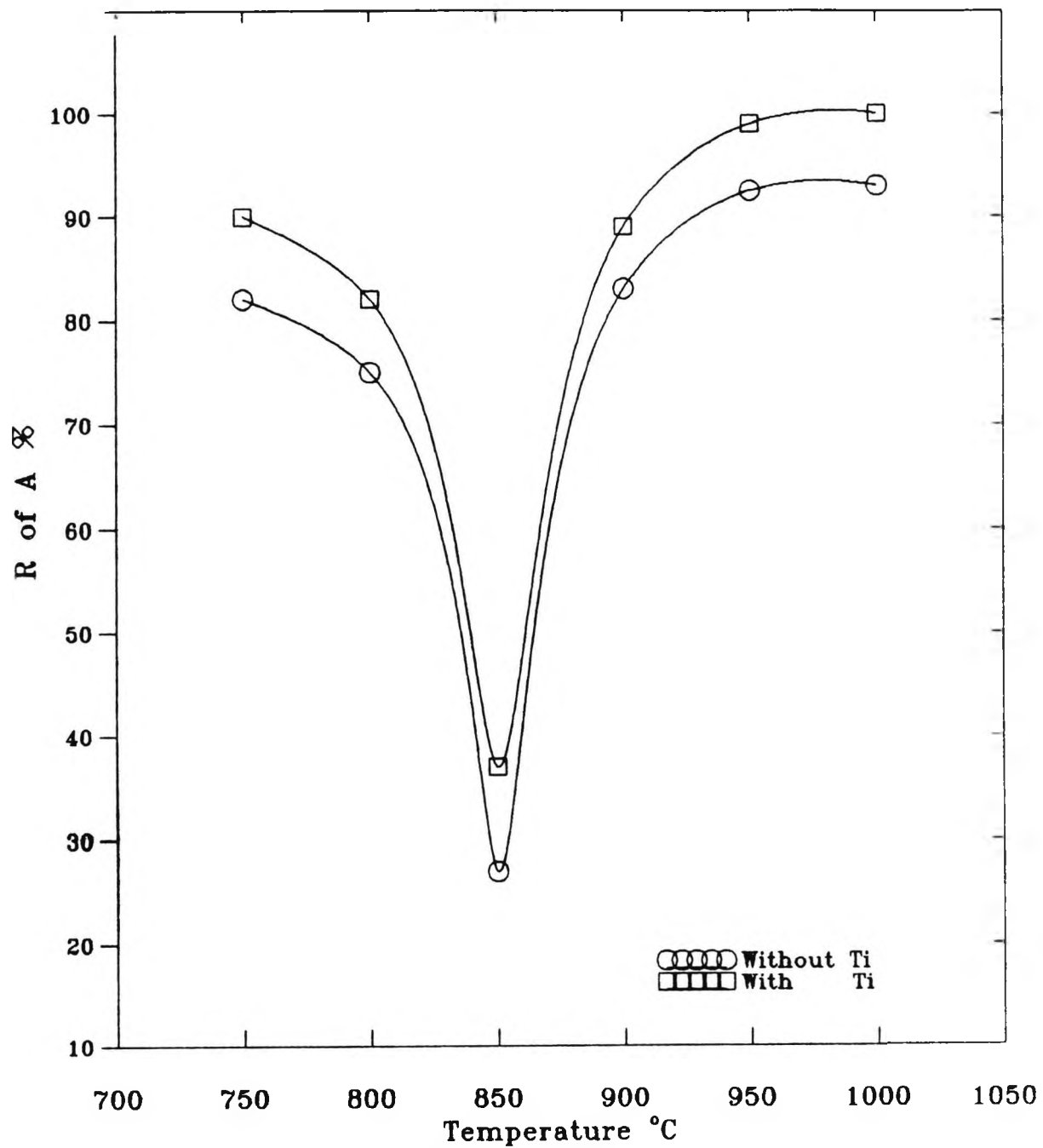


Fig 7.1 Hot ductility curves for 0.05%C.

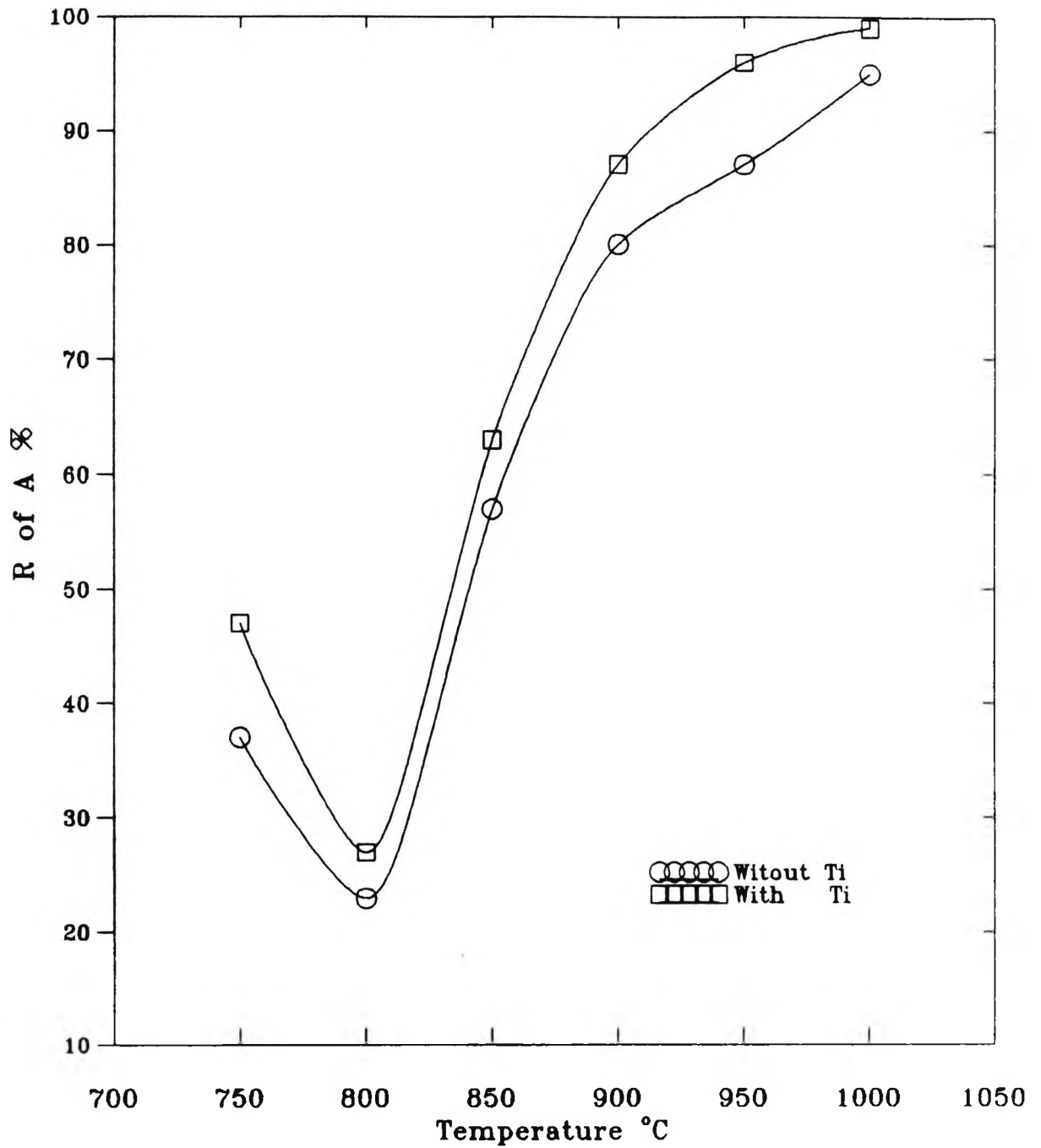


Fig 7.2 Hot ductility curves for 0.15%C.

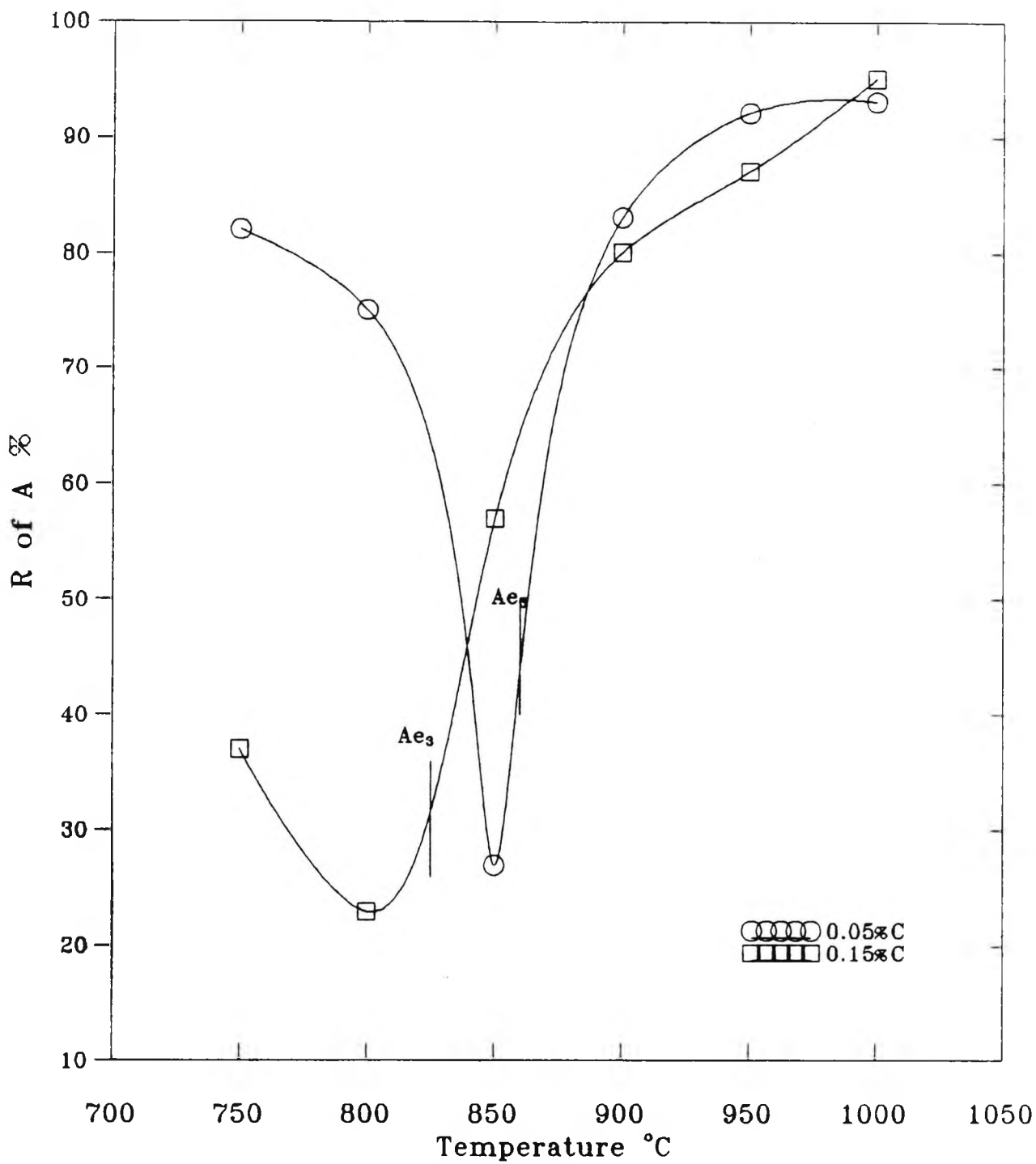


Fig 7.3 Influence of C on hot ductility for Ti free steels.

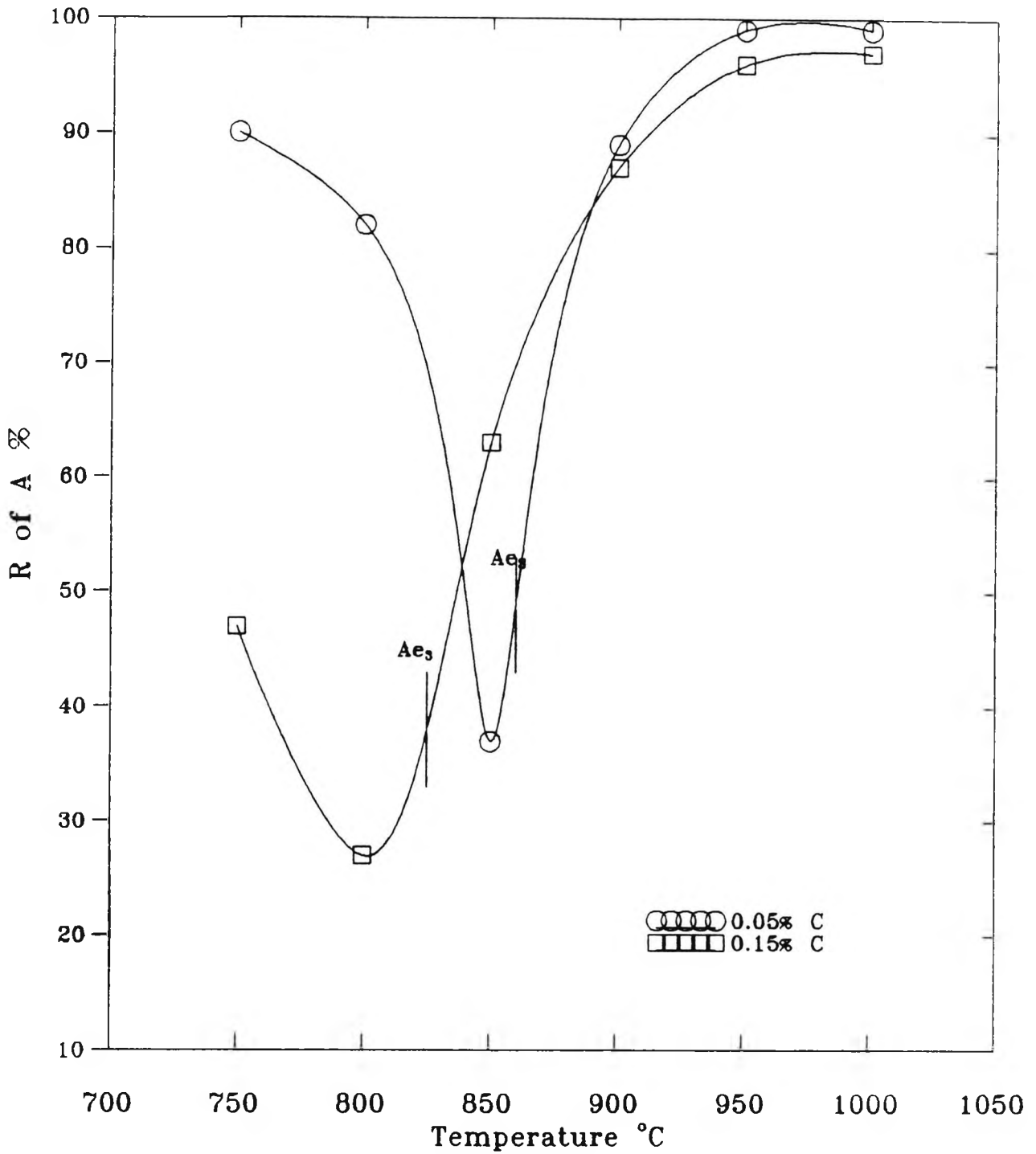


Fig 7.4 Influence of C on hot ductility for Ti steels.

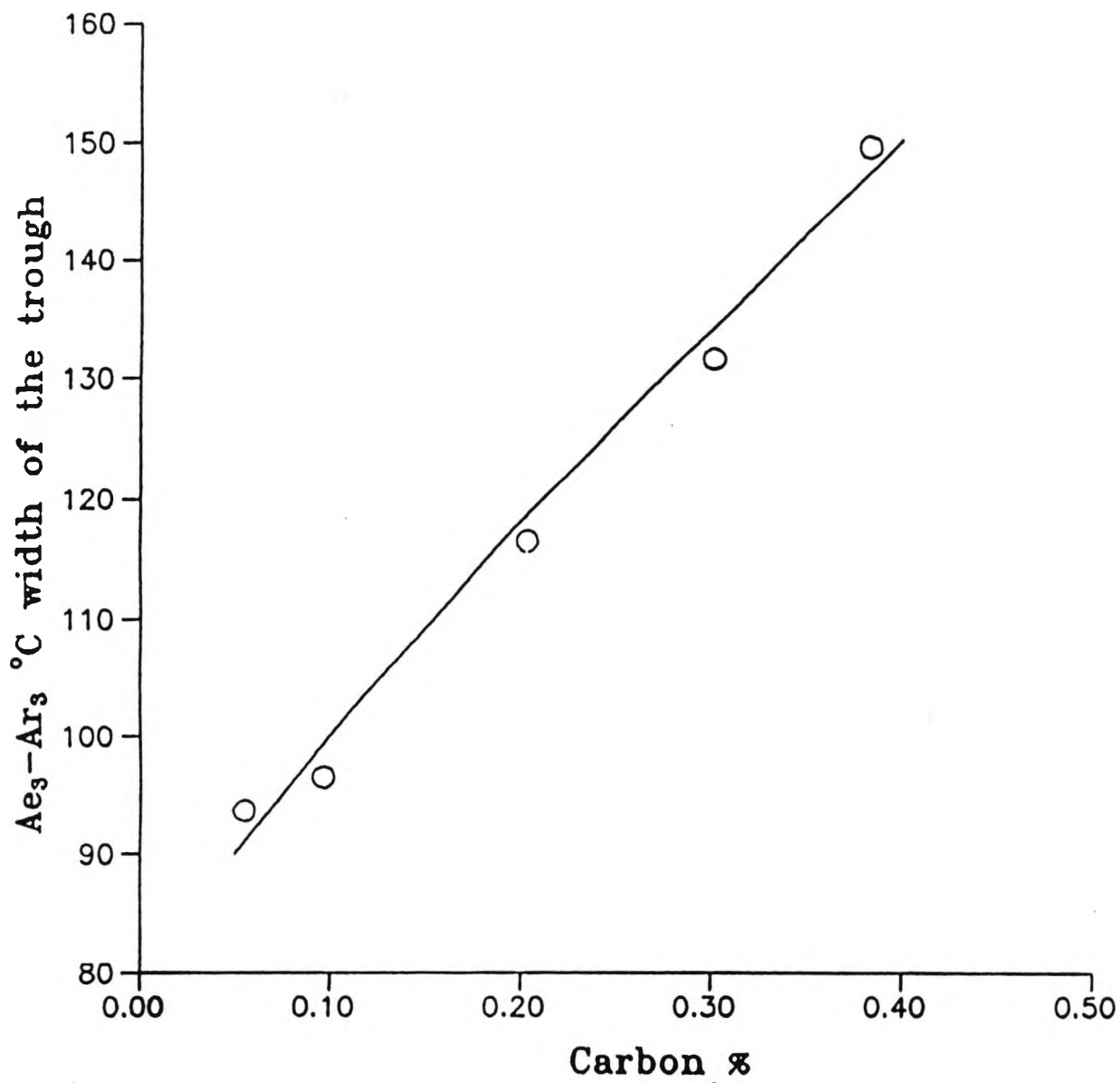


Fig 7.5 Influence of carbon content on the difference in temperature between the A_{e3} temperature and the A_{r3} temperature.

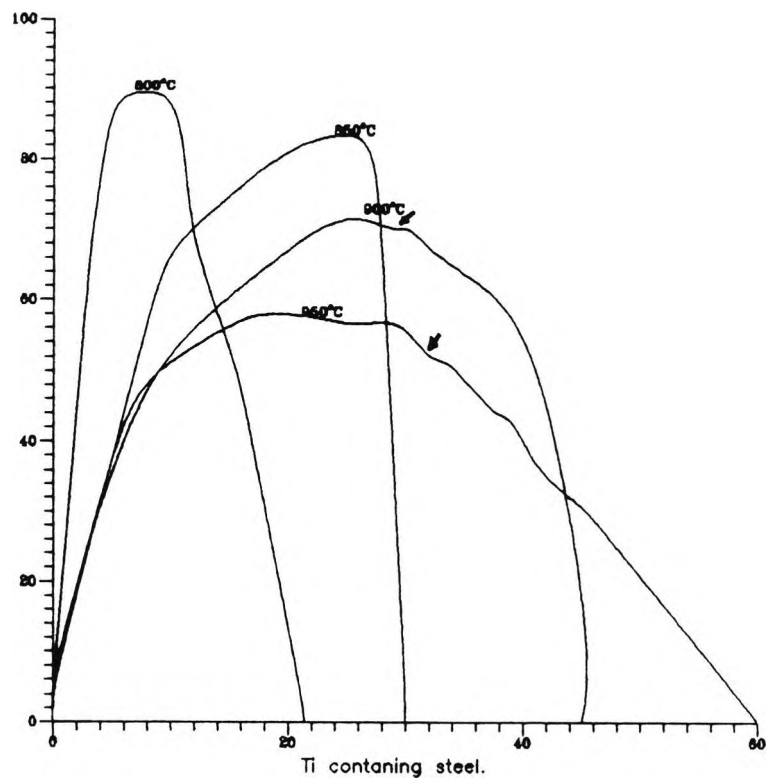
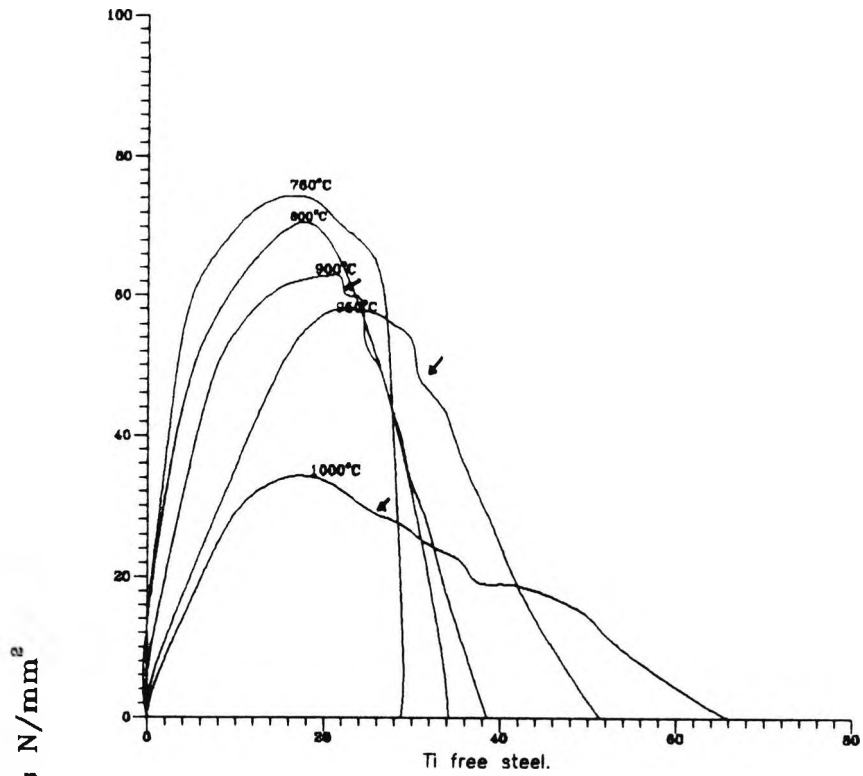


Fig. 7.6 Stress/Elongation curves for the low C steels.
Elongations
(Arrows indicate dynamic recrystallization).

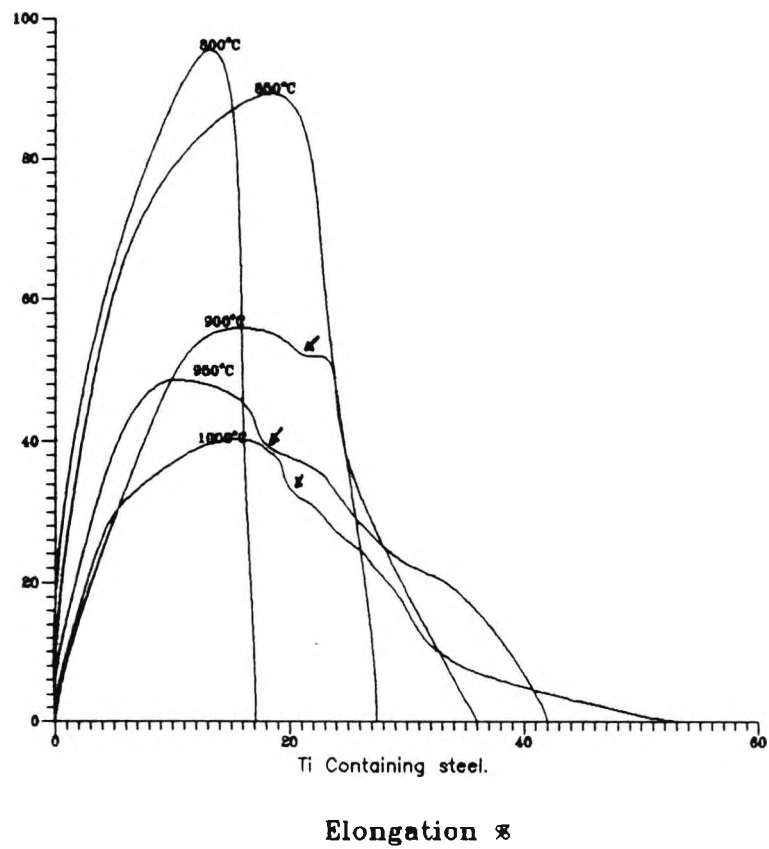
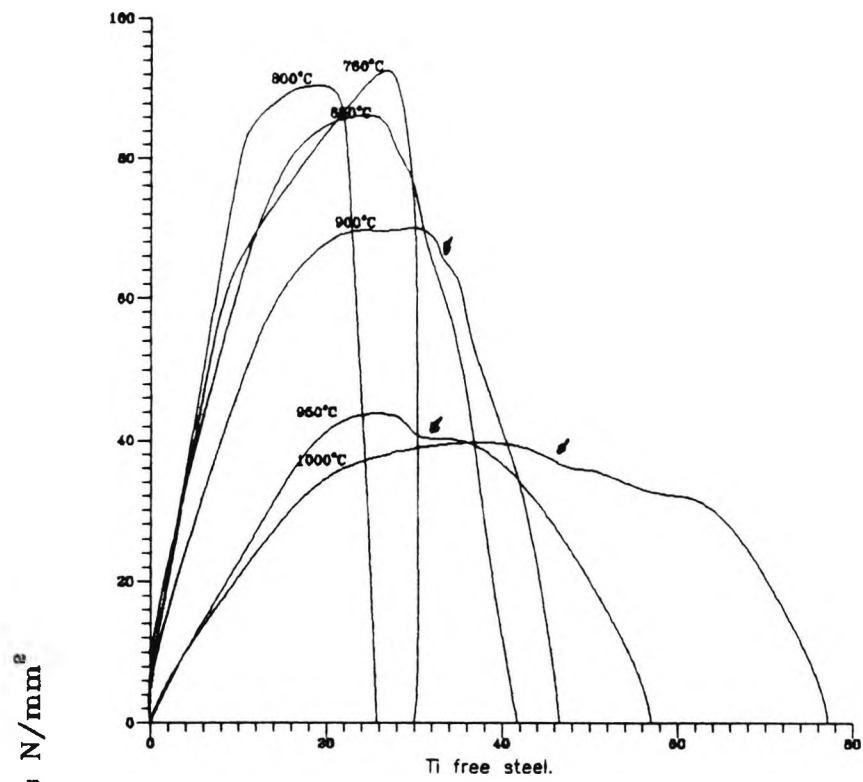
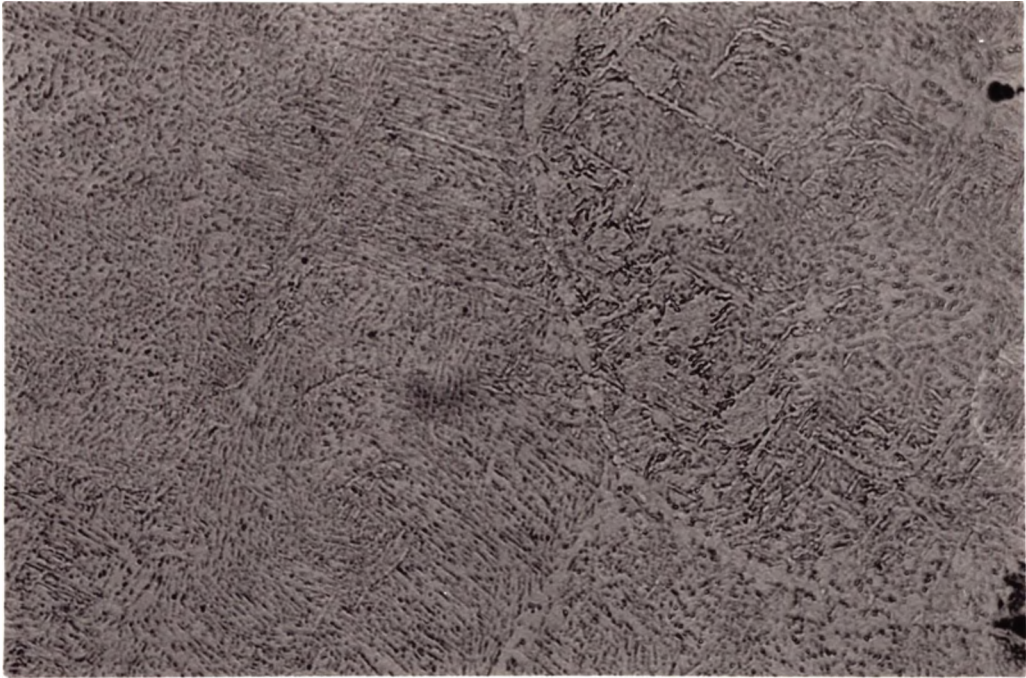
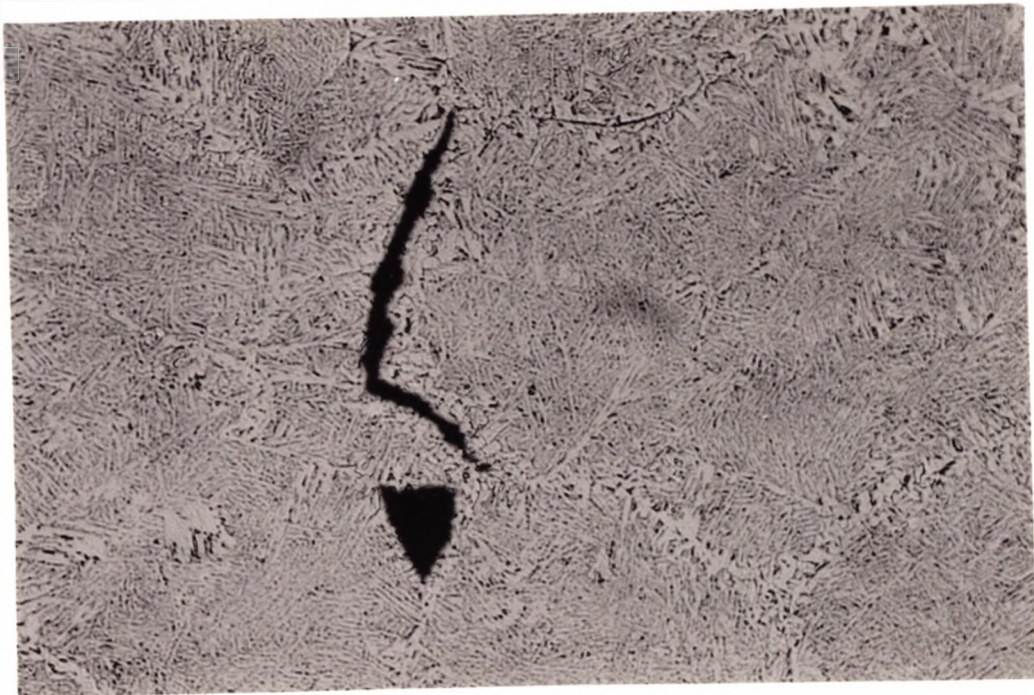


Fig. 7.7 Stress/Elongation curves for the high C Steels.
(Arrows indicate dynamic recrystallization).



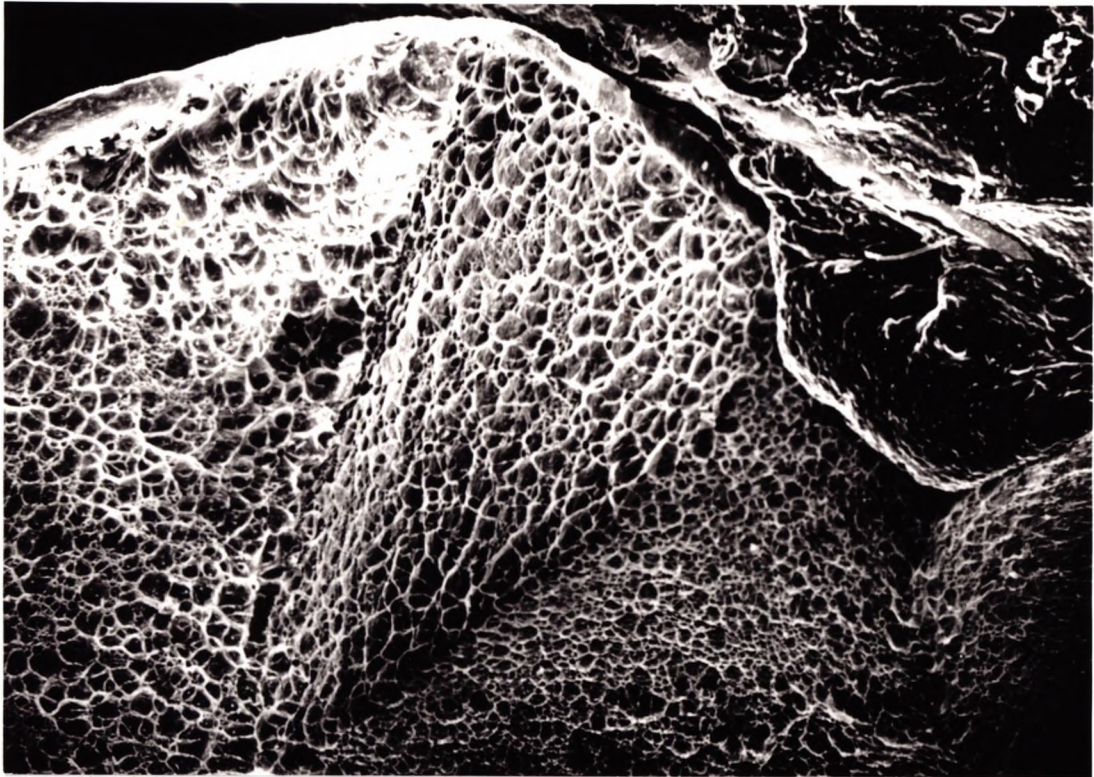
200 μm

Fig.7.8 Evidence of deformation induced ferrite in Ti free, 0.15% C steel, tested at 800°C.

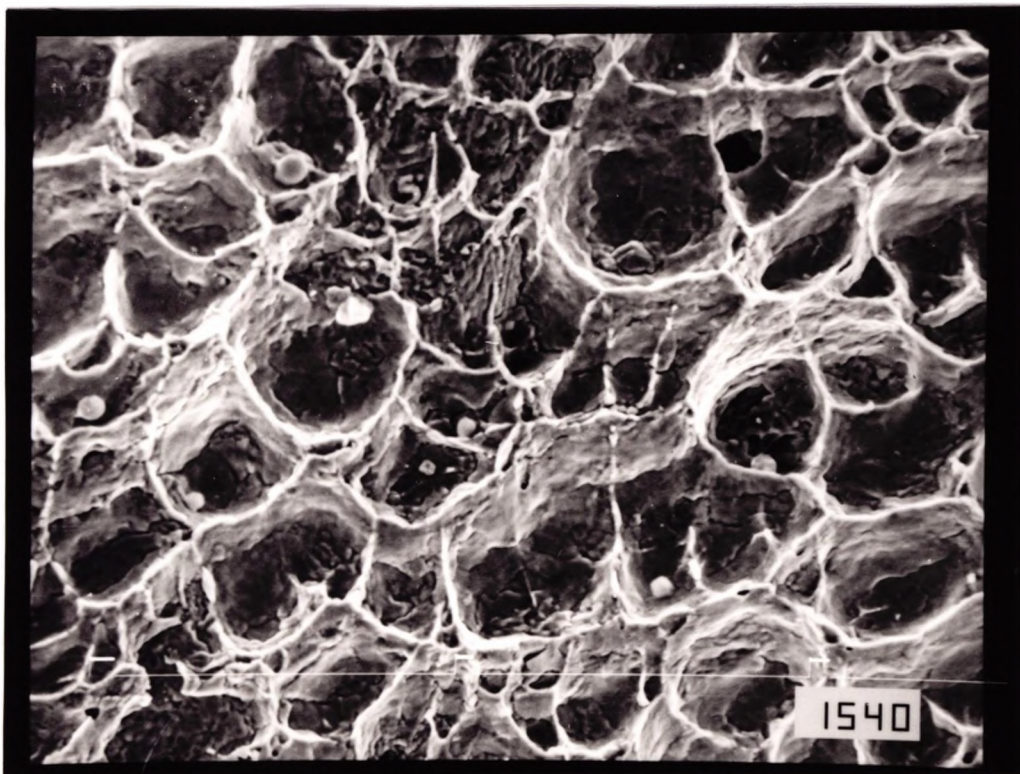


200 μm

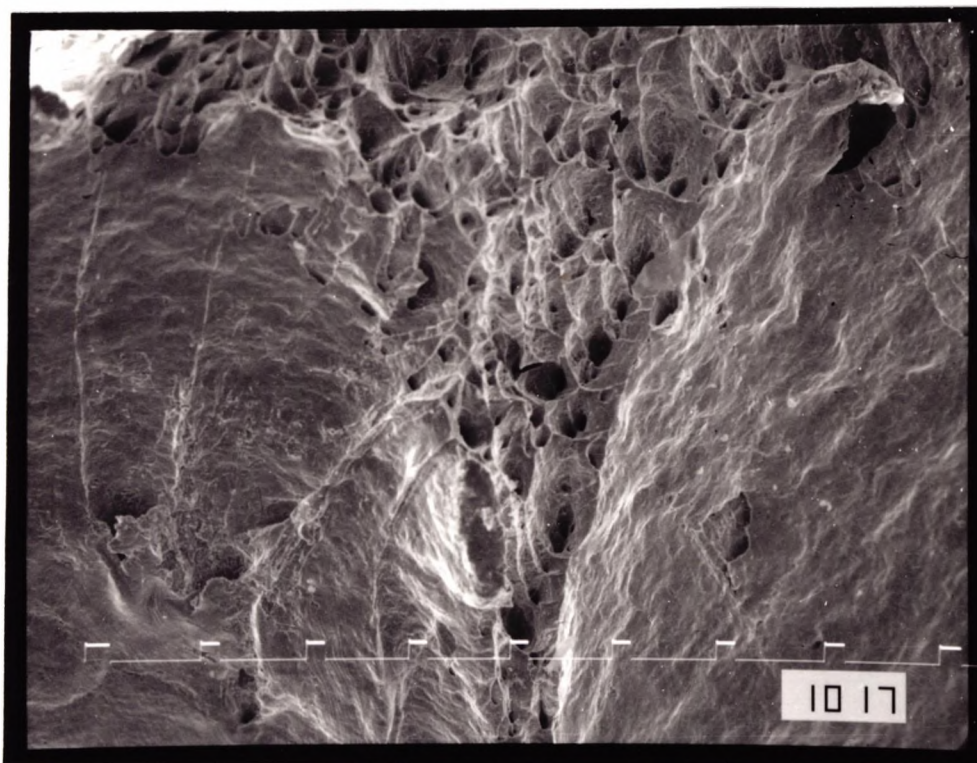
Fig.7.9 Typical wedge crack found in Ti free, 0.15% C, steel tested at 900°C.



185 μm
Fig.7.10 Fracture surface of Ti containing, 0.15% C steel , showing intergranular microvoid coalescence, tested at 800°C. R of A 23%.

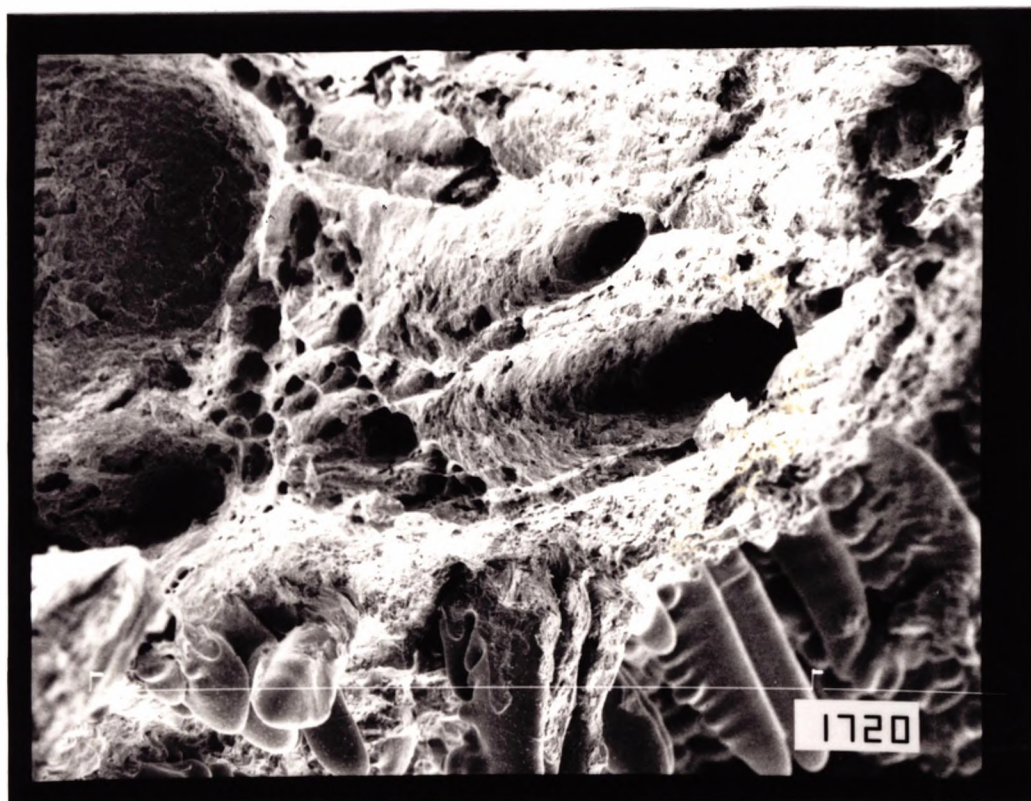


20 μm
Fig.7.11 Fracture surface of Ti containing, 0.15% C steel , showing intergranular microvoid coalescence, tested at 800°C. R of A 23%.



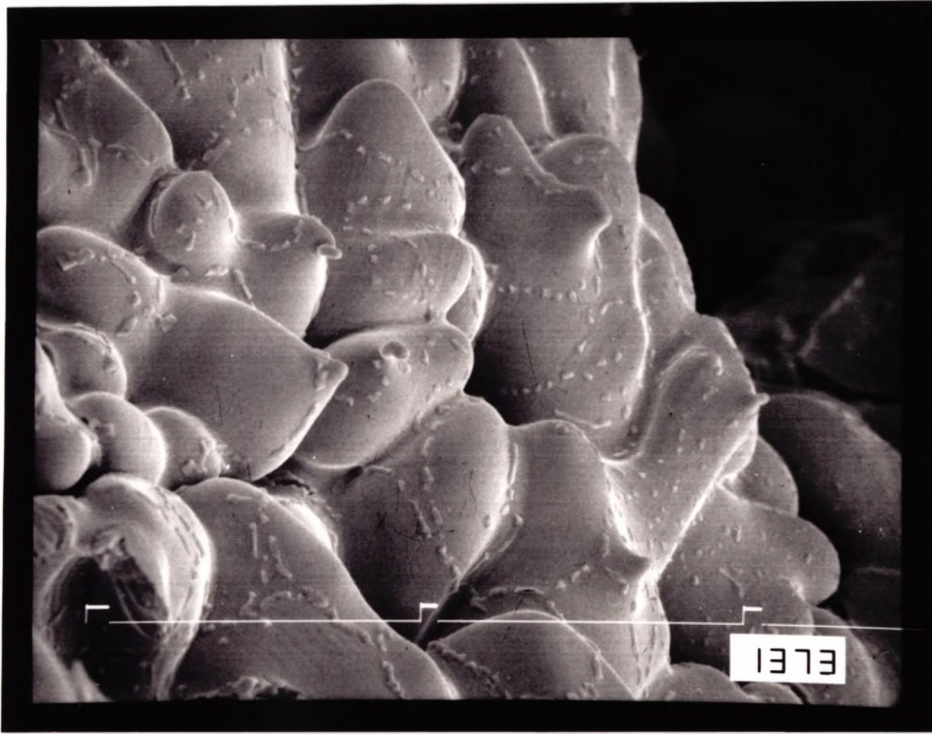
66 μm

Fig.7.12 Fracture surface of Ti containing, 0.15% C steel, Showing grain boundary sliding, steel tested at 900°C R of A 83%.



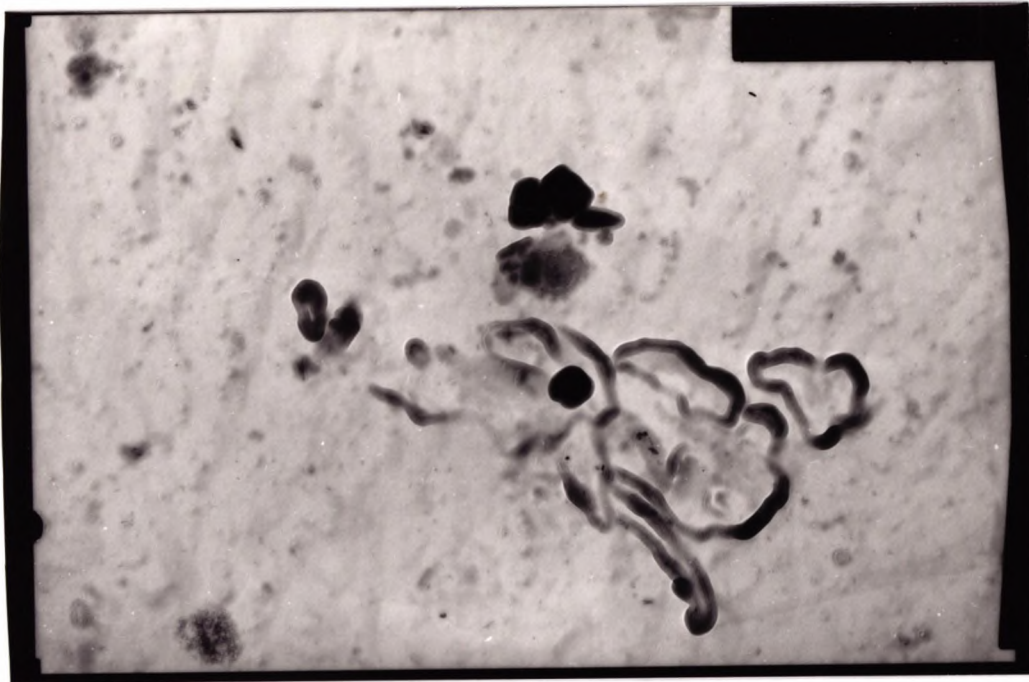
100 μm

Fig.7.13 Fracture surface of Ti free, 0.05% C steel showing ductile voiding, steel tested at 900°C.R of A 83%.



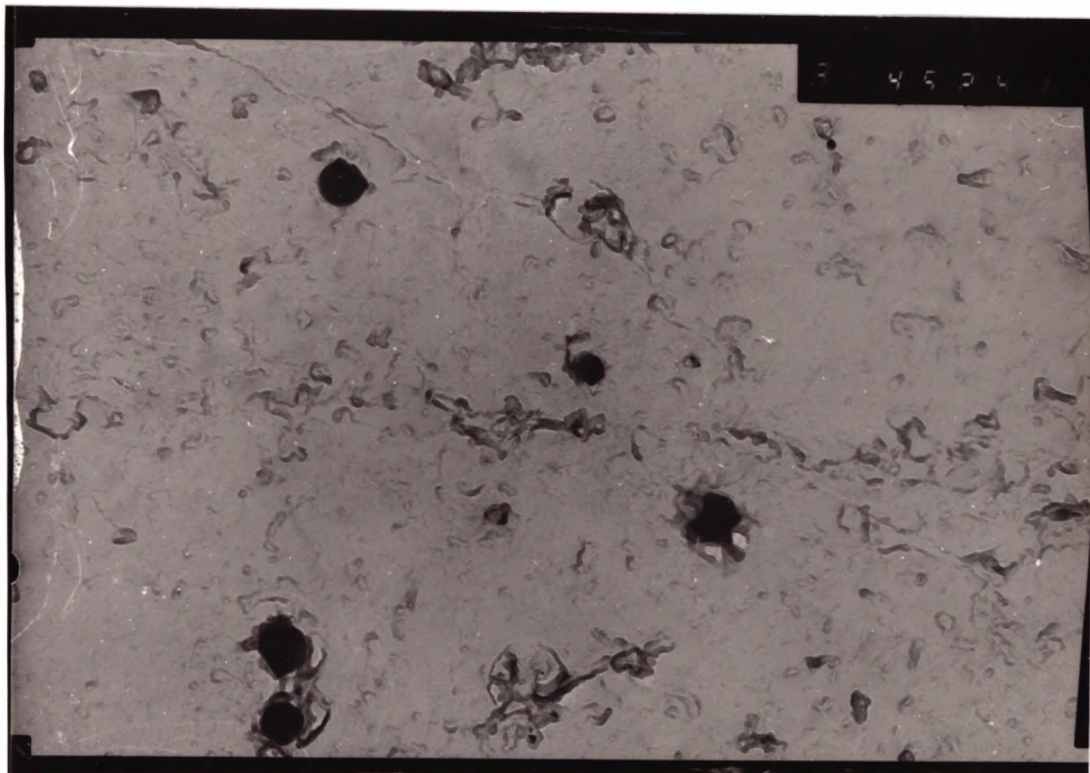
50 μm

Fig.7.14 Fracture surface of Ti free 0.15% C steel showing isolated dendritic region, tested at 900°C. (R of A 57%).



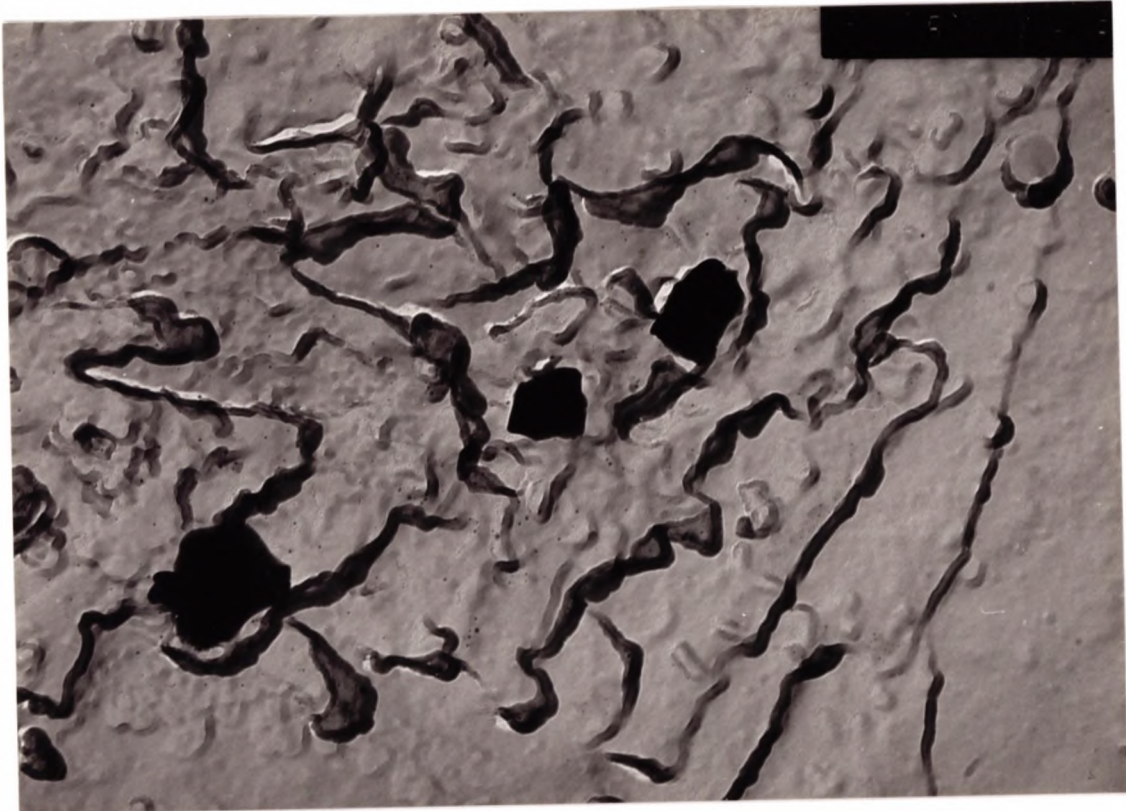
0.353 μm
||

Fig.7.15 TiN precipitation found in 0.15% C steel tested at 850°C.



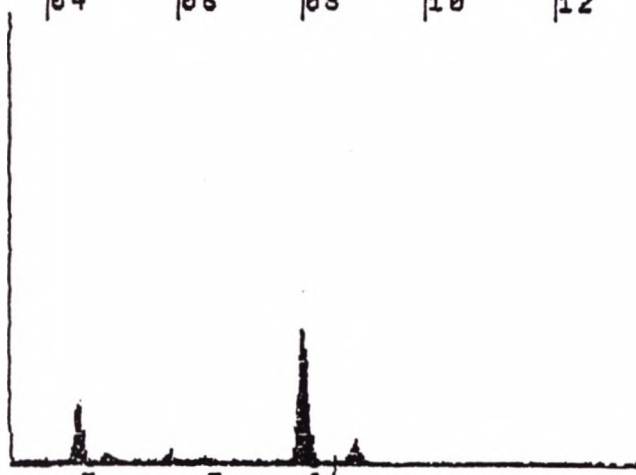
0.780 μm
||

Fig.7.16 TiN precipitation found in 0.15% C steel tested at 850°C.



0.26 μm

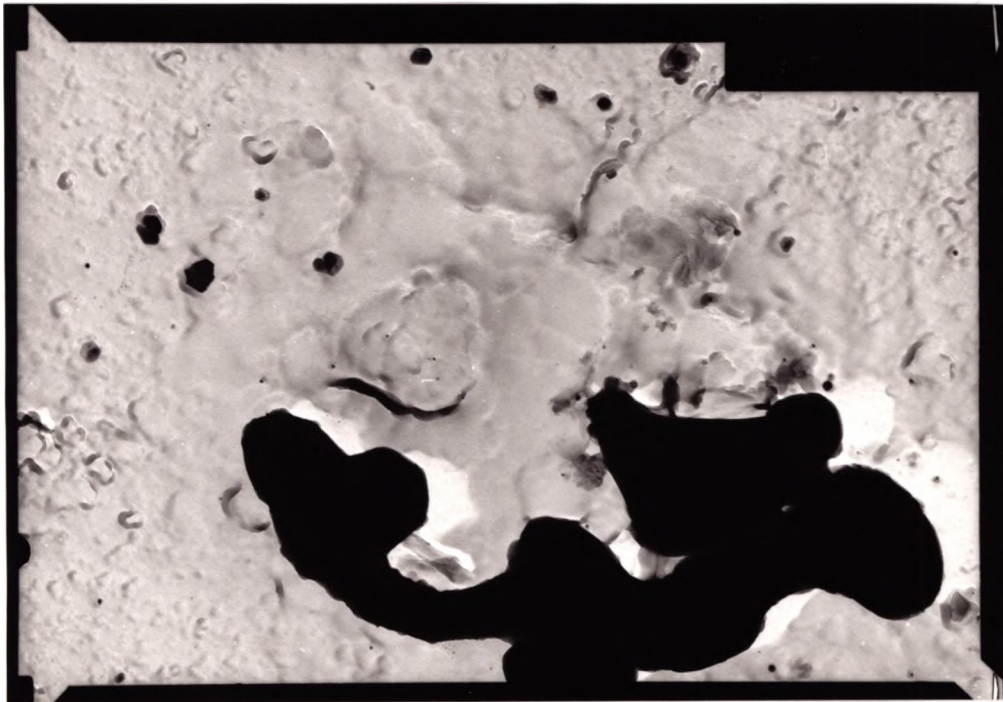
09-MAY-90 06:51:46 EDAX READY
RATE: 2012CPS TIME: 44LSEC
00-20KEY: 10EV/CH PRST: OFF
A: B:
FS= 2023 MEM: A FS= 200
|04 |06 |08 |10 |12



CURSOR (KEY)=08.560

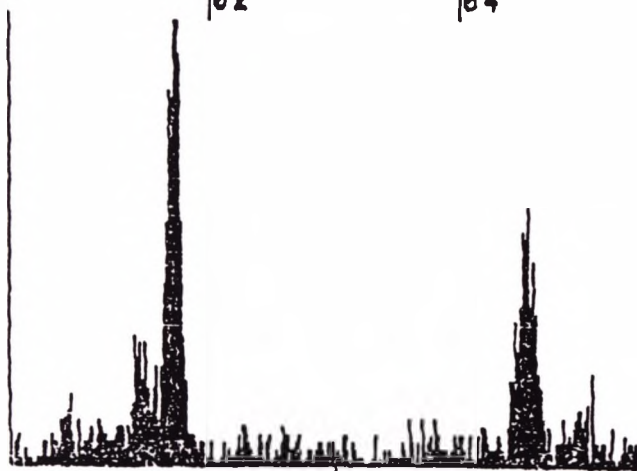
EDAX

Fig. 7.17 TiN precipitation found in 0.05% C steel tested at 850°C.



0.35 μ m

29-SEP-90 12:14:44 EDAX READY
RATE: 225CPS TIME: 60LSEC
00-20KEV: 10EV/CH PRST: OFF
A: B:
FS= 50 MEM: A FS= 50
|02 |04



CURSOR (KEV)=03.020

EDAX

Fig .7.18 TiN and Al rich particles found in 0.15% C steel tested at 850°C.



0.35 μm

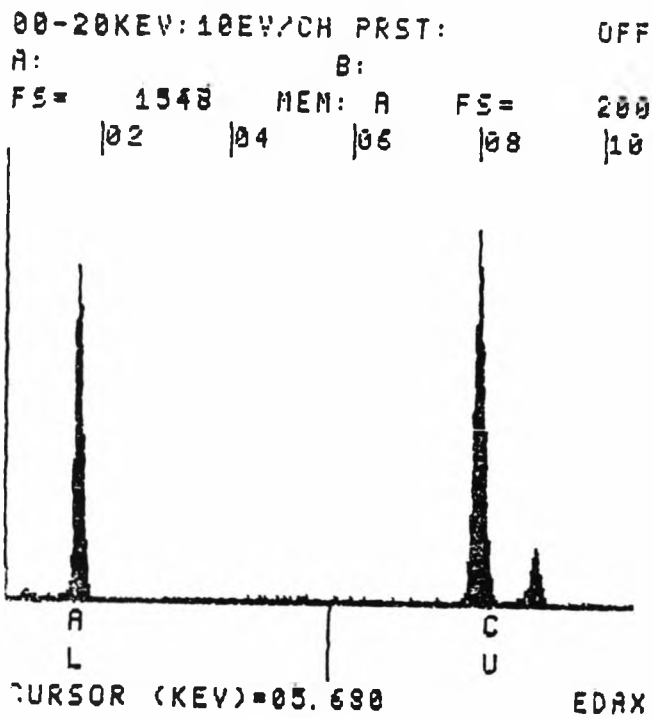


Fig.7.19 Al rich particles found in 0.15% C Ti free steel tested at 850°C.

CHAPTER 8

EFFECT OF Al AND N ON HOT DUCTILITY

8.1 INTRODUCTION

When solution treating prior to testing is used Al containing steels usually have good hot ductility-unless the solubility products are very high. Cooling under continuous casting cooling rates from the solution temperature at 60°C/min Crowther et al, (1987) reported that AlN did not precipitate out either statically or dynamically in a steel containing 0.03% Al and 0.005% N after holding 6 hours at 850°C prior to testing. Gladman and Pickering, (1967) have also reported that for the same cooling rate the precipitation of AlN is very sluggish.

However the temperature cycling that occurs during cooling of the continuously cast strand can accentuate AlN precipitation and this can be very detrimental to ductility particularly as AlN often precipitates at γ boundaries.

Obviously the level of Al and N present in the steels is important, the higher the solubility product, the greater being the driving force for precipitation. Mintz et al, (1991) suggested that for steel having 1.4% Mn, the solubility product has to approach 2.5 to 3×10^{-4} for precipitation to occur.

The majority of work into the influence of Al and N on hot ductility has concentrated on high N steels (0.01%) and

precipitation of AlN is always observed or inferred from a reduction in ductility.

In contrast, Mintz et al, (1987) working on low N steels have not observed AlN precipitated except at very high Al levels, ($\geq 0.07\%$)

The possibility that for given solubility product N has a more powerful influence than Al in encouraging precipitation, therefore needs investigation, and this has formed the basis of study, in the present examination.

Three steels were chosen for examination a plain C-Mn, and two C-Mn-Al steels of similar base composition, both having similar solubility products but one low in N and the other high.

8.2 EXPERIMENTAL

All the steels were supplied as vacuum melts. All casts were hot rolled to 12 mm thick plate. The full compositions are given in Table 8.1. Although the same solubility product had been aimed for on casting the lower N steel had a higher solubility product.

Tensile samples having a length of 70 mm and diameter 7.94 mm were machined from the plates with their axes parallel to the rolling direction. Hot ductility tensile tests were carried out on a Hounsfield Tensometer and heating was supplied by an induction heater, as described in chapter (3).

This study was carried out on two heat treated conditions, these being as following:-

- 1- Samples were heated in 15 minutes to 1330°C, held for 5 min. prior to cooling to test temperature in the range 700 to 1000°C at a cooling rate of 60°C/min. This heat treatment would probably redissolve most of the AlN precipitates and lead to a coarse grain size representative of conditions pertaining to the continuous casting process. Samples were held for 5 min. at test temperatures before straining to failure at 10^{-3} s^{-1} . This treatment will be referred to as a short holding time heat-treatment in the text.

2- The second heat treatment was the same as the previous one, except that samples were held for longer times, 20 min at the solution temperature of 1330°C, and 20 min at the test temperature. This treatment would ensure complete resolution of the AlN and also give more opportunity for it to re-precipitate during holding at test temperature. This second heat-treatment will be referred to as long in the text.

In the case of plain C-Mn steel, the γ grain size after heat-treatment (1) was found to be considerably finer than present in the Al containing steels. In order to be able to use the steel for precise comparisons, the steel had to be heated to 1330°C and held at this temperature for 2 1/2 hr to obtain the same grain size as for the C-Mn-Al steels, and this heat treatment was given to this steel for all the long heat-treatments.

Fracture surfaces were examined using a JEOL T100 SEM operating at 25 KV. Carbon extraction replicas were prepared as described in chapter (3) from transverse sections approximately 1 mm behind the fracture surface, and examined using a JEOL 100 KV, TEM, operating at 60 KV.

Austenite grain sizes were determined using the linear

intercept method before deformation after heating the steels to 1330°C followed by quenching in ice water.

8.3 RESULTS

8.3.1 Hot ductility curves

The curves of Reduction in Area against test temperature for the C-Mn-Al and C-Mn steels are shown in Figs 8.1 and 8.2 for short and long holding time heat treatments respectively. The calculated Ae_3 temperatures for the steels examined are marked on the curves. It can be seen from Fig 8.1 that the C-Mn-Al steels showed a marked ductility trough. The curves for these two steels are almost identical, the higher N steel having the slightly worse ductility. The C-Mn steel had the best hot ductility, but note this steel had a much finer grain size.

For the C-Mn-Al steels with different N contents, i.e. 0.0058% and 0.01% N, ductility started to fall at 900°C and reaches a minimum at 800°C of 35% and 30% R.of.A temperature for the low and high N containing steels respectively. The ductility started to recover when the test temperature was further lowered to 750°C.

The C-Mn steel had a narrow ductility trough, the lowest value for Reduction of Area value being ⁶⁵70% obtained at 800°C.

For the long time heat treatments, Fig. 8.2 the ductility troughs for the C-Mn-Al steels have deepened and widened. The ductility started to fall at 950°C, and was very poor at 850°C reaching R.of.A values of 43% and 38% for high and low N containing steels respectively. Further lowering of the temperature to 800°C caused the ductility to reach minimum values of 29% and 25% for the high and low N steel respectively. Ductility again recovered when the test temperature was further lowered.

The C-Mn steel which now had a similar grain size, gave better ductility than the C-Mn-Al steels, the ductility reaching a minimum value of 45% at 800°C.

8.3.2 Stress/Elongation curves

The stress total elongation curves are shown in Figs. 8.3 and 8.4 for both the short and long holding time heat-treated conditions respectively. The fall in the rate of strain hardening leading to the peak in stress followed by work softening and fluctuations (Jonas et al, 1968) is evidence of dynamic recrystallization. For the short holding time heat treatments the onset of dynamic recrystallization was first detected from the curves at 900°C.

On the other hand in the long time heat treatments dynamic recrystallization was delayed to 950°C for C-Mn-Al steels. However for the C-Mn steel, the temperature for the onset of dynamic recrystallization was not changed, remaining at 900°C.

8.3.3 Metallography

a Short holding times

SEM examination of the fracture surfaces of the C-Mn-Al steels tested at the minimum ductility temperature of 800°C showed intergranular failure, the main mode of failure for both steels being by micro-void coalescence as in Fig. 8.5. Intergranular failure occurs when the temperature is low enough to allow thin films (~ 5 to 20 μm) of ferrite to form around the γ grains as shown in 8.6. At temperatures of 850°C and above when R.of.A values were high, a large area of the fracture surface was normal ductile rupture as shown in Figs. 8.7

For the more ductile plain C-Mn steel, ductile voiding was observed even at the minimum R.of.A value of ⁶⁵70% as shown in Fig.8.8.

It is important to note that coarse grain sizes ~300 μm were obtained for C-Mn-Al steels, while the grain size for C-Mn steel was only ~100 μm as in Fig 8.9. These measurements were obtained after heating small samples to 1330°C for 5 mins, followed by quenching in water.

b- Long holding times

For this heat-treatment, for the C-Mn-Al steels, intergranular fracture due to grain boundary sliding was also observed. This was especially marked for the high Al, C-Mn-Al steel tested at 900°C as shown in Fig 8.10. For both the high and low Al containing steels, lowering the temperature to 850°C caused the intergranular fracture mode to change to a mixture of micro-void coalescence and grain boundary sliding as shown in Fig. 8.11. Wedge cracks characteristic of steels which fail by grain boundary sliding were observed as shown in Fig.8.12

8.3.4 Transmission electron microscope results

a- Short holding times

Carbon extraction replicas revealed the presence of very coarse Al_2O_3 and alumina-silicates with about 75% of these inclusions being $\geq 0.5 \mu m$. No difference in inclusion distribution could be found between the two aluminium containing steels. No AlN precipitation was observed. Fig 8.13 shows a very coarse alumina-silicate found in the 0.058% Al containing steel and Fig. 8.14 shows a coarse Al_2O_3 particles. Similar inclusions were observed in the 0.23% Al, Figs. 8.15

b Long holding times

Again no AlN precipitates were observed. Inclusions of aluminium-silicate and aluminium oxides were again present, this time being somewhat finer.

8.4 DISCUSSION

No AlN precipitation has been found in the present examination. However this may arise because of the difficulty in detecting AlN on sections taken through the fracture samples. Coleman and Wilcox, (1985) have shown that AlN precipitates as very thin films at the γ grain boundaries and that it is necessary to take replicas directly off the fracture surface of samples which have failed intergranularly in order to clearly see them. Unfortunately time was not available to do this. The present discussion is based on the assumption that AlN is indeed present, and this accounts for why the Al containing steels have worse ductility than the plain C-Mn steel and also why long holding times can be more effective in reducing ductility. However until more definite evidence is forthcoming this can only be regarded as speculative.

The present work has shown only small differences in ductility between the high and low N steels. For short holding times the high N containing steel had the worse ductility, but when the time was extended, the lower N steel had the slightly worse ductility. However differences were small indicating that precipitation of AlN if it does occur must be controlled by the value of the solubility product rather than the N level. The hot ductility curves for the Al containing steel and plain C-Mn steel shown in Fig 8.2. clearly indicate that at the same

grain size both Al steels had worse ductility indicating that precipitation is likely to have occurred and is having an adverse influence on ductility. If comparison is made between the plain C-Mn steel (dashed curve in Fig. 8.1) and the Al containing steel at the same grain size, it can be seen that the Al containing steels still show the worse ductility, although differences are smaller. The manner in which AlN precipitation can influence hot ductility is not clear. There seems little evidence from the literature that it can precipitate dynamically during test as can Nb(CN) except at very high Al and N concentrations, solubility product $\geq 7 \times 10^{-4}$ (Michel and Jonas, 1981).

Coleman and Wilcox, (1985) have shown that it can precipitate as very thin plates covering the γ grain boundaries, and this may account for the flat, intergranular decohesion fractures often observed in these steels. They also make the point that because it is so thin it is often very difficult to extract from replicas and as already explained this may account for it not being detected in the present exercise. Wilcox and Honeycombe, (1987) have also found AlN precipitation in the grain boundaries in tensile samples cooled from 1300°C to 800-900°C, followed by reheating to the test temperature of 1100°C. Ductility was found to be poor after this thermal heat treatment.

Similarly Crowther et al, (1987) have found AlN precipitation in a C-Mn-Al steel, after directly heating the steel to the test temperature in the range 600-1000°C,

as have Funnell and Davies, (1978). The latter investigators have observed that the finer grain boundary particles (≤ 100 nm), the closer was the interparticle spacing for a given volume fraction, and the worse the hot ductility. AlN precipitation however occurs readily on heating up through the α/γ transformation and their precipitation would have been formed statically prior to deformation.

Previous work by Crowther et al, (1987) with a steel of similar solubility product to the presently examined steels indicated that a 10 min hold at 1330°C was not sufficient to completely redissolve the precipitates of AlN. Hence it is unlikely that the 5 min hold in the present work would have completely redissolved the coarse AlN particles. In their work they noted coarse AlN particles which had not dissolved and fine AlN particles which were precipitated while holding at the test temperature prior to test. They also noted that this fine precipitation took place very rapidly (after a 2 min hold at 850°C) and reduced ductility. Longer holding times resulted in worse ductility as more fine AlN precipitation was allowed to take place. It is likely that similar behaviour is occurring in the present exercise. The longer hold treatments allow all the coarse AlN precipitates to redissolve and this ensures a greater volume fraction of AlN precipitated during holding at test temperature.

The mechanism of intergranular failure is believed to be by pinning of the boundaries by these precipitates

encouraging grain boundary sliding. As noted in previous chapters finer precipitation always lead to worse ductility as cracks can more readily join up. Thus the longer holding times treatments by encouraging a greater volume fraction of finer precipitation results in lower ductility. Another possible explanation for the present results is that the longer time at 1330°C may allow more S to go back into solution and be available for precipitating in a fine form at the austenite boundaries. However against this argument is the better ductility shown by the plain C-Mn steel which was given even longer extended holding times at 1330°C (2 1/2 hr).

Finer precipitation is always found to be more detrimental to ductility and the raising of the temperature for the onset for dynamic recrystallization by this finer precipitation ensures a widening of the trough.

In contrast to the C-Mn-Al steels, the C-Mn steel showed excellent ductility. Unfortunately after short holding times this plain C-Mn steel had a significantly finer grain size than the Al containing steels (probably because of its higher S level and hence higher volume fraction of MnS), so the results can not be compared directly. Such a refinement in grain size is likely to account for most of the improvement in ductility shown in Fig. 8.1. Nevertheless when the grain size coarsened to

~250 μm , by heating the steel at 1330°C for two and half hours, the C-Mn steel still gave better ductility when compared with the C-Mn-Al steels indicating that precipitation of AlN had occurred in the Al containing steel. Again if the S in solution was of the most importance the longer time at 1330°C given to the C-Mn steel might be expected to result in worse hot ductility not better.

8.5 CONCLUSIONS

- 1- Ductility is found to deteriorate when Al is added to steels and the AlN solubility product is in the range 2.3 to 3.3×10^{-4} .

- 2- The fall in ductility seems to be controlled by the solubility product rather than the amount of N present in the steels.

- 3- The widening of the trough and increase in depth is due most likely to the precipitation of AlN, which probably occurs prior to deformation. Unfortunately AlN was not detected in the presence exercise and more work is required to confirm its presence.

- 4- Longer holding times in the Al containing steel resulted in worse ductility. This again is most likely to be interpreted in terms of more AlN going back into solution and more being precipitated in a finer detrimental form prior to tensile testing.

Table 8.1

Composition of the steels examined (Wt.%)

Code	C	Si	Mn	P	S	Total * Al	N	Solubility product
Steel 1	0.11	0.29	1.34	0.015	0.007	0.058	0.0058	3.3×10^{-4}
Steel 2	0.1	0.3	1.39	0.015	0.007	0.023	0.01	2.3×10^{-4}
Steel 3	0.1	0.29	1.39	0.008	0.028	<0.005	0.0077	0

* British steel state that soluble Al levels are typically 0.002-0.003% less than the total Al levels.

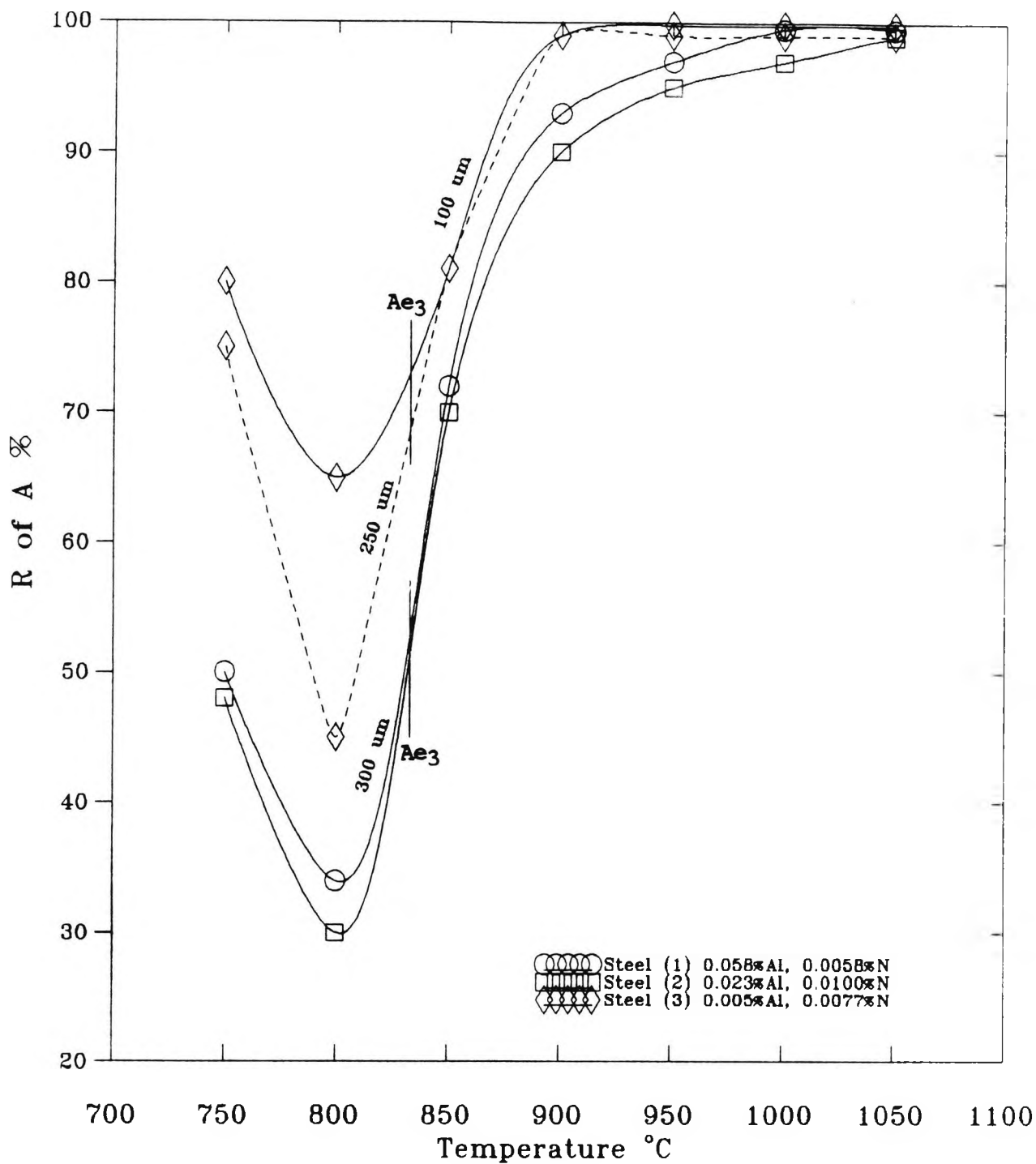


Fig. 8.1 Hot ductility curves for C-Mn-Al steels and C-Mn steel. Steels were given short holding times. Dashed curve is for C-Mn steel heat-treated to give a coarse grain size.

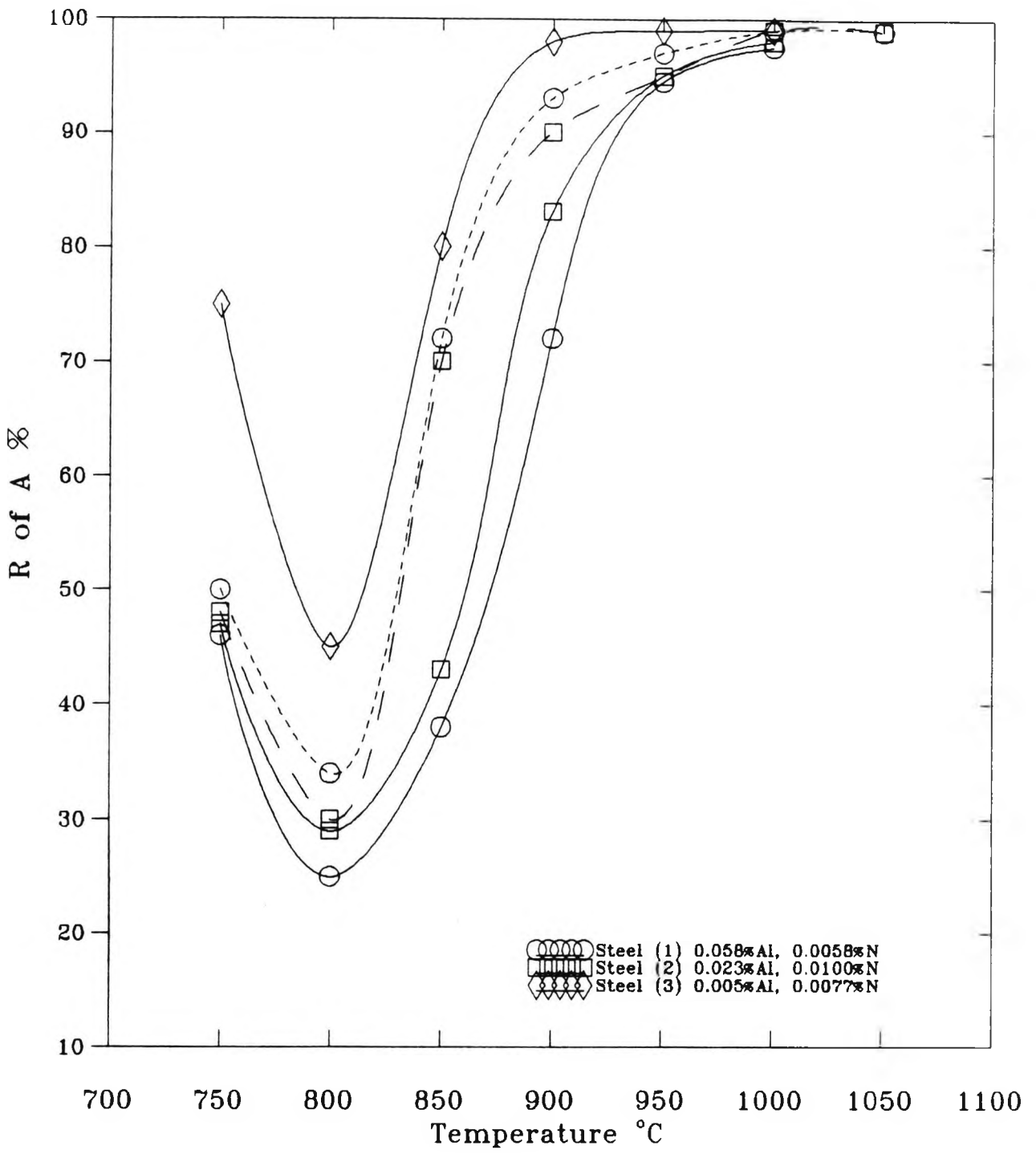


Fig. 8.2 Hot ductility curves for C-Mn-Al steels and C-Mn steel. given long holding times. Dashed curves are for short holding time heat-treatments for the C-Mn-Al steels.

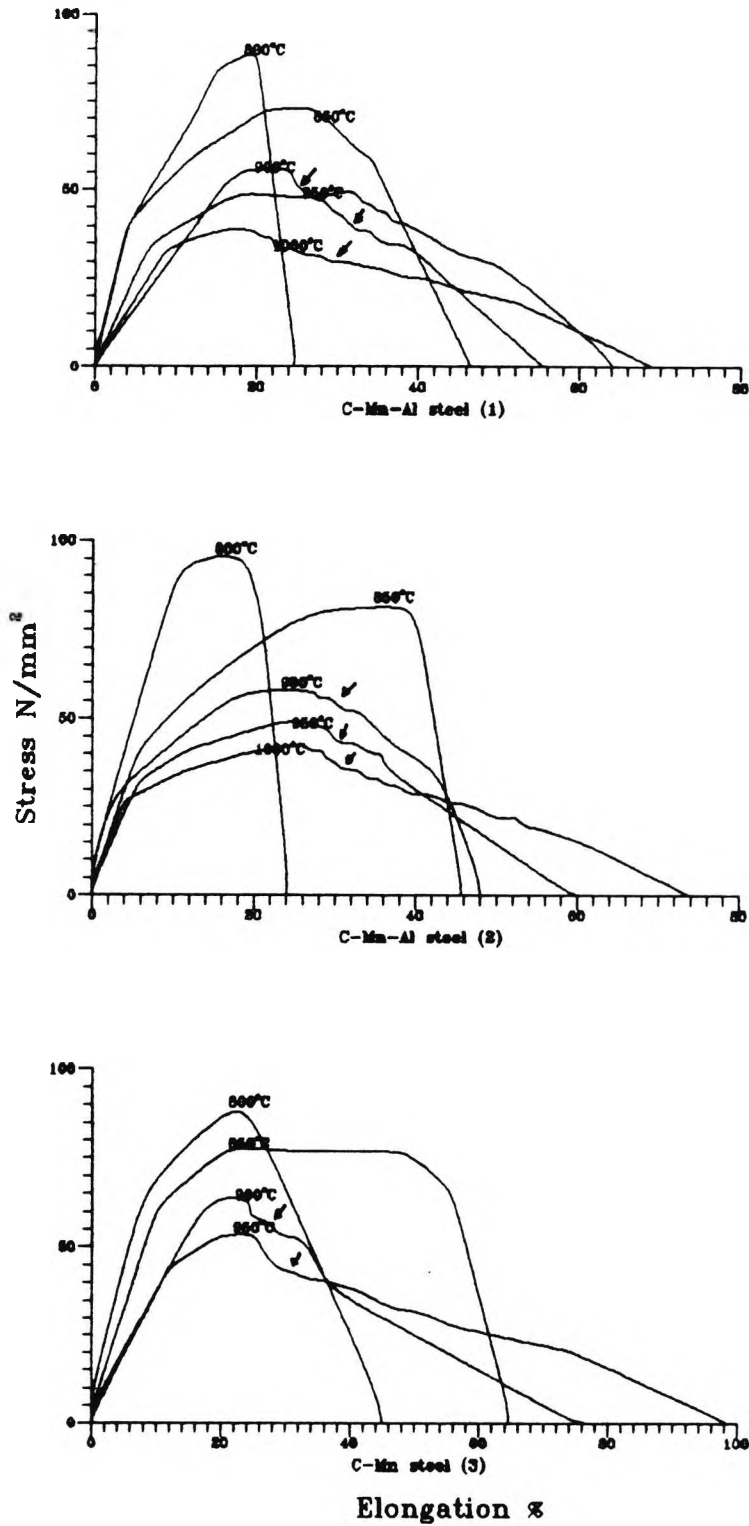


Fig. 8.3 Stress/Elongation curves for the steels examined, after the short holding times. (Arrows indicate dynamic recrystallization).

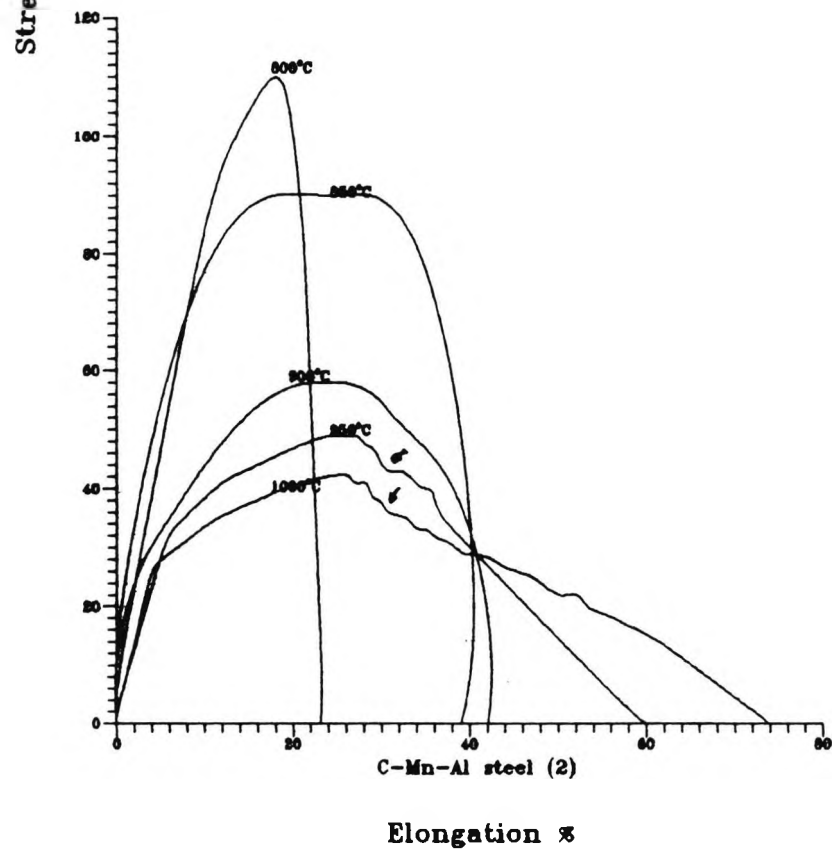
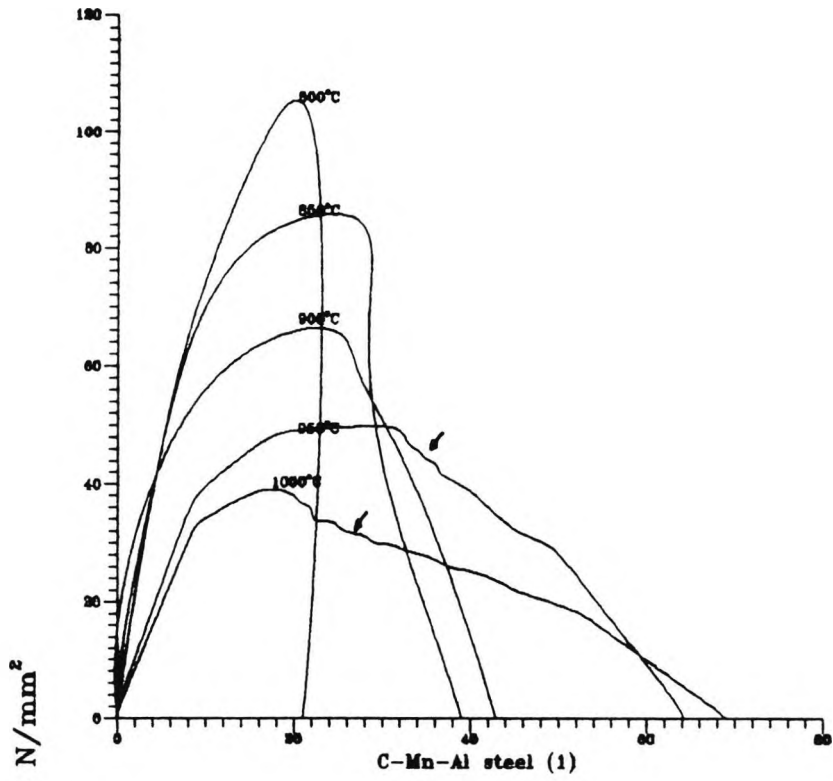
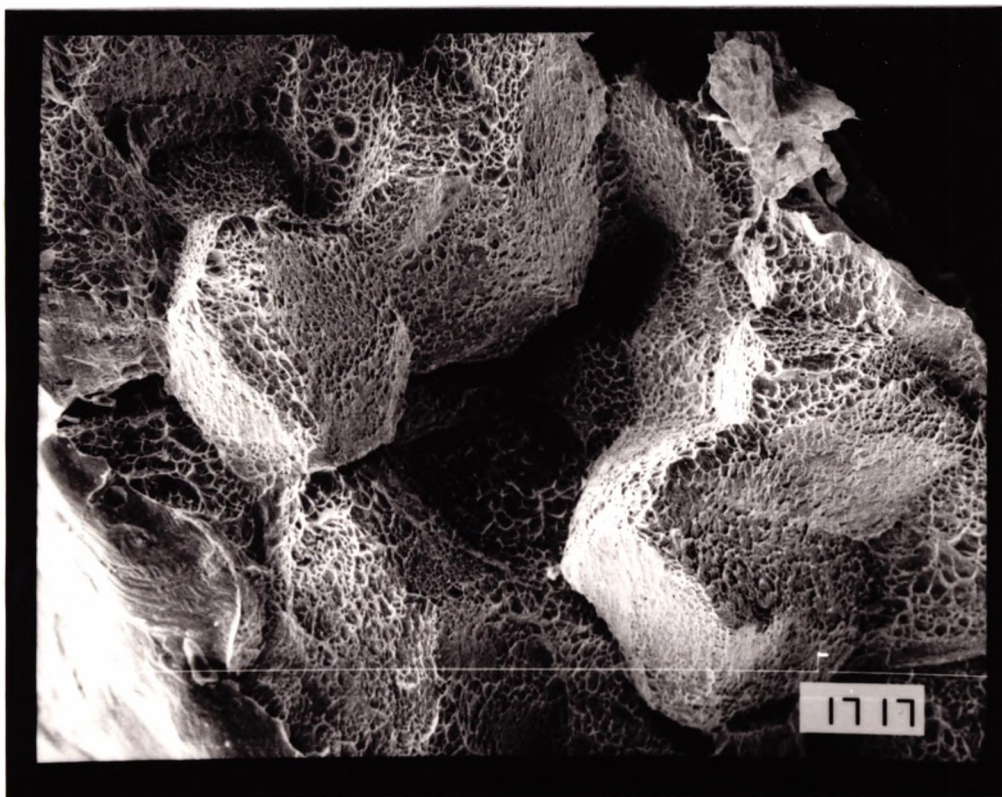
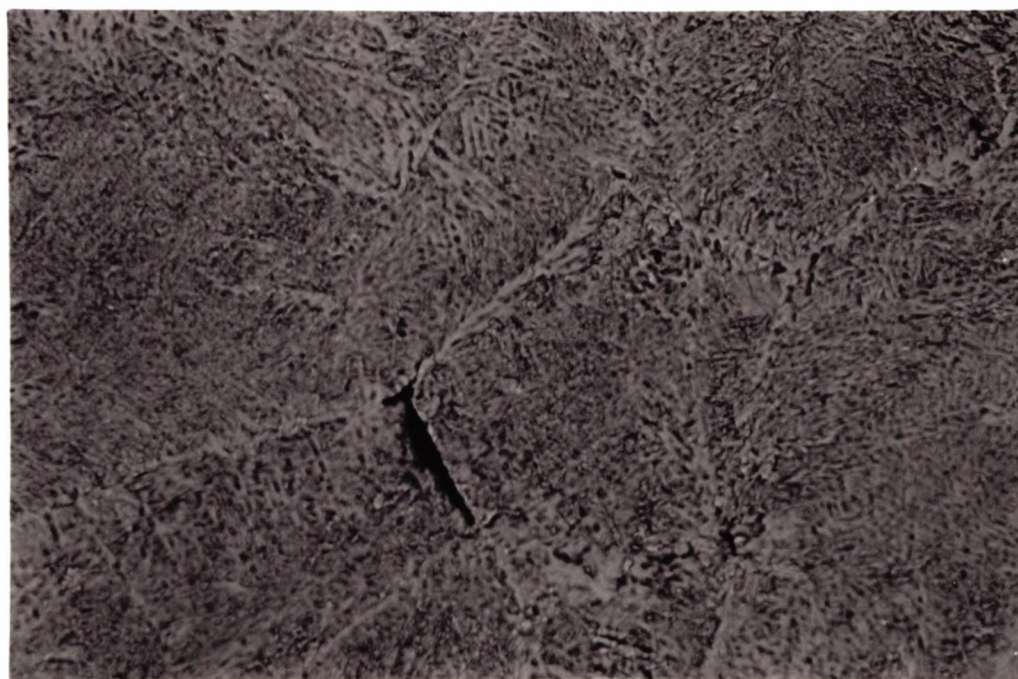


Fig. 8.4 Stress/Elongation Curves for the C-Mn-Al steels, after given long holding times. (Arrows indicate dynamic recrystallization).



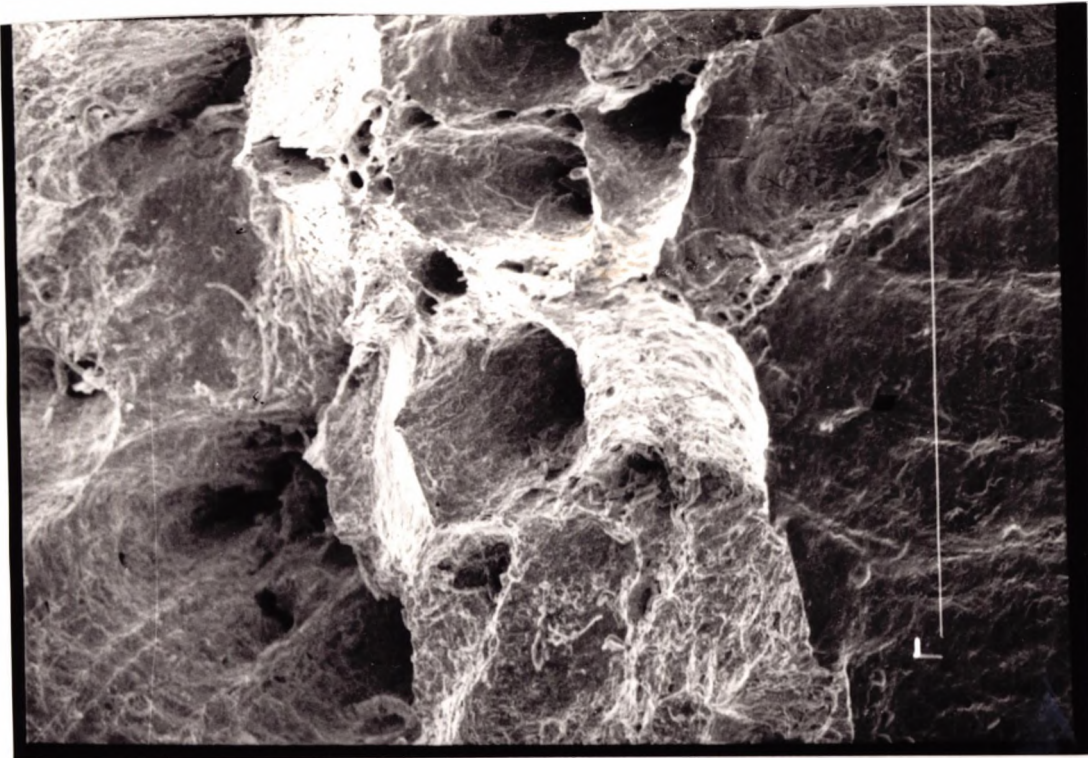
100 μm

Fig. 8.5 Example of intergranular micro-void coalescence fracture observed in the 0.023% Al steel tested at 800°C and given the short holding time treatment.



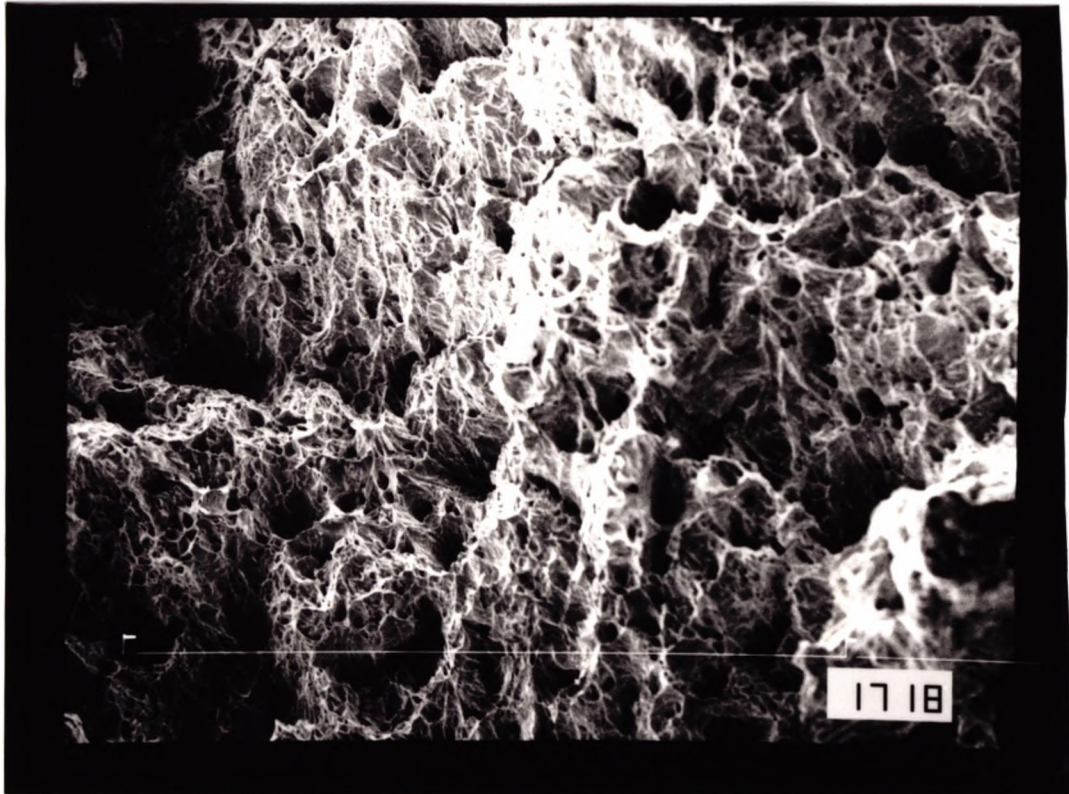
200 μm

Fig. 8.6 Example of deformation induced ferrite observed in the 0.058% Al steel tested at 850°C and fast cooled after fracture. Calculated A_{e3} temperature was $\approx 850^\circ\text{C}$. Steel given short holding times.



66 μm

Fig. 8.7 Example of ductile rupture observed in an 0.058 Al steel tested at 850°C and given the short holding time.



100 μm

Fig. 8.8 Example of ductile voiding observed in an C-Mn steel tested at 800°C. The steel was given the short heat treatment and had a fine grain size.



200 μm

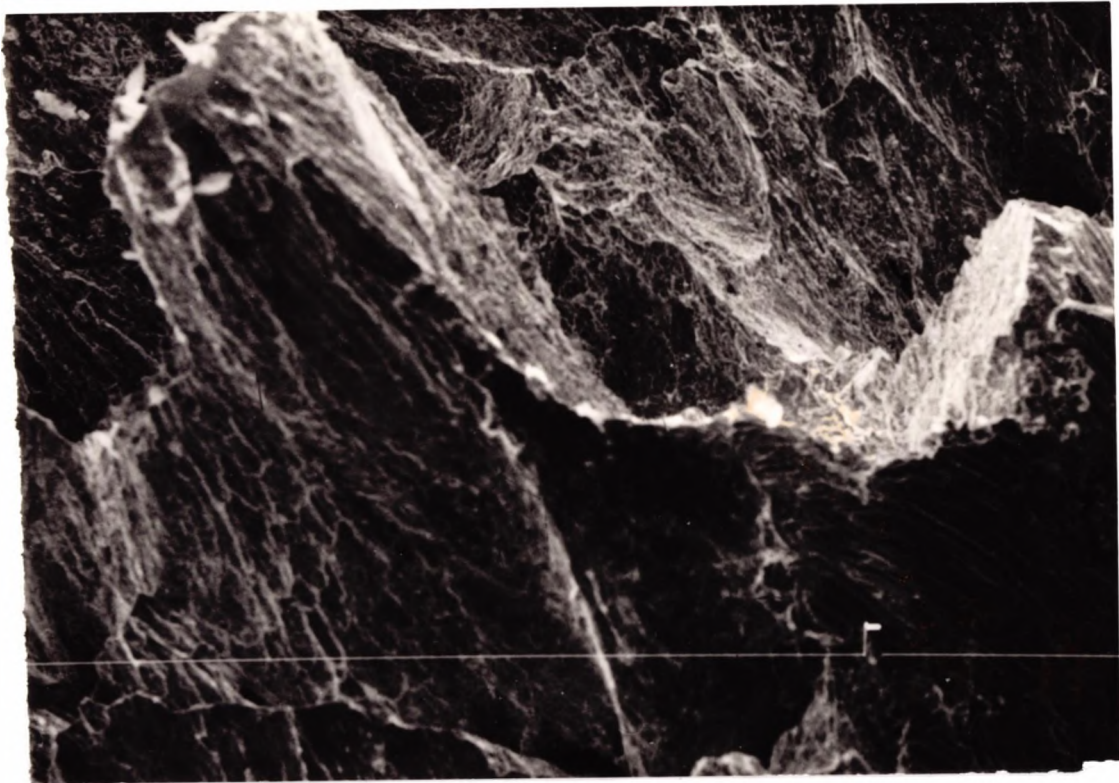
C-Mn-Al steel



200 μm

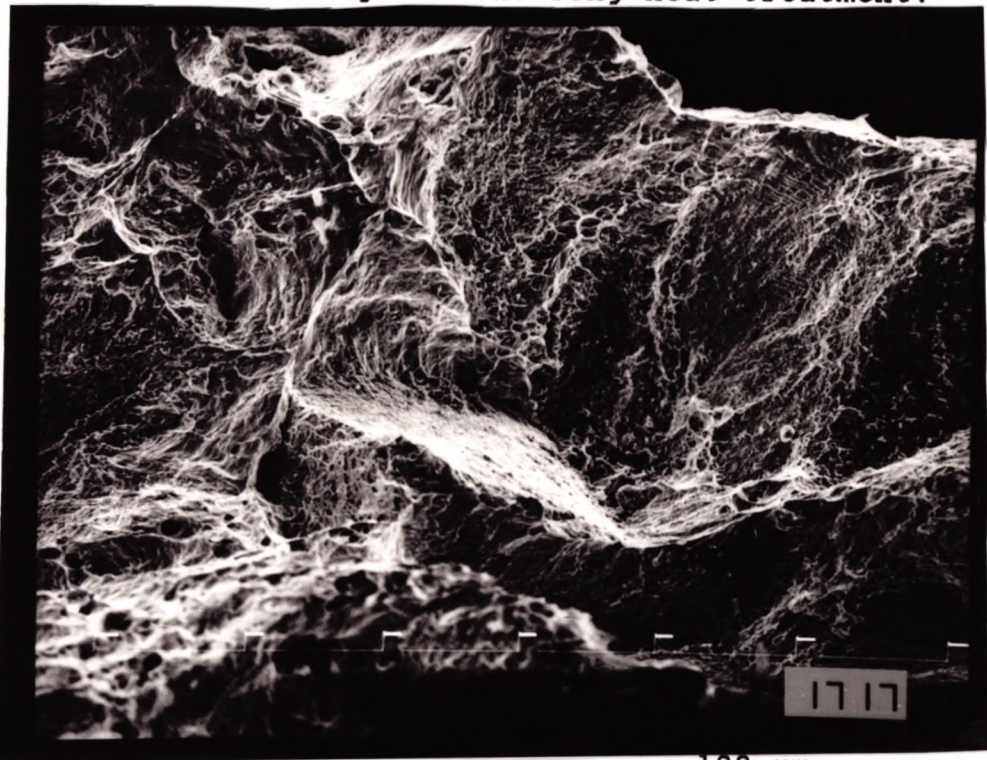
C-Mn steel

Fig. 8.9 Austenite grain size for C-Mn-Al and C-Mn steels, after solution treatment to 1330°C. for 5 mins, and quenching in water.



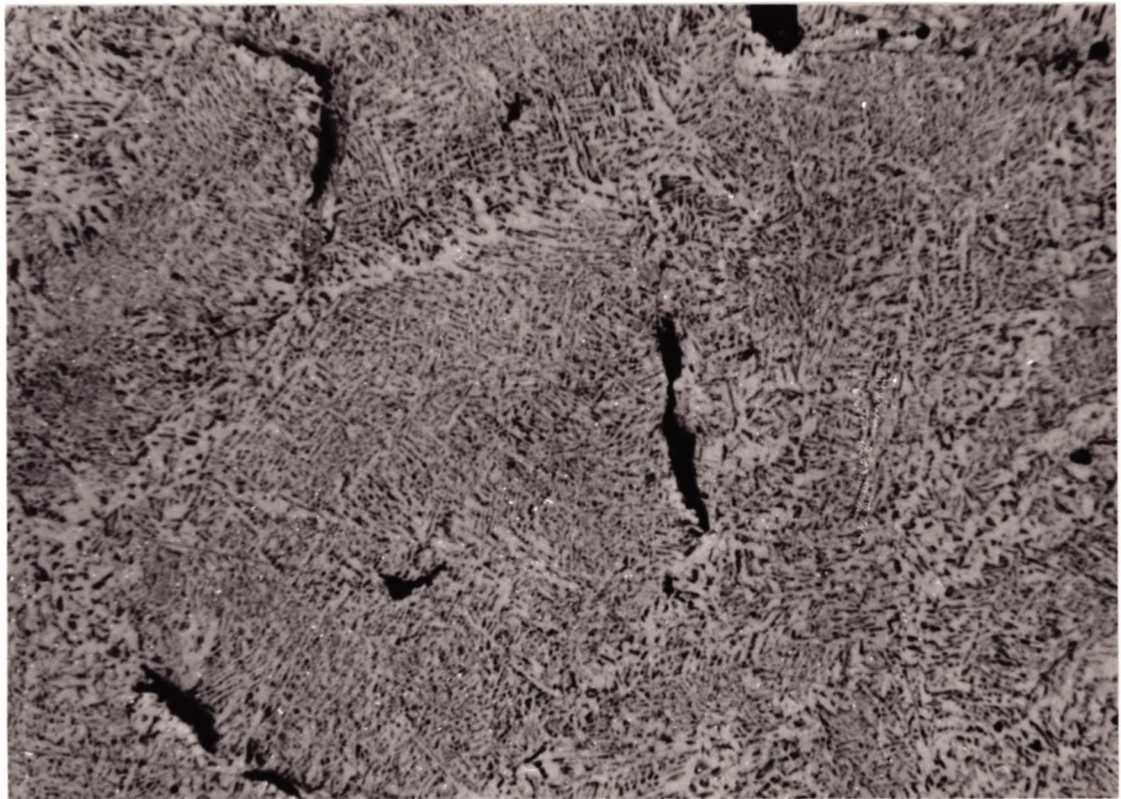
67 μm

Fig. 8.10 Example of intergranular fracture due to grain boundary sliding and micro-void coalescence observed in the 0.058% Al steel tested at 900°C. The steel was given the long heat-treatment.



100 μm

Fig. 8.11 Example of intergranular fracture due to grain boundary sliding and micro-void coalescence observed in the 0.058% Al steel tested at 850°C. The steel was given the long heat-treatment.



200 μm

Fig. 8.12 Wedge cracks observed in the 0.058% Al steel tested at 850°C. Steel had been given the long heat-treatment prior to testing.



2 μ m

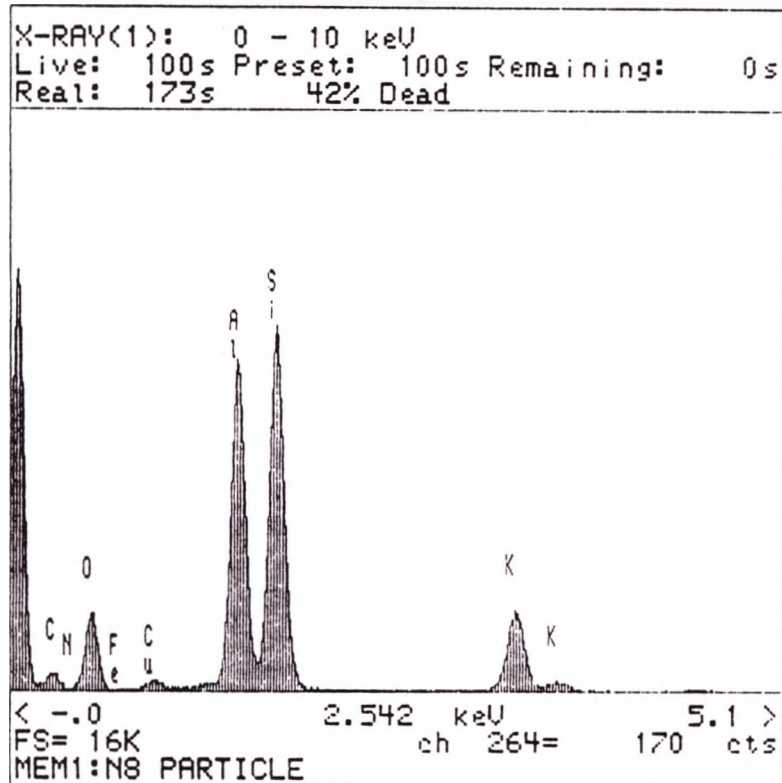
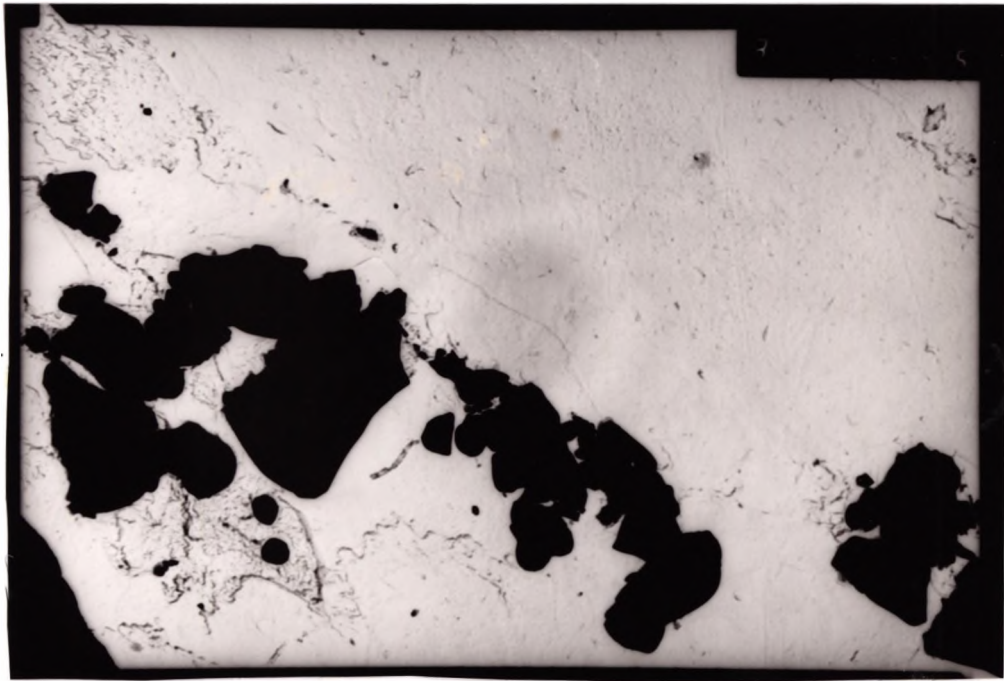


Fig. 8.13 Very coarse AlSiO_2 particles found in 0.023% Al steel tested at 850°C . Steel was given short holding times.



30 μ m

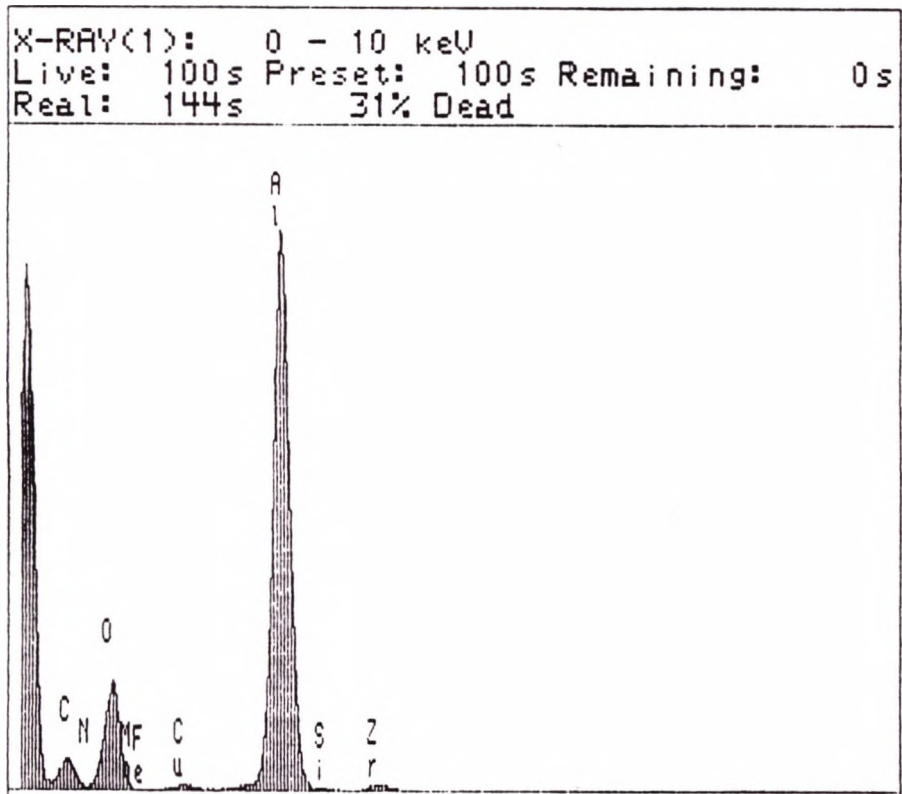


Fig. 8.14 A very coarse Al_2O_3 precipitation found in 0.058% Al steel tested at 850°C. Steel was given short holding times.



0.36 μm

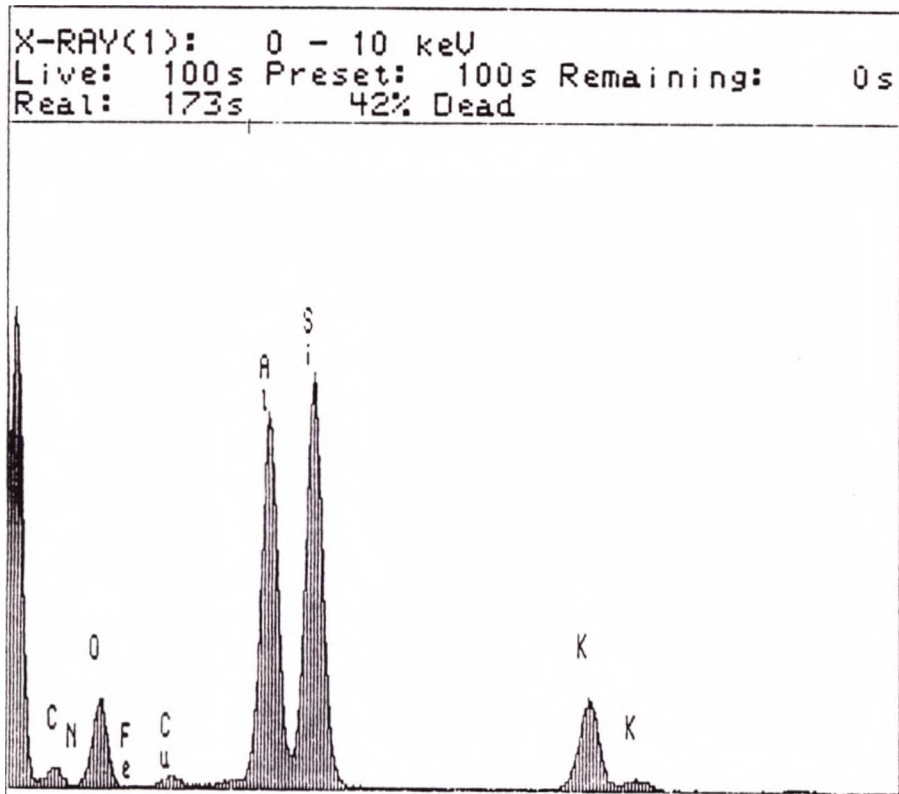


Fig. 8.15 Alumina silicate $\text{Al}_2\text{O}_3 \cdot \text{SiO}_2$ found in 0.023% Al steel tested at 850°C. Steel was given short holding times.

CHAPTER 9

EFFECT OF 'RESIDUAL ELEMENTS' ON
HOT DUCTILITY

9.1 INTRODUCTION

Metallic elements that remain in the steel in small quantities after refining is complete, and which are not deliberately added to steel, are defined as residuals, they are always present to some degree. Some elements like copper and tin remain because they cannot be preferentially oxidized with the use of normal steel making methods (Hartley et al, 1980).

The presence of residual elements in steels may be beneficial or detrimental, depending on the particular end application. The main processing problem caused by the presence of residual elements in carbon and low alloy steels is hot shortness. Hot shortness results directly from the fact that residual elements more noble than iron, such as copper, tin, nickel and antimony, are not oxidized when steel is reheated. Consequently, as iron is removed preferentially from the surface layers, these residual elements enrich progressively in the subscale layer. Copper is the key element in this area, without it hot shortness does not occur since it can enrich to a level exceeding its solubility limit in austenite (9%) and such an enrichment is possible under conditions of severe oxidation. At reheating temperatures in the range 1100-1200°C the Cu rich phase that precipitates is molten (melting point 1080°C) and tends to penetrate the austenite grain boundary leading to surface fissuring when any tensile stress is applied (Melford 1980). In contrast, nickel has been shown to have a beneficial effect since it

stabilizes austenite and increases the solubility of copper in austenite. Fisher, (1969) has also studied the effect of nickel additions on the prevention of the molten, copper rich phase formation. His work indicates that the Cu:Ni ratio must be in range 1.5 or 2:1 to increase the solubility of Cu in austenite and hence avoid hot shortness.

Nowadays Cu is often added in a very small amounts as a cheap way to increase the strength of the steels (Jackson and Southall, 1980). The use of Cu as an alloying element in low carbon HSLA steels gives rise to increased strength by Cu precipitation while retaining good toughness, weldability and formability, even at very low temperatures and this is combined with excellent corrosion resistance (Fenn and Roberts, 1983). The corrosion resistance effect of Cu additions to steel exposed to the atmosphere is well known in terms of structural weathering steels (Le May et al, 1987)

Oil platform steels (C-Mn-Nb-Al) have Cu and Ni added to enable them to meet the strength requirement for thick plate. However it has been noted that the addition of these elements at somewhat higher levels than normal residual levels (1/4 %) ^{0.02-0.03} has resulted in a decrease in surface quality, and hot shortness from Cu is suspected. In this chapter the hot ductility of four C-Mn-Nb-Al steels were examined; a normal steel without Cu or Ni, a steel containing 0.5% Cu, a steel containing 0.5% Ni and finally

a steel which had equal quantities of Cu and Ni (0.25% Cu as well as 0.25% Ni).

9.2 EXPERIMENTAL

The composition of the steels are given in Table. 9.1. The steels were air melts supplied as hot rolled to 12 mm thick plates. Longitudinal tensile samples having a length of 70 mm and diameter of 7.95 mm were machined from the plates with their axis parallel to the rolling direction. Hot tensile tests were carried out on a Hounsfield Tensometer and heating was supplied by an induction heater, as described in chapter (3).

The hot rolled samples were heated to 1330°C, held for 5 minutes prior to cooling to test temperature in the range 750 to 1000°C, at a cooling rate of 60°C/min, so as to simulate the continuous casting process. Samples were held for 5 minutes at test temperature before straining to failure at 10^{-3}s^{-1} . These tests were carried out firstly in an inert atmosphere using an argon flow, and secondly without the presence of argon, in air. In addition, the steels were also examined after direct casting. The tensiles were melted at 1540°C for 5 minutes resolidified and cooled at 60°C/min to the required test temperature in the range 750 to 1000°C, then held for 5 minutes at test temperature and strained to failure using a strain rate of $2 \times 10^{-3}\text{s}^{-1}$ (these samples will be referred to in the text as as-cast. Note the slightly higher strain rate used is due to a smaller gauge length in the melted samples). Again the influence of argon and an air atmosphere was examined. This time in the first series of tests the argon gas flow surrounding the tensiles was left on until the test was

finished. In the second series, the argon gas flow was left on until the sample reached the melting point and then the gas was turned off and the test continued without argon in air.

The fracture surfaces were examined using a JEOL T100 SEM, operating at 25 KV.

The optical microscope was also used to examine the structure of the steels.

9.3 RESULTS

9.3.1 Hot ductility curves

The hot ductility curves of reduction in area (R.of.A) against test temperature for all the steels examined and for the various test conditions are given in Figs 9.1 to 9.8.

Unfortunately the base steel which contained no additions of Cu and Ni was found to give very poor ductility after solution treatment, and fracture was along planes parallel to the rolling plane. Examination of the delaminated fracture surface indicated that large amounts of slag or refractory had become entrapped in the steel, and subsequently elongated out on rolling. Results from these samples have therefore not been included in this analysis. However the part of this plate used for melting exercise was found to be free of slag entrapment and hence these results have been included.

For the hot rolled solution treated steels Figs. 9.1 to 9.5 all the steels examined showed a marked ductility trough. Ductility started to fall at 1000°C and continued to fall to at least 800°C. Ductility was generally about 5 to 10% R.of.A higher for the samples tested in argon but there was no significant difference in ductility between the three steels as shown in Figs. 9.4 and 9.5. Unfortunately because samples tended to break outside the gauge length, it was not generally possible to obtain R.of.A values below 850°C.

In the as-cast condition for samples tested in argon, Fig. 9.6 ductility again started to fall at 1000°C and reached the minimum at 800°C. The hot ductility curves for all four steels were very similar, the minimum R.of.A being 23% to 25%.

However for the as-cast steels tested in air a clear separation of the hot ductility curves occurred. The 0.5%Cu containing steel gave the worst R.of.A values Fig. 9.7 while the 0.5% Ni containing steel gave the highest values. There was, however, no significant difference in ductility between the steel with no addition of Cu and Ni and the steel with the 1/4% Cu and 1/4% Ni addition. This tends to suggest that the adverse influence of Cu on ductility is balanced by the beneficial influence of Ni and that this combination is to be recommended.

The temperature for the onset of dynamic recrystallization seemed little influenced by residual level or whether tests were carried out after solution treatment or in the as-cast condition; its value being $\geq 1000^\circ\text{C}$ as shown in Figs 9.9 to 9.12.

9.3.2 Fracture examination

Scanning electron microscope examinations revealed two distinct fracture modes, high temperature ductile rupture and intergranular fracture. At temperature $\geq 1000^{\circ}\text{C}$ only high temperature ductile rupture was observed as shown in Fig. 9.13. Lowering the temperature to 900°C reduced ductility and intergranular fracture was mainly due to grain boundary sliding although some micro-void coalescence was also observed, as shown in Figs. 9.14 and 9.15. At 800°C , intergranular fracture due to micro-void coalescence was the main mode of fracture as can be seen in Figs. 9.16 and 9.17.

The 0.5% Ni containing steels Ni steel, seemed to show more ductile voiding than the other steels, Fig. 9.18

9.3.3 Metallography

Grain sizes in as-cast condition were very coarse ~ 1 mm, while on reheating the grain size refined to ~ 300 μm . Grain size measurements were taken after fracture on transverse sections of samples giving low ductility values. Wedge cracks typical of failure by grain boundary sliding were observed for all the steels in all conditions, Fig. 9.19.

Examination of polished surfaces of both longitudinal and transverse sections close to fracture of steels tested in air or in the as-cast condition after switching off the argon, revealed that most of the surface had some internal oxidation and decarburization. Cracks were also seen to be associated with these areas as shown in Figs. 9.20 and 9.21. In contrast, steels heated or cast with a protective atmosphere of argon showed little oxidation and decarburization as shown in Fig. 9.22.

9.4 DISCUSSION

The present work has shown that oxidation has a very marked influence in reducing ductility. Previous work by Iacocca and Woodford, (1990) have also shown that oxidation can result in a weakening of the austenite grain boundaries, increasing the degree of grain boundary sliding. Melford, (1980) has reported that Cu becomes enriched in the subscale region whenever steel is subsequently reheated in an oxidizing environment. In the present instance this oxidation results in a 10% reduction in R.of.A. values.

For the solution treated condition there is a little evidence of Cu having any influence on ductility. This may be because the level of Cu at the boundaries is low and not sufficient to exceed the solubility limit, i.e. less than 9% the maximum solubility of Cu in austenite.

However after melting and cooling in air it is a clear that Cu does have an effect. This may arise because Cu would be expected to segregate to the boundaries on solidification so that its concentration there will be high. These results suggest that provided air is not allowed to enter the system the build up of Cu is not high enough to cause local melting. However when oxidation can take place, the solubility of Cu in austenite may be exceeded and if so melting can readily occur.

Nickel has been shown to increase the solubility of Cu in austenite and so would be expected to be beneficial as has been demonstrated in the present exercise.

The temperature range in which ductility is reduced by Cu (i.e. 950 to 850°C) is not the range normally associated with hot shortness (>1000°C). However at temperatures >1000°C dynamic recrystallization occurs and this prevents linkage of cracks which may be present at the boundaries due to localized melting. If Cu is present at the boundaries, then it is possible that it will act as a soft

film encouraging strain concentration and grain boundary sliding.

The changes in ductility are in general small and this probably arises because the steels contain Nb, and the hot ductility is very much influenced by the degree of Nb(CN) precipitation at the grain boundaries (Mintz and Arrowsmith, 1979). Cu additions may well have a more detrimental influence on the ductility of C-Mn-Al steels where precipitation is often absent.

Care must be taken in applying the results to the commercial continuous casting operation, as both the casting conditions and cooling conditions are very different to the laboratory situation. The laboratory cast tensiles often show more intense segregation than observed at the surface of the continuously cast slab. The oxidizing conditions in laboratory work are also less severe than during continuous casting as has been discussed by Melford, (1980). The water spray cooling and reheating through the rolls provides enhanced conditions for oxidation. Burden et al, (1979) have shown that vigorous spraying, by a combination of enhanced oxidation coupled with intermittent descaling can produce very severe enrichment of residual elements in a very short time.

CONCLUSIONS

- 1- The residuals Cu and Ni have no significant influence on the hot ductility of C-Mn-Nb-Al steels when these steels are solution treated prior to testing. This is independent of the presence of a protective atmosphere.
- 2- These residuals also have no significant influence on the hot ductility of directly cast tensiles when a protective atmosphere of argon is applied
- 3- Cu is detrimental to ductility when samples are directly cast and oxidation can occur. In these conditions Ni is found to be beneficial.
- 4- The results indicate that the beneficial effects on hot ductility of small amounts of Ni are exactly balanced by the detrimental effect of the same amount of Cu.
- 5- It is believed that these observations can be interpreted in terms of hot shortness. Segregation during casting probably causes a build up of Cu at the boundaries and this is increased when oxidation of Fe occurs to such a degree that the solubility of Cu in austenite is exceeded. Ni is able to increase the solubility of Cu in austenite and so is beneficial.
- 6- It is recommended that when Cu is added to continuously cast steel an equal amount of Ni should also be added.

Table 9.1

Composition of the steels examined (Wt.%)

Code	C	Mn	Si	P	S	Ni	Al	Cu	N	Nb
Normal steel	0.10	1.36	0.48	0.010	0.010	0.010	0.051	0.015	0.008	0.039
Cu steel	0.10	1.33	0.44	0.009	0.009	<0.020	0.047	0.490	0.007	0.039
Ni steel	0.10	1.30	0.44	0.010	0.008	0.500	0.057	0.020	0.034	0.034
Cu,Ni steel	0.10	1.30	0.44	0.010	0.010	0.250	0.059	0.250	0.004	0.033

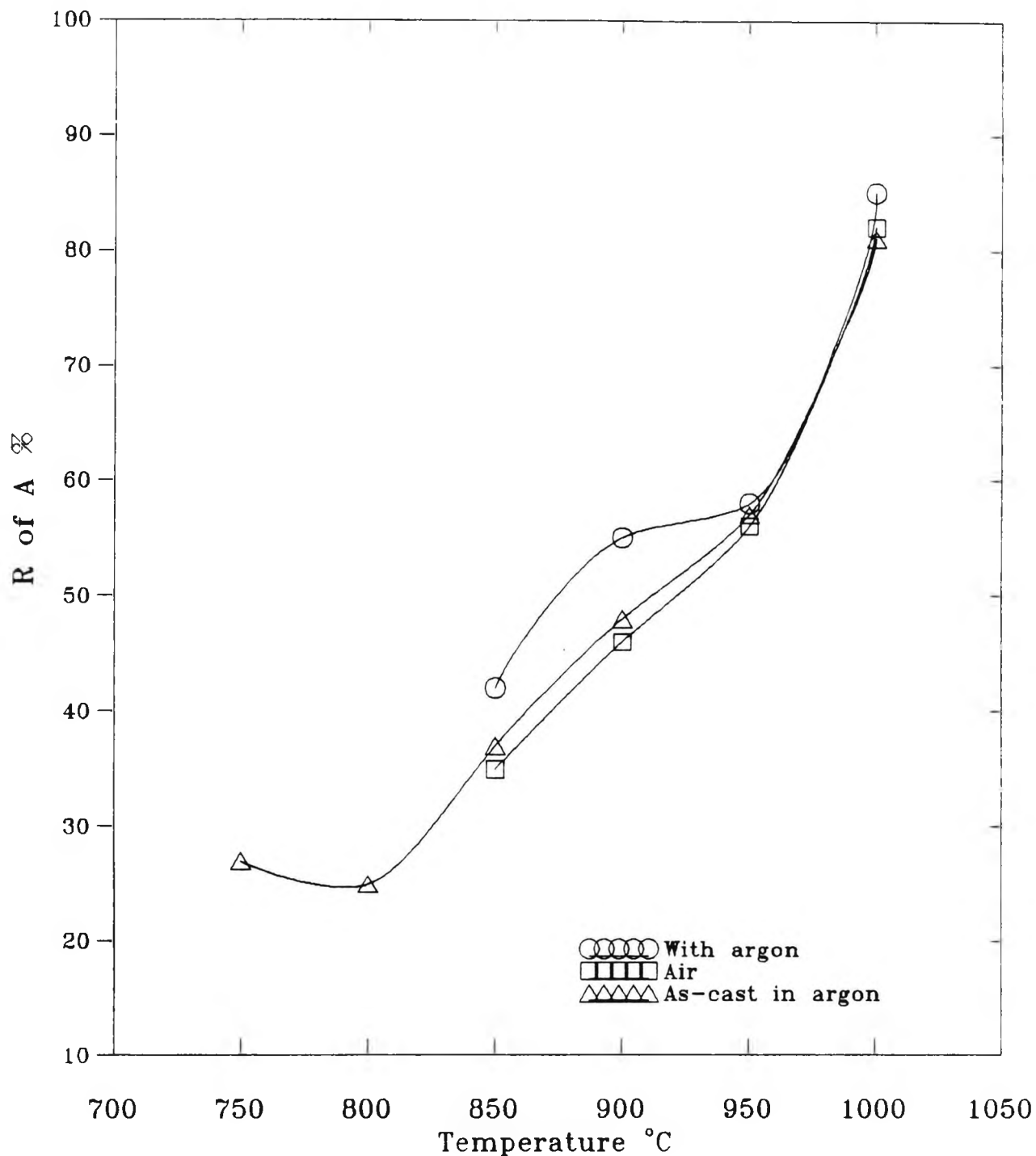


Fig 9.1 Hot ductility curves for 0.5% Cu steel in the solution treated condition with and without argon, and after casting and testing in an argon atmosphere.

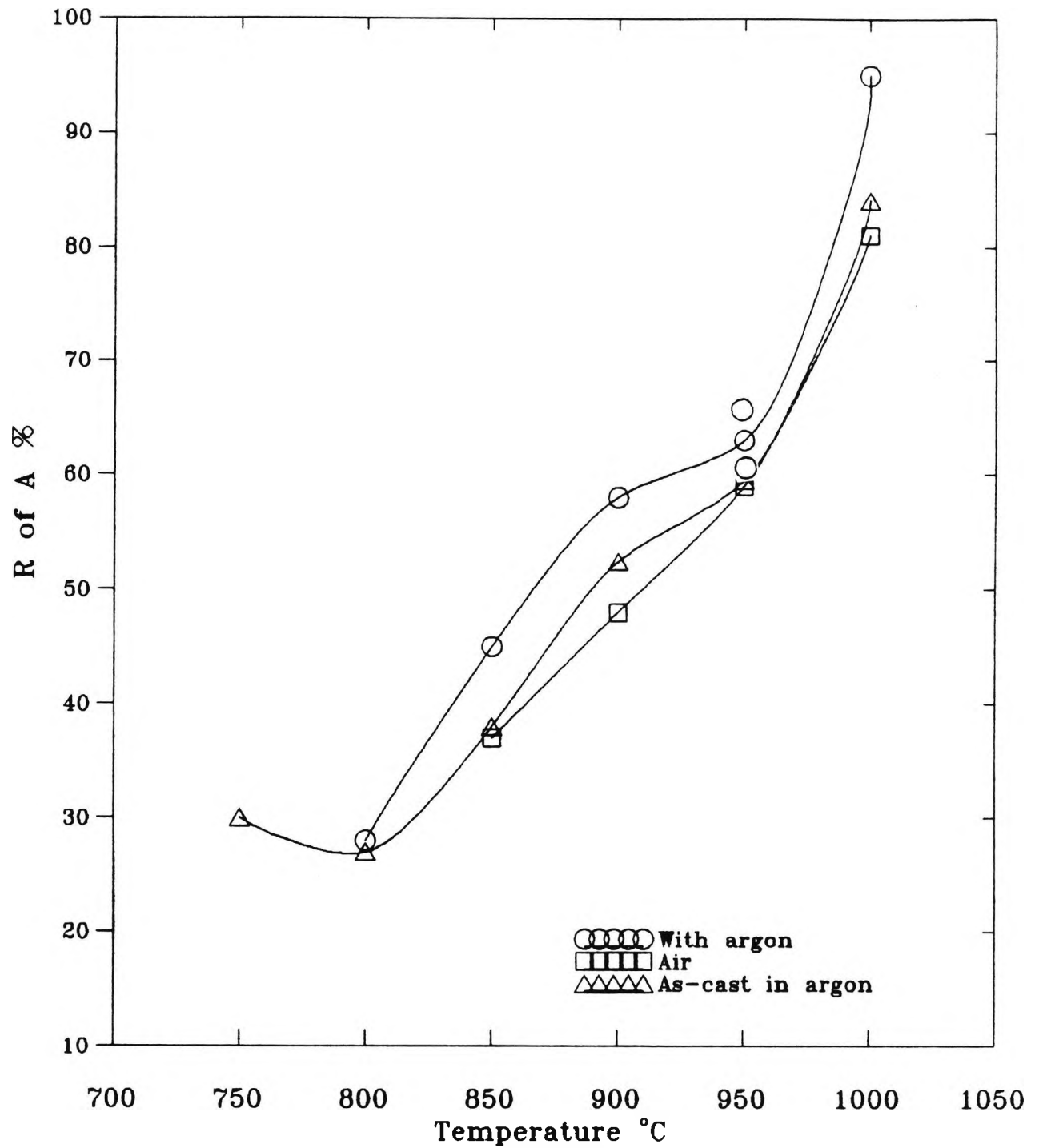


Fig 9.2 Hot ductility curves for 0.5% Ni steel in the solution treated condition with and without argon and after casting and testing in an argon atmosphere.

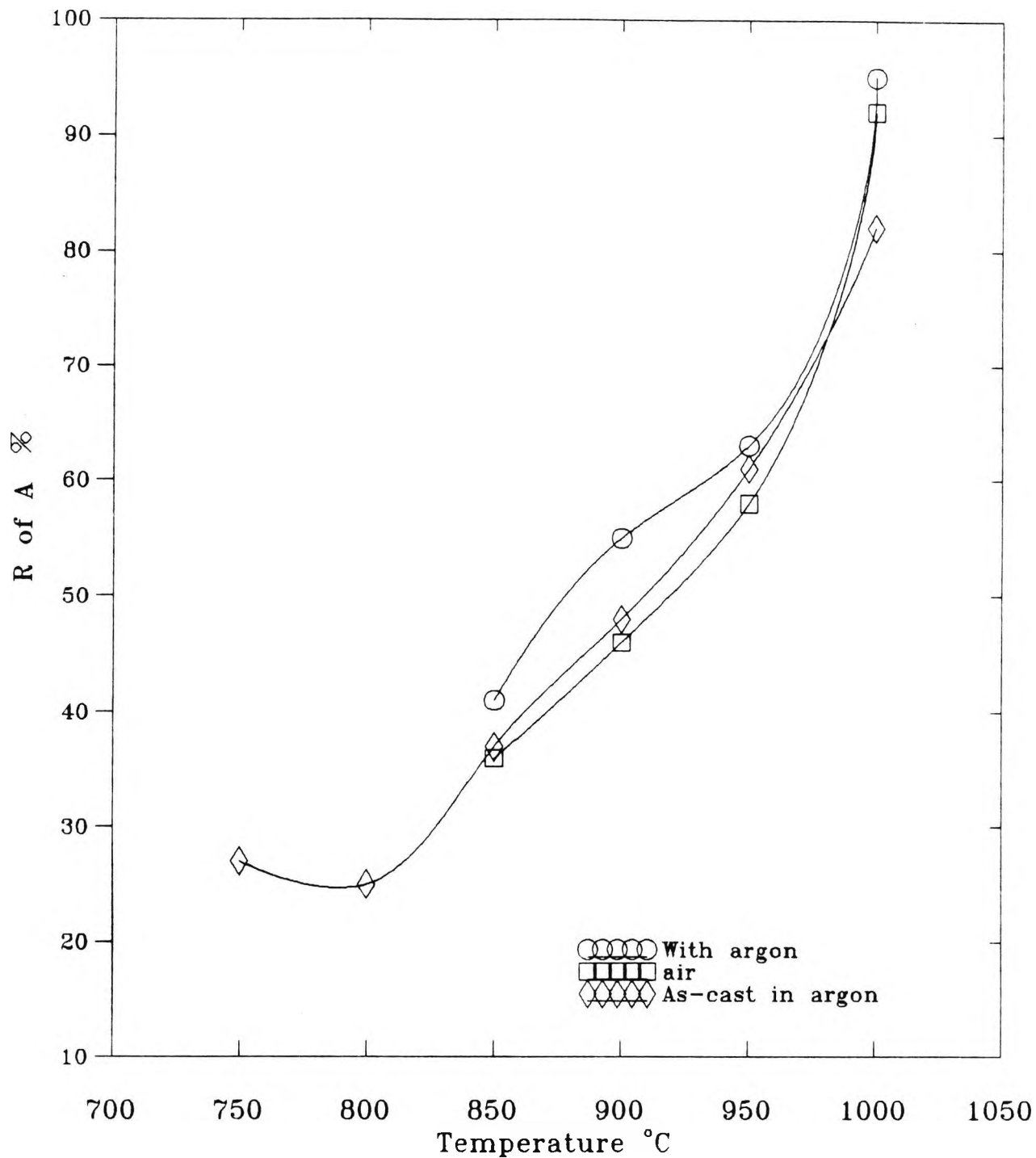


Fig. 9.3 Hot ductility curves for CuNi steel in the solution treated condition with and without argon, and after casting and testing in an argon atmosphere.

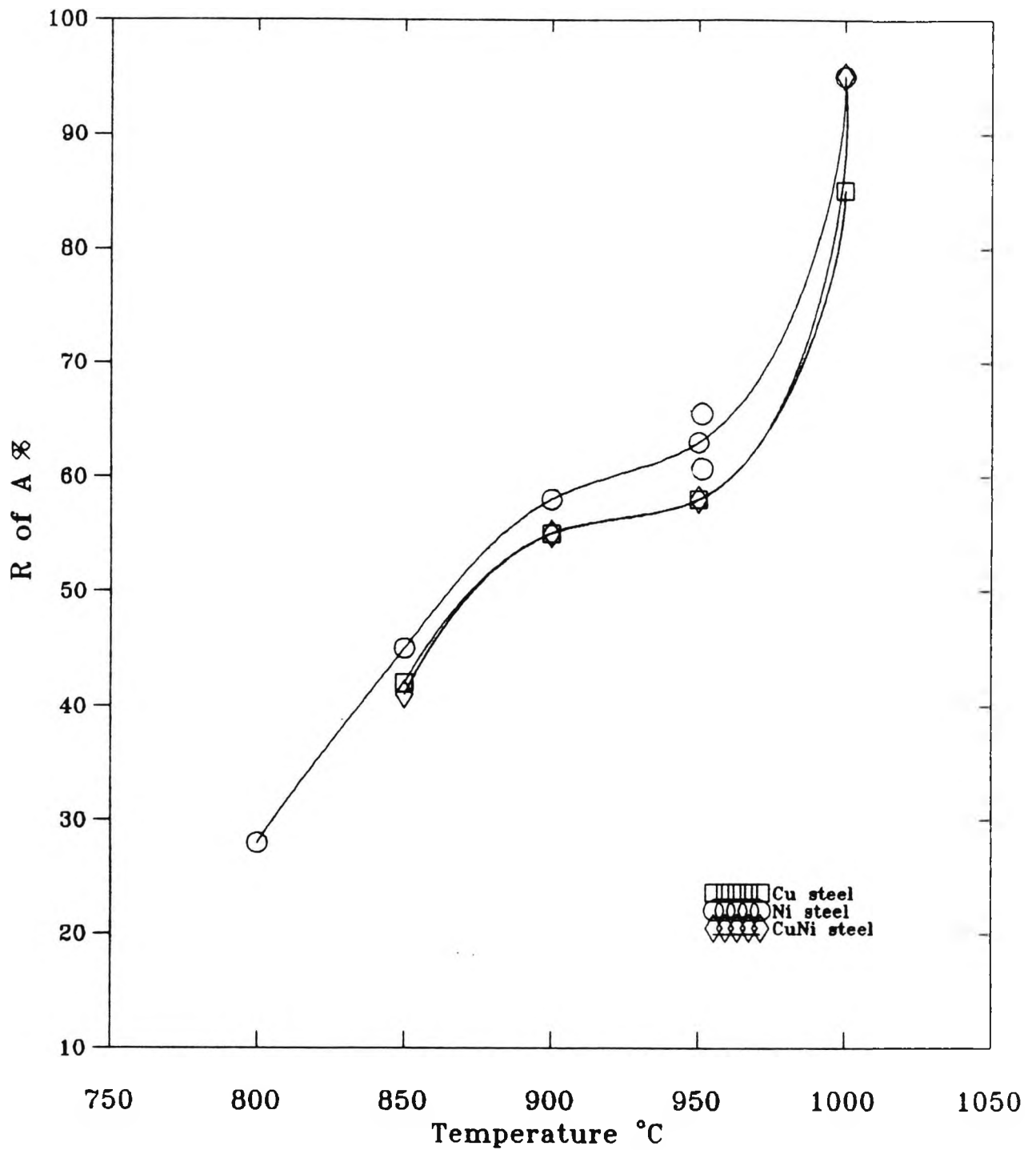


Fig. 9.4 Hot ductility curves for all the steels examined after solution treating, using an argon atmosphere through out the tests.

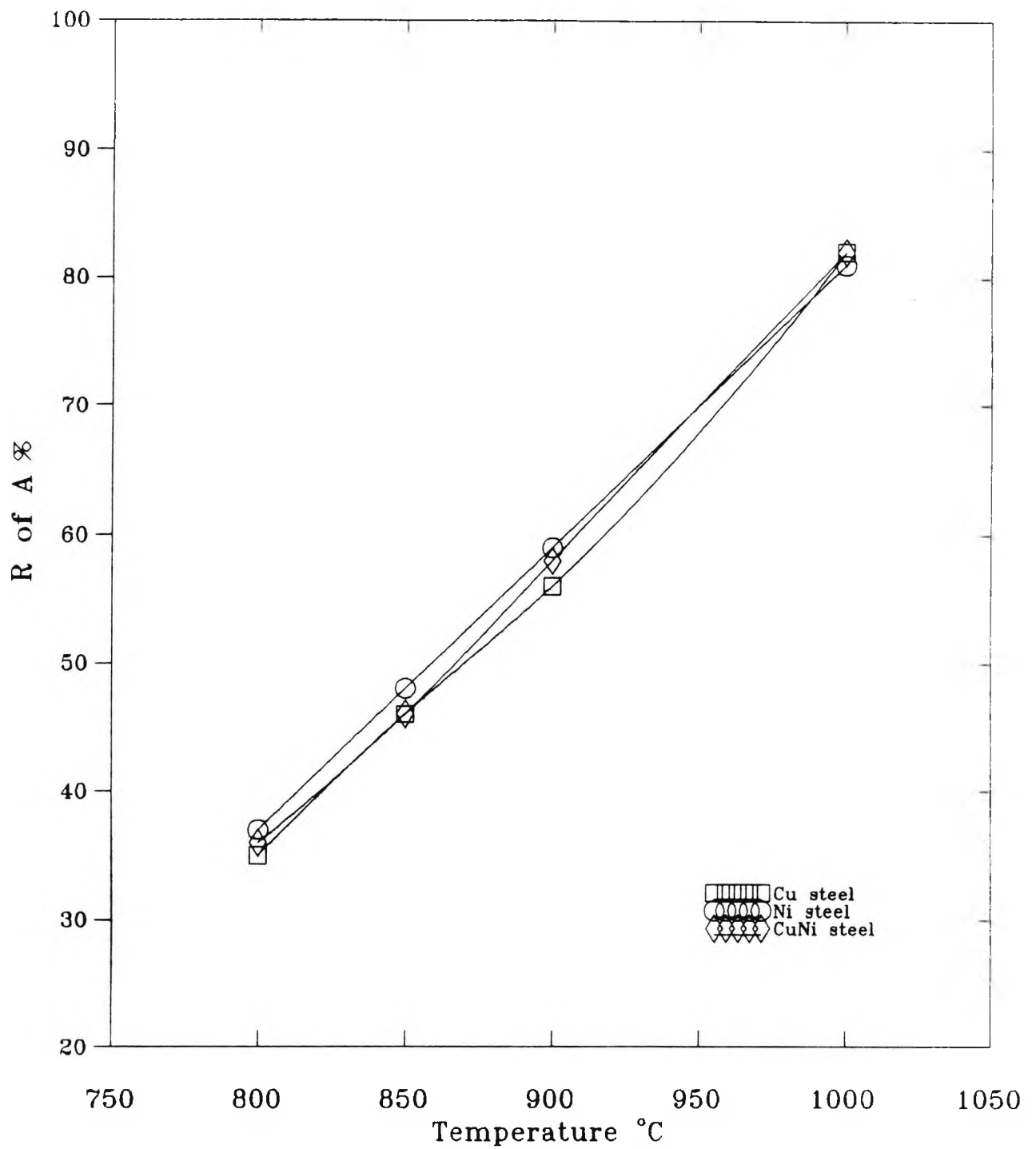


Fig. 9.5 Hot ductility curves for all the steels examined after solution treating in air.

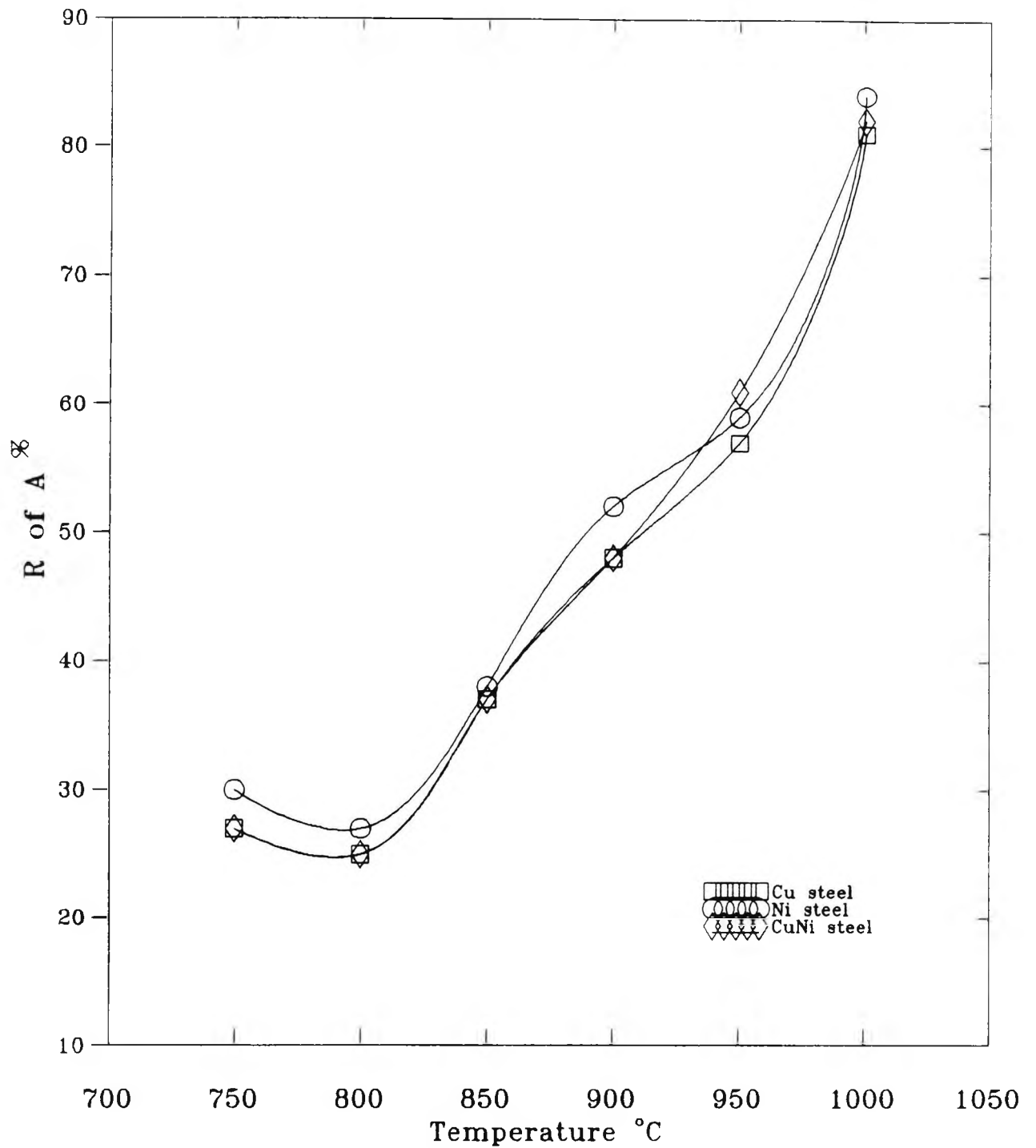


Fig.9.6 Hot ductility curves for all the steels examined in the as-cast condition using an argon atmosphere for protection.

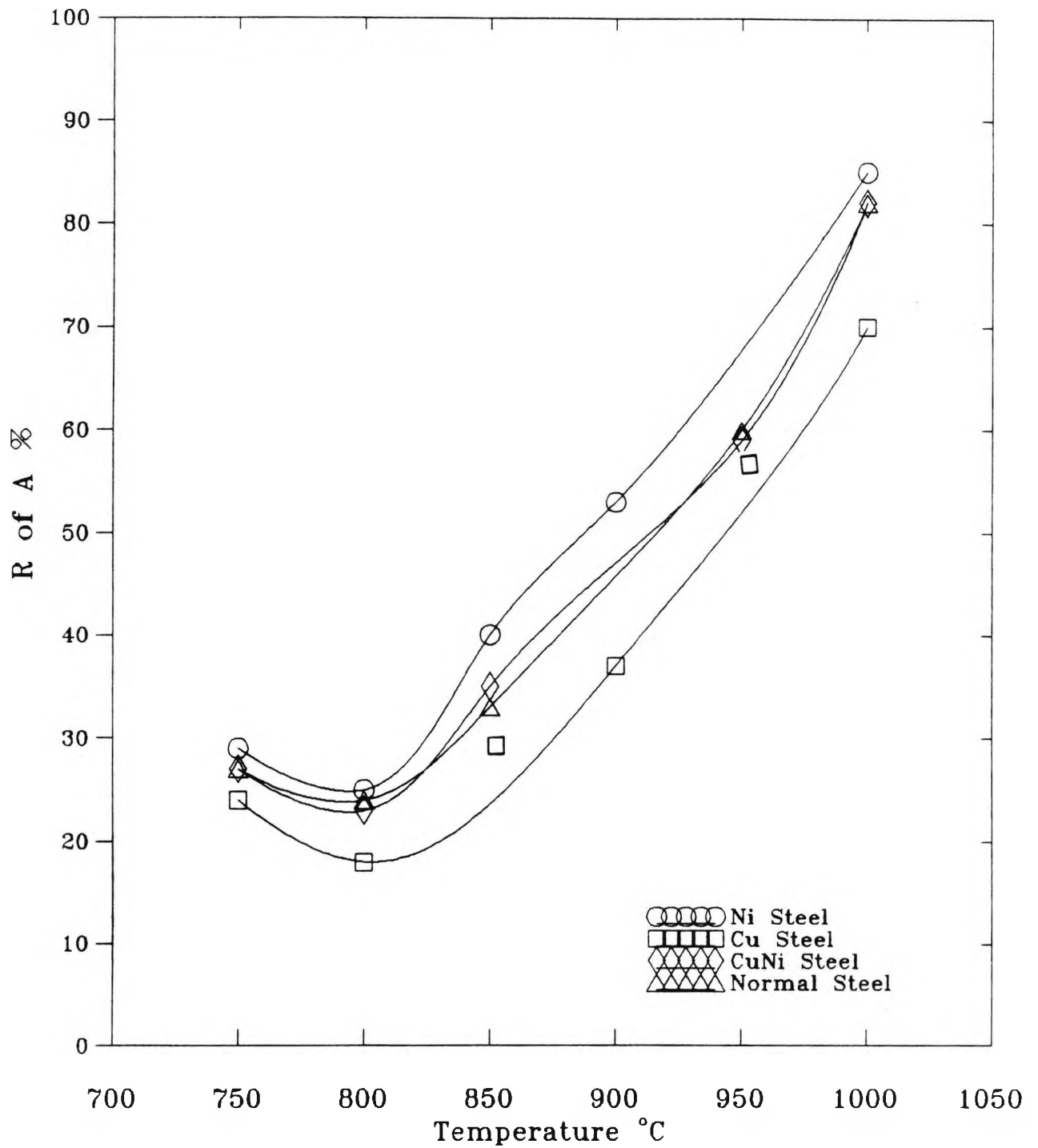


Fig. 9.7 Hot ductility curves for all the steels examined in the as-cast condition. Argon was switched off at 1500°C.

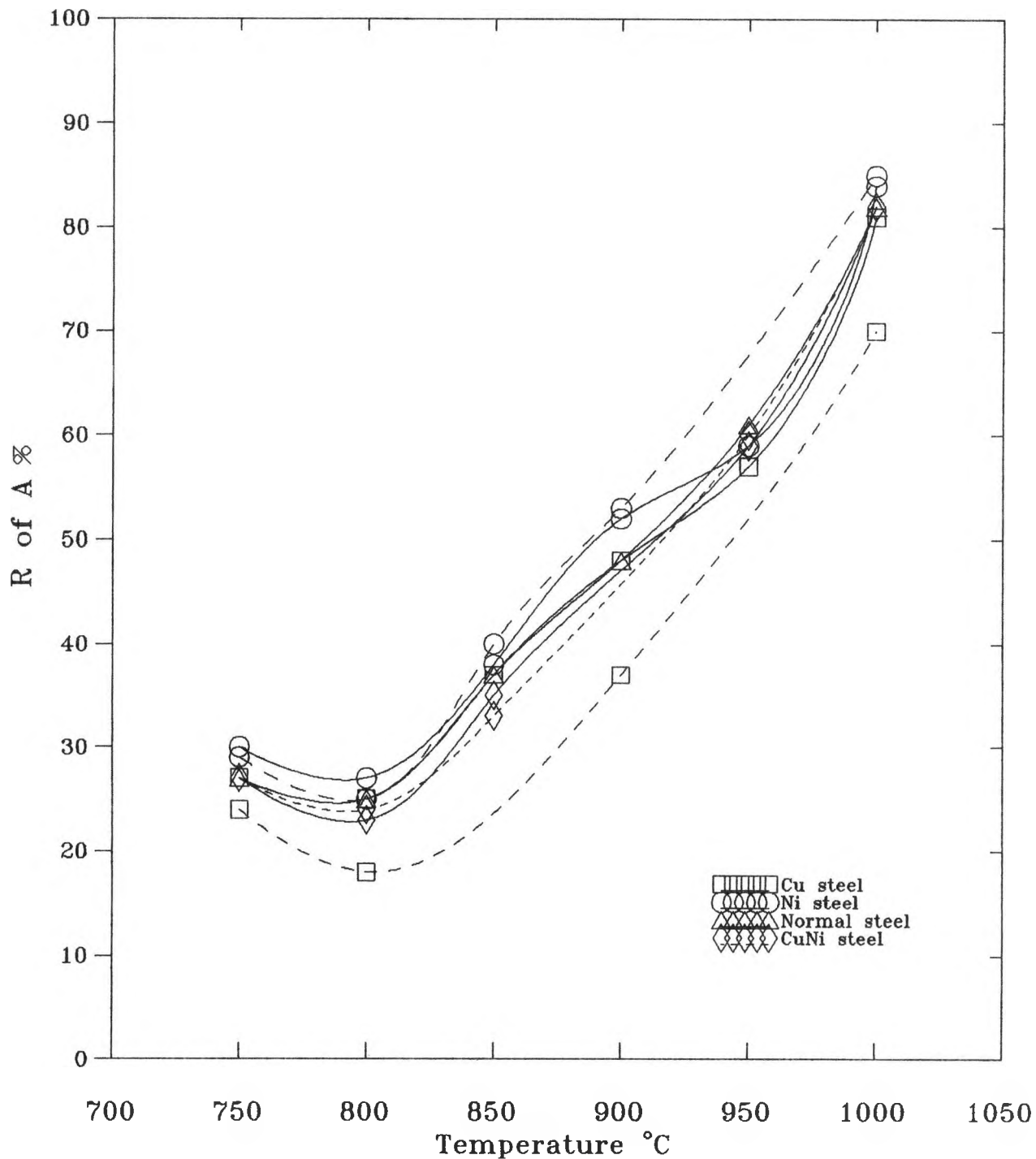


Fig. 9.8 Hot ductility curves for the all steels examined in the as-cast condition using an argon atmosphere for protection. The dashed lines are for the steels when the argon was switched off after melting.

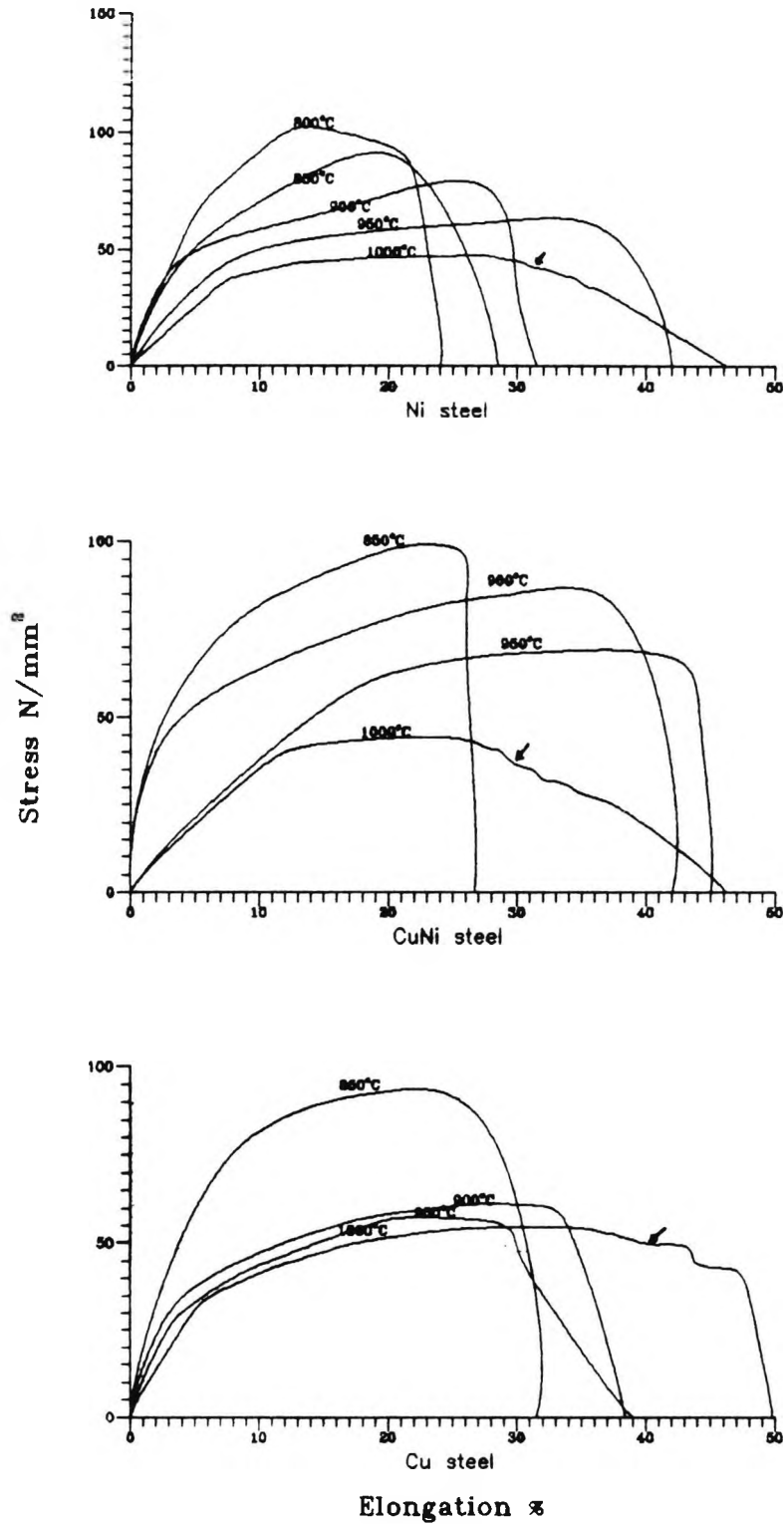


Fig. 9.9 Stress/Elongation curves for the reheated solution treated steels tested in an argon atmosphere.
(Arrows indicate dynamic recrystallization)

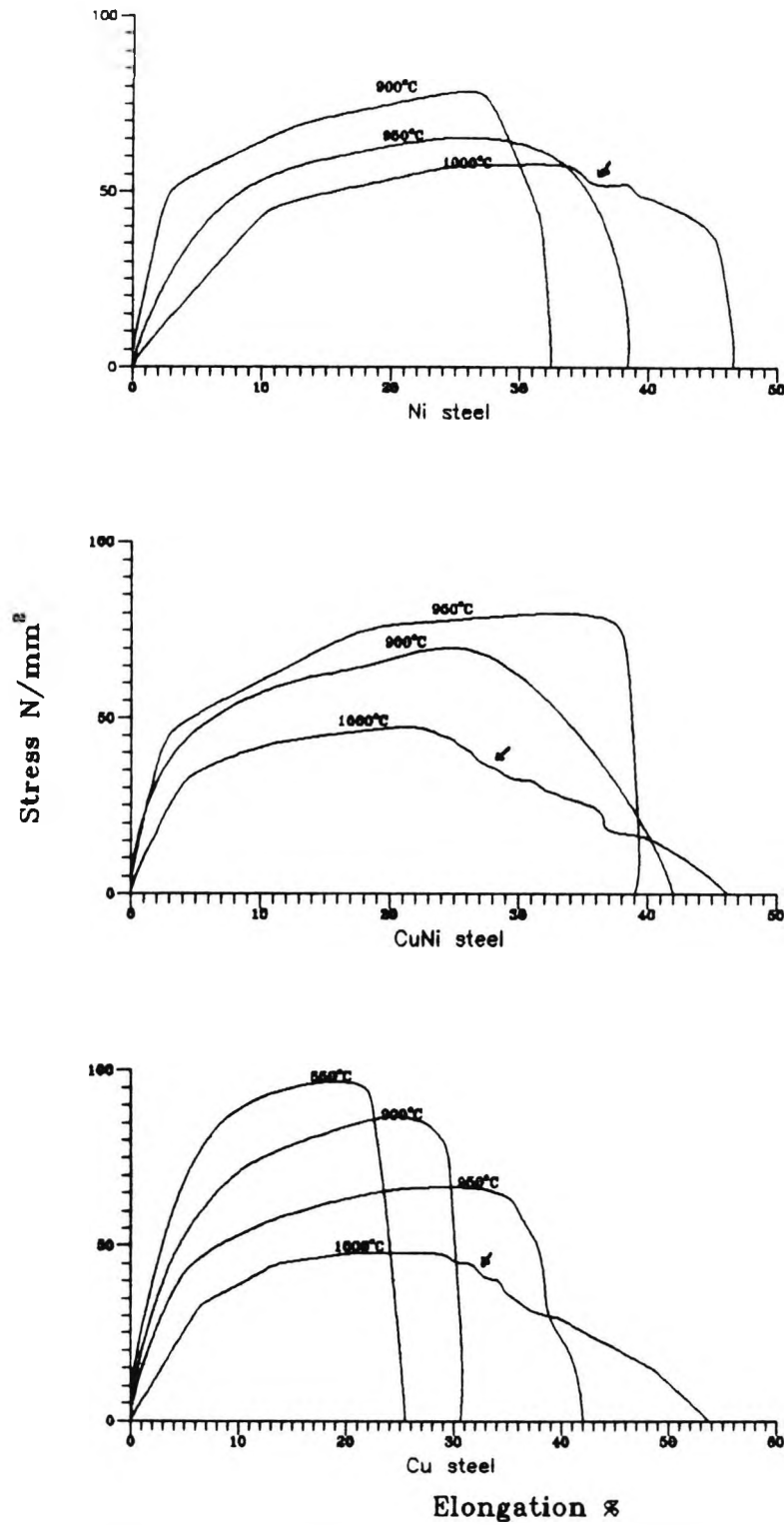


Fig. 9.10 Stress/Elongation curves for reheated steels solution treated and tested in air. (Arrows indicate dynamic recrystallization).

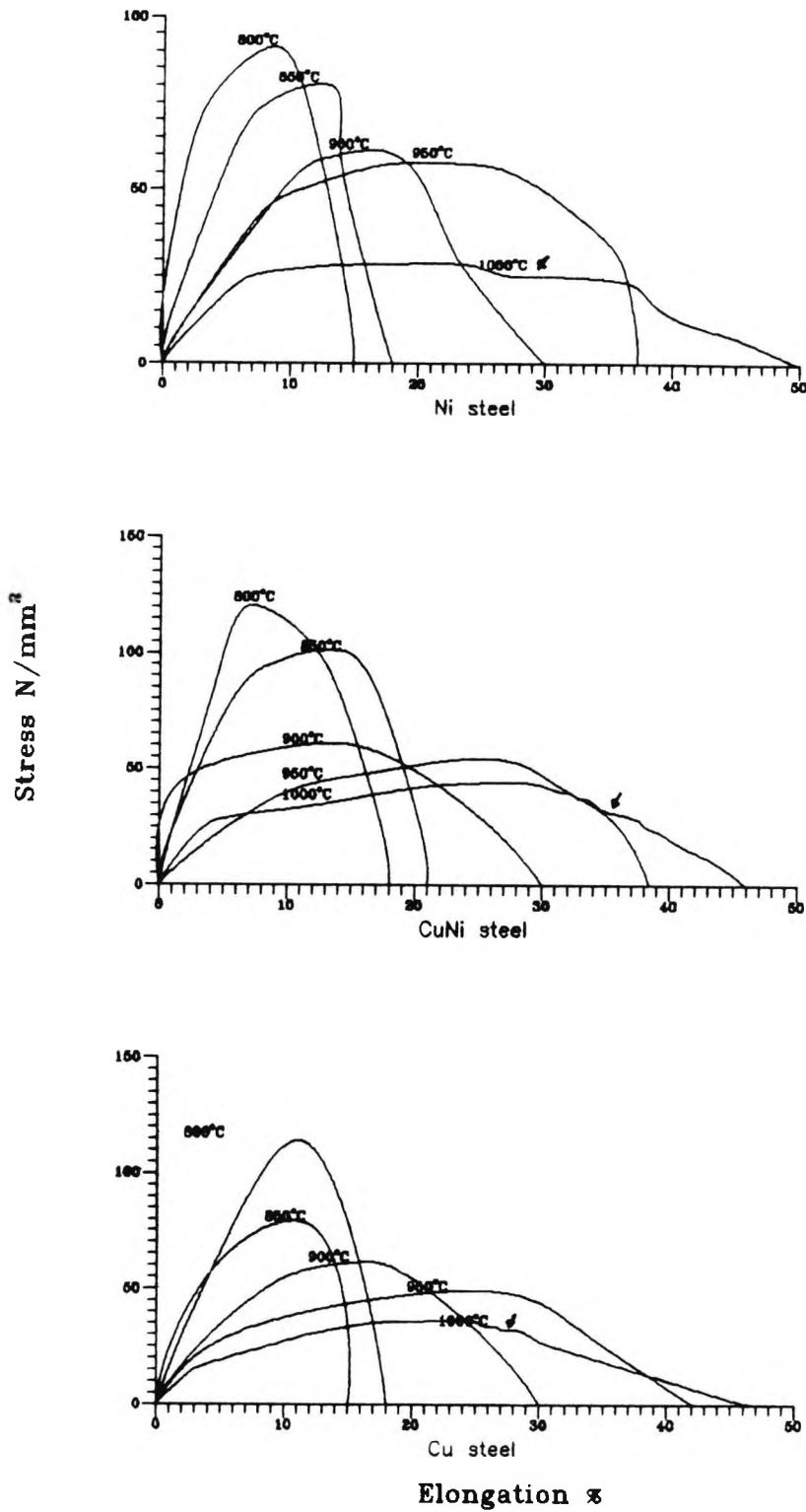


Fig. 9.11 Stress/Elongation curves for the as-cast steels protected within an argon atmosphere. (Arrows indicate dynamic recrystallization).

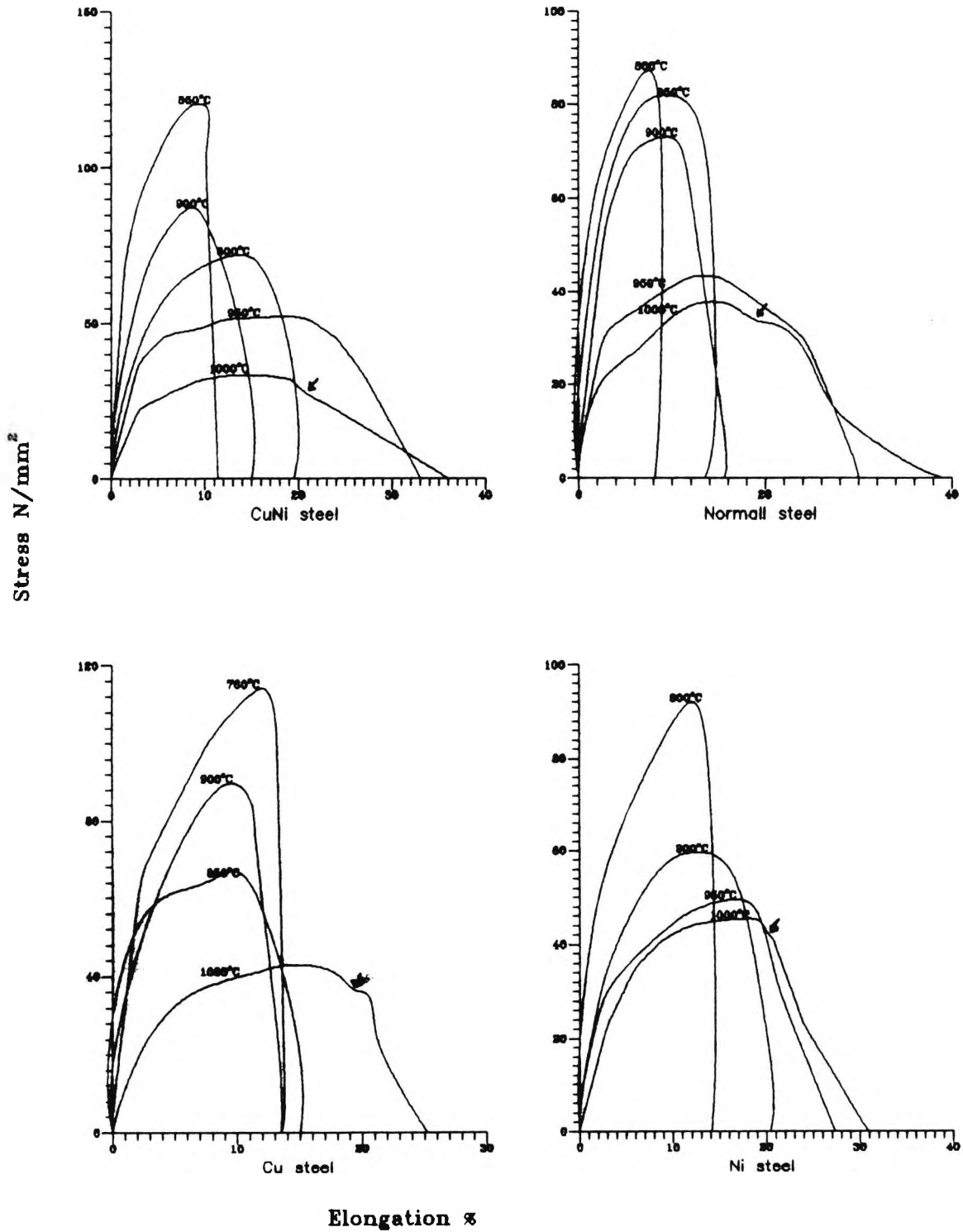
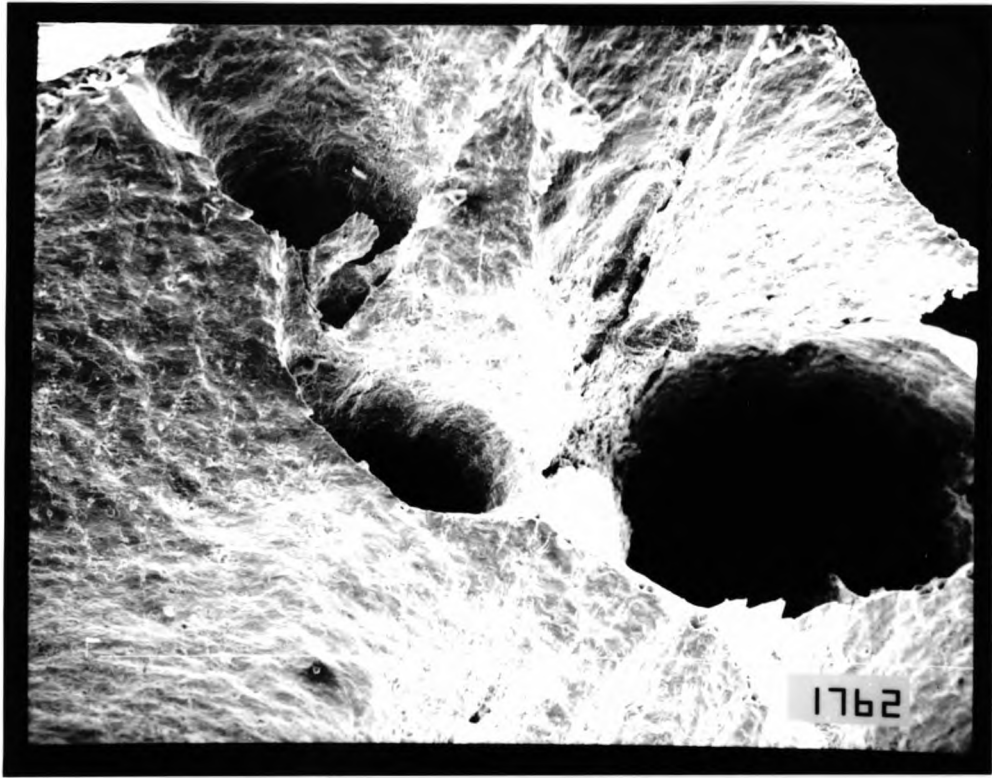


Fig 9.12 Stress/Elongation curves for all the steels examined, in the as-cast condition with the argon flow discontinued at a temperature of 1500°C. (Arrows indicate dynamic recrystallization).

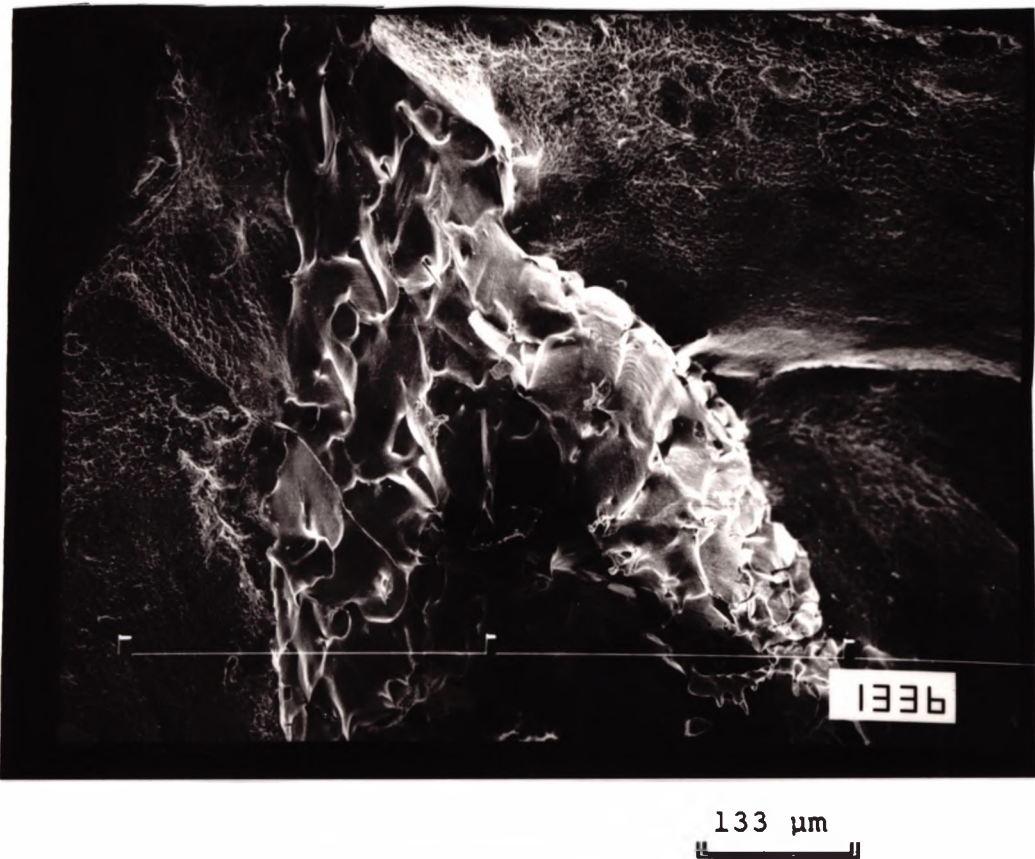


100 μm

Fig. 9.13 Ductile rupture fracture found in 0.5% Ni containing steel reheated to 1300°C, and protected with argon. Sample tested at 1000°C.



(a) Argon switched off at 1500°C



(b) with Argon

Fig. 9.14 Grain boundary sliding found in the CuNi steel in the as-cast condition. Steel tested at 900°C
 (a) argon flow stopped at 1500°C
 (b) argon flow on all the time.

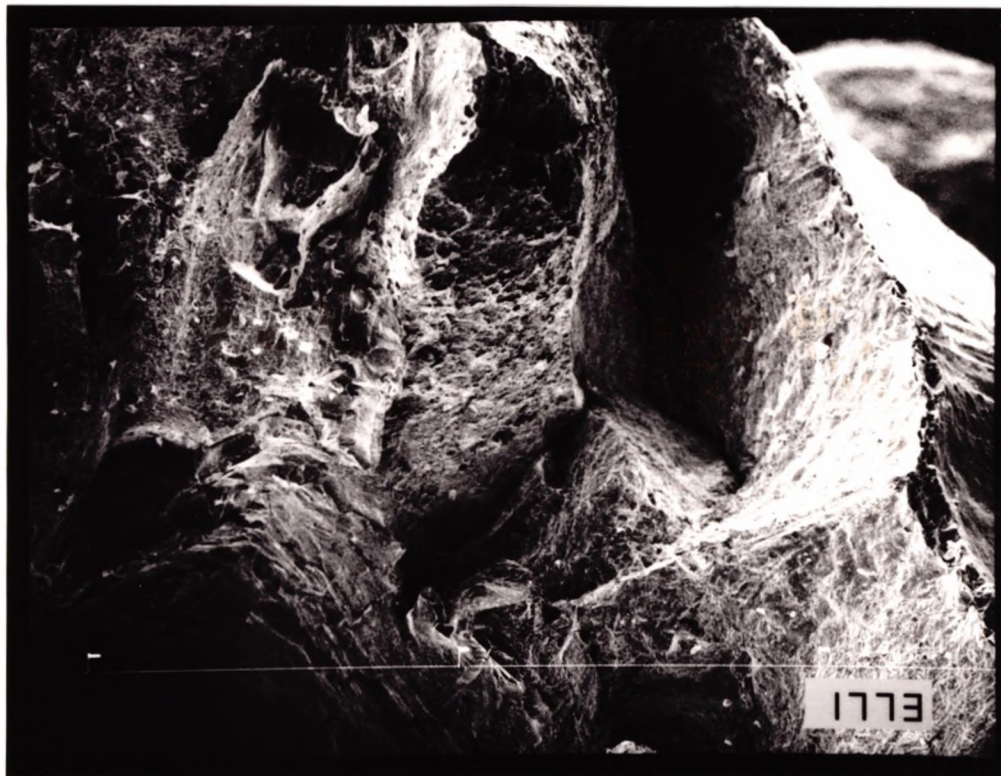


Fig. 9.15 grain boundary sliding found in 0.5% containing Ni steel. Steel was solution treated ,tested at 900°C. Sample was protected by argon.

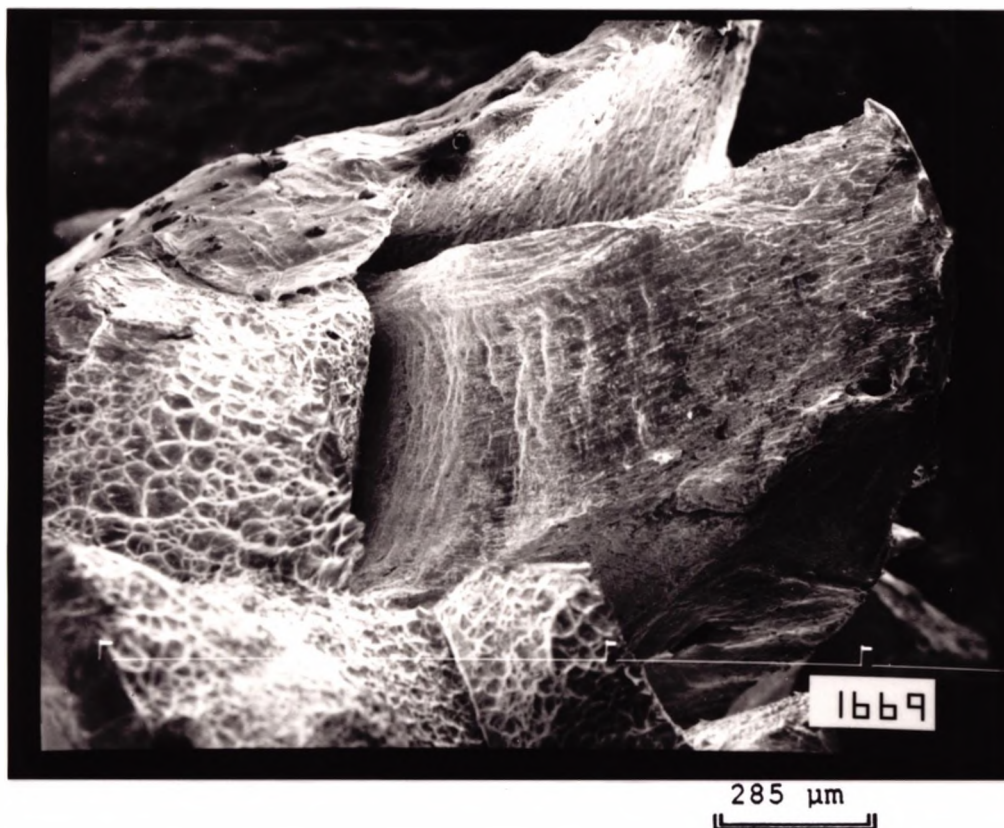
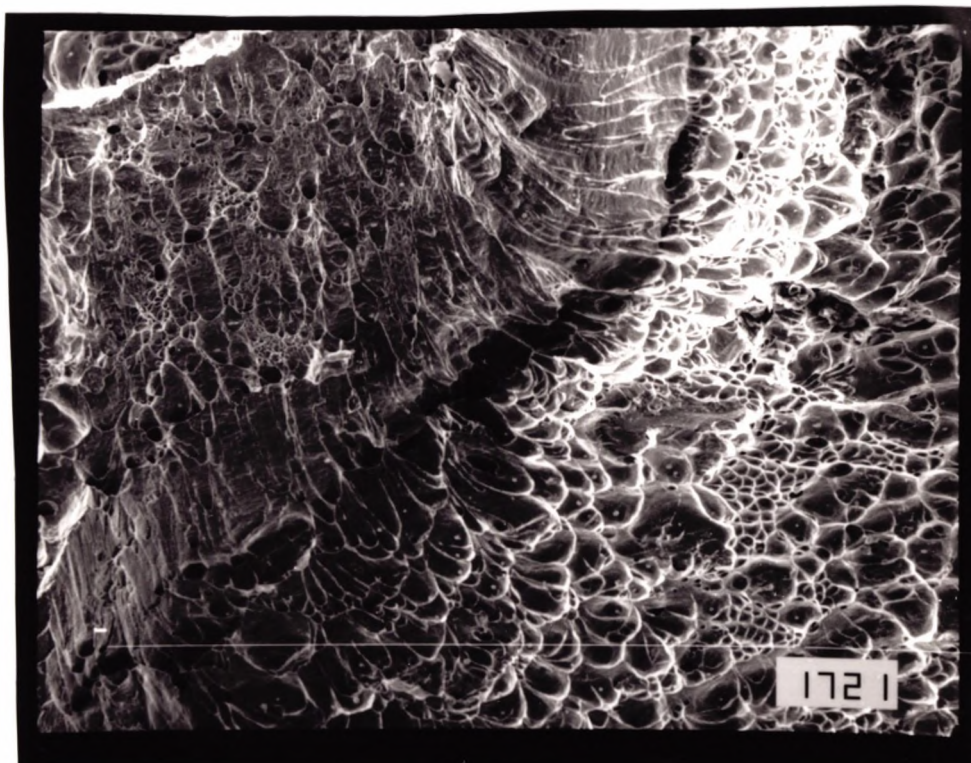


Fig. 9.16 As-cast 0.5% Cu steel ,tested at 800°C, showing a mixture of grain boundary sliding and micro-void coalescence. Argon flow was discontinued at 1500°C.



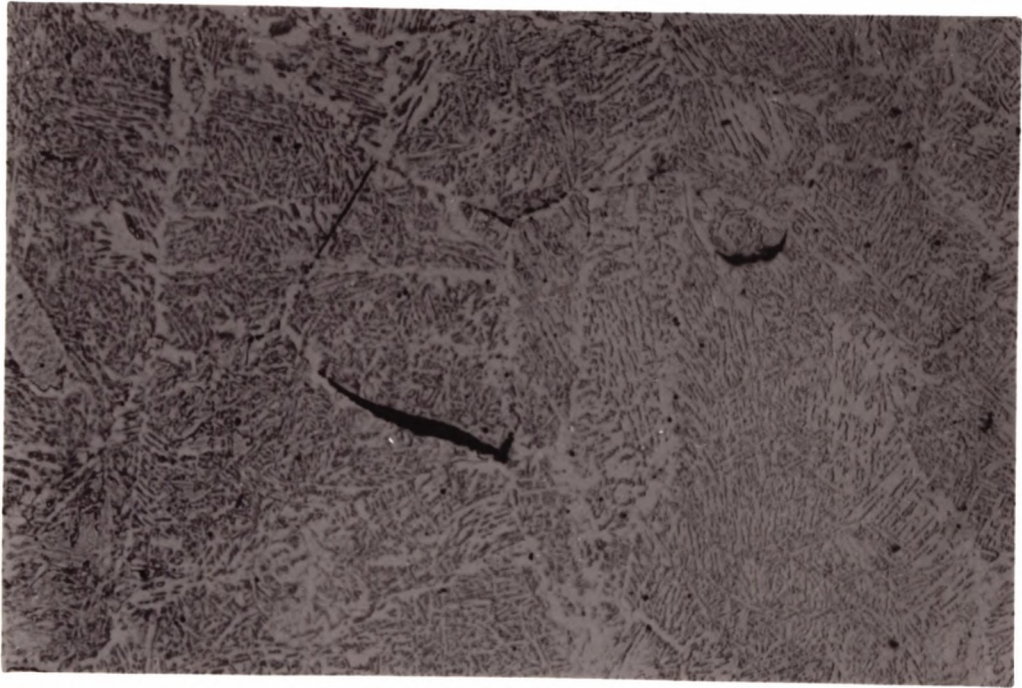
285 μm

Fig. 9.17 Intergranular fracture due to micro-void coalescence, found in the CuNi steel tested at 800°C. Sample was protected by argon.



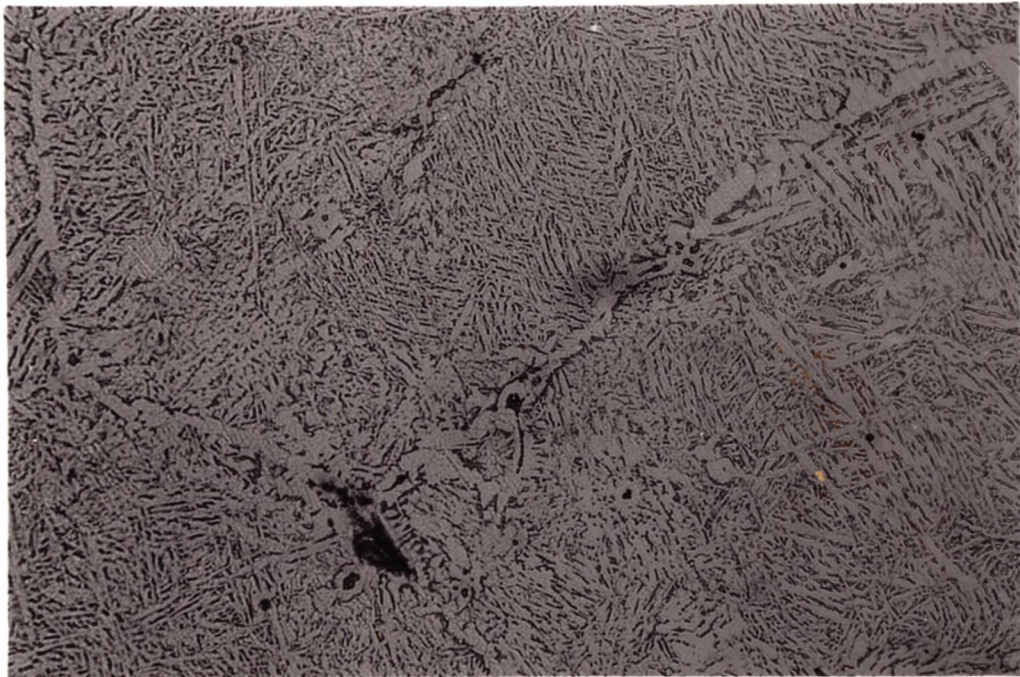
100 μm

Fig. 9.18 Ductile voiding found in 0.5% Ni steel, tested in air at 850°C.



200 μm

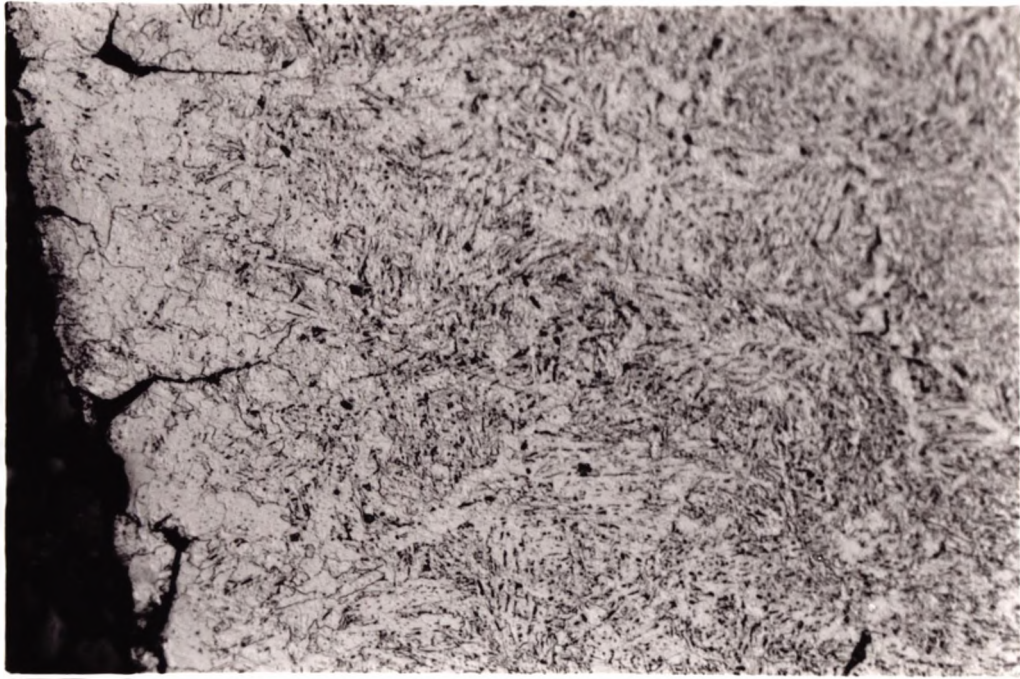
Steel was solution treated and tested at 900°C



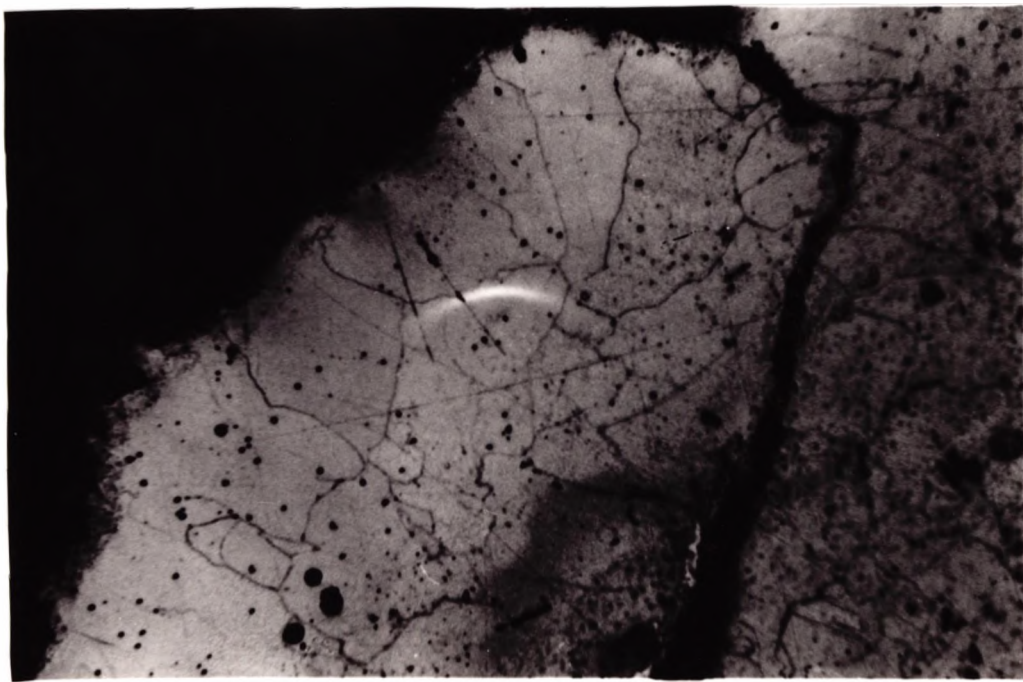
100 μm

Steel was as-cast and tested at 900°C, (argon flow discontinued at 1500°C)

Fig. 9.19 Wedge cracks found in 0.5% Cu steel.

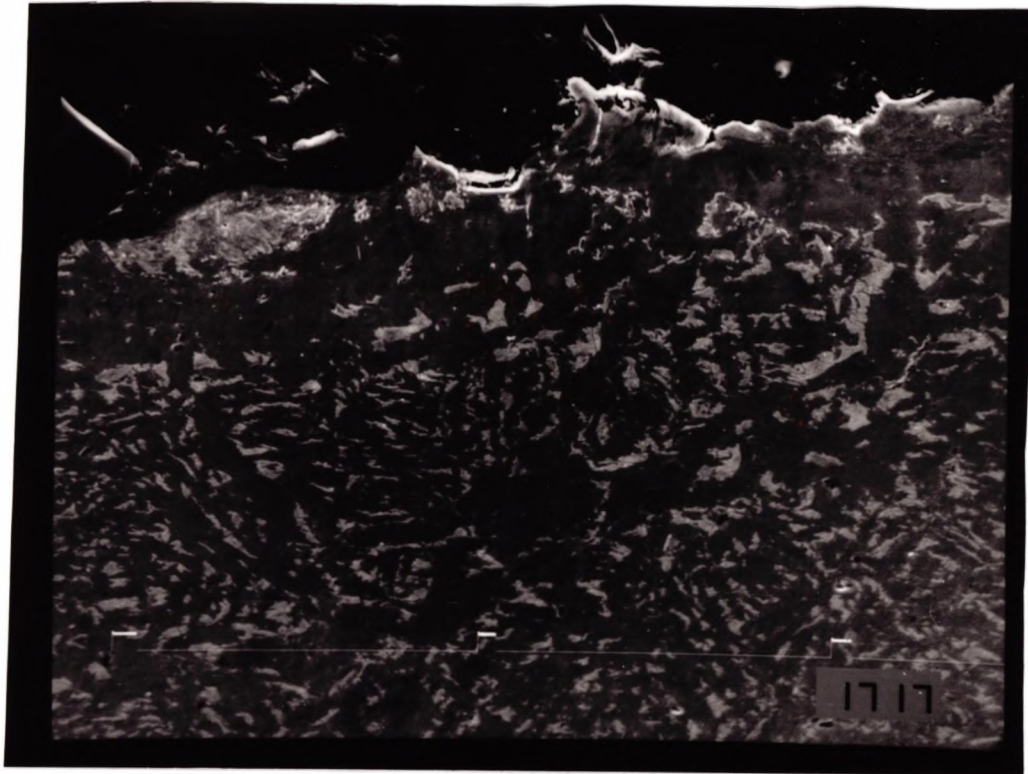


100 μm

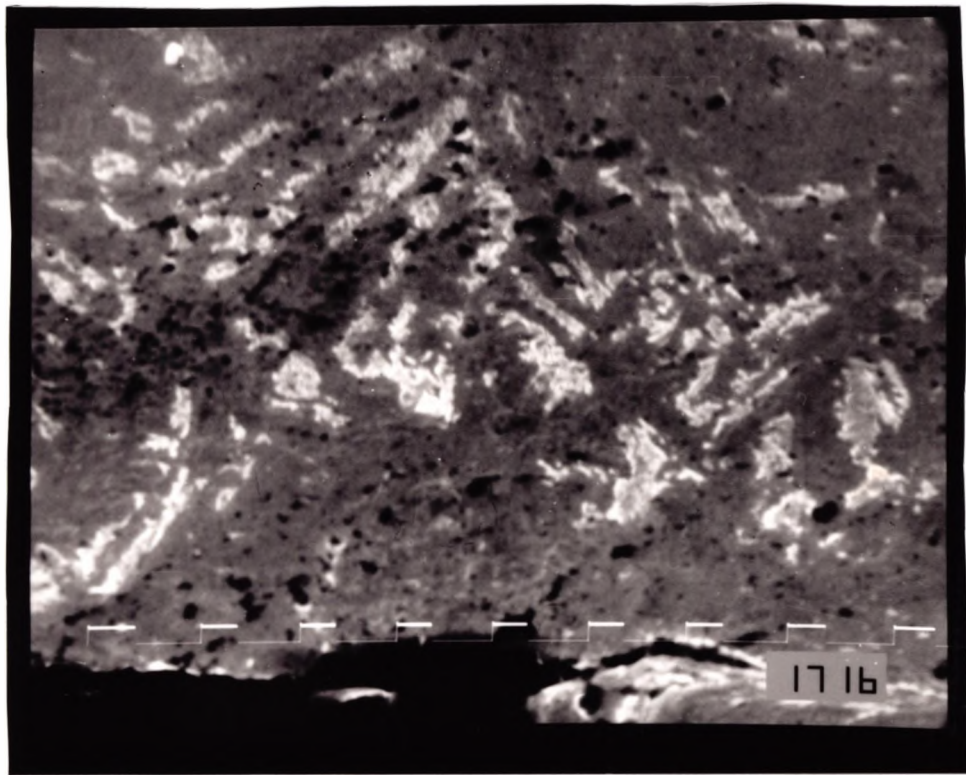


50 μm

Fig. 9.20 Decarburization and internal oxidation found in 0.5% Cu containing steel solution treated and tested in air at 900°C (R.of.A is 35 %)

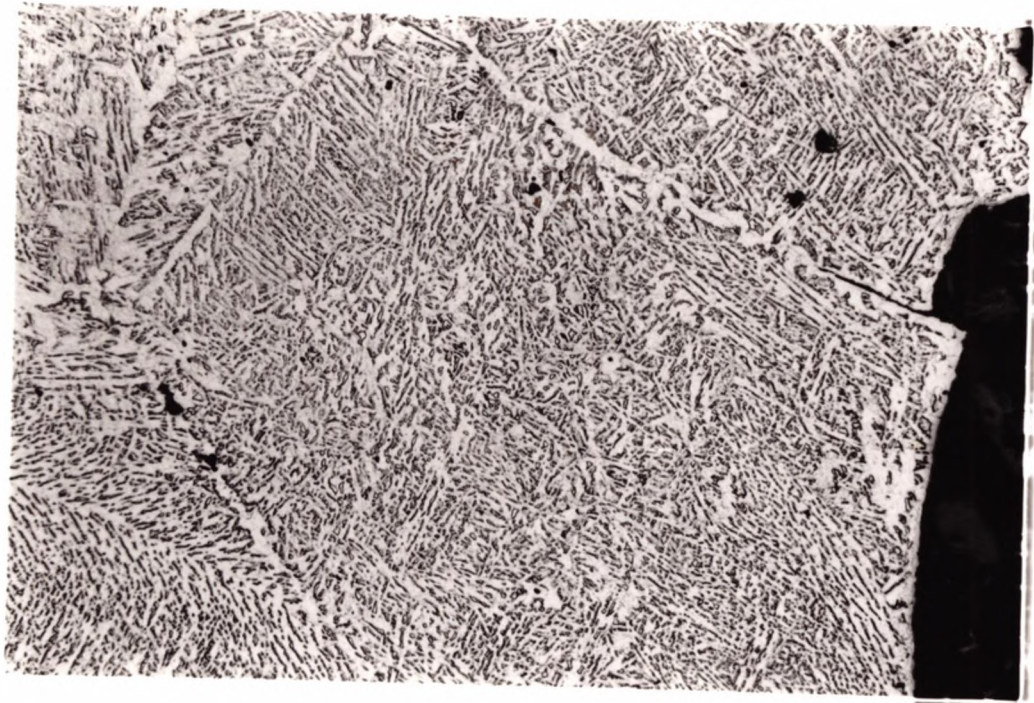


20 μm



13.3 μm

Fig. 9.21 Decarburization and internal oxidation found in as-cast CuNi steel tested at 900°C. Argon was turned off at 1500°C.



100 μm

Fig. 9.22 Virtual absence of decarburization and internal oxidation found in the as-cast 0.5% Cu steel protected throughout the test by argon. Steel was tested at 900°C.

CHAPTER 10

EFFECT OF C ON HOT DUCTILITY

10.1 INTRODUCTION

Crowther and Mintz, (1986) have examined the influence of C on the hot ductility of plain C-Mn steels of the same base composition, but with differing carbon levels in the range 0.04% to 0.65%. Tests were carried out using the Gleeble machine which uses electrical resistance heating in an argon atmosphere. Test pieces were heated to 1330°C, then cooled at a rate of 60°C/min to the test temperature range of 550 to 950°C where they were strained to failure at a strain rate of $3 \times 10^{-3} \text{ s}^{-1}$. The cooling rate and strain rate were chosen to simulate the cooling rate undergone by the strand and the strain rate of the straightening operation. In all cases a trough was obtained and for C levels up to 0.3%, this trough was controlled by the transformation from γ to α . On lowering the temperature the micro-structure changes from one which is totally austenitic to one in which thin films of ferrite form around the austenitic grains and strain concentration occurs.

Raising the C level was found to move the trough bodily to lower temperature in accord with the trough being controlled by the transformation from γ to α . The thin films of ferrite were in fact found to be deformation induced.

However, raising the C level above 0.3% caused a change in the fracture mode. Instead of fracture being by micro-void coalescence at the MnS particles situated at the

boundaries, failure was by grain boundary sliding in the single phase austenite. This change in the fracture mode was not understood. Furthermore the temperature for the onset of dynamic recrystallization was not recorded in their work making interpretation difficult.

The present study has therefore been instigated in order to obtain a greater understanding of this unusual behaviour.

Two steels were examined, a low C steel with 0.11% carbon, and a high C steel with 0.75% carbon.

10.2 EXPERIMENTAL

The experiment was carried out on two steels of different carbon levels. One steel was a commercial rail steel with a high carbon content 0.75% C, and the other steel was supplied as a laboratory vacuum melt, hot rolled to 12 mm thick plate, with a low carbon level, 0.11% C. The full composition of the two steels are given in Table 10.1.

Tensile samples with diameter 5.04 mm and gauge length 25.4 mm were machined longitudinally from each steel. Hot tensile tests were performed using the Instron equipment described in chapter 3. Tests were conducted in a flowing Argon atmosphere, and the samples were also nickel plated as described by Crowther, (1986) to prevent decarburization.

An additional thermocouple was used independently of the furnace thermocouple to give the temperature of the sample.

The nickel plated test sample and the grip were pasted with Alumina (alumina powder in a suspension of methanol) to prevent sticking of the sample to the grip. The sample was surrounded by a silica sheath in which the argon flowed in order to protect the sample from oxidation and decarburization. The argon flow was turned on at a rate of 4 L/min. The sample was then heated to 1330°C and it took an hour to reach this temperature. During the heating the sample would expand and the tension was released at regular intervals. The sample was held at

1330°C for 5 minutes, then the argon flow was increased to 40 L/min and the sample was cooled at a rate of 25°C/min, this being the maximum cooling rate attainable using the platinum wound furnace. The samples were cooled to the test temperature in the range 1000 to 550°C and held for 5 minutes at the test temperature and then strained to failure using a strain rate of $3 \times 10^{-3} \text{ s}^{-1}$. After failure half of the test sample dropped automatically into a quenching unit, the other half of the sample remaining in the furnace and being subsequently slow cooled to room temperature (not all samples were water quenched after fracture as the quench unit was not fully operational until the later stages of this work. It was developed during this investigation and is shown in detail in Fig 10.1)

A Vickers projection microscope was used to measure reduction of area. The fracture surfaces of the samples were examined with a T100 JEOL Scanning electron microscope. An Optical microscope was also used for examination of longitudinal sections of polished samples. Austenite grain sizes were obtained before deformation. The start of the pearlite transformation was obtained by heating small samples to 1330°C for 5 minutes then cooling at 25°C/min to temperatures below 700°C at 20°C intervals followed by quenching. This established the pearlite start temperature as being between 650°C and 670°C.

10.3 RESULTS

10.3.1 Hot ductility curves

The Curves of reduction in area against test temperature for both the low and high carbon steels are shown in Fig. 10.2. The calculated Ae_3 temperature using Andrew's equation, (1965) have been marked on the curves. For the high carbon steel it was 725°C and for low carbon steel it was 870°C .

Both of the steels showed a significant ductility trough. The ductility for low carbon steel started to fall from 99% reduction of area at 900°C and reached a minimum of 30% at 850°C . The trough was narrow and ductility recovered rapidly on lowering the temperature further and was fully recovered at 800°C

For the high carbon steel ductility probably falls in two stages. The ductility first started to fall at 800°C reaching a low value of 40% R of A at 700°C . This probably corresponds to the temperature range in which deformation induced ferrite can form, and the R.of.A value is similar to that found in the low C steel. Below 700°C ductility continues to fall to a low value of 15% R.of.A at 670°C and remains constant at this value to temperatures as low as 550°C , the lowest temperature used in the exercise. This region probably corresponds to the region in which pearlite is able to form.

10.3.2 Stress/Elongation curves

Dynamic recrystallization was first observed from the flow stress curves for the low carbon steel at 900°C as in Fig. 10.3, while in high carbon steel there was some evidence of dynamic recrystallization at temperatures as low as 750°C although it is not fully pronounced until 850°C. Polished samples which had been quenched after test revealed there was some limited dynamic recrystallization at temperatures as low as 750°C as shown in Fig 10.4. and marked dynamic recrystallization at 780°C as is shown in Fig 10.5.

10.3.3 Metallography

Austenite grain size before deformation was measured on polished samples using the intercept method. The grain size for high C steel was found to be 550 μm and for the low C steel 450 μm .

SEM examination revealed that for the low carbon steel there are three modes of failure; high temperature ductile rupture on the right hand side of the trough, low temperature ductile rupture at the left hand side of the trough, and intergranular failure due to micro-void coalescence in the trough at 850°C as illustrated in Fig 10.6

For the high carbon steel, the fracture surface was ductile rupture on the right hand side of the trough from temperatures $\geq 750^\circ\text{C}$ as shown in Fig.10.7. Large ductile

voids were present on the fracture surface. At 700°C the main mode of fracture changed to micro-void coalescence as in Fig 10.8. This type of fracture is typical of that resulting from the formation of the thin films of deformation induced ferrite as in Fig. 10.9. Lowering the temperature further to 670°C caused the mode of fracture to change again to give flat facets characteristic of grain boundary sliding in the γ as in Fig. 10.10. Further lowering of the temperature to 620°C produced a very craggy looking surface which probably corresponds to the establishment of large volume fraction of pearlite as shown in Fig 10.11. Pearlite was observed at 650°C, as shown in Fig.10.12. At 670°C, the structure was completely austenitic except for a thin film of ferrite surrounding the austenite grain boundaries as shown in Fig. 10.13.

10.4 DISCUSSION

For the low carbon steel tested in the temperature range 900 to 1000°C, failure was in a ductile manner and high R.of.A values were obtained. When the test temperature was lowered to the 850 to 875°C temperature range there was a marked fall in ductility. As the A_{e3} temperature is 870°C, this fall of ductility most likely corresponds to the presence of thin films of deformation induced ferrite forming around the surface of the austenite grains. Ferrite is softer than austenite and so strain concentration occurs in the thin films. Inclusions present in the ferrite films cause micro-voiding. These microvoids grow and link up, thus leading to intergranular failure. Crowther and Mintz, (1986) have shown that the ferrite is deformation induced and forms at temperatures as high as the A_{e3} . The A_{e3} temperature for this steel was 870°C in accord with the temperature range in which the ductility is observed to fall. Ductility is seen to recover at 800°C due to an increase in the volume fraction of ferrite dispersing the strain more uniformly.

Dynamic recrystallization was first observed at a test temperature of 900°C, a temperature at which ductility was high. Thus at the right hand side of the trough recovered ductility corresponds to both removal of the thin film of ferrite and the onset of dynamic recrystallization.

For the high C steel again good ductility was observed at the high temperature side of the trough when both

deformation induced ferrite was eliminated and dynamic recrystallization was apparent. Although from the Stress/Elongation curves the first detected temperature for the onset of dynamic recrystallization was at 850°C, examination of the polished section from fractured samples showed some evidence for this at temperatures as low as 750°C. Lowering the test temperature to 700°C caused the ductility to fall and this fall is probably due to the presence of the thin films of deformation induced ferrite forming around the austenite grains. Lowering the test temperature further to 670°C caused a further drop in ductility to 15% R.of.A after which ductility remained constant. The fracture observations and measured pearlite start temperature (650 to 670°C) suggest that this temperature range corresponds to when pearlite is forming. The brittle nature of the steel is hence due to the austenite to pearlite transformation. Pearlite is much harder than austenite and hence is more brittle.

The results show initially the austenite to ferrite transformation is the controlling factor in the ductility of both the steels. In the high carbon steel, the austenite to pearlite transformation causes the ductility to decrease further and remain at a low level. Raising the carbon level caused a lowering of the transformation temperatures and, as a consequence, the ductility trough moved to lower temperatures. The movement of the A_{e3} temperature was 150°C, and assuming in the high C steel that fall in ductility between 750°C and 700°C corresponds

to when deformation induced ferrite first forms, a similar movement of the trough is apparent.

The work carried out by Crowther and Mintz, (1986) showed that for steels with carbon content between 0.04 and 0.24%, the factor controlling the position of the ductility trough was as in the present instance the austenite to ferrite transformation. For this range of carbon, raising the carbon level caused a lowering of the transformation temperature and, as a consequence, the ductility trough moved to lower temperatures. However, for their higher carbon steels 0.35 and 0.65% C, the mode of fracture was found to change from micro-void coalescence to flat fracture surfaces characteristic of grain boundary sliding in the austenite. Instead of the trough shifting to a lower temperature as the C level increased from 0.24 to 0.35% the left hand side of the trough remained fixed in the temperature range 600 to 650°C, while the right hand of the trough moved to a higher temperature as is shown in Fig. 10.14. For the higher carbon steels, the ductility was observed to fall before the onset of the austenite to ferrite transformation. Intergranular failure was found to occur due to grain boundary sliding in the austenite. The hot ductility trough extended over a much wider temperature range because in addition to failure being in the austenite by grain boundary sliding, on the lowering the test temperature below the A_{e3} temperature, thin ferrite films were seen to form around the austenite grains. Thus two different fracture modes were responsible for the poor

ductility. This behaviour is very different to that found in the present work.

However, whether intergranular failure first occurs in the austenite or at the onset of transformation has been shown to be finely balanced (Crowther and Mintz, 1986). The balance, in this case, may have been tilted by the aluminium content of the steel. There was no aluminium in the steels in the previous work. In the present work, the steels were aluminium killed. The low carbon steel contained 0.037% Al, and the high carbon steel 0.014% Al. It is suggested that this difference in behaviour between the steels may have been caused by the variation in oxide contents as grain boundary sliding in the γ is enhanced by the presence of particles at the boundaries (precipitates, sulphides, oxides, etc).

10.5 CONCLUSIONS

- 1- The low carbon steel shown a marked ductility trough due to the presence of thin films of deformation induced ferrite around the austenite grains. The ductility recovered on lowering the temperature due to an increase in the volume fraction of the softer ferrite phase. At the high temperature side of the trough removal of deformation induced ferrite lead to dynamic recrystallization. Both these processes might be expected to improve ductility, but because they occur together it is not possible to separate there individual contributions to the improved ductility.

- 2- Raising the carbon content, by lowering the transformation temperature, moved the trough to lower temperature. Again the temperature for the onset of dynamic recrystallization and removal of deformation induced ferrite (Ae_3) were similar. However, ductility did not recover due to the austenite to pearlite transformation.

Table 10-1

Composition of the steels examined (Wt.%)

<u>Code</u>	<u>C</u>	<u>Si</u>	<u>Mn</u>	<u>P</u>	<u>S</u>	<u>Al</u>	<u>Ni</u>	<u>Cr</u>	<u>Cu</u>	<u>N</u>
Low Carbon steel	0.11	0.32	0.32	0.01	0.003	0.037	0.02	<0.005	—	0.007
High Carbon steel	0.75	0.22	0.91	0.016	0.02	0.014	0.06	0.02	0.05	

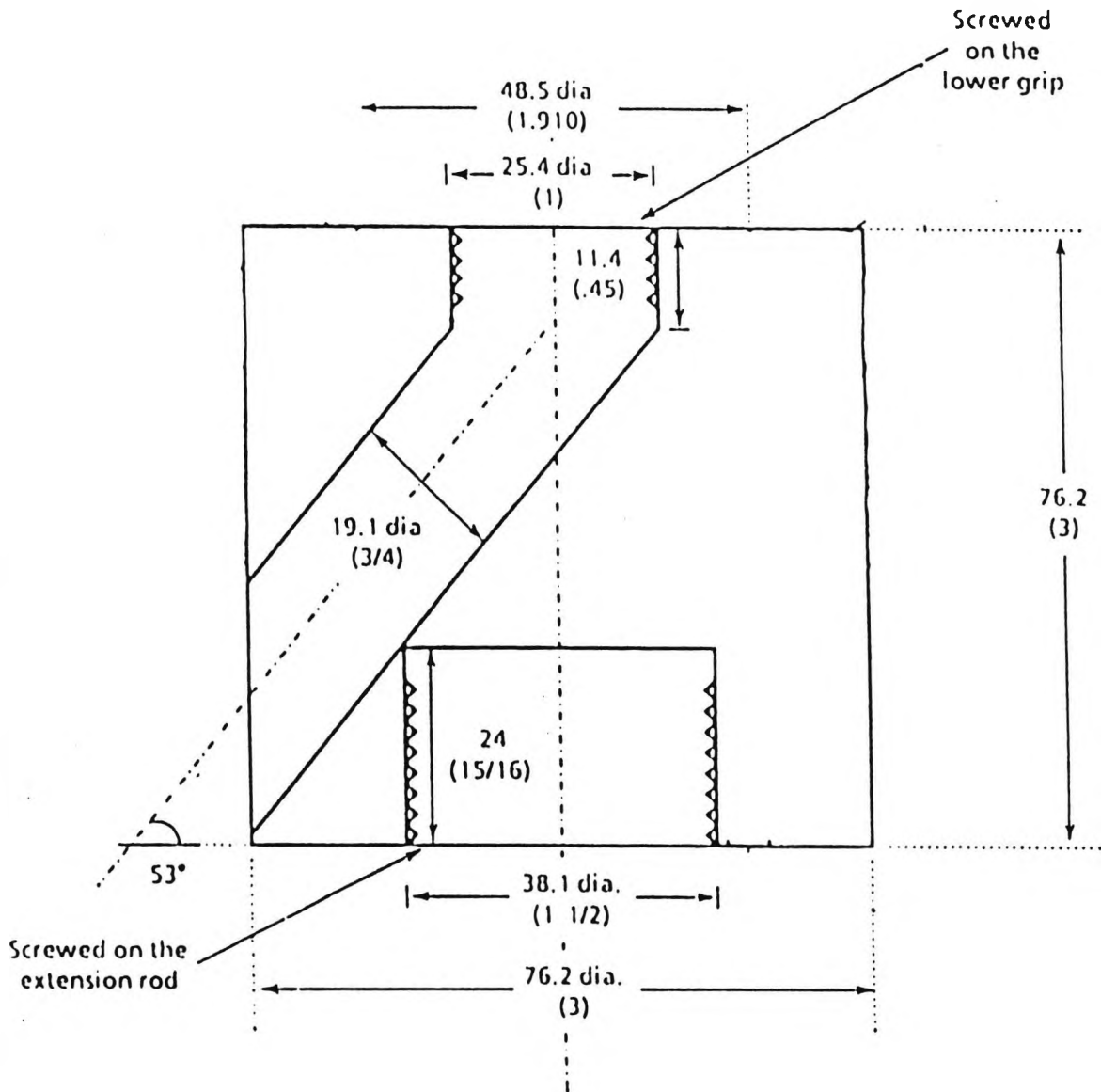


Fig. 10.1 Schematic diagram of the quenching unit
 (Approximate dimensions in mm (original dimensions
 in inches are shown in parentheses)

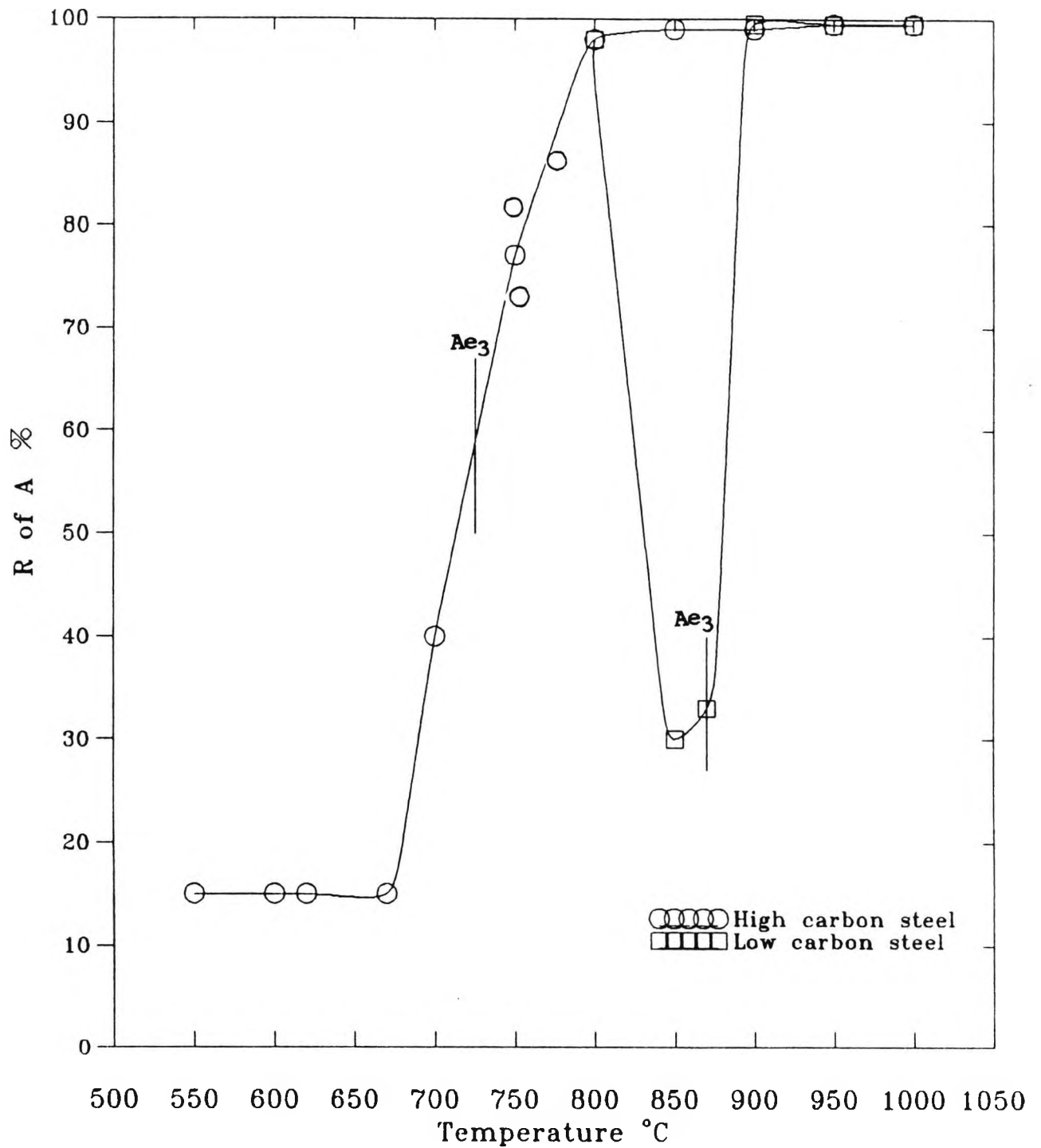


Fig. 10.2 Hot ductility curves for low and high carbon steels.

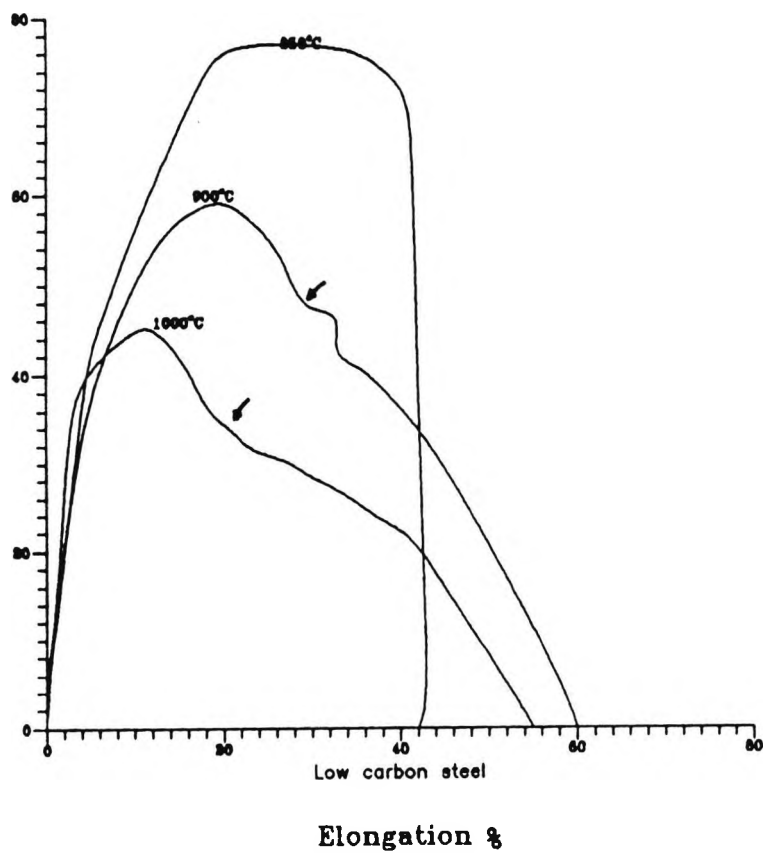
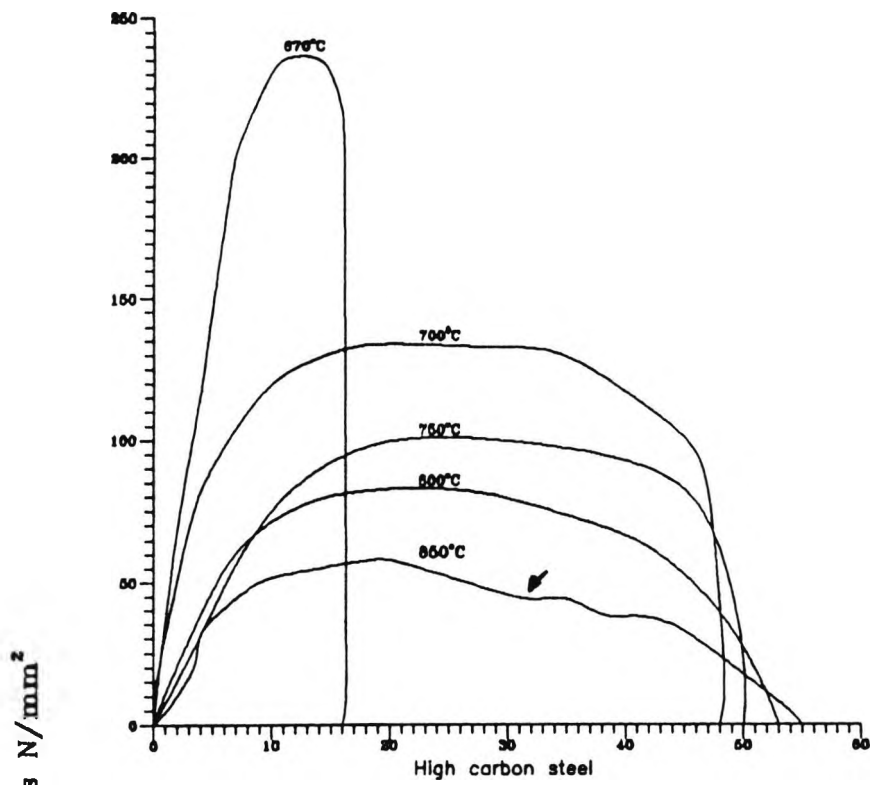
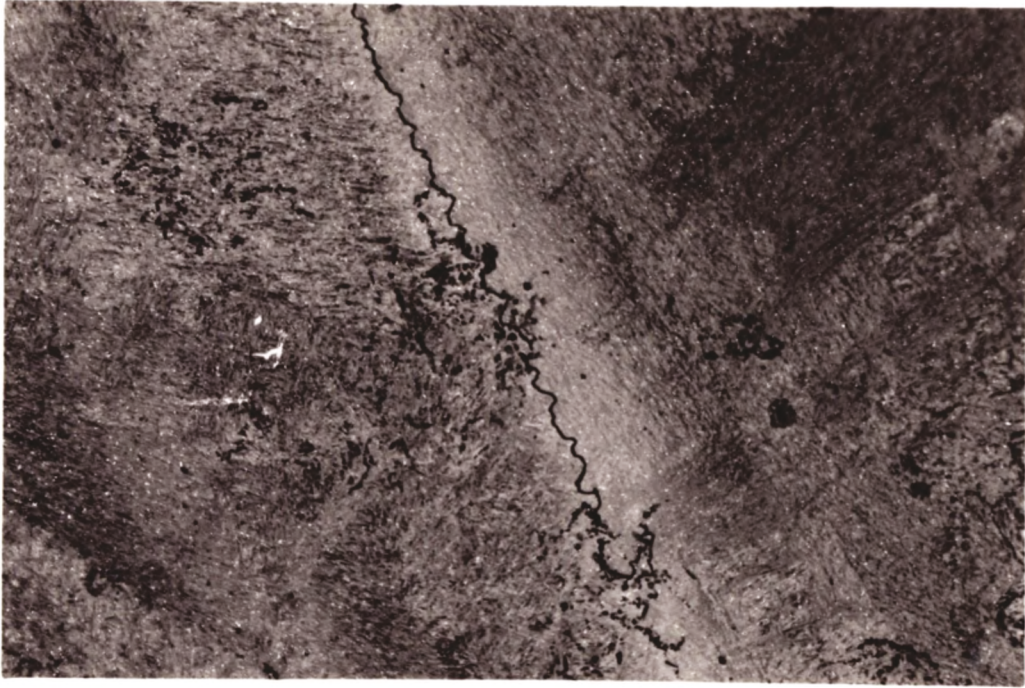
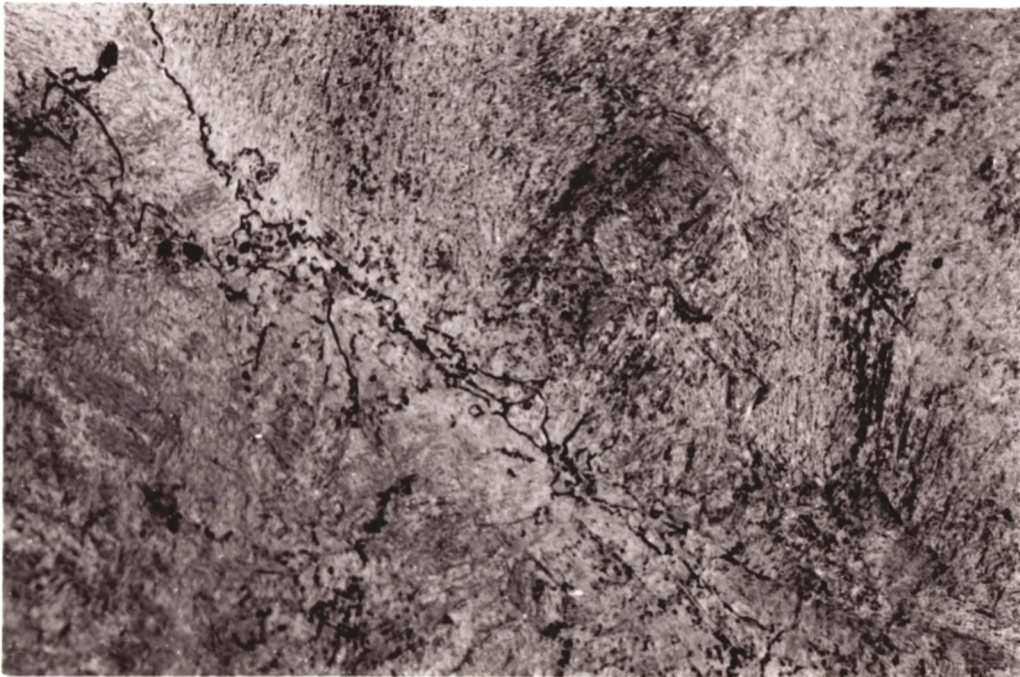


Fig. 10.3 Stress/Elongation curves for high and low carbon steels.

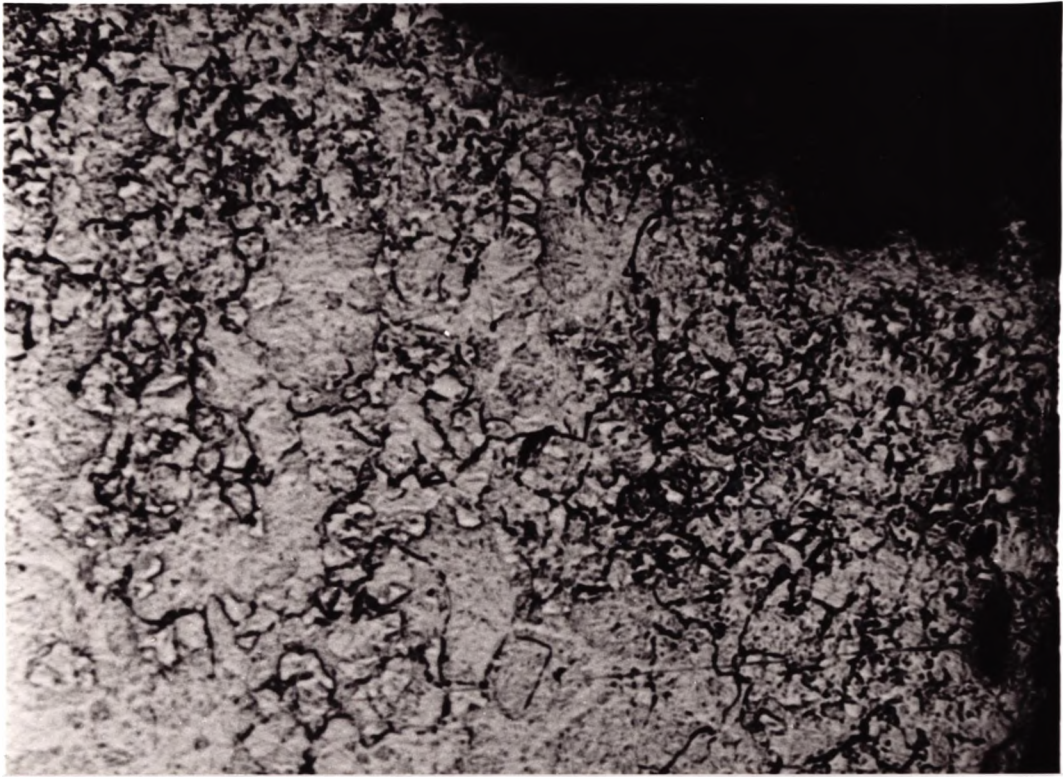


100 μm



100 μm

Fig. 10.4 Evidence of dynamic recrystallization for high carbon steel, tested at 750°C. (*quenched*)



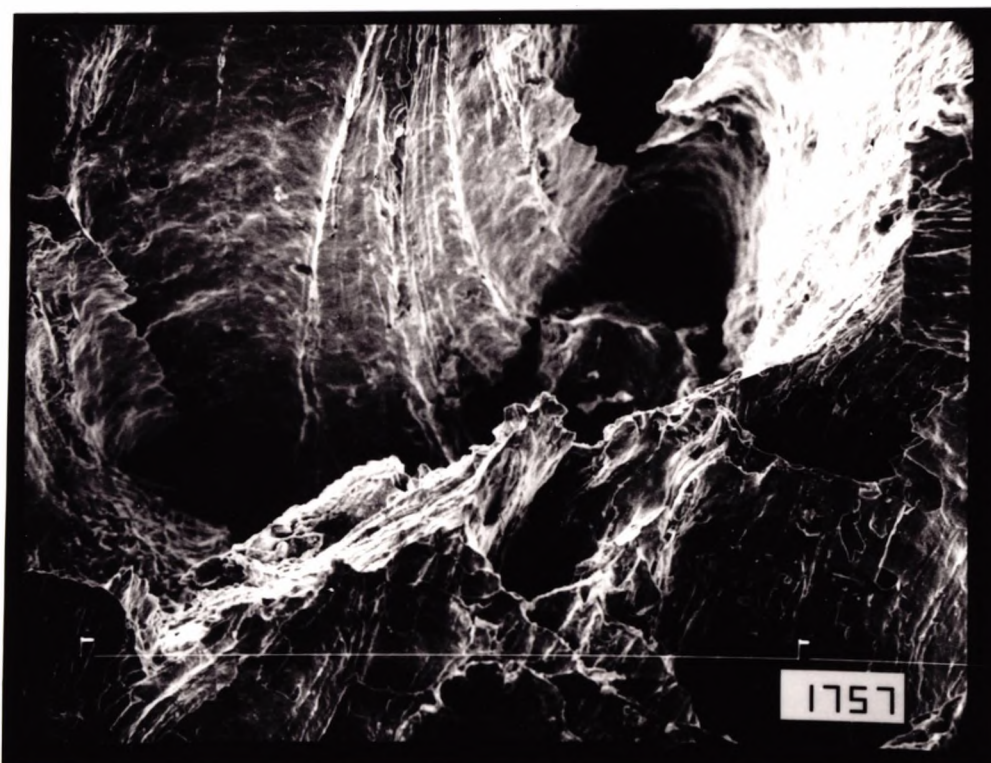
50 μm

Fig. 10.5 Evidence of dynamic recrystallization for high carbon steel, tested at 780°C. (quenched)



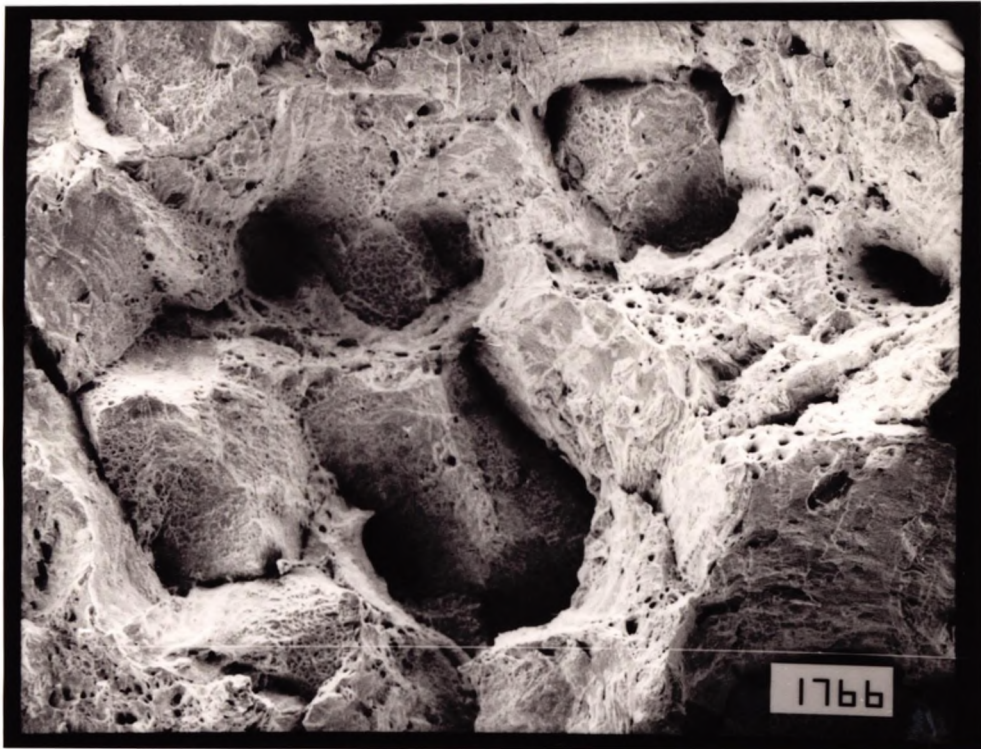
285 μm

Fig. 10.6 Example of intergranular micro-void coalescence fracture observed in low carbon steel, tested at 850°C.

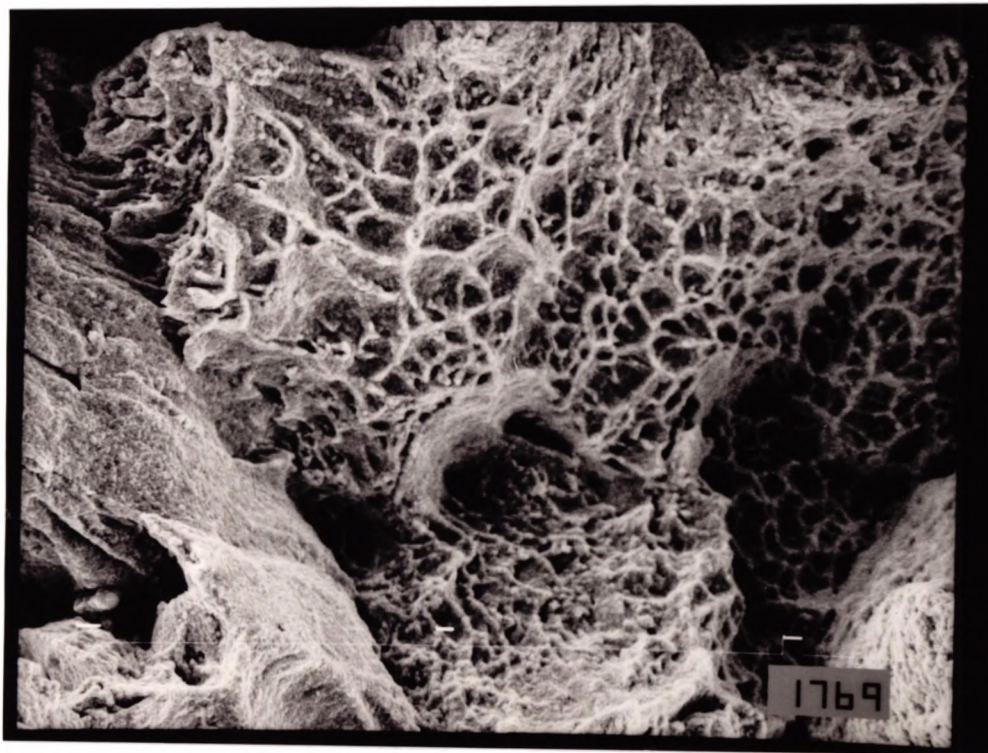


50 μm

Fig. 10.7 Example of high temperature ductile rupture fracture found in high carbon steel tested at 750°C.

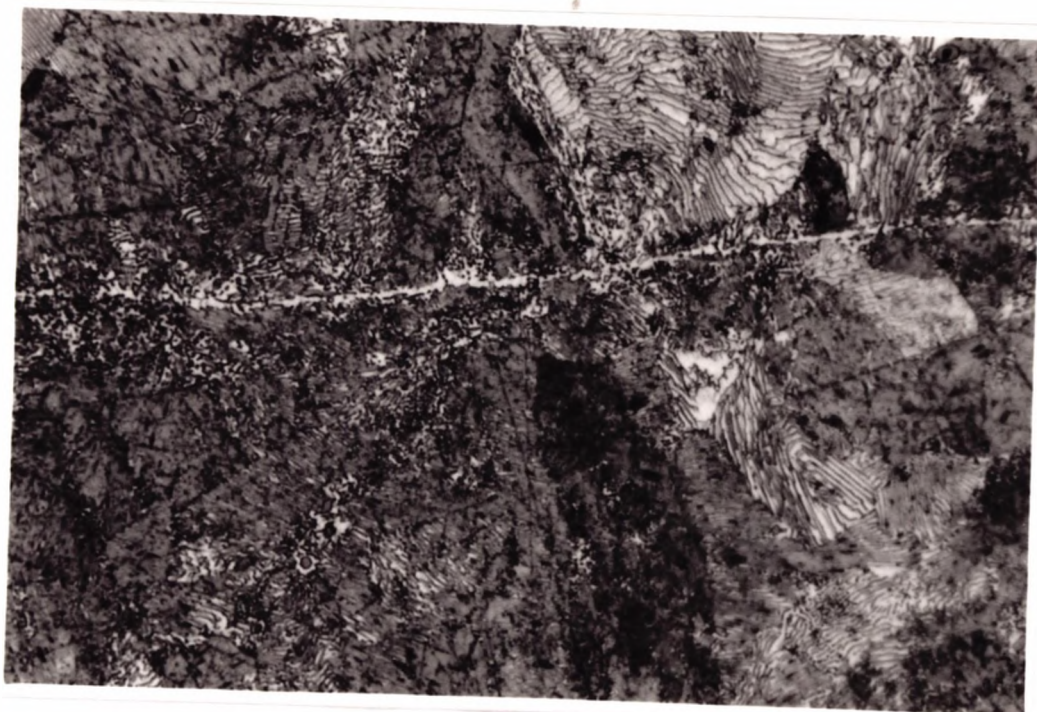


133 μm



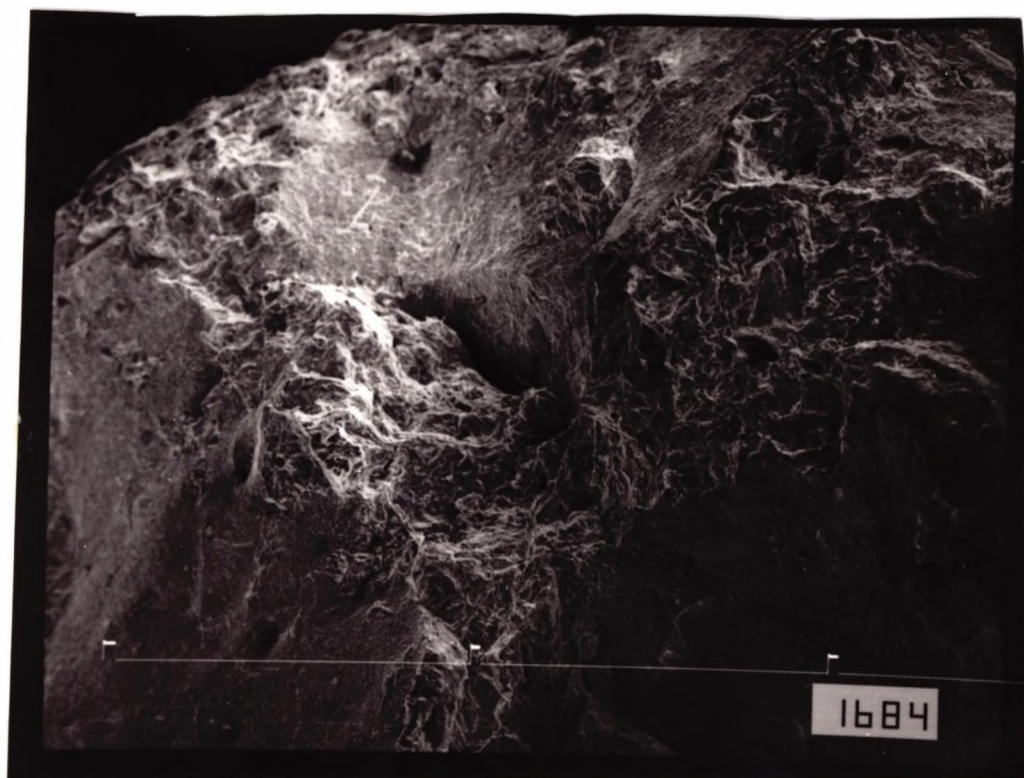
30 μm

Fig. 10.8 Example of intergranular micro-void coalescence fracture observed in high carbon steel, tested at 700°C



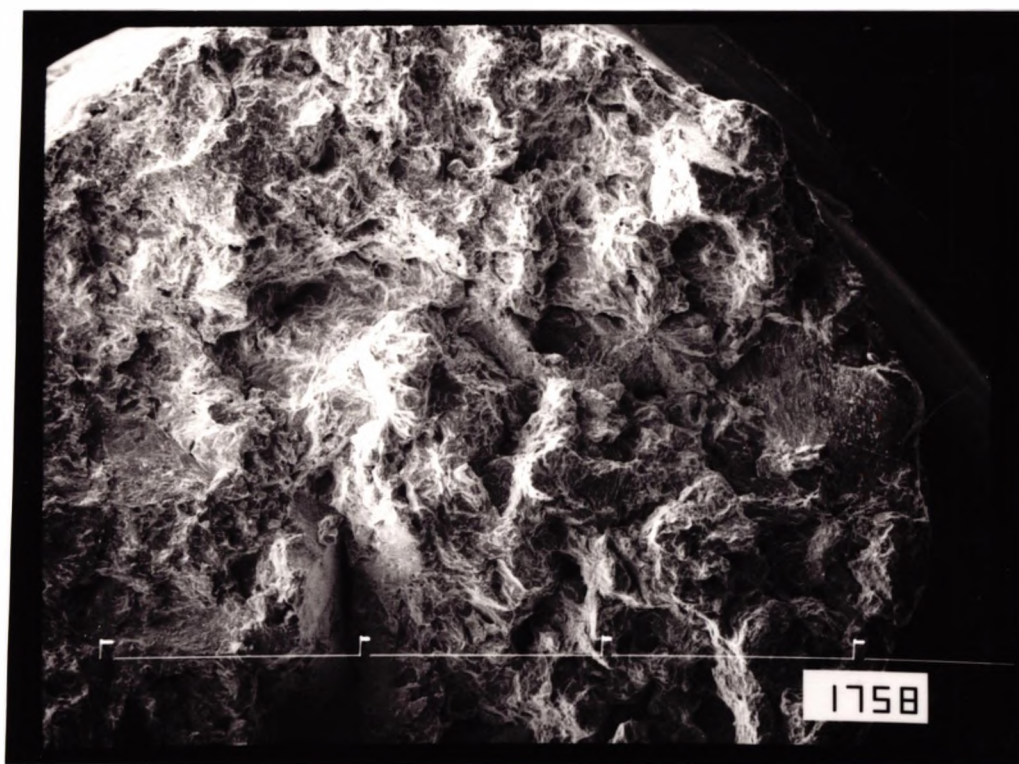
50 μm

Fig. 10.9 Evidence of deformation induced ferrite in high carbon steel tested at 700°C. (quenched)



200 μm

Fig. 10.10 Grain boundary sliding found in high carbon steel, tested at 670°C.



285 μm

Fig. 10.11 Typical pearlitic fracture found in high carbon steel tested at 620°C.

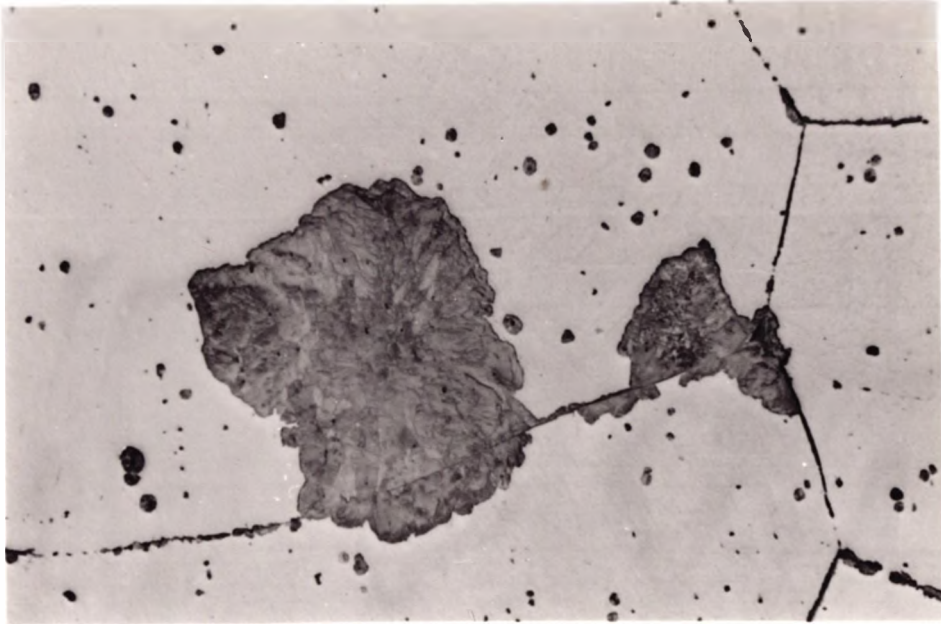


Fig. 10.12 First evidence of pearlitic structure formation in high carbon steel. Steel heated to 1330°C, held for 5 min, cooled at 25°C/min to 650°C, held 5 min, and then quenched in water. 200 μm



Fig. 10.13 High carbon steel tested at 670°C showing austenite grains with ferrite films surrounding the grains. (not quenched) 200 μm

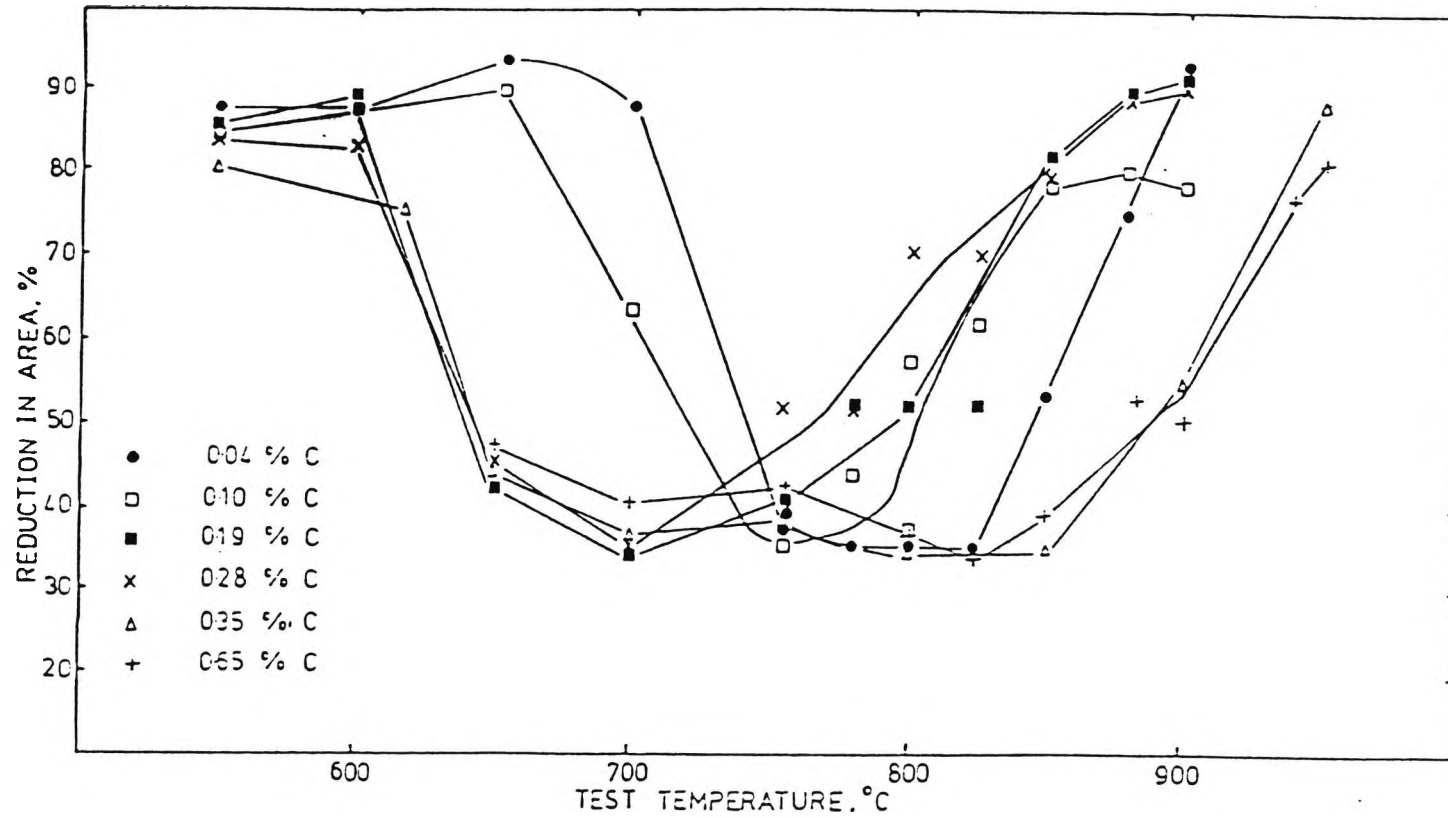


Fig. 10.14 Hot ductility curves for series of plain C-Mn steels with different carbon levels. (After Crowther and Mintz, 1986)

CHAPTER 11

SUMMARY AND RECOMMENDATIONS

11.1 INTRODUCTION

The hot ductility behaviour of micro-alloyed and plain C-Mn steels has been examined in the as-cast condition or after heating the steels to 1330°C, and cooling to test temperatures in the range of 700 -1000°C. Low strain rates of 10^{-3}s^{-1} - 3.10^{-3}s^{-1} have been used to simulate the conditions experienced during the straightening operation in the continuous casting process.

It is intended in this chapter to summarise the results obtained in these studies and to compare the hot ductility behaviour of all the steels examined.

From the conclusions reached in the present study and previous studies, recommendations will be suggested to help in the prevention of transverse cracking, and recommendations will be made for future work.

11.2 Summary

For the steels in the as-cast condition, cooled to the test temperatures in the range 700-1000°C, and tested at a strain rate of $2 \times 10^{-3} \text{ s}^{-1}$, the following conclusions can be drawn:-

1- Ca treatment for the C-Mn-Al and C-Mn-Nb-Al steels improves hot ductility due to the total S being reduced, so reducing the amount of sulphides precipitated at the interdendritic grain boundaries which later become the austenite grain boundaries. The reduction in the number of fine sulphides precipitated at the boundaries reduces voiding at the boundaries and makes it more difficult for cracks formed by grain boundary sliding to join up. A reduction in the fine matrix precipitates of sulphides also lowers the temperature for the onset of dynamic recrystallization.

2- Nb and S have a similar influence on the hot ductility, both producing fine precipitation in the matrix as well as at the austenite grain boundaries. These precipitates encourage cracks formed by grain boundary sliding to link up and delay the onset of dynamic recrystallization to higher temperatures. In this way ductility is reduced and the trough is widened.

3- A Ti addition to a Nb containing steel has only a slight effect on the hot ductility when cooled at 100°C/min to the test temperature, but a marked improvement has been shown to occur when the cooling rate is reduced to 25°C/min. This marked improvement arises because the precipitation is found to be coarser. It is likely that the coarse Ti rich particles provide nucleation sites for precipitation of Nb at higher temperatures so that there is less available to precipitate out at lower temperatures in a finer detrimental form.

4- Raising the C level from 0.05% to 0.15% in a C-Mn-Al, Ti containing and Ti free steel was found to move the ductility trough bodily to lower temperatures in accord with the change in transformation temperature. Intergranular failure was mainly micro-void coalescence as a result of the stress concentration acting on the thin films of the softer deformation induced ferrite causing voiding at the particles and inclusions, these linking up to give failure.

5- Addition of Cu to as-cast C-Mn-Nb-Al steels was found to be detrimental to the hot ductility when the steels were tested in air but not in argon. It is believed that segregation of Cu to the boundaries on solidification, combined with the surface oxidation of Fe causes a build up of Cu to

a value exceeding its solubility in austenite, (9%) resulting in hot shortness. Nickel was found to be beneficial to as-cast hot ductility probably because it increases the solubility of Cu in austenite.

6- Reheating the steels after casting refines the grain size and the hot ductility significantly improves, when no precipitation occurs. On the other hand, ductility deteriorates (deeper and wider troughs) when C-Mn-Nb-Al steels (even when Ti is present) and high S, C-Mn-Al steels are reheated after casting. This is due to more Nb and S being able to redissolve on reheating and be available for precipitating in a fine detrimental form on cooling to the test temperature.

7- For solution treated steels, raising the solubility product for Al and N containing steels to $2-3 \times 10^{-4}$ causes a small deterioration in hot ductility. For C-Mn-Al steels solution treated at 1330°C and cooled to the test temperature in the range $750-1000^{\circ}\text{C}$ and tested at a rate of 10^{-3} s^{-1} , it is likely that the precipitation of AlN depends only on the solubility product (i.e. N does not have a more deleterious effect on hot ductility than might be indicated from the solubility product). However, longer hold times at 1330°C and at test temperatures resulted in reduced

ductility, probably because more finer AlN precipitation is allowed to occur prior to test temperature. Unfortunately, no direct evidence for AlN precipitation could be found and more work is required to confirm this view point.

11.3 Future work and recommendations

- 1- In all the previous and present work on hot ductility it has been shown that the recovery in ductility on the left hand side of the trough is caused by the presence of an increasing volume fraction of ferrite. This has been linked to the fact that ferrite is believed to be more ductile than the austenite and less prone to grain boundary sliding. Certainly ferrite has more slip systems and also has a higher stacking fault energy than austenite and so will cross slip more readily. However another factor which may be more important in giving rise to improved ductility is the difference in grain size between the ferrite and austenite grain structures. Whereas the austenite grain size is typically 300 μm , the ferrite grains is an order of magnitude smaller, and finer grain sizes are known to give improved ductility. In order to examine this possibility the influence of ferrite grain size on hot ductility in the temperature range 600 to 700°C needs to be established and this is best carried out on a ferritic stainless steel.

- 2- Certain aspects of the hot ductility curve and its relationship to transverse cracking are still not understood. For C-Mn and C-Mn-Al (low Al and N levels) steels solution treated and cooled to the

test temperature, the majority of the trough is associated with the presence of deformation induced ferrite. Little is known about the development of this ferrite and in particular it is not known whether it can form at the low strains applied during the straightening operation, or what influence grain size has on its formation. It is suggested that samples of plain C-Mn steels be heat-treated into the γ to give a variety of grain sizes should be cooled to the minimum ductility temperature and given various strains (2,5,10 % etc) followed by quenching to determine the presence of deformation induced ferrite.

3- It has been shown in Chapter 8, that adding Al so that the solubility product is in ^{excess of} ~~the range~~ 3.2×10^{-4} causes ductility to deteriorate, and longer holding times at 1330°C and at test temperatures cause further deterioration in ductility. This strongly suggests that AlN precipitation is responsible for the loss of ductility, but no direct evidence was found. Further work, taking replicas directly off the fracture surface may reveal the presence of AlN, and confirm the interpretation of the results. Although the simple hot ductility test has been of immense help in alleviating the problem of transverse cracking especially when the tests are

carried out in the as-cast condition as in the present instance, conditions are still far removed from the commercial operation. In the commercial continuous casting operation the strand undergoes a cycling in temperature, due to the impingement of the sprays on the strand each time the strand goes in and out of the rolls.

The present testing technique needs to be further developed to incorporate this cooling cycle.

4- The study of the effect of Cu on the hot ductility of as-cast steels indicates that Cu is detrimental especially when the tests are carried out without the protection of an atmosphere. Further work is required on this to clarify the mechanism which causes this fall in ductility.

5- The relative contribution of grain boundary sliding, deformation induced ferrite, and dynamic recrystallization to hot ductility is still not clear as it is very difficult to separate the individual contributions. The improvement in ductility which occurs at the high temperature side of the trough in C-Mn and C-Mn-Al steels always corresponds to both the onset of dynamic recrystallization and the removal of deformation induced ferrite films and it is not clear which factor is more effective in improving the hot ductility. More work is needed to separate the

importance of these mechanisms. It is likely that more information could be obtained if the strain rate is lowered to $3 \times 10^{-4} \text{ s}^{-1}$, as this will encourage grain boundary sliding and widen the trough without influencing the Ae_3 temperatures. Such an exercise should be carried out on a plain C-Mn steel heated to give a coarse grain size (300 μm) and cooled to the test temperature range of 650-1000°C. A higher C steel (0.4 %C) would be preferred for this exercise as these steel have been found to be more prone to grain boundary sliding. The new quenching rig will enable the presence of deformation induced ferrite to be readily identified.

11.4 INDUSTRIAL RECOMMENDATIONS

The present work suggests that Ca is an excellent addition to make to steels to reduce transverse cracking. Reducing S levels in general are likely to be beneficial and this is one method of achieving a low volume fraction of sulphides at the γ grain boundaries. Ti additions are also likely to be beneficial but the cooling rate during solidification may have to be reduced if full benefit is to be achieved (25°C/min is to be recommended).

Finally in order to prevent hot shortness it is suggested that if Cu is added to a C-Mn-Nb-Al steel to increase strength, an equal amount of Ni should also be added.

Appendix

Appendix 1 (Publications)

Some of the results presented in this thesis have been published or accepted for publication.

- 1- Influence of calcium on the hot ductility of steels has been published in Material Science and Technol. Vol 5, P,.682 ,.1989
- 2- The influence of Ti on hot ductility of as-cast steels has been published in Material Science and Technol. Vol 7, P,.613 ,.1990
- 3- The Influence of S and Nb on the hot ductility of as-cast steels has been accepted for publication, in Material Science and Technol. 1991
- 4- The hot tensile test as mean of physically stimulating the straightening operation in continuous casting has been accepted for publication, in Material Science and Technol. 1991

REFERENCES

Akben, M G., Weiss, I., and Jonas, J.J., (1981). Acta Met., 29, 111.

Andrade, E.N.da C. (1948)., Nature, Lond, 162, 410.

Andrew, K.w., (1965). JISI, 203, 721.

Banks, T.M. and Gladman, T., (1979). Met.Technol., 3, 81.

Bernard, G., Birat, J.P., Conseil, B., and Humbert, J.C., (1978). Rev. Met., 75, 467.

Burden, M.H., Funnell,G.D., Whitaker, A.G.& Young, J.M. (1979). In Proc. Sheffield Int. Con. on Solidification and Casting., 279, London.

Biggs, B.L., (1959). JISI., 192, 361.

Birat, J.P., Larrecq, M., Le Bon, A., Jeanneau, M., Poupon M., and Senaneuch, D., (1981). Steel Making Procs., 64, 53.

Brimacombe, J.K., and Sorimachi, K. (1977)., Metall.Trans., 8B, 489.

Bywater, K.A., and Gladman, T. (1976)., Met.Technol., 3, 358.

Cardoso, G.I., and Yue, S. (1989)., Proc. of 31st Mechanical and Steel Processing Conf. Iron and Steel Soc.of AIME. Chicago., 585.

Carlsson, C.G. (1964)., Jernkot, Ann., 184, 152.

Chang,W.H. and Grant, N.G. (1956). Trans. AIME, 206, 544.

Chang,W.H. (1972)., "Superalloys Processing", AIME, MCIC.

Cochrane, R.C. (1982)., unpublished work.

Coleman, T.H., and Wilcox, J R. (1985)., Mat.Sci and Technol.,1, 80.

Copeland, M.I., and Howe, J.S., (1975). U.S.Bureau of Mines **Report** no. 8080.

Cordea, J.N.,and Hook.,R.E., (1970). Met.Trans.,1,111.

Coward, M.D., Richardson, G.J., and Sellars., C.M., (1976). Met.Tech., 12, 550.

Crowther, D.N. and Mintz, B., (1986d). Proc.Int.Con. "On The Effects and Control of Inclusions and Residuals in Steels", Toronto, Canada, 3, 83.

Crowther, D.N., (1986). PhD Thesis, The City University.

Crowther, D.N., and Mintz, B., (1986a). Mater.Sci and Technol., 2, 671.

Crowther, D.N., and Mintz, B., (1986b). Mater.Sci and Technol., 2, 951.

Crowther, D.N., and Mintz, B., (1986c). Mater.Sci and Technol., 5, 1099.

Crowther, D.N., Mohamed, Z. and Mintz, B., (1987). Trans.ISIJ, 27, 366.

Davies, P.W. and Evans, R.W., (1965). Acta.metall., 13, 353.

Desai, S.C., (1959). JISI, 191, 250.

Dieter, G.E., (1968)., In: "Ductility", Metals Park, Ohio, 1.

Lucke, K., and Stuwe, H.B., (1963). In "Recovery and Recrystallization of Metals". New York, ed. L. Himmel.

Dudley, D., (1665). Metallum martis.

Evans, H.E., (1969). Met.Sci.J., 3, 33.

Evans, H.E., (1984). In "Creep Fracture", Pergmon Press.

Farkas, S., Shaw, J.W., and Gricol, J.D., (1971). Open
Hearth Proc., 54, 68.

Fenn, R., Roberts, S.B, (1983). Conf. COPPER IN STEEL.
LUXEMBOURG. 25-27 May.

Fu, J.Y., Garcia, C.I., Pytel, S., and De Ardo, A.J.,
(1988). The Mineral Metals and Material Soc., 27.

Fisher, G.L., (1969). J. Iron Steel Inst. 207, 1010.

Fujii, H., Ohashi, T., Hiromoto, K. and Oda, M. (1975).
Testsu To Hogana, 61, 5556.

Funnell, G.D., and Davies, R.J., (1978). Metals Technol.
5, 150.

Gifkin, R.C., (1956). Acta.metall., 4, 98.

Gifkin, R.C., (1958). Institute of Metals., 87, 255.

Gittins , A., (1977). Int.Met.Rev., 22., 212.

Gittins , A., and Tegart, W.J.McG., (1981). Metals Forum., 4., 57.

Gladman, T.and Pickering,F.B., (1967). JISI, 205,653

Glover, G. & Sellars, C.M., (1973). Metall.Trans., 4, 765.

Greenwood, J.N. and Worner, H.K., (1939). J.Inst.Metals 64 135.

Guo, H., Zhang, H., and Dong, C., (1988). Int. Symp. on "Physical simulation of welding, hot forming and continuous casting". Ottawa, , ASM, Duffer Scientific Inc. (in press).

Hannerz,N.E., (1985). Trans.ISIJ, 25, 149.

Harada, S., Tanaka, S.,Misumi,H., Mizoguchi, S., and Horiguchi,H., (1990). Trans.IJIS, 30, 310

Harding,R.A., Sawle, R., and Sellars, C.M., (1977). Met.Techol., 4, 142.

Hardwick, d., Sellars, C.M., and Tegart, W.J.McG., (1961) J.Inst.Metals 90 , 21.

Hasebe, T., (1972). Tetsu to Hagane, 58, 227.

Hater, M., Klages, R., Redent, B., and Taffner, K., (1973). Open Hearth Proc., 56, 202.

Hilty, D.C. and Farrel, J.W., (1974). In "inclusions and their effects on steel properties", Con. Paper No4, University of Leeds.

Irvine, K.J. Pickering, F.B. and Gladman, T. (1967) JISI, 205, 161

Honeycombe, R.W.K., (1987). Processing, Microstructure and properties of HSLA STEELS.

Jonas, J.J., Sellars, C.M., and Tegart, W.J.McG., (1968). In "Deformation Under Hot Working Condition", Special Report No. 108, London. ISI, 21.

Lankford, W.T., (1972). Metall.Trans., 3, 1331.

Le Bon, A., J.Rofes-Vernis, and Rossard, C., (1975). Metall.Trans., 9, 36.

Le May, I., Schetky, L,McD., and Krishnaev, M.R., (1984). Int.Con.of Metallurgical Soc of the American Institute A.I.M.E., 64.

Luton, M.j., and Sellars, C.M., (1969). Acta metall., 17., 1033.

Luyckx, L., Bell, J. John., McLean, A. and Korchynsky, M., (1970). Met. Trans., 12, 3341.

Maehara, Y., and Ohmori, Y., (1984). Met. sci and Eng., 62., 109.

Maehara, Y., Yasumoto, K., Tomono, H., Nagamichi, T., and Ohmori, Y., (1990). Mat. Sci, 6., 793.

Maehara, Y., Yasumoto, K., Sugitani, Y., Gunji, K., (1985). Trans ISIJ, 25, 1045.

Maki, T., Nagamichi, T., Abe, N., and Tamura, I., (1985). Tetsu-to-Hagane., 71., 1367.

McQueen, H.J., and Jonas, J.J., (1975). In "Treatise on Materials Science Technology" New York Academic Press, Vol. 6., 396.

Melford, D.A., (1980). Phil. Trans. R. Soc. Lond. A 295, 89-103.

Mercer, R.E., and Macpherson, N.A., (1980). Iron Making and Steel, 7, 167.

Michel, J.P., and Jonas, J.J., (1981). Acta metall., 29, 513.

Mintz, B., (1980) Private Communication.

Mintz, B., and Mohamed, Z. (1988). Met.Sci.Technol. 4,pp. 895-902.

Mintz, B., Stewart, J.M., and Crowther D.N., (1987). Trans.ISIJ., 27. 366.

Mintz, B., and Arrowsmith, J.M., (1979). Met.Technol., 6, 24.

Mintz, B., and Arrowsmith, J.M., (1980). In 'Hot Working and Forming Processes ',Met.Soc. Book No. 264, 99.

Mintz, B., Wilcox, J.R., and Crowther, D.N., (1986). Mat.Sci and Technol., 2, 589.

Mintz, B., Yue, S., and Jonas, J.J., (1990). Accepted for publication. Int. Materials Review.

Mohamed, Z., (1988). PhD Thesis, The City University.

Mori, H., (1974). Tetsu To Hagane, 60, 784.

Mushet, R., (1857). British Patent no. 1660.

Nachtrab, W.T., and Chou, Y.T., (1986). Met. Trans., 17a 1955.

Narita, K., (1975). Trans.Iron Steel Inst. Japan., 15, 147.

Noberg, H., And Aronsson, B., (1968). J.Iron Steel Inst., 206,1263.

Nozaki, T., Matsuno, J., Murata, k., Ooi, H., and Kodama, M., (1978). Trans.ISIJ, 18, 330.

Offerman, C., Dacker, C.A., and Enstrom, C., (1981). Scan.J.Met , 10, 115.

Ouchi, C., and Matsumoto, K. (1982)., Trans.ISIJ, 22, 543.

Osinkolu., G.A., Tacikowski., M., and Kobylanski., A., (1985). Mater. Sci. and Technol., 1, 520.

Paul, S.K., Chakrabarty, A.K., and Basu, S., (1982). Met. Trans., 6, 185.

Pickering, F.B., (1989). Mecanical Working and Steel Processing Conf., 10, 381

Pircher, H., and Klapdar, W., (1977). In "Micro-alloying 75", New York, United carbide Crop., 232.

Portevin, P.A., (1962) Thesis, University of Paris.

Rizio, D.P., Oldland, R.B., and Borland, D.W., (1988). Proceeding of Thermec.Con., 178.

Robbins, J.L., Shepard, O.D., and Sherby, O.D., (1967).
Trans. ASM, 60, 205.

Roberts, W., Boden, H., and Ahblom, B., (1979).
Met.Sci., 13, 195.

Rogberg, B., (1983). Scand.J.Met., 12, 175.

Ruibal, E. , Urcola, E.E., and Fuentes, M., (1984).
Met.Technol., 11, 189.

Sandström, R., and Lagneborg, R., (1975). Acta
Metall. 23, 387.

Sanker, J., Hawkins, D.N., and McQueen, H.J., (1979).
Met.Technol., 6, 325.

Schmidt, L., and Josefsson, Å., (1974). Scan.J.Met., 3,
193.

Sekine, H., and Maruyama, T., (1979). Trans ISIJ, 16,
427.

Sellars, C.M., (1980). In "Hot Working and Forming
Processes", Metals.soc. Book No. 264, 3.

Sellars, C.M., and Tegart, W.J.McG., (1966).
Met.Sci.Rev., Met., 63, 731

Sellars.C.M., (1979). Hot Working and Forming Processes
Con.

Smaill, J.S., Keown, S.R., and Erasmus, L.A., (1976).
Metall. Technol, 5, 194.

Stroh., A.N., (1955). Proc.Roy.Soc., London, A232., 548.

Suzuki, H.G., Nishimura, S., Imamura,J., and Nakamura,Y.,
(1984). Trans.ISIJ, 24, 54.

Suzuki, H.G., Nishimura,S., and Yamaguchi, S., (1982).
Trans.ISIJ, 22, 48.

Suzuki, H.G., Nishimura,S., Imamura,J., and Nakamura,Y.,
(1984). Trans.ISIJ, 24, 169.

Takeuchi,E., and Brimacombe,J.K., (1985). Met.Trans 16B,
605.

Taplin, .M.R., and Whittaker, V.N., (1963). J.Ins.Met.,
92, 426.

Tegart, W.J.McG., and Gittens, A., (1977). In "The hot
Deformation Of Austenite "Met.Soc.AIME, New YORK 1

Tegart,W.J.,McG., (1968). In: "Ductility", Metals Park,
Ohio, 133.

Thomas, B.G., Brimacombe, J.K., and Samarasekera.
(1986)., ISS Trans., 7, 7.

Tipnis, V.A., Joseph, R.A., and Doubrava, J.H., (1973).
Met.Eng Quarterly., 73.

Tomono, H., (1977). In; CONAST Slab Seminar, Zurich.

Turkdogan, E.T., (1987). Steelmaking Con.Proceeding.,
Pittsburgh, 70, 399.

Turkdogan, E.T., Ignatawice, I., and Pearson, J., (1955).
JISI, 180, 349.

Vodopivec, F., (1973). JISI, 211, 664.

Vodopivec, F., (1978). Metals Technol., 5, 118.

Weiss, I., and Jonas, J.J., (1979). Metall.Trans..
10A.,831.

Weiss, I., and Jonas, J.J., (1980). Metall.Trans. 11A.,
403.

White, F.E. and Rossard.C., (1966). In "Deformation
under Hot Working Conditions". Conference Uni. of
Sheffield.

White, F.E., and Rossard, C., (1968). "Deformation Under Hot Working Conditions". Spec.Rep., No 108., Lond, ISI, 14.

Wilcox, J.R , and Honeycombe, R.W.K. (1987), Mat.Sci and Technol., 3, 849.

Wilcox, J.R , and Honeycombe, R.W.K., (1984). Met.Technol., 11., 217.

Iacocca, R.G., and Woodford, D.A., (1990). Polytechnic institute. To be published. Proc. Int. Symp. on "Physical simulation of welding, hot forming and continuous casting", 1991, . Ottwa, Canada. CANMET (in press).

Woodfine, B.C., and Quarrell, A.G., (1960). JISI., 19s, 409.

Wray., P.J., (1981). Met.Technol., 8., 466.

Wright, J.A., and Quarrell, A.G., (1962). JISI, 200, 299.

Yamaguchi, S., Kobayashi, H., Matsumiya, T., and Hayami, H., (1979). Met.Technol., 5., 170.

Yasumoto, k., Maehara, Y., Ura, S., and Ohmori, Y., (1985). Mat, Sci. and Technol., 1., 111